CHAPTER SEVEN

SUMMARY AND CONCLUSION

Evaporites have been the focus of renewed attention through the last century concerning its origin and bio-saline roles effects on mineral solubility. The last decades witnesses more interest initiated particularly by sedimentologists (e.g. Shearman, 1963; Haride and Eugster, 1971; Schreiber *et al*, 1976) and still actively going by many authors with expanding the field of applications (e.g. Geisler-Cussey, 1997; Orti, 1997; Schreiber and Nury, 1997; Alderman, 2000 and Wali, 2004), whom recognizing that evaporites can not only be treated as chemical deposits and/or precipitates, but can also be interpreted as sediments with facies assemblages characterizing a certain environment of deposition.

The combined work of sedimentologists and biologists on the modern salt setting emphasizes and indicates relationship between the evaporative media and its organic content (e.g. Orti Cabo *et al* 1984; Cornee, 1988, 1984; Gerds and Krumbein, 1987; Evans and Kirkland, 1988; Javor, 1989 and others). These achievements had led petroleum geologist to re-scope and propose evaporites as a source rock for hydrocarbons (e.g. Friedman, 1980; Evans and Kirkland, 1988; Kerkland and Evans, 1981; Eugster, 1985; Warren, 1986 and Benali *et al* 1995).

The evaporite contribution to some of the world's major oil reserves (e.g. Hunt, 1967; Palacas, 1984 and others) based on the unusual composition and habitat of the organic content of many evaporite deposits (e.g. Connan *et al* 1988, 1986; ten Haven *et al* 1988, 1985; Sinnighe Damste *et al* 1988, 1986; Mello *et al* 1988; Benali and Schriber1995) leading to intensive continual efforts to improve and to strengthen the belief that evaporites are capable to act as a source rock. However, different cases allover the worlds were proved that the evaporites are the

source rock, none of the published source rock data in Gulf of Suez and Mediterranean Sea emphasize or reefer that evaporites could be the source rock in Egypt, hence both basins enclosed high thick evaporite sections during their development.

The present study aims to execute comparative study including recent site as sabkhas to prove their capabilities offering the required conditions as to prevent their biomasses from being oxidized with tentative available cores of older evaporite sections in order to tie-up their products with the recent one and to prove that the evaporite could act as source rock in Egyptian producing areas and horizons.

The stratigarphy and geologic structure (faults, folds and unconformities) of the Gulf of Suez and Northern Sinai were reviewed with especial emphasis to detailed core description of the cored intervals from the study areas (Ras Shukeir Coastal Sabkha, Ras Gemsa, Ras Dib, South East Zeit, Shagar and Gubal Island fields with North Sinai and Esh Mallah Fields).

The Miocene stratigarphy in Gulf of Suez region gained its importance and was studied by many workers due to exploration and exploitation for oil, where the Gulf of Suez is considered as the most important oil province in Egypt. As a result of the increasing exploration activities within the Gulf of Suez, the Stratigraphic subdivision of Miocene rock was of prime interest for the oil companies in order to elucidate suitable and well defined mappable time-rock units where the majority of oil production from the Miocene sediments. Generally, the Miocene section in Gulf of Suez region represented by a lower clastic Group (Gharandal Group) and an upper evaporite Group (Ras Malaab Group). The Gharandal Group is characterized by the dominance of sandstone, shale, marl and limestone. The Ras Malaab Group consists mainly of anhydrite and salt with numerous intercalations of shale and marls. The Miocene section is overlain

unconformably by a very thick Pliocene and Pleistocene succession of gravel and sand with intercalation of marl and shale (Hassan and El Bashlouty, 1970).

The Miocene sequence of north Sinai (Mediterranean Sea region) is known only from subsurface coring (Said, 1990). Concerning the Miocene rocks in north Sinai, detailed palaeobathymetric, nannoplankton biostratigraphy and facies analyses of exploratory boreholes indicated that the beginning of Messinian (Upper Miocene), Said, 1990. It's evident that the Miocene succession in the Gulf basin is characterized by a remarkable lateral change in thickness and facies as a result of the Miocene block faulting (Sadek, 1958; Garfunkel and Bartov, 1977).

The geologic structure of the Western side of Gulf of Suez and north Sinai, (Mediterranean Sea), were studied by many workers. The brief and simplified reviews indicate that: 1- The rocks of the Gulf of Suez are characterized by rapid central changes in thickness and facies in response to Miocene block faulting (Sadek, 1959, Garfunkel and Bartov, 1977). 2- Almost all the linear structures in the Gulf of Suez are strike-slip faults of different trends. These major fractures system are identified as three left lateral trending N35W, N60E-SSW and N8SE. 3- The Gulf of Suez seems to have been subjected to three phases of tectonism associated with five cycles of deformation (Bayoumi, 1983). Also Meshref, 1990, suggested a rifting model for Gulf of Suez showing sense of major faulting that extend and bounded the Gulf of Suez on both sides (Fig.22). He also mentioned that the Gulf of Suez rift comprises a northwest trending intracratonic basin that separated from Red Sea by the Aqaba transform fault. There is a great similarity between this model and the dogleg model proposed by Harding, 1984. The detailed structure of area is mentioned in Chapter Two.

Field observations of recent site of evaporite deposits (Ras Shukeir sabkha) were crucial for characterizing formation and preservation of organic matter contents. The observations show that Ras Shukeir sabkha is divided into three zones of different elevation: an outer higher zone is covered with tepee structure, an intermediate central zone contain gypsum and mud mounds, which contains algal remains and organic odour as well as the mud mound of algal origin surrounding seasonal pans suggesting and indicating the high organic activity and productivity of such evaporitic environment (saline-hypersaline pans). The permanent hypersaline pans occupy the lowest zone. Gypsum is the only sulphate mineral occurring with clastic sediments in-between crystals but halite is precipitating insitu along the upper most surface of the sabkha. The water supply into the sabkha is almost entirely from the sea by seepage-reflux through the coastal sediments and never by flooding. The hypersaline pans are permanent due to continuous and constant re-charge of seawater by seepages and strong evaporation rates would lead to evaporite accumulation and/or precipitation from concentrated and saturated brines. The pans are different in size and have distinctive associations, the eastern pan is shallower but the western is deep with an evaporitic sequence of carbonate, algal mat at the margins and gypsum and halite at the crust. The solar ponds are in western part of the sabkha, which are shallow and produce annual layering of salt. The presence of gypsum mound with algal relics and mat and mud mound with algal mats and organic odour as well as mud mound of algal origin are forming and supporting a rich organic life and activity with high productivity such as green algae, halophytes and the red tomato soup color. Their presence represents indicators of prolific biological activity and productivity. Knowing that evaporitic environments can be organic matter productive and so hydrocarbon potentialities upon reaching optimum maturation. The sampling and all applied technique were carried on brines and rocks were described in detailed in Chapter Four and the pathway as well as laboratory procedure are shown in Table-1 and Fig. 35.

Mineralogical identification and characterization of evaporite core samples were based on polarizing microscope, XRD and SEM (with EDAX attachment units) to determine structure phases and composition. Also illustrating the textural and fabric relationships as well as the required details for understanding the process(es) as well as the type(s) of how organic matter involvement(s) formulating the basic measure for hydrocarbon generation. Peterographic investigation of the evaporite boreholes rocks, were based on more than 100 thin sections and fresh rock fragments covering the existing lithofacies.

The study revealed that the anhydrite, gypsum, halite, polyhalite, sylvite and wavellite are the main sulphate minerals with minor amounts of clays and calcite, dolomite, torona and pyrite as well as hematite, illmenite and siderite.

The bio-mineralized microbial matts, algal matts and algal remains and biocapsule as well as dense, black-opaque organic matter, which recording different modes of occurrences within the evaporite sediments, support the high organic contents of these sediments.

Gypsum, also occurred as lenticels, mostly composite reflecting the influence of organic material under specific salinity and temperature conditions of rich evaporite depositional regime during the deposition. Presences of halite or step-shaped irregular and square shaped voids reflect the higher salinity and hypersaline condition of the depositional regime. The intense deformation of evaporite as well as disintegration and brecciation reflect the influence of compaction stress and strain of evaporite rock as a result of high tectonic effect of the areas.

Diagenetic changes associated with pressure growth. Is the intense deformation, which includes both fragmentation and brecciation effect. Other diagenetic effects include the formations of composite lenticular gypsum and stellate texture of gypsum/anhydrite nodules and

mineralogical changes as well as dissolutions. The formation of composite lenticular gypsum crystals represents the continual growing with compaction as the main factor to merge the single lenticular crystals into one composite crystal. The stellate textures reflect the influence of exhumation that occurred during or after uplifting of depositional area due the tectonism. Mineralogical changes include mineral changes, mineral replacive and displacive and neomorphism, which appear in formation of sparitic size of carbonate and dolomitization. Dissolutions appear as unfilled voids, irregular step shaped and square shaped molds which due to dissolution the pre-existing halite or transformation of minerals phases leading to the porosity enhancements of evaporite sediments.

Fluid inclusions investigations support the petrographic study, while the microthermometric data were used to deduce the brines condition of salt bearing deposits and investigating the relationships between the hydrocarbons and evaporite rocks. The studies revealed that the inclusions include solid and fluid inclusions. The solid inclusions include calcite, anhydrite and organic matter. Calcite and anhydrite inclusions were identified by their morphology and birefringence. Organic matters are rounded, dark in color and appear as unicellular bacteria or organic residues, where they fluoresced by using ultraviolet light. Two-phase (Liquid-solid) inclusions were recorded where the solid was organic matter or carbonate. The presences of organic matter inclusion as a primary inclusion support the high organic content of evaporite sediment to be yielding hydrocarbons at optimum maturity. The primary fluid inclusions are relatively large 20-90 mm in diameter and occurred as single- phase (liquid), two-phase (liquid-solid) and three-phase (liquid-solid-algae). The compositions of these primary fluid inclusions are hydrocarbon droplet, brines and organic material or algae, which are considered to be organic remains and or unicellular cyanobacteria, where they fluoresced by using ultraviolet light attached to microscope. Also, many single-phase liquid inclusions appear to have two immiscible liquids, where with freezing one liquid phase, was increased in size

between -145C° to -150 C°. The increasing in size of these inclusions indicates the existence of hydrocarbons droplets as primary fluid inclusions. The Petrographic evidences of the primary fluid inclusions are supported by microthermometric results where final melting temperatures of ice in these primary inclusions show zonations. Large number of single-phase (liquid) primary fluid inclusions in the studied samples especially Gypsum indicates precipitation from relatively low-temperature solutions (40 C°-50 C°). Salinity variations in fluid inclusions from single growth bands, as indicated by final melting temperature of ice, are relatively small which indicates that the individual growth bands developed under relatively uniform conditions. Thermometric results indicate that there are three possibilities for the origin of the parent waters: 1-recycled Seawater. 2- mixed marine-nonmarine waters. 3- fresh water with calcium sulfate derived from the pre-existing marine deposits. Because of the salinity is too high for fresh water, the parent waters of the most samples of the old evaporite are probably either mixed marine-nonmarine or recycled Seawater. The structural setting of Gulf support the thermometric results which indicate that these evaporite deposits formed from mixed marine-nonmarine, where the faulted block were flooded by Seawater or water from land which supported by shallow, subaqeous, subsiding marginal rift basin (lagoon or salina) environment setting.

Geochemical characteristics of hypersaline pans and ponds based up on brine samples, which covered profile of different vertical depths for Ras Shukeir sabkha pools, were analyzed to identify their physical, chemical composition and their water source(s). The samples were analyzed for their major Cations and Anions, TDS, pH, salinity and physical properties (specific gravity with density). The Salinity values are high and vary with depth. pH values indicate slightly acidic to slightly alkaline as the salinity increased. TDS values are high and categorize the water pools as hypersalline. The specific gravity, Density and Salinity were suggesting introducing the layering within the water body even if it very shallow as it were confirmed by hydrochemical composition. The water types are belonging to a sandstone types with a

composition of Mg-Na- (Ca)-Cl-SO4 and path (i), which represent the manner of evolution of the reached composition. The structural configuration of the area (fault) facilitates recharging the sabkha pools by seawater.

The above considerations would strongly suggest that the Ras Shukeir sabkha is hypersalline environment as all hypersaline environments. These environments are very productive with its exposed surface, on the margin and water brine body as a whole (Evan and Kirkland, 1981). These organic matters that were generated in this hypersalline environment have several possible fats it may be preserved or may partly or completely destroy. The detailed analyses of water/brines of Ras Shukeir sabkha approved that the destruction of the generated organic matter within the water column are insufficient due to the following:

1. The oxygenated destroyer water column is very thin and the destructive capacity is very low due to the density of hypersaline pans where the solubility of oxygen decreases.
2. The viscous behavior of the highly mineralized water brines of these hypersalline pans permits their stratification and layering within the water body even if it was very shallow, which permit the flourishing the organic on the top, lighter, less saline, surface.
3. The existence of these stratification and layering prevents contact of more oxygenated destructive water with underlying sediments rich in decayed organic, which led to their preservation.
4. The alkalinity nature of brines proved the reducing environment for preservation of the originated organic matter.

For all these reasons, we can conclude that the hypersalline environment at Ras Shukeir has the capability of preserving at least a part of organic matter generated by the biological

activity in their brines and then the further evaporitic source beds would exist. Organic geochemistry study aims to investigate the relationships between organic material accumulation, preservations and evaporite.

Since the main target of this study is to answer whether or not the thermal and source rock evaluation of evaporite deposits through studying recent and restricted evaporative environments (coastal sabkha and old evaporite of Miocene age) from the Gulf of Suez and Mediterranean Sea regions. The source rock and thermal maturity evaluation based on different techniques preformed on the whole rock samples, insoluble organic matter (kerogen) and soluble organic matter (bitumen) for both evaporite sediments of recent coastal sabkha and evaporite cores of Miocene age found in Gulf of Suez and Mediterranean Sea.

The results data showed the following:

1-Ras Shukeir sabkha has moderately high total organic carbon (TOC) content, which suggesting marginal organic richness with poor to excellent potential for hydrocarbon generation. The kerogen content of the organic matter is belong to type I and II, which believed to be derived from algal and planktonic biomass together with microbial that accumulated under saline to hypersaline and moderately to highly reducing condition. Thermal maturity of the organic matter is of low grade to yield hydrocarbon.

2- Ras Gemsa area has moderately TOC contents, which indicating fair to excellent organic richness with generally low potential for hydrocarbon generation; however, some intervals show good to excellent potential for hydrocarbon generation were detected in different wells. The organic matter is characterized by kerogen contents belong to type I and II with significant amount of type II/III and III. The kerogen type I and II are oil prone and derived mainly from algal and planktonic biomass together with bacterial residues accumulated under saline to hypersaline and moderately to moderately high reducing condition and Kerogen type II/III

derived mainly from oxidation during the deposition but the type III derived mainly from land derived materials or terrestrial origin. The thermal maturity is generally low grade for hydrocarbon generation.

3- Southeast Zeit area have generally low TOC contents, however, some intervals have high TOC contents indicating good organic richness. The hydrocarbon potentialities are low yields for hydrocarbon generations. . This low generation may be attributed to the poor preservation or oxidation of organics after deposition by subaerial exposure due to the tectonic up lift that characterized the Gulf region). The characteristic kerogen of evaporite sediments from this area is type II and/or II/III with presence of type III. The organic matters are marine source with significant amount of terrestrial source and thermally immature for hydrocarbon generations.

4- Ras Dib area generally is lean to fair organic richness; however, some intervals show good to excellent organic richness with excellent generation of hydrocarbon potential. The organic matter characterized by kerogen contents belonging to types II and I with presence of type II/III and III. The source of these organic matters is mainly marine source with significant contribution from terrestrial source that deposited under saline to hypersaline and moderately to moderately high reducing (anoxic) conditions and mostly immature with high potential for oil and/or gas.

5-Shagar area is lean to fair organic richness with lean hydrocarbon potential for hydrocarbon generations. The high sedimentation rate of evaporite over other sediments dilutes the organic matter, which cause lowering the TOC values of the evaporite sediments. The kerogen contents are belonging to types II and/or II/III of oil or gas prone nature, indicating the organic matter of marine source mixed with terrigenous derived organic debris, while the type II/III indicates the oxidation during the depositions. The thermal maturation is generally low grade.

6- Gubal Island area is generally lean to fair organic richness and low yields for hydrocarbon generations, which belived to dilution of organic matter content by the high rate of sedimentations and/or poor preservation as tectonic influence. The organic matter is characterized by kerogen content belong to type I, II and/or II/III. These types of kerogen

indicate the marine algal and planktonic biomass together with microbial or bacterial source accumulated under saline to hypersaline and moderately high reducing conditions (anoxic), while the presences of type II/III indicate the oxidation during the deposition. The thermal maturation is low grade for this area.

7- Esh El-Malaha area is characterized by low to moderate TOC contents. The TOC contents, which suggesting lean to fair organic richness. The hydrocarbon generation is low. The kerogen contents are belonging to type II and/or II/III, i.e. marine origin derived from bacterial and algal source and oxidized during the deposition. The organic matter in all studied samples generally immature for hydrocarbon generations.

8- North Sinai area, Mediterranean Sea, is characterized by its low total organic carbon contents (TOC), which suggesting lean to marginal source rock. The potentialities are low yields than the potential of the samples from the Gulf of Suez, which suggesting poor potentialities for hydrocarbon generations. The organic matter is characterized by kerogen belong to kerogen types II and/or II-III. The II of kerogen are derived manly from marine source (algal and planktonic population together with microbial residues mixed with terrigenous source, while the type II-III of kerogen is belived to be due to the oxidation during the deposition. The maturity is low mature state for oil generation.

The reached and recorded data base of the previous chapters would definitely urge the candidate as to consider these data as courageous enough to confirm the basic fact that evaporative environments are capable for both generating enough bio-masses and to prevent their oxidation as it was approved by Knoret *et al* , 2001 Pollastro,1999 in Gkaba and Fahud salt basin, Oman. Consequently, the possibility would support the first part of the postulated question whether or not evaporites can be a source for hydrocarbons. Now, at the particularly studied case i.e. Gulf of Suez region, the study of a recent sabkha site had proved its efficiency as to preserve organic population from being deteriorated and/or oxidized. The structural framework of the

Gulf of Suez area was devoted for thorough discussions about "How and Where a trap is suitable to hosting hydrocarbons?", but the critics concerning from where such hydrocarbons were generated did not have so much attention although some researches were focused on other sources. Moreover, the structural setting and its complicated framework did offer the required pattern for isolated to semi-isolated basins of different magnitudes i.e. sabkha sites. The present work proofs that such environment would be capable enough to produce and to preserve the organic matters, hence it worse to ask ourselves "why not evaporites would act as a source of hydrocarbons in the Gulf of Suez area?" The answer is now more sticking to positivism, but farther data (analytical and core samples) would definitely support the reached one, hence the required cost to cover these matters is huge. "The first step is a start for a thousand miles" although the sentence was among literature as application, long time ago, but it is as evaporites still expanding its flexibility to cover more fields.

REFERENCES

REFERENCES

Abdallah, A.M., Abu Khadra, A.M. and Zahran, M., 1983, Structural evolution of West Rudies oil field, Gulf of Suez, Egypt: Sixth conf. in African Geolo. Nairobi, Kenya (ABS).

Abdel Azim, M.E., 1970, Crude oil composition due to its migration in the Gulf of Suez Region: 7th Arab Petroleum Congress: pp. 37(B-2), Kuwait: 7p.

Abdel Azim, M. E, 1970, Crude oil composition – A clue to its migration in the Gulf of Suez Region 7th Arab Petroleum Congress: pp. 37 (B-2), 7p, Kuwait.

Abdel Gawad, M., 1969, Geological structure of Red Sea inferred from satellites pictures in hot brines and recent metal deposits in the Red Sea: New York, Springer-Verlag, Inc., pp. 25-37.

Abu El Ezz, A.R, 1993, Sedimentology, mineralogy and chemistry of sabkhas sediments, Central Red Sea coastal zone of Egypt. Al-Azhar. Bull. Sci., 4: pp. 77-98.

Adams, J.E. and Frenzal, H. N., 1950, Capitan barrier reef, Texas and New Mexico. Jour. Geol., 58: pp. 289-312.

Adams, J. E. and Rohodes, M.I., 1960, Dolomitization by seepage reflux: Bull. Of Amer. Assoc. of Pet. Geol, 44: pp.1912-1920.

Afifi, 1997, Geology, Mineralogy and Geochemistry of sabkha deposits and associated Uranium accumulation of Lake El Arag-lake Sitra area, northern Western Desert, Egypt (unpublished) Ph.D.Thsis, Cairo, Univ, 1, 126pp

Al Droubi, A., Fritz, B., Gas, J, and Tartoly, Y., 1980, Generalized residual alkalinity concept; Application to prediction of the chemical evolution of natural water by evaporation. Amer. Jour. Of Sci., 280: pp. 560-572

Albaiges, J., Algaba, J., Clavell, E. and Grimatt, J., 1985, Petroleum geochemistry of the Tarragona basin. Spain Mediterranean off shore. Organic Geochemistry, 10/1-3: pp. 441-450.

Alderman, M. H., 2000, Dietary sodium, surrogate markers and human health, 8th Intern. Symposium on Salt, Holland, Den Hag, (R. M. Geertman Ed.), Elsevier, 1:pp: 33-37.

Alderman, S.S., 1983, Geology of the Owens lake evaporite deposits in Schreiber, B.C., and Harner, H.L., editors: Sixth international symposium on salt, 1: pp.75-83.

Ali, Y.A. and West, I., 1983, Relationship of modern gypsum sum nodules in sabkhas of loess to compositions of brines and sediments in Northern Egypt, Jour. Sed. Petrol, 53/4:pp1151-1162.

Ali, Y.A., 1989, Petrography and environment of deposition of some subsurface Miocene evaporites (Markha evaporites) from North El Morgan, Gulf of Suez, Egypt. M.E.R.C. Ain Shams Univ., Earth Sci.Ser., 3: pp. 63-76.

Allard, G.O and Hurst, Vol. J., 1969, Brazil –Gabon geologic link supports continental drift. Sci., 193: pp. 528-532

Allen, G., 1984, Subsurface sedimentological study of Rudeis formation in Kareem, Ayun, yusr and Shukeir fields, E.G.PC., 7th petrol. Explor. Seminar, 13pp, Cairo, Egypt

Allen, G., Ayyad, A., Desforgess, G., Haddadi, M. and Pizon, J., 1984, Subsurface sedimentological study of the Rudies Formation in Kareem, Um Yuser and Shukeir fields, E.G. P.C. 7th Pet., Explo., seminar, 13pp, Cairo, Egypt.

Anderson, N.L; Brown, R. G. and Hinds, R. S., 1988, Geophysical aspects of wahomun salt distribution in southern Alberta: Canadian Jour. Of Exploration Geophysics, 24: pp.166-178.

Angels B., Grimaet, J.O, Pveyo, .J, and Albaiges, J., 1990, Characterization of model evaporitic environments through the study of lipid components. Organic Geochemistry, 16/4-6: pp. 815-828.

Arakel. A., 1980, Genesis and digenesis of Holocene evaporite sedimentation in Hutt and Leeman lagoons, Western Australia, Jour. Sed. Petrol, 50: pp.1305-1326.

Aref, M. A.M., 1998, Holocene stromatolites and microbial laminates associated with lenticular gypsum in a marine-dominated environment, Ras El Shetan area, Gulf of Aqaba, Egypt. Sedimentology, 45: pp. 245-262.

Arthurton, R.S., 1973, Experimentally produced halite compared with Triassic layered halite-rock form Cheshire, England: Sedimentology, 20: pp145-160.

Artjushkov, E., 1963, The possible genetics and general laws governing the growth of convection instability in sedimentary rocks; Diklady Akad. Nauk USSR, 153/ 1: pp.162-165.

Attia, E.A., 2003, Sedimentological and fluid inclusions characteristics of the middle Miocene gypsum dunes at Gebel Khoshera, Sinai, Egypt, Fifth international conference on Geology of the Middle East: pp.347-356.

Attia, O. E., Lowenstein T. K. and Wali, A. M. A., 1995, Middle Miocene Gypsum, Gulf of Suez: Marine or Nonmarine. Jour. of Sediment. Petrol., A65:pp.614-626.

Attia, O., Lowenstein, T.K., and Wali, A.M.A. 1995, Middle Miocene gypsum, Gulf of Suez: Marine or Nonmarine. Jour. Of Sed. Research, A65/4: pp.614-625.

Ball, J., 1916, The geography and geology of West central Sinai, Egypt, Survey Depart, Cairo, 219pp

Barakat, H., 1982, Geochemical criteria for source rock, Gulf of Suez. E.G.P.C.: 6th Petrol, Explor, Seminar, 13 p., Cairo, Egypt.

Barakat, H., 1982, Geochemical criteria for source rock, Gulf of Suez, E.G.P.C. 6th Annual offshore. Tech. Conf., HOUSTON, Texas: pp. 375-380.

Barakat, M.G., 1982, General review of petroliferous provenances of Egypt with special emphasis on their Geological setting and oil potentialities research project on resources development and policy in Egypt. Pet and natural gas, Cairo, Egypt: pp. 1-78.

Bayomi, A.I., 1983, Tectonic origin of the Gulf of Suez, Egypt as deduced from gravity data: CRC Handbook of Geophysical Explo. At Sea: pp .417-432.

Bazhenova, O.K and Arefiev, D.A., 1990, Immature oil as the products of early catagenetic transformation of bacterial – algal matter. Org. Geoch, 16: pp.307-311.

Beicha, G., 1966, Fantomes d'accroissement dans le gypse des salines de villeroy. Bull. De. Academie des science, Comptes Rendus, t.263, serie D: pp. 457-461.

Beleity, A., 1982, The composite standard and definition of palaeoevents in the Gulf of Suez. Sixth Egyptian General Petroleum Corporation Seminar, Cairo: 23pp

Benali C., Schreiber, B.C., 1995, Characterization of organic matter from restricted evaporative environment: Late Miocene of Lorca basin, Southeastern Spain, Amer. Assoc. Petroleum Geologists Bull., 79: pp.816-830.

Benali, S., Schreiber, B.C., Holman, M. L., Philips, R.PP. , 1995, Characterization of organic matter from a restricted/evaporative sedimentary environment: Late Miocene of Lorca Basin, Southeastern Spain. Amer. Assoc. Petroleum Geologists Bull., 79/6: pp. 816-830.

Berner, R.A., 1982, A new geochemical classification of sedimentary environments. Jour. Sed. Petrology, 51/2: pp.359-365.

Beydoun. Zr., 1989, Hydrocarbon prospects of red sea, Gulf of Aden: A review. Jour. Of Petroleum geology, 12/ 2: pp .125-144.

Billo-Saleh.M., 1996, Geology of marine evaporites favorable for oil gas exploration. Oil and gas Jour., 94/. 6: pp. 69-73.

Blankenhorn, M., 1901, Naues zur geologie und palantologie Aegypten III: Das Miozene: deut. Geol. Ges, 53: pp.52-132.

Blankenhorn, M., 1921, Handbuch der regionaten geologie, Bd. VIII, Abt.9, heft 23, Aegypten. Corl winters Univ, Titates buchhandlung, Heidelbeberg, 224pp

Bobbit, J. and Gallegher, J.O., 1978, The petroleum Geology of the Gulf of Suez, 10th Annals offshore Tech. Conf. Texas: pp.375-380.

Bodine, Marc W, 1998: Clay mineralogy of insoluble residues in marine evaporite. Publ by Society of mining engineers of Aim, New York USA: pp. 133-156.

Bowman, T.S., 1931, Report on boring for oil in Egypt, section III: E.D and adjoining island: Report to ministry of finance, mines and quarries department, 353A9.

Braitsch, O., 1971, Salt deposits, their origins and composition New York, Springer .297.

Brantley, S.L., Crerar, D,A., Moller, N.E., and Weare, J.H., 1984: Geochemistry of a modern marine evaporite: Becana de verrila, Peru, Jour. of Sed. Petrol., 54: pp. 447-462.

Brassel, S.C., Wardroper, A.M.K., Thmson, I.V, Maxwell, J.R. and Eglinton.G, 1981, Specific a cyclic isoprenoids as biological markers of methanogenic bacteria in marine sediments, -Nature 29, 693-696, London.

Brassell, S.C.; Gvoying, F. and Eglington, G., 1988, Biological markers in lacustrine Chinese oil shales, in. AJ. Fleet, K, kelts and M. R Talbot, eds., lacustrine petroleum source rocks. Geol. Soci. of London, special publication. 40: pp.299-308.

Brassell, S.C., Eglinton, G. and Howel, J., 1987, Paleoenvironmental assessment of Marine organic-rich sediments using Molecular organic geochemistry: In Brocks, J. and Fleet, A.J. (eds.), Marine petroleum source Rocks, Geol. Soc. Spec. Publ., 26: pp 79-98.

Brewster, D., 1923, On the existence of two new fluids in the cavities of minerals, which are immiscible and possess remarkable physical prosperities. Edinburgh new philos, J., 9: pp.94-107.

Brochert, H., and Muir, R.O., 1964, Salt deposits –The origin, metamorphism and deformation of evaporites: London, D. van Nostrand Co., ltd. 338 pp

Burrus, J., and Audebert, F., 1990, Thermal and compaction processes in young rifted basin containing evaporite; Gulf of Lois, France: Bulletin, 74: pp.1420-1440.

Bush, PP., 1998, Some aspect of the diagenitic history of the sabkhas in Abu Dhabi, Persian. : pp. 396-405.

Busson, G., 1991, Relationship between different types of evaporitic deposits, and the occurrence of organic-rich layers (potential source-rocks). Carbonates and evaporites, 6: pp. 177-191.

Butler, G.P, 1969, Modern evaporite deposition and geochemistry coexisting brine, sabkha, Trucial Coast, Arabian Gulf. Jour. Sed. Petrol., 39:pp.70-89.

Canals A, Carpenter B, Guithaumou H. A. and Rasmsey Mh, 1993, Microanalysis of primary fluid inclusions in halite: constraints for an evaporitic sedimentation modeling. Application to the Mulhouse, France, Organic Geochemistry, 20/ 8: pp. 1139-1151.

Carpenter, A.B and Miller, J.C., 1969, Geochemistry of saline subsurface water, saline County (Missouri): Chem. Geol, 4: pp.135-167.

Castanier, S., Perthuisot, J.P., Rouchy, J.H., Mourin, A. and O.Guelorget, 1992, Halite and ooids in lake Asal, Djibouti; biocrystalline build- cups: Geobis, 25: pp. 811-821.

Ceccionini, G., Meyerhoff, A. A, Teitz H. H., 1988, Geology, Geomorphology and Petroleum possibilities of the Godo Area, Tquqe, Chile. Jour. Pet. Geol, 11: pp.245-276.

Chape, B., Michaelis, Albrecht, PP., 1980, Molecular fossils of as selective degradation products of kerogen, in A.G. Douglas and J.R. Maxwell, eds. Advances in organic Geach.,1979: Oxford, England, PEREAMON press: pp.268-5-274.

Chenet, PP Y., Letovzey, J., and Zagloul, E., 1984, Some observation on the rift tectonics eastern part of the Suez rift: Seventh General Petroleum corporation Exploration seminar, Cairo, 33PP

Chenet, PP Y., Zaghloul, E.S., 1982, Stratigraphic and structural study in ASL Nobwi inshore zone including surrounding areas. : Institute Francais du Petrole (Arch of APGC) 24P.

Chowdhary, L. and Taha, S., 1987, Geology and Habitat oil in Ras Budran field, Gulf of Suez, Egypt, Amer. Assoc. Petroleum Geologists Bull., 10: pp. 1274-1293, Tulsa.

Christian, S. and Gunther W., 1991, A proposed extension of Folk's (1959 and 1962) textural classification of carbonate rocks. Carbonates and Evaporites, 6: pp. 23-28.

Christiansen, G., Piasecki, S., Stemmerik, L. and Telnaes, N., 1993, Depositional environment and organic Geochemistry of the Upper Permian Ravne field Formation source rock in East Greenland. Amer. Assoc. Petroleum Geologists Bull., 77: pp .1519-1537.

Chvng, H.M., Rooney, M.A., Toon, B. and Claypool, G.E., 1992,Carbone isotope composition of Marine crude oil, Amer. Assoc. Petroleum Geologists Bull., 76:pp.1000- 1007.

Clarke, F.W, 1924, The data of Geochemistry. 5th ed. US. Geol. Survey Bull. , 707: pp.156-180.

Cody, R.D., 1991, Organo-crystalline intercalations in evaporite system; the effects of crystallization inhibition: Journal of sedimentary Petrology, 61: pp. 851-859.

Cody, R.D. and Cody, A.M., 1988, Gypsum nucleasion and crystal morphology in andog saline terrestrial environment: Jour. Sediment. Petrology, 58: pp. 247-255.

Connan, J., Bouroulle, J., Dessort, D., and Albveche, PP., 1986, The microbial in put in carbonate – anhydrite facies of a sabkha paleoenvironment from Guatemala-a molecular approach, in D.Leythaeuser and j. Rullkotter, Eds, Advances in organic Geoch., 1985,Oxford Pergamon pross, pp .29-50.

Connan, J., Bouroullec, J., Dessort, D. and Albrecht, 1986, The microbial input carbonate, anhydrite facies of a sabkha paleoenvironment from Guatemala: a Molecular approach, in D. leythaeuser and J, Rullkotter, eds., Advances in Organic Geochemistry 1985: Oxford, Pergamon: pp. 29-50.

Connan, J., 1981, Biological markers in crude oils, -in J.F. Mason (ed), petroleum geology in China, 48-70 Tulsa, Penn well books.

Damaste, J., Ten Haven, H. and De Leevw, J., 1998, Application of biological markers in the recognitions of paleo-hypersaline environment, in, lacustrine Petroleum source rocks (A.J. Fleet, et al., eds.) Ged. Soci. Spec. Publ., 40, Blackwell Science, Oxford: pp.304-329.

Damste, Joan .S. Sinning He, Betts Susannah, Ling Yue, Hoffmann, 1993, Hydrocarbon biomarkers of different lithofacies of salt TV formation of the Mol house basin, France. Organic Geochemistry, 20/8: pp.1187-1120.

David Newell, K., Robert C. Burruss and James G. Palacas, 1993, Thermal maturation and organic richness of potential petroleum source rocks in Proterozoic Rice Formation, North American Mid-Continent Rift system, Northeastern Kansas. Amer. Assoc. Petroleum Geologists Bull., 77: pp.1922-1941.

De Leeum, J. W., and Sinninghe Damste, J.S., 1990, Organic sulfur compounds and other biomarkers as indicators of paleosalinity, in W.I. Orr and C.M. white, eds., Geochemistry of sulfur in fossil Juels: Washington, D.C., American Chemical Society.: pp. 417-443.

Dikyk, B. M., Simoneit, B. R.T., Brassell, S.C. and Eglinton, 1978, Organic geochemical indicators of paleoenvironment conditions, Nature, 272: pp.216-222, London.

Dincer, T., 1968, The use of oxygen –18 and Deuterium concentrations in the water balance of lakes: Water Resources Research, 4: pp. 1289-1306.

Dow, W.G, 1977, Kerogen studies and geological interpretation: Jour. Geoch. Explor, 7: pp. 79-99.

Duncan, A.D., and Hammitton, R.L.M., 1988, Paleolimnology and organic Geochemistry of Middle Devonian in the Orcadian basin in: lacustrine pet. Source rock. Geol. Soc. Special publication, 40: pp. 173-301, Oxford.

Durand, B., Alpern, B., Pittion, J. L. and Pradier, B., 1986, Reflectance of vitrinite as a control of thermal history of sediments: in Burrus, J. (ed.), thermal Modeling in sedimentary Basins, Technip ed., Paris.

Dvrand D., 1980, Sedimentary organic matter and kerogen, definition and quantitative important of kerogen, in B., Durand, ed., kerogen: Paris, Eddtitions Technip: pp. 13-34.

Egyptian General Petroleum Corporation (EGPC), 1963, Oligocene and Miocene rock-stratigarphy of Gulf of Suez region: Report of Stratigraphic committee, 142pp.

Ekweozor, C.M., Okogum, J., I. Ekong, D.E.U. and Maxwell, J.R., 1979, Preliminary organic geochemical studies of samples from the Niger delta, Nigeria, I analysis of crude oils for triterpanes: Chemical Geol, 27: pp.11-28.

El-Tabakh. M., Grey, K., Pirajno, F. and Schreiber, B.C., 1999, Pesudomorphs after evaporitic minerals interbedded with 2.2 Ga Stromatolites of the Yerrida basin, Western Australia: Origin and significance. Geology, 27: pp.871-874.

El-Tabakh, M., Schreiber, B. C. and Warren, J. K., 1998, Origin of fibrous Gypsum in the Newark Rift Basin Eastern North America: Jour., of Sedimentary Research, 68: pp. 88-99.

El-Tabakh, M., Schreiber, B.C., Cherdsak Utha-Aroon Lee Coshell and Warren, J. K., 1998,Diagenetic of Basal Anhydrite in the Cretaceous Maha Sarakham salt: Khorat Plateau, NE Thailand. Sedimentology, 45: pp.579-594.

El-Tabakh, M., Riccioni, R., Schreiber, B.C., 1997, Evaluation of late Triassic rift basin evaporites (Passaic Formation): Newark Basin, Eastern America, Sedimentology, 44: pp.767-790.

El-Tarabili, E., 1964, General outline of the structures of the sedimentary formation in the general part of Eastern Desert, Quseir, Safaga-Wadi Qara's Southern part: Institute of desert Bull., 14: pp.22-43.

El-Zaraka and Mostafa, A.R. 1988, Oil prospects of the Gulf of Suez, Egypt, A case study- Org. Geochem, 12: pp.109-121, Oxford.

El-Zaraka, M.H, 1975, Geochemical relations of fluids in oil field of Gulf of Suez, Egypt, , Amer. Assoc. Petroleum Geologists Bull., 59: pp. 1667-1684.

El-Zarka, M. H and Wally, M .M, 1987, Physiographic features of Miocene Ras Malaab group, south baker oil field, Gulf of Suez, Egypt. Jour. Pet. Geol., 10: pp. 295-318.

El-Zarka, N.H. and Wally, M.M., 1982, Subsurface geological studies on Miocene Gharandal Group of Suez Baker oil field, Gulf of Suez Egypt (in press): 30pp.

Essam Abd El Gawad, A., 1995, Application of Infrared spectroscopy to the classification of Kerogen types and evaluation of Miocene source rocks in South-central and Southern parts of the Gulf of Suez region, Egypt, Al Azhar Bull. Sci, 6: pp.1937-1950.

Eugster, H.P and Jones, B.F., 1979, Behavior of major solutes during closed –basin brine evolution: Amer. Jour. of Sci, 279: pp .609-631.

Eugster, H.P, 1970, Chemistry and origin of brines of lake Magadi, Kenya: Contrib. Mineral Petrology Beitr. Mineral Petrologic, 22: pp. 1-31.

Eugster, H.P, Harvie, C.E. and Weare. J.H, 1980, Mineral equlibria in six-component sea water system, Na-K-Mg-Ca-SO4-Cl-H2O, at 25C, Geochimica et Cosmochimica Acta, 44: pp.1335-1347.

Eugster, H.P, 1986, Lake Magadi, Kenya: a model for rift valley hydrochemistry and sedimentation? In L.E. Frostick, R.W. Renaut, I. Reid, and J.J.Tiercelin, eds. , Sedimentation in the African rifts, Geology society special publication: pp.177-189.

Eugster, H.P, and Hardie, L.A., 1978, Salina lake in A. Lerman, ed., Lakes; chemistry, geology, physics, New York, NY, Springer, Verlag: pp .237-243.

Eugster, H.P, 1980, Geochemistry of evaporitic lacustrine deposits, Annual Review of the Earth and planetary science, 8: pp.35-63.

Evamy, B.D, 1973, The precipitation of aragonite and its alteration to calcite on Trucial coast of the Persian Gulf: in the Persian Gulf (B.H. Pruser, ed). Springer Verlag, Berlin, Heidelberg, New York: pp .329-342.

Evan, A. L., 1988, Neogene tectonic and Stratigraphic events in the Gulf of Suez rift area, Egypt: Tectonophysics, 153: pp.235-247.

Evans, R., and Kirkland, D.W., 1988, Evaporitic environments as a source for petroleum, in B.C.Schreiber, ed., evaporite and hydrocarbons: New York, Columbia University Press: pp. 256-299.

Evans, R, 1978, Origin and significance of evaporites in basins around Atlantic margin. Amer.Assoc. Petro. Geolo.Bull, 62: pp .223-234.

Feth, J. H. Robenson, C.E. and Polzer, W.L, 1964, Source of mineral constituents in water from granitic rocks Sierra Nevada, California and Nevada U.S – G. Survey water supply: pp. 1535-1538.

Forsman, J.PP and Hvnt, J.M., 1958, Insoluble organic matter (Kerogen) in sedimentary rocks. Geochim. et Cosmochim. Acta, 15: pp .170-182.

Frass, E., 1988, Aus dem orient. Geologische Beobachtungon Am euf der Sinai: Halbinsal, und in sutein Edner und sebert. Stuttaert. 22pp

Friedman. G. M., 1965, Terminology of crystallization textures and fabric in sedimentary rocks, Jour. Sedimen. Petrol, 35: pp643.

Friedman, G. M., 1982, Significance of red Sea in the evaporites and basinal limestone. Amer. Assoc. Petroleum Geologists Bull., 56: pp .1072-1086.

Friedman, G. M., 1980, Petrographic data and comments on the depositional environment of the Miocene sulphate and dolomites at sites 124,132 and 134 western Mediterranean Sea: pp. 695-707.

Ganz, H., 1987, Geochemical evaluation of hydrocarbon source rock characteristics and facies analysis –methods and application, Berliner Geowiss Abh, (A) 75: pp. 669-690, Berlin.

Ganz, H. and Robison, vol. D, 1985, Newly developed infrared method for characterizing kerogen type and thermal maturation.13th inter. Meeting on organic Geochemistry 16-20Sept, 1985 in Julich: pp 69(abstract).

Ganz, H., Kalkeruth, W., Nakhjiri Ganz, S., Oner.F, Pearson, M.J and Wehner, H., 1990, Infrared analysis –state of art-Berliner Geowiss: Abh. (A).

Ganz, H., 1987, Geochemical Evaluation of hydrocarbon source rock characteristics and facies analysis methods and application Berliner Geowiss. Abh., (A), 75/3:pp.669-690, Berlin.

Ganz, H., and Kalkreuth, 1987, Enhanced geochemical screening analysis- Accurate Determination of petroleum source rock characteristics and comparison with standard techniques in: petroleum geology of North west Europe (edited by Brooks, J. and Glennie, K.), Garahom and trotman Itel, 847-851, London.

Ganz, H., Kalkrevth, W. Oner, F., Pearson, M.T and Small, J.S., 1989, Enhanced geochemical screening analysis –accurate determination of petroleum source rock characteristics and comparison with standard techniques in: Petroleum Geology of North West Europe. (Edited by Brooks, J. and Glennie, K.) Garahtn and Trst, Ltd 847-851. London.

Ganz, H, 1987, petroleum geochemistry of oil and source rocks from the Ras Gharib and Abu Rudies area, Gulf of Suez. 13th international meeting on organic geochemistry, Sept.21-25, Veneziz: pp.251.

Ganz, H, Kalkreuth and Pearsonm, 1990,Infrared analysis state of Art, Berliner Geowiss. Abh. (A) 120-2, pp.1011-1026, Belin.

Ganz, H, S Robisow, and Vol. D., 1985, Newly developed infrared method for characterizing Kerogen type and thermal maturation 13th Intern. Meeting on Organic Geochemistry, 16-20sept 1985 in Julich: pp 69, (abstract).

Garfunkel, Z. and Barotov, 1977, The tectonics of the Suez rift, -Geol. Survol. Israel Bulletin: 71, pp.1-44.

Garfunkel, Z. and Bartov, 1977, The tectonic of Gulf rift: Geological survey of Israel Bulletin, 71: pp.1-44.

Garrels, R.M and Mackenize, F.T., 1999, Origin of chemical composition and some springs and lakes in equilibrium concept in natural water system, Washington, D.C, Am. Chem. Soc., Advances in chemistry, 67; pp. 222-242.

Geisler-Cussey, D., 1997, Modern depositional facies developed in evaporite environments (marine, mixed and nonmarine). In Sedimentary deposition in rift and foreland basins in France and Spain. "Paleogene and Neogene" (G. Busson and B.C. Schreiber Eds.). Columbia Univ. Press. pp. 3-42.

Gezeery, M.N., and Marzouk, I. M. (Eds), 1974, Miocene rock stratigarphy of Egypt: Jour. Of Geol, 18: pp.1-59.

Ghorab, M.A., 1964, Oligocene and Miocene rock stratigarphy of Suez region. : Egyptian General Petroleum Corporation, Cairo, and 142p.

Ghorab, M.A and Marzouk, 1967, A summary report on the rock Stratigraphic classification of the Miocene non-marine and coastal facies in the Gulf of Suez and Red Sea coast. : Unpublished report. G.P.C, Cairo, E. R.; 601,12pp

Girmalt, J.O., Wit, R De, Teiaidor, PP. and Abaiges, J., 1991, Lipid biogeochemistry of phormidium and micro coleus mats: Org. Geochem. 19:pp.509-540.

Grishina, S., Pironon-Jacques, Mazurou-Mikhail, Goryainov-Sergy, 1998, Organic inclusions in salt.Part3.Oil and gas inclusions in Cambrian evaporite deposits from East Siberia: A contribution to the understanding of nitrogen generation in evaporites. Organic Geochemistry, 28: pp.297-316.

Grotzinger, J.PP, and Kasting, J.F., 1993, New constraints on Precambrian ocean composition: Jour. Of Geology, 101: pp. 235-243.

Guiyangi A. S., 1986, Peculiarities of salt lake sediments as source in China. Organic Geochemistry, 10: pp. 119-126.

Hand, C.R., 1981, Coastal sabkhas and salt pan deposition of the Lower clear Fork formation (Permian), Texas: Journal of Sedimentology, 51: pp.761-778.

Handford, C.R., 1991, Marginal marine halite; sabkhas and Salinas, in J.L Melvin, ed., Evaporite, petroleum and minerals resources, Elsevier Developments in Sedimentology, 50: pp.1-66.

Hardie, L. A., 1984, Evaporites: Marine or non-marine? : American Journal of science, 284: pp.193-240.

Hardie, L. A., 1991, On the significance of evaporites: Annual review Earth and planetary science, 19: pp. 131-168.

Hardie, L. A., 1996, Secular variation in seawater: Chemistry an exploration for coupled secular variation in mineralogy's of marine limestone and patch evaporites over the past 600my. Geology, 24: pp. 279-283.

Hardie, L. A., 1991, On the significance of evaporites. Annul. Revol. Earth planet. Sci., 19: pp.131-168.

Hardie, L. A., Lowenstein, T .K. and Ronald J. S., 1983, The problem of distinguishing between primary and secondary features in evaporites. Sixth International Symposium on salt, 1.

Haride, L.A. and Eugster, H.P, 1971, The depositional environment of marine evaporite: a case for shallow, clastic accumulation., Sedimentology., 16: pp.187.

Haride, L.A, Smoot, T.PP. , Eugster, H.P, 1978, saline lakes and their deposits; a sedimentological approach I A. Matter and M.A.Tucker, eds., Modern and ancient lake sediments, international Association Sedimentology special publication 2: pp.7-41.

Haride, L.A and Eugster, H.P., 1970, The evolution of closed-basin mineral. Soc. America. Spec. , Paper 3: pp.273-290.

Haride, L.A., Eugster, H.P. and Weare, J. H., 1982, Mineral equlibria in the six component sea water system, Na –K-Mg-Ca-So4-Cl-H2O at 25C: Composition of saturated solutions: Geochimica at Cosmochimica act, 46: pp.1603-1618.

Haride, L.A., 1990, The role of rifting and Hydrothermal $CaCl_2$, brines in the origin of potash evaporites: a hypothesis: Amer. Jour. Of Sci., 290: pp. 43-106.

Harvie, C.E and Wear, J.H., 1980, The prediction of mineral solubilities in natural waters: The Na-K-Mg-Ca-$S0_4$-Cl-H_20 from zero to high concentration at 25C: Geochim-Cosmochim. Acta, 44: pp .1666-1676

Harvie, C.E., Weare, J.H., Hardie, L.A., and Eugster, H.P, 1980, Evaporation of seawater: Calculated mineral sequences. Science, 208: pp. 498-500.

Hassan, F. and El Dashlom, S., 1970, Miocene Evaporites of Gulf of Suez Region and Their Significance: Amer. Assoc. Petroleum Geologists Bull., 54 :pp. 1686-1696.

Hassan, F. and El –Bashlouty, S., 1970, The Miocene evaporites of the Gulf of Suez region and their significance, Amer. Assoc. Petroleum Geologists Bull., 54/9: pp.1686-1695.

Hassan, M.M., 1996, Sedimentary and chemical nature of recent sabkhas, central part of Red Sea coastal zone, Egypt. Sedimentology of Egypt, 4: pp .41-52.

Haven, H. L., Deleeum, J.W., Sinninghe Damste, J.S. and Zumberge, J.E, 1988, Application of biological markers in the recognition of paleo-hypersaline environments in j. fleet, k. kelts and M.R. Talbot eds., lacustrine petroleum source. Geolo. Soci, special publication, 40: pp.123-130.

Heybrock, F., 1949, The Miocene and Pliocene at the Gulf of Suez region: Unpublished report, G.R., 735pp

Heybrock, F., 1965, The Red Sea Miocene evaporite basin, salt basins around Africa, London pet. Institute: pp.17-40.

Hite, R.J., and Anders, D.E., 1991, Petroleum and evaporites in J.L. Melvin, ed., Evaporites, Petroleum and resources Amsterdam, Elsevier Developments in Sedimentology: pp. 477-533.

Hofmann, P., Huc Ay, Carpentier, B., Schaeffer, Albrecht, P., Keely, B., Moxwell, JR., Basmte, JS., De Leew, JW., Leythaeuser, 1993, Organic matter of Millhouse basin, France: A synthesis. Organic Geochemistry, 20/ 8: pp .1105-1123.

Hofmann, P., Leythaeuser, D., Carpentier, 1993, Palaeoclimatic controlled accumulation of organic matter in Oligocene evaporite sediments of the Mulhouse basin. Organic Geochemistry, 20/ 8: pp. 1125-1138.

Holliday, D .W., 1970, The petrology of Secondary gypsum rocks; a review: Journal of sedimentary petrology, 40: pp.734-744.

Hollister, L.S and Crawford, M. L, 1981, Short course in fluid inclusions: Application to petrology. Min.Ass.Con., 304 pp

Hosny, W., Gaafer, I., and Sabour, A., 1986, Miocene Stratigraphic nomenclature in the Gulf of Suez region. : 8th Pet. Explo. Seminar. EGPC, Cairo: 124pp

Hosny, W., Gaafer, I. and Sabour, A.A., 1986, Miocene Stratigraphic nomenclature in the Gulf of Suez region: Egypt 6th Exploration Conference.

Huc, A. and Durand, B., 1977, Occurrence and significance of humic acids in ancient sediments. Fuel, 59: pp. 308-325.

Huiton, A.C, Cook, A.C, Kanster, A. J. and Mckirdy, D.A, 1980, Organic matter of oil shales, SPEA. Jour., (20): pp .44-67,Sydny-Australia.

Hume, W.F., Madgwick, T.G., Moon, F.W and Sadek, H., 1920, Preliminary general report on occurrence of petroleum in western Sinai. Pet. Research Bull.2, Cairo: pp.1-15.

Hunt, J.H., 1996, petroleum Geochemistry and geology: 2nd., freeman and company, New York : pp743.

Hutechinson, G.F, 1957, A treatise on limnology: New York, John Wiley and sons, 978pp.

Hutton, A. C., Cook, A.C and Nckirdy, D.M, 1980, Organic Matter of oil shales. APEA Jour., 20(1): pp. 44-67, Sydney.

Hvang, W.Y and Meinschein, W.G, 1979, Sterols as ecological indicators: Geochim. Cosmochimica Acta, 43: pp739-745.

Isaken, G.H., 1991, Molecular indicators of lacustrine fresh water depositional environment: Org. Geoch., Advances and Applications in Energy and Natural environment, 15th FAOG, meeting, Manchester Univ., press: pp .361-364.

Jacobson, G., and J. Jankowski, 1989, Ground water discharge processes at a central Australian playa: Jour. Of hydrology, 105: pp.275-295.

Jacques, P., Maurice, P., Frederic, W. and Barres, 1995, organic inclusions in salt. Part2: Oil, gas and ammonium in inclusions from the Gabon Margin. Organic Geochemistry, 23: pp.739-750.

Jankowski, J., and Jacobson, 1990, Hydrological processes in ground water discharge playas, central Australia: Hydrological processes, 4: pp.59-70.

Jankowski, J. and Jacobson, G., 1980, Hydrochemical evolution of regional ground waters to playa brines in central Australia: Jour of hydrology, 108: pp.123-173.

Jauor, B., 1989, Hypersaline environments, microbiology and biochemistry: Berlin. Springer Vertag. 328 pp.

Jenyon Mk, 1988, Some deformation effects in a clastic overburden resulting from salt mobility. Jour. Pet. Geol, 11/ 3: pp.309-324.

Jones, B. B., 1965, The hydrology and mineralogy of deep springs Lake Injo county, California: U.S. Geol. Survey Prof. Paper 502-A, 56pp.

Jones, B. F., 1966, Geochemical evolution of closed basin water in Western Great basin M. Ram.J.I, editor, Northern Ohio. Geol. Soc., 2nd symposium on salt: Cleveland, Ohio, 1: pp.181-200.

Jones, B.F., Eugster, H.P, and Retting, S.T., 1977, Hydrochemistry of the lake Magadi basin, Kenya, Geoch. Et Cosmo. Acta, 44: pp.53-72.

Jowett, C. E., Lawrence, C. M., and Davis Bruce W, 1993, Predicting depth of gypsum dehydration in evaporitic sedimentary basins: Amer. Assoc. Petroleum Geologists Bull., 77/3 : pp. 402-403.

Jowett, E.C., Lawrence, M.C., Bruce W. Davis, 1993, Predicting depth of gypsum dehydration in evaporitic sedimentary basin: Amer. Assoc. Petroleum Geologists Bull., 77/3: pp. 402-413.

Katz, B.J., Bissada, K. K. and Wood, J. W., 1987, Factors limiting potential of evaporites as hydrocarbon source rocks (abs), Amer. Assoc. Petroleum Geologists Bull., 71: pp. 575.

Kaufman D.W and Slawson, C.B., 1950, Ripple marks on rock salt of the Salina formation. Jour. Geol., 58: pp.24-29.

Kendall, A.C, 1992, Evaporites in N.PP James, ed., facies models: Responses to sea level change, Geo. Assoc. Of Canada: pp. 375-409.

Khalaf, F. and Shennawy, H. M., 1979, Drilling of Gulf of Suez evaporites: SPE: pp. 7749.

Kholef, M.M. and Barakat, M.A., 1986, New evidence for petroleum source in a Miocene evaporite sequence, Gulf of Suez, Egypt. Jour. Of Pet. Geol., 9: pp.217-226.

Kholef, M.M. and Barakat, M. A., 1986, New evidence for a petroleum source rock in a Miocene evaporite sequence Gulf of Suez, Egypt. Journal of petroleum geology, 2: pp .217-226.

Kinsman, D.J.J, 1969, Mode of formation, sedimentary associations and diagenitic features of shallow water and supratidal evaporites, Bull. Amer. Assoc. Petrol. Geol, 1: pp.302.

Kinsman, D.J.J., 1966, Gypsum and anhydrite of recent age, Trucial coast, Persian Gulf. In Second Symposium on Salt Northern Ochio: Geol. Soci., Cleveland, 1: pp.302-326.

Kirkland D. W., and Evans, R., 1981, source rock potential of evaporitic environment. Amer. Assoc. Petroleum Geologists Bull., 65: pp.181-190.

Kirkland, D.W., and Evans, R., 1981, Source –rock potential of evaporitic environment, American Association of Petroleum Geologist Bulletin, 65: pp.181-190.

Knoret, 2001, Stratigraphy and hydrocarbon habit of Arabian platform, Amer. Assoc. Petroleum Geologists Bull., 74: pp 4582-522.

Kribek. B., 1991, Metallageny, Structural. Lithology and time controls of ore deposition in anoxic environments: Mineralism Deposita,.26: pp .477-533.

Krupp, R., Oberthur, T.T. and Hirdes, W., 1994, The early Precambrian atmosphere and hydrosphere: Thermodynamic constraints on Precambrian ocean composition: Jour. Of Geol., 89: pp.1581-1598.

Kul'chitskaya, A.A, 1973, Two-phase liquid inclusions in gypsum, In A. Kazlowski, ed., Abstracts of papers from Fourth regional conference on thermobarageochimestry of mineral forming processes, Rostov Univ., Press: pp.128-129.

Kul'chitskaya, A.A, 1974, Inclusions of mineral-forming solution in gypsum and their significance, In Y.K.Lazarenko, ed, Mineralogy of sedimentary deposits. Naak.Duinka, Kiev: pp.34-38.

Kul'chitskaya, A.A, 1985, The use of inclusions in gypsum for resolving some problems of sedimentary mineral-formation (Abstracts). In D.Brown,ed., Abstracts of seventh All union conference on thermobarametry and geochemistry of ore-forming fluids, USSR, 1: pp.191-192.

Kyle, J.R., and Posey, H. H., 1991, Halokinesis, cap rock development and salt dome mineral resources: Developments in Sedimentology, Amsterdam, Elsevier: pp.413-474.

Lagan, B.W., 1987, The Maclead Evaporite basin, western Australia: Tulsa Ok, American Association of Petroleum Geologist Memoir 44,140 pp.

Last, W.M., 1989: Continental brines and evaporites of the Northern Great Plains of Canada, Sed. Geol., 61: pp.170-177.

Lopatin, N. Vol., 1971, Temperature and geological time as factors in Coalification. Akad. Nauk. SSSR IZVOL. Ser Geol., 3: pp.45-105.

Lowenstein, T.K., 1988, Origin of depositional cycles in a Permian (saline gain): The Salado evaporites of New Mixco and Texas: geol. Sci of Amer, Bull., 100: pp.592-608.

Lowenstein, T. K., Spencer, R.J., 1990, Syndepositional origin of potach evaporites: Petrographic and fluid inclusion evidence, Am Jour. of Science, 290: pp.1-24.

Lowenstein, T. K and Hardie L. A., 1985, Criteria for the recognition of saltpan evaporite: Sedimentology, 32: pp. 627-644.

Lyberis, N., 1988, Tectonic evolution of the \Gulf of |Suez and the \Gulf of Aqaba: Tectonophysics, 153: pp.209-220.

Mackenzie, A. S., 1984, Application of biological markers in petroleum geochemistry. In books, J. and Welte, D. H. (ed.), Advances in petroleum geochemistry, academic press, London: pp. 115-214.

Maefaydyen, W.A., 1930, The Miocene Foraminifera from the clysmic area of Egypt and Sinai. : Geol. Sur. Of Egypt, Cairo, 149pp.

Mello, U.T., Anderson, R.N. and Karner, G.D., 1995, Role of salt in retaining the maturation of subsalt source rock; marine and petroleum Geology, 12: pp .101-102-104-107.

Michael S. Stecker and Uri S. Ten Brink, 1986, Lithospheric strength variations as a control on boundaries: examples from the northern Red sea region. Earth and planetary science letters: pp. 120-132.

Michaelis, B. and Alhrecht, PP, 1979, Molecular fossils of archaebacterial in kerogen: Naturwissenschoften, 66: pp. 420-422.

Mitchell, Djw., Allen, RB. , Salama, W., Abu Zakm, A., 1993, Tectonostratigraphic framework and hydrocarbon potential of the Red sea, J.P.P. Geol, 15: pp.187-210.

Moldowan, J.M., Seifert, W.F., and Gauogos, E. J., 1985, Relationship between petroleum composition and depositional and depositional environment of petroleum source rock Amer. Assoc. Petroleum Geologists Bull., 69: pp .1255-1268.

Moldowan, J.M., Dahl, J., Huizinga, B.J., Fogo, F.J, Hickly, F.J., Peakman, T.M., and Toylo, D.W., 1994, The molecular fossil record of Oleanane and its relation to angiosperms: Scre, 265: pp .768-771.

Moldowan, J.M., Dahl, J., Jacobson, S.R., Huizizga, BJ., Fogo, F.J., Shetty, R., Watt, D.S., and Peters K.E., 1996, Chemostratigraphic reconstruction of biofacies Molecular evidence linking cyst-forming dinoflagellates with pr-Jurassic ancestors, Geol., 24: pp. 159-162.

Monty C.L.V, Rouchy J.M and Marin A, 1987, Reef-stromatolites-evaporites facies relationships from Middle Miocene examples of Gulf of Suez and the Red Sea. Lecture Notes in Earth Science, 13: pp.134-188.

Moon, F.W. and Sadek, H., 1923, Preliminary geological reports on wadi Gharandal area north of Gebel Hammam Faraun western Sinai. : Pet. Res. Bull, Cairo, 12, 42pp.

Mostfa A.R. and Ganz H., 1990, Source rock evaluation of a well in Abu Rudies Area, Gulf of Suez. Berliner. Abh (A) 120/2: pp.1027-1040.

Murray, R.C., 1964, Origin and diagenesis of gypsum and anhydrite. Jour. Sed. Petro, 34: pp.512-523.

Nicol, W., 1828, Observations on the fluids contained in crystalline minerals. Echriburgh New philos. J., 9: pp. 94-96.

Obermajer.M, Fowler.G.M and Snowdon, 1998, Geochemical characterization and biomarker re-appraisal of oil families from southwestern Ontario, Canada. Bull. Of Canada Petroleum geology, 46/ 3: pp.350-378.

Ogninen. L., 1957, Secondary gypsum of sulphur series, scicily and the so-called integration. Jour. Of Sed.Petro, 27: pp. 64-79.

Orit, F. and Rosel, L., 2000, Evaporite system and digenetic patterns in the calatayud basin (Miocene, central Spain). Sedimentary, 47(suppl.1): pp .665-685.

Orti, F., 1997, Continental evaporitic sedimentation on the southeast border of the Ebro basin (Cata'la'nides). In Sedimentary deposition in rift and foreland basins in France and Spain

"Paleogene and Neogene" (G. Busson and B.C. Schreiber Eds.). Columbia Univ. Press. pp. 338-396.

Orti, F., Hevai, Rosell, C., and Gundogan, I., Helvaci, L. 1998, Sulphate- borate relations in evaporitic lacustrine environment: the sultancayir Gypsum (Miocene, Western Anatolia): Sedimentology, 45:pp. 697-710.

Orti, F. and Rosel, L., 1993, Sulfate plateform-Basin transition of lower WERRA anhydrite (Zechsten, Upper Permian) Western Poland, facies and petrography, Jour., Sed. Perolo. , 63: pp .646-658.

Ower, J., 1980, Elements geochemistry in petroleum exploration. Robertson Research international LTD. North Wales, U.K.

Passeri C., G., and Schreiber, B. C., 1985, Una proposta di classification delle evaporitti solfatiche. Geologica Rom., 24(1985): pp.219-232, Roma.

Peryt. T.M, 1989, Basal zasal zechstein in southwestern Poland: sedimentation, diagenesis and gas accumulation: Geological Associa. Of Canada paper, 36: pp. 601-625.

Peryt, T.M., Pierre and Gryniv, S.P, 1998, Origin of polyhalite deposits in the Zech stein (upper Permian) zdrada platform (northern Poland): Sedimentology, 45: pp.565-578.

Peters. K.E., Kontorovich, A. Eh. , Moldowa. J., Huziinga, B.J., Demaison, G.J. and Sasova, O.F., 1993, Geochemistry of selected oils and rocks from the central portion of the west Siberian, Russia. Amer. Assoc. Petroleum Geologists Bull., 77: pp . 863-887.

Peters, K.E., 1986, Guidelines for evaluation petroleum source rock using programmed pyrolysis. Amer. Assoc. Petroleum Geologists Bull., 70: pp .318-329.

Petrichenko, O.I., 1973, Methods of study of inclusions in minerals of saline deposits, In E. Roedder, ed., Translation in fluid inclusions Research proceeding of caffi, 12: pp.214-273, 1979.

Philip, R.PP, 1985, Biological markers in fossil –full production Mass spectrometry, Reviews, 4: pp1-54, Amsterdam.

Piere, C. and Rouchy J.M., 1986, Oxygen and sulfur isotopes in anhydrites from Givetain and Visean evaporites of northern France and Belgium. Thermal Geology,(Isotope Geoscience section), 58: pp. 245-252.

Pierre, C. and Rouchy, J.M., 1988, Carbonate replacement after sulphate evaporites in the Middle Miocene of Egypt. Jour. Of Sedimentary Petrology, 58/3: pp. 446-456.

Pierre, C., and Rouchy, J.M., 1988, Carbonate replacements after sulphate evaporites in Middle Miocene of Egypt: Jour. Of Sedimentary petrology, 58: pp. 446-456.

Pierre, C., Letouzey, J. and Zaghloul, S., 1984, Some observation on the rift tectonics in the Eastern part of the Suez Rift. Institute Francais du Petrole.

Ping'an, P., Jiamo, Fu, Guoying, S., and Eglinton, G., 1991, Biological markers in ancient Chinese sediments II-aliphatic and geoporphyrines in application of Paleoenvironmental assessments: Org. Geocchem., advances and Application of in Energy and Natural Environment, 15th EAOG Meeting, Manchester Univ. Press, pp. 375-378.

Pollastro.R.M., 1999, Ghaba salt basin province and Fahud salt basin province, Oman-Geological overview and total petroleum system: Us. Geological Survey open –file Report 99-50D.

Potter, R.W., Clynne, M.A., and Brown, D.L., 1978, Freezing point of concentrated aqueous sodium chloride solutions. Economic Geology, 73: pp. 284-285.

Powell, T.G. and Mckirdy, D. M., 1973, The effect of source material rock type and diagenesis on the n-alkane content of sediments: Geochim. Cosmochim. Acta, 37: pp. 623-633.

Powell, T. G. and Mckirdy, D. M., 1973, Relationship between ratio of pristane to phytane, crude oil composition and geological environment in Australia. Nature, 243: pp. 37-39.

Presley, M. W., 1987, Evolution of Permian evaporite basin in Texas Panhandle. The American Association of Petroleum Geologists (Bulletin), 71/2: pp. 167-190.

Radke, M, Vriend, S.PP and Schaefer, R.G., 2001, Triassic oils geochemical characterization of lower Toarcian source rocks from NW Germany: Interpretation of aromatic and saturated hydrocarbons in relation to depositional environment and maturation effects. Jour. Petrol. Geolo, 3: pp.287-307.

Read, J.F., Kerans, C., Weber, L.J., Sarg, J.F. and Wright, F.M., 1995, Milankovitch sea level changes, cycles and reservoirs on carbonate platforms in green house and ice-house worlds: SEPM/society for Sedimentology short course notes, 35: pp81.

Riding, R., 2000, Microbial carbonates: The geological record of calcified bacterial-algal mats and biofilms. Sedimentology, 47 (suppP1): pp. 17-214.

Robison, D., 1986,Organic geochemical characterization of late cretaceous- early transgressive sequence found in the Duwi and Dakhla formations, Egypt. Ph. D. Thesis, Univ. Oklahoma, 176 pp.122-133.

Robson, D.A., 1971, The structure of Gulf of Suez (Clysmic) rift with special reference to eastern side. : Jour. of Geol. Soci. Of London, 127: pp.245-276.

Roedder, E., 1958, Technique for the extraction and partial chemical analysis of fluid filled inclusions from minerals. Economic Geology, 53: pp.235-269.

Roedder, E., 1972, Composition of fluid inclusions. U.S. Geological Survey, professional paper, 164pp

Roedder, E., 1984, Fluid inclusions, Reviews in mineralogy. Mineralogical Socity of America: 12, 646pp.

Roedder, E., 1963, Studies of fluid inclusions, III: Extraction and quantitative analysis of inclusions in milligram range. Economic Geology, 26: pp.353-373.

Roeddere, E., Anglo, W.M.D., Fdorrzapf, A., and Aruscvage, Jr., 1987, Composition of fluid inclusions in Permian salt beds, Palo Duro basin, Texas, U.S.A. Chemical Geology, 61: pp. 97-90.

Roeder, E., 1984, Fluid in salt, American Mineralogist, 69: pp. 413-439.

Rohbrback, B.G., 1982, Organic geochemistry of cores and cuttings from the Gulf of Suez and western desert oil provinces, Egypt, Internal report No. 75, 24PP, Tulsa Oklahoma U.S.A.

Rohbrback, B.G., 1980, Crude oil geochemistry of Gulf of Suez: E.G.P.C. 6th the petrol. Explor. Seminar: 14 pp., Cairo, Egypt.

Rona. PPA., 1981, Evaporites at passive margins, in Dynamics of passive margins. Geidyn. Ser, 5: pp.116-132, Washington, DC, American Geophysical Union.

Rouchy, A. L. and Groessens, E., 1987, Lower Carboniferous (Visean) evaporites in northern France and Belgium: Depositional, diagenitic and deformational guides to reconstruct a disrupted evaporation basin. Lecture Notes I earth discipline, vol. 13T. M.peryt(ed): Evaporite basins. Springer Verlag Berlin Heidelberg 1987.

Rouchy, J.M., Catherine Pierre and Frederic, 1995, Deep-water resedimentation of anhydrite and gypsum deposits in Middle Miocene (Belayim Formation) of the Red Sea, Egypt. Sedimentology, 42: pp.267-282.

Rouchy, J.M., Noel, D., Wali, A.M.A., and Aref, 1995, Evaporite and biosiliceous cyclic sedimentation in the Miocene of the Gulf of Suez-depositional and Diagenitic aspect. Sedimentary Geology 94(1995): pp. 277-297.

Rouchy, J. M., 1987, Authigenic natroalunite in meddle Miocene evaporites from the Gulf of Suez (Gemsa, Egypt). Sedimentology, 34: pp. 807-812.

Rowan, L. C., Poole, F. G., Pawlewicz, M. J., 1995, The use of visible and Near-Infrared reflectance spectra for estimating organic matter thermal maturity. Amer. Assoc. Petroleum Geologists Bull., 79: pp .1464-1480.

Russell, J. D., 1987, Infrared methods: In Wilson, j. m. (ed) A handbook of Determinative method in clay mineralogy, champan and Hall, New York: pp 133-173.

Sadek, H., 1959, Miocene in the Gulf of Suez region, Egypt. Geol. Sur. Of Egypt, Cairo, 118pp

Said, R., 1961, Tectonic framework of Egypt and its influence on distribution of Foraminifera. Amer. Assoc. of Pet. Geol. Bull., 45: pp.198-218.

Said, R., 1962, The geology of Egypt: Amsterdam El-Sevier Publisher, 377pp.

Said, R., 1990, The geology of Egypt. : Blakema Rotterdam. Brookfield Publisher, 734pp

Said, R. and Basionni, M.A., 1958, Miocene Foraminifera of Gulf of Suez region. Amer. Assoc. Petroleum Geologists Bull., 42/ 8: pp.1958-1977.

Said, R., and El Heiny, I.A., 1967, Planktonic Foraminifera from Miocene rocks of the Gulf of Suez, Egypt. : Conf. Cushman found froman, Ras.,18: pp.14-26.

Samer Salih and Abdulghi Waleek, M., 1995, Lithostratigraohy and deposional environment of the Upper Jurassic Arab-c carbonate and associated evaporites in the Abquiq field Eastern Saudia Arab. Amer. Assoc. Petroleum Geologists Bull., 79/ 3: pp.394-409.

Sanbouavd-Rosset, C., 1976, Solid and liquid inclusions in gypsum: These de ETOT, Univ. Paris Sud., Center d,Orsay,168pp.

Sanchezmaral, S., S. Ordonez, M.A.G. Delcura, M. Hoyas and J.C. Canaveras, 1998, Penecontemporaneous diagenesis in continental saline sediments-Bioeditization in quero playa lake (La Mancha, central Spain): Chemical Geology, 149: pp.189-204.

Sanford and Wood, 1991, Brine evolution and mineral deposition in hydrologically open evaporite brines, Amer. Jour. Of Sci., 291: pp.687-710.

Sanford, W. E., and Wood, W.W., 1991, Brine evolution and mineral deposition in hydrologically open evaporite basin. American journal of science, 29: pp.687-710.

Sawlowicz. Z., 1992, Primary sulphide mineralization in Cu-Fe-S zones of kupferschiefer, fore-sudetic monocline, Poland: Transaction-Instion of mining and metallurgy, section B, 101: pp.81-88.

Schlumberger, 1984, Well evaluation conference, Egypt: Schlumberger Middle East, S.A.P: pp.9-18.

Schreiber B.C. and El Tabakh, 2000, Deposition and early alteration of evaporite. Sedimentology, 47(suppl.1): pp. 215-238.

Schreiber, B. C. and Nury, D., 1997, The Paleogene basins of southern province. In Sedimentary deposition in rift and foreland basins in France and Spain "Paleogene and Neogene" (G. Busson and B.C. Schreiber Eds.). Columbia Univ. Press. pp. 240-299.

Scott, R.W and Govean, F.M., 1985, Early depositional history of a rift basin: Miocene in Western Sinai. : Palea., Paleeo and palaeoecology, 52: pp.143-158.

Sellwood, B.W., and Netherwood, R.E., 1984, Facies evolution in the Gulf of Suez area: sedimentation history as an indicator of rift Initiation and development –Modern Geology, 9, 43-69, Amsterdam.

Sellwood, B.W and Netherwood, R.E., 1984, Facies evolution in the Gulf of Suez area. Sedimentation history as indicator of rift initiation and development: Modern Geolo., 9: pp. 43-69.

Shahin, A.N and Sharaf L.M., 1994, Assessment of petroleum potential in the Northern Gulf E.G.P.C., 12TH Petrol Explor: pp.152-174.

Shahin, A.N., 1988,Oil window in the Gulf of Suez Abc. Amer. Assoc. Petroleum Geologists Bull., 72/ 8: pp .1024-1025.

Shahin, A.N and Shehab, M.N, 1984, Petroleum generation, Migration and Occurrence in Gulf of Suez off shore of south Sinai, E.G.PC., 7th petrol. Explor. Seminar: pp.126-151, Cairo, Egypt.

Shanmugam, G., 1985, Significance of coniferous rain forest and related organic matter in generating commercial quantities of oil G. Gipsland basin, Australia. Amer. Assoc. Petroleum Geologists Bull., 69: pp. 1241-1254.

Shearman, D.J and Fuller, J.G., 1969, Anhydrite diagenesis, calcitization and organic laminitis, Winnipeg sis Formation, Middle Devonian, Saskatchewan: Bulletin. Pet., geol.,17: pp. 496-525.

Shearman, D.J, 1978, Evaporites of coastal sabkhas: in marine evaporites (W.E Dean and B.C. Schreiber, eds), Short courses no. 4, Soc. Econ. Paleant. Mineralogists: pp. 6-42.

Shearman, D. J., 1978, Evaporites of coastal sabkha, in W.E. Dean and B.C. Schreiber, eds., Marine Evaporites : SEPM short course , no. 4:pp. 6-42.

Shinn, E.A., 1969, Submarine lithification of Holocene carbonate sediments in Persian Gulf: Sedimentology, 12: pp.109-1.

Simoneit, B. R. T. and Stuermer, D. H., 1982, Organic geochemical indicators for sources of organic matter and paleoenvironmental conditions in Cretaceous Oceans. IN schlanger, S.O. and Cita, M.B. (eds.), Nature and origin of cretaceous carbon- rich facies, Academic press: pp. 145-163.

Simon-Robertson and Gwyneedd Wales, 1992, Sedimentary evaluation of the red sea and Gulf of Aden. Jour. Pet. Geol, 15: pp .157-172.

Sinnighe Damste, J. S., Deleeuw, J. W., Rock- Van Dlallen, A. C., Dezeeuw M. A. and Schenk, PP A., 1987b, The Occurrence and identification of series of organic sulfur compounds

in oils and extracts I: A study of Rozel point oil (U.S.A). Geoch. Et. Cosmoch. Acta, 51: pp. 2369-2391.

Sinnighe Damste, J. S., Ten Haven, H. L., De Leeum, J.W., and, Schenk, PPA., 1986, Organic geochemical studies of a Messinian evaporite basin, Northern Apennines (Italy) II, isoprenoids and n- alkyl thiophenes and thinpanes. Org., Geoch., 10: pp. 791-805.

Sinninghe Damste, J. S., Rock- Van Dullon, A. C., De Leeuw, J. W., 1987a, The identification of mono., di, trimethyl-2-(4,8,12 trimethltrid ecyl) chromans and their Occurrences in geogpshere. Geochema ET Cosmochimica Acta, 51: pp .2393-2400.

Sjogren, J.H., 1893, On large fluid inclusions in gypsum from Sicily: (Uppsala Institute Bulletin, 1/2: pp.277-291), In E.Roedder, 1984,fluid inclusions; Reviews in mineralogy: Mineralogical Socity of America, 12, 646pp.

Smith, F.G., 1953, Historical development of inclusions thermometry: Univol. Of Toronto press, Toronto, Canada: 1449pp.

Smmot, J.PP. and Lowenstein, T.K., 1991, Depositional environments non marine evaporites, in J.D. Melvin,ed., Evaporites , Petroleum and mineral resources, Elsevier science, Development in Sedimentology: pp.189-347.

Sorby, H.C., 1858, On microscopical structures of crystals indicating the origin of minerals and rocks. : Geological Socity of London Quat. Jour., 14: pp.453-500.

Southgate, PP. N., 1982, Cambrian skeletal halite crystals and experimental analogues: Sedimentology, 29: pp.391-407.

Spencer, R.J. and L.A. Hardie, 1990, Control of sea water composition by mixing of river waters and mid-ocean ridge hydrothermal brines to H.P Eugster, san Antoino, Geochem. Soc. Spec.Publ.2: pp.409-419.

Spencer, R.J., and Lowenstein, T.K., 1990, Evaporites: Geoscience Canada, Reprint series, 4: pp.141-163.

Spencer, R. J., Moller, N., and Warre, J. H., 1990, The prediction of minerals solubilities in natural waters: A chemical equilibrium model for Na-K-Ca-Mg-Cl2-SO4-H2O system at temperatures below 25C: Geochemica et Cosmochimica Acta, 54: pp.575-590.

Swennen, R., Viaene, W., Jacobs, L. and Connelissen, C., 1990, Petrography and Geochemistry of Belle Roche breccias (Lower Visean, Belgium): evidence for brecciation by evaporite dissolution: Sedimentology, 37: pp.859-878.

Tellam. J. H., 1995, Hydrochemistry of the saline groundwater of the lower Mersey basin Permo-Triassic sandstone aquifer. Jour. Of Hydrology, 165/ 1-4: pp .45-84.

The Stratigraphic Sub-Committee Of Geological Science, 1974, Miocene rock stratigarphy of Egypt: Egyptian Jour. Of Geolo., 18: pp.1-69.

Tissot, B. PP, Welte, D.H. and Durand, B., 1987, The role of geochemistry in exploration risk evaluation and decision-making. Proc. 12th world Pet. Cong.2: pp.99-122, London.

Tissot, B., and D.H. Welte, 1984, Petroleum formation and occurrence, 2nd ed: Berlin, Springer, Verlag, 538 pp.

Uliann Ma and Legarreta L, 1993, Hydrocarbon habitat in a Triassic-to Cretaceous sub-Andean setting: Neaquen basin, Argentina. Jour. of Petrol, Geol., 16: pp397-420.

Vewkatesan, M. I. and Kaplan, I. R., 1982, Distribution and transport of hydrocarbon in surface sediments of the Alaskan Outer continental shelf. Geochem. Cosmochim. Acta, 46: pp. 2135-2149.

Wait and Pooly, 197, Report on Nukul Formation: Unpublished Report, G.R., 952.

Wali, A.M.A., 1983, Origin and composition of recent sabkha, Ayun Musa, Sinai, Egypt. Geol. Soci., In press.

Wali, A.M.A., 1986, Some supratidal feature Ras Shukeir Coastal subkha, Red Sea, Egypt: EGPC, eight Explor. Conf., E.G.P.C., 1: pp.232-343.

Wali, A.M.A., 2004, Resoning morphologies of the evaporative precipitates and origin of domal habit: The sixth international conference on geochemistry. Alex. Univ.: in Press.

Wali, A. M.A., Abdel Wahab, A. and Taher, A. G., 1995, On some superatidal features, Ras Shukeir costal sabkha, Gulf of Suez, Egypt. (In press)

Wali, A.M.A, Morsy, M.A. and Afifi, 1998, Brine chemistry of recent continental saline lakes and their origin, Western Desert, Egypt, Envol. and Soc.J. (Chemistry administration,.1: pp.1-420.

Waples, D.W., and Machihara, T., 1992, Biomarker for geologist AAPG methods in exploration series: 9, 91 PP,

Waples, D.W., 1985, Geochemistry in petroleum exploration: Inter Human Resources Development CarPP, Boston, 232pp.

Waples, D.W., 1980, Time and temperature petroleum formation; application of lopatins method to petroleum exploration. Amer. Assoc. Petroleum Geologists Bull., 64: pp.916-926.

Waples, D, 1985, Geochemistry in petroleum exploration- International human Resources Development Corporation, Boston, 232 pp.

Warren, J. K, 1986, Source rock potential of shallow water evaporite setting: Journal Sedimentary Petrology, 56: pp.442-454.

Warren, J.K., 1991, Sulphate dominated sea-marginal and platform evaporite setting in J.L. Melvin, Ed. Evaporites, Petroleum and resources: Developments in Sedimentolgy 50th, Amsterdam, Elsevier: pp. 477-533.

Warren, J.K, 1990, Sedimentology and mineralogy of dolomitic Coorang lake, south Australia: Journal of Sedimentary petrology, 60: pp. 843-858.

Warren, J.K., 1988, Sedimentology of Coring dolomite in the salt Creek region, south Australia: Carbonate and evaporites, 3: pp.175-199.

Warren, J.K., and Kendall, C.G.S.C., 1985, Comparison of sequences formed in marine sabkhas (subaerial) and Salina (subaqeous setting, modern and ancient: American Association Petroleum Geologist Bulletin, 69: pp.103-123.

Warren, J.K., 1982, The hydrogical setting, occurrence and significance of gypsum in late Quaternary salt and lakes South Australia. Sed., 29: pp. 609-639.

Welte, D.H. and Waples, D.W., 1973, Uber die Bevorzugung geraetzahliger n- alkane in sedimentgesteinen –Nature wissenschaften, 60, 516-517, Heidelberg.

White, D.E., Hem, J.D and Warring, G.A., 1963, Chemical composition of subsurface waters. U.S. Geol. Sur: pp.4440-l, 67PP.

Young, M.J., Gawthrope, R.L. and Sharp, R., 2000, Sedimentology and sequence stratigarphy of transfer zone coarse-grained delta, Miocene Suez rift, Egypt. Sedimentology, 47(suppl.1): pp. 1081-1104.

APENDDICES

APPENDEX-1

1. LIST OF TABLES

TABLE NO.

APPENDEX-2

2. LIST OF FIGURES

FIGURE NO.

FIGURE NO.

FIGURE NO.

FIGURE NO.

FIGURE NO.

FIGURE NO.

Table -1: Executed analysis for chosen samples with respect to adopted techniques.

WELL	DEPTH	S NO.	TECHNICAL ANALYSIS							
			TOC	RE Pyrolysis	Gc	IR	T.S	SEM	F. I	XRD
GS-89-02	39.3	1	*TOC*	*RE*			*T.S*			
	43.1	2								
	43.4	3	*TOC*	*RE*						*XRD*
	48.6	4	*TOC*	*RE*			*T.S*			
	49	5	*TOC*	*RE*						
	73	6								
	75.7	7	*TOC*	*RE*			*T.S*			*XRD*
	101.6	8								
	106.3	9	*TOC*	*RE*						*XRD*
	89.6	10	*TOC*	*RE*			*T.S*			
	88.3	11	*TOC*	*RE*						
	131.1	12								
	133.4	12	*TOC*	*RE*			*T.S*	*SEM*		*XRD*
	149.4	13	*TOC*	*RE*						
	161.7	14					*T.S*	*SEM*		
	168.9	15								
	171.7	16								*XRD*
	179.5	17								
	182.3	18	*TOC*	*RE*						
	210.1	19	*TOC*	*RE*						
	219.8	20								
	221.6	21	*TOC*	*RE*			*T.S*			*XRD*
	210.8	22	*TOC*	*RE*						
	281.4	23								*XRD*
	283.4	24								
	356.3	25	*TOC*	*RE*			*T.S*	*SEM*		
	368.7	26								
	370.2	27	*TOC*	*RE*						*XRD*
	386.5	28					*T.S*	*SEM*		
GS-89-03	62.3	30								
	61.2	31								
	89.7	32	*TOC*	*RE*			*T.S*			
	102.5	33	*TOC*	*RE*			*T.S*			*XRD*
	131.3	33"								
	147.3	34								
	151.7	35								
	157.9	36	*TOC*	*RE*			*T.S*			*XRD*
	196.7	37								
	203.1	38	*TOC*	*RE*						
	218..80	39					*T.S*	*SEM*		
	219.8	40	*TOC*	*RE*						
	234.6	41	*TOC*	*RE*						*XRD*

TOC: Total organic carbon *IR: Infrared Analysis* *F.I: Fluid inclusions analysis*
RE: Rocky-Eval Pyrolysis *T.S: Thin Section* *XRD: X-ray diffractions*
Gc: Gas Chromatographs *SEM: Scanning electronic microscope*

(Cont.) Table -1: Executed analysis for chosen samples with respect to adopted techniques.

WELL	DEPTH	S NO.	TECHNICAL ANALYSIS							
			TOC	RE Pyrolysis	Gc	IR	T.S	SEM	F. I	XRD
GS-89-03	245.6	42								
	247	43								
	249.5	44								
	270	45	*TOC*				*T.S*			*XRD*
	272.5	46								
	275.4	47								
	277.2	48	*TOC*	*RE*			*T.S*	*SEM*		*XRD*
	295.1	50	*TOC*							
	333.5	51	*TOC*							
	335.3	52								
	338.7	53	*TOC*	*RE*			*T.S*			
	344.6	54								*XRD*
	405.45	55	*TOC*	*RE*						
	405.2	56	*TOC*	*RE*	Gc	*IR*	*T.S*	*SEM*		*XRD*
GS-89-04	95.6	57	*TOC*	*RE*			*T.S*	*SEM*		*XRD*
	107.6	58								
	117.9	59	*TOC*				*T.S*			
	121.3	60	*TOC*				*T.S*	*SEM*		
	132.8	61								
	135.7	62	*TOC*				*T.S*			*XRD*
	220	63								
	244.6	64	*TOC*				*T.S*	*SEM*		
	246.3	65	*TOC*	*RE*			*T.S*	*SEM*		*XRD*
	247.8	66								
	268.5	67	*TOC*	*RE*			*T.S*			
	259.3	68	*TOC*							
	284.2	69	*TOC*				*T.S*			*XRD*
	280.9	70		*RE*		*IR*				
	305.7	71	*TOC*	*RE*						
	316	72	*TOC*	*RE*		*IR*	*T.S*			
GS-89-05	81.5	77	*TOC*	*RE*			*T.S*	*SEM*		*XRD*
	83.9	78								
	108.6	79								
	109.8	80	*TOC*	*RE*			*T.S*	*SEM*		
	116.1	81								
	118.2	82	*TOC*	*RE*		*IR*				
	139.1	83								
	140.3	84	*TOC*				*T.S*			*XRD*
	154.7	85								

TOC: Total organic carbon *IR: Infrared Analysis* *F.I: Fluid inclusions analysis*
RE: Rocky-Eval Pyrolysis *T.S: Thin Section* *XRD: X-ray diffractions*
Gc: Gas Chromatographs *SEM: Scanning electronic microscope*

(Cont.) Table -1: Executed analysis for chosen samples with respect to adopted techniques.

WELL	DEPTH	S NO.	TECHNICAL ANALYSIS							
			TOC	RE Pyrolysis	Gc	IR	T.S	SEM	F. I	XRD
	155.3	86	*TOC*	*RE*			*T.S*			
	209.7	87								
	208	88	*TOC*	*RE*			*T.S*	*SEM*		
	208	88	*TOC*	*RE*			*T.S*	*SEM*		
	221.6	89								
	223.7	90								
	234.7	91	*TOC*	*RE*	Gc		*T.S*			*XRD*
	235.7	92								
	234.1	93								
	240.6	94								
	249.6	95	*TOC*	*RE*			*T.S*			*XRD*
	247	96								
	269.5	97	*TOC*	*RE*						
	272.2	98								
GS-89-06	46	99	*TOC*				*T.S*	*SEM*	*F.I*	
	48.1	100								
	79.2	101								*XRD*
	81.4	102								
	99.2	103	*TOC*	*RE*		*IR*	*T.S*			
	111.3	105	*TOC*	*RE*						*XRD*
	111.8	106								
	116.9	107					*T.S*			
	117.6	108	*TOC*	*RE*						
	158	109					*T.S*			
	160	110	*TOC*	*RE*						*XRD*
	201	111								
	203.2	112	*TOC*	*RE*			*T.S*	*SEM*		
	211	113								*XRD*
	211.8	114	*TOC*	*RE*	Gc		*T.S*			
	238.2	115								
	250.8	116	*TOC*	*RE*						

SOUTH ZEIT AREA

WELL	DEPTH	S NO.	TECHNICAL ANALYSIS							
			TOC	RE Pyrolysis	Gc	IR	T.S	SEM	F. I	XRD
GS-89-07	50.7	117					*T.S*	*SEM*	*F.I*	
	53	118								
	56.1	119	*TOC*							*XRD*
	58.2	120								

TOC: Total organic carbon *IR: Infrared Analysis* *F.I: Fluid inclusions analysis*
RE: Rocky-Eval Pyrolysis *T.S: Thin Section* *XRD: X-ray diffractions*
Gc: Gas Chromatographs *SEM: Scanning electronic microscope*

(Cont.) Table -1: Executed analysis for chosen samples with respect to adopted techniques.

WELL	DEPTH	S NO.	TECHNICAL ANALYSIS							
			TOC	RE Pyrolysis	Gc	IR	T.S	SEM	F. I	XRD
	73.8	121	*TOC*				*T.S*			
	75.8	122								
	84.5	125					*T.S*	*SEM*		
	87.2	126	*TOC*	*RE*						*XRD*
	98	127	*TOC*							
	95.9	128								
	101.5	129	*TOC*				*T.S*	*SEM*		
	103.8	130		*RE*		*IR*				
	131	132	*TOC*							
	158.6	133	*TOC*				*T.S*			*XRD*
	174.4	134	*TOC*							

RAS DIB AREA

WELL	DEPTH	S NO.	TECHNICAL ANALYSIS							
			TOC	RE Pyrolysis	Gc	IR	T.S	SEM	F. I	XRD
GS-89-08	76.4	136	*TOC*				*T.S*		*F.I*	*XRD*
	78.8	137								
	81.5	138	*TOC*				*T.S*			
	88.7	139					*T.S*			
	89.3	140	*TOC*	*RE*		*IR*				
	95.3	141								*XRD*
	96.1	142	*TOC*				*T.S*	*SEM*		
	100.7	143					*T.S*			
	102.8	144	*TOC*							*XRD*
	120.1	145	*TOC*	*RE*	Gc	*IR*				
	123	146	*TOC*				*T.S*	*SEM*		*XRD*
	154.8	147								
	162.7	148	*TOC*							
	177.6	149					*T.S*			
	220.2	152					*T.S*			
	219	153								
	225	154	*TOC*							
	227.1	155					*T.S*			*XRD*
	237.2	156	*TOC*							
	238.6	157	*TOC*	*RE*						*XRD*
	162.7	148	*TOC*							
	177.6	149					*T.S*			
	220.2	152					*T.S*			
	219	153								
	225	154	*TOC*							
	227.1	155					*T.S*			*XRD*

TOC: Total organic carbon *IR: Infrared Analysis* *F.I: Fluid inclusions analysis*
RE: Rocky-Eval Pyrolysis *T.S: Thin Section* *XRD: X-ray diffractions*
Gc: Gas Chromatographs *SEM: Scanning electronic microscope*

(Cont.) Table -1: Executed analysis for chosen samples with respect to adopted techniques.

WELL	DEPTH	S NO.	TECHNICAL ANALYSIS							
			TOC	RE Pyrolysis	Gc	IR	T.S	SEM	F. I	XRD
GS-89-08	237.2	156	*TOC*							
	238.6	157	*TOC*	*RE*						*XRD*
	162.7	148	*TOC*							
	177.6	149					*T.S*			
	220.2	152					*T.S*			
	219	153								
	225	154	*TOC*							
	227.1	155					*T.S*			*XRD*
	237.2	156	*TOC*							
	238.6	157	*TOC*	*RE*						*XRD*
GS-89-09	40.1	160	*TOC*	*RE*						
	41.2	161								*XRD*
	48.2	162					*T.S*			
	47.1	163	*TOC*							
	52.5	165								
	52.4	169	*TOC*		Gc	*IR*	*T.S*			
	60.7	166								
	59.1	167								*XRD*
	68.5	168	*TOC*	*RE*			*T.S*	*SEM*	*F.I*	
	67.9	169	*TOC*	*RE*			*T.S*		*F.I*	
	72.2	171		*RE*						*XRD*
	73.6	172	*TOC*				*T.S*	*SEM*		
	95.3	173								
	96.6	174	*TOC*	*RE*						
	103.4	175								*XRD*
	112	177	*TOC*				*T.S*		*F.I*	
	113.6	178								
	119.1	179	*TOC*							
	120.2	180	*TOC*							*XRD*
	127.7	181					*T.S*	*SEM*		
	129.1	182	*TOC*	*RE*		*IR*				
GS-89-10	40.5	183					*T.S*			*XRD*
	40.8	184	*TOC*	*RE*						
	114.6	185					*T.S*			
	116.6	186	*TOC*							*XRD*
GS-89-11	24.1	187	*TOC*	*RE*		*IR*	*T.S*	*SEM*		
	25.8	188								*XRD*
	32.8	191								
	56.6	192	*TOC*				*T.S*			
	60.2	193								

TOC: Total organic carbon *IR: Infrared Analysis* *F.I: Fluid inclusions analysis*
RE: Rocky-Eval Pyrolysis *T.S: Thin Section* *XRD: X-ray diffractions*
Gc: Gas Chromatographs *SEM: Scanning electronic microscope*

(Cont.) Table -1: Executed analysis for chosen samples with respect to adopted techniques.

WELL	DEPTH	S NO.	TECHNICAL ANALYSIS							
			TOC	RE Pyrolysis	Gc	IR	T.S	SEM	F. I	XRD
	68.3	194	*TOC*							*XRD*
	70.6	195	*TOC*	*RE*						
	71.2	196	*TOC*				*T.S*		*F.I*	
	82.2	197	*TOC*							
	99.6	198					*T.S*			
	97.6	199	*TOC*	*RE*		*IR*				*XRD*
	134	200	*TOC*				*T.S*			
	136.4	201	*TOC*				*T.S*			
GS-89-12	65.5	202								*XRD*
	68.2	203	*TOC*	*RE*						
	72.5	204					*T.S*		*F.I*	
	74.6	205	*TOC*	*RE*						*XRD*
	88.9	206	*TOC*							
	126.6	208	*TOC*							
	215.8	210	*TOC*							
GS-89-13	52.8	213	*TOC*	*RE*		*IR*	*T.S*		*F.I*	*XRD*
	53.2	213	*TOC*				*T.S*			
	102	214								
	100.8	215	*TOC*				*T.S*			*XRD*
GS-89-14	49	216	*TOC*				*T.S*			*XRD*
	48.5	217								
	67.8	218	*TOC*							
	69.1	219								
	76.8	220								
	84.8	24	*TOC*	*RE*	Gc					
	102	223	*TOC*							
	96.5	224					*T.S*			*XRD*
	131.1	225	*TOC*							
	153.2	226	*TOC*							
	151.1	227					*T.S*			*XRD*
	78/178.1	228	*TOC*	*RE*						
	177	229					*T.S*			
	188.1	230	*TOC*	*RE*						
	191	231					*T.S*			*XRD*

GUBAL ISLAND

WELL	DEPTH	S NO.	TECHNICAL ANALYSIS							
			TOC	RE Pyrolysis	Gc	IR	T.S	SEM	F. I	XRD
GS-89-17	6.3	232					*T.S*	*SEM*	*F.I*	*XRD*
	8.3	233	*TOC*							
	25.9	234	*TOC*							

TOC: Total organic carbon *IR: Infrared Analysis* *F.I: Fluid inclusions analysis*
RE: Rocky-Eval Pyrolysis *T.S: Thin Section* *XRD: X-ray diffractions*
Gc: Gas Chromatographs *SEM: Scanning electronic microscope*

(Cont.) Table -1: Executed analysis for chosen samples with respect to adopted techniques.

WELL	DEPTH	S NO.	TECHNICAL ANALYSIS							
			TOC	RE Pyrolysis	Gc	IR	T.S	SEM	F. I	XRD
	35	235	*TOC*	*RE*						
	54.6	236					*T.S*			*XRD*
	58	237	*TOC*	*RE*		*IR*				
	70	238	*TOC*				*T.S*			
	278.6	239								
	313.7	240	*TOC*	*RE*			*T.S*	*SEM*		*XRD*
GS-89-18	179.8	241	*TOC*				*T.S*			*XRD*
	205.5	242								
	207.3	242	*TOC*				*T.S*			
	249.7	245	*TOC*	*RE*	*Gc*					*XRD*
	263.7	246					*T.S*			
	274.7	247								
	282	248	*TOC*							
	310.7	249					*T.S*			
	336.9	250	*TOC*							*XRD*

SHAGAR AREA

WELL	DEPTH	S NO,	TECHNICAL ANALYSIS							
			TOC	RE Pyrolysis	Gc	IR	T.S	SEM	F. I	XRD
GS-90-15A	150.7	251	*TOC*	*RE*			*T.S*	*SEM*	*F.I*	*XRD*
	185.6	252	*TOC*							
	214.6	253					*T.S*			
	223.7	254	*TOC*				*T.S*			*XRD*
	255.4	256								
	256.2	257	*TOC*				*T.S*	*SEM*		*XRD*
GS-90-16	175.2	259	*TOC*	*RE*			*T.S*			*XRD*
	199.2	260	*TOC*							
	256.1	261	*TOC*				*T.S*	*SEM*		
	288.5	262	*TOC*				*T.S*			*XRD*

NORTH SINAI

WELL	DEPTH	S NO,	TECHNICAL ANALYSIS							
			TOC	RE Pyrolysis	Gc	IR	T.S	SEM	F. I	XRD
88-15	431.0	434.0	*TOC*				*T.S*			
88-26	447.5	450.4	*TOC*	*RE*			*T.S*		*F.I*	
88-34	496.0	498.7	*TOC*				*T.S*			
88-34	506.0	508.9	*TOC*				*T.S*		*F.I*	
88-38	379.5	387.5					*T.S*			
88-44	585.0		*TOC*				*T.S*			
89-42	571-574						*T.S*			

TOC: Total organic carbon *IR: Infrared Analysis* *F.I: Fluid inclusions analysis*
RE: Rocky-Eval Pyrolysis *T.S: Thin Section* *XRD: X-ray diffractions*
Gc: Gas Chromatographs *SEM: Scanning electronic microscope*

(Cont.) Table -1: Executed analysis for chosen samples with respect to adopted techniques.

WELL	DEPTH	S NO.	TECHNICAL ANALYSIS							
			TOC	RE Pyrolysis	Gc	IR	T.S	SEM	F. I	XRD
88-44	578.0		*TOC*	*RE*			*T.S*			
88-44	580.0	583.2	*TOC*							
88-44	585.0		*TOC*							
88-44	592.0		*TOC*							
88-44	592.0	595.0	*TOC*				*T.S*			

Esh El Malaha

WELL	DEPTH	S NO.	TECHNICAL ANALYSIS							
			TOC	RE Pyrolysis	Gc	IR	T.S	SEM	F. I	XRD
DH7	663.0	664.0	*TOC*	*RE*			*T.S*			
DH7	664.0	665.0	*TOC*				*T.S*			
DH3R	686.0	687.0	*TOC*				*T.S*		*F.I*	
DH3R	689.0	690.0	*TOC*	*RE*			*T.S*			
DH3R	705.0	706.0	*TOC*				*T.S*		*F.I*	
DH3R	724.0	725.7	*TOC*	*RE*			*T.S*			
DH3R	730.0		*TOC*							
DH3R	738.0	739.9	*TOC*	*RE*			*T.S*		*F.I*	
DH3R	739.0	741.0	*TOC*				*T.S*			
DH3R	741.0	742.0	*TOC*				*T.S*			

RAS SHUKEIR AREA

WELL	DEPTH	S NO.	TECHNICAL ANALYSIS							
			TOC	RE Pyrolysis	Gc	IR	T.S	SEM	F. I	XRD
RS#3			*TOC*	*RE*						
RS#4										
RS#5			*TOC*	*RE*						
RS#6										

TOC: Total organic carbon *IR: Infrared Analysis* *F.I: Fluid inclusions analysis*
RE: Rocky-Eval Pyrolysis *T.S: Thin Section* *XRD: X-ray diffractions*
Gc: Gas Chromatographs *SEM: Scanning electronic microscope*

Table-2: ICP operating conditions.

Tourch	High flow
Axuillary gas flow	0.5 L/min
Rf power	1200 W
Flush pump rate	200 rpm
Analysis pump rate	100 rpm
Nebulizer pressure	30 psi
No. of repeats	4
Wavelength	315.887 nm

Table-3: SEMI-QUANTITATIVE OF XRD DATA FOR ANALYZED EVAPORITE CORE SAMPLES FROM THE STUDIED AREAS

Area	SNO.	Sulphate Minerals										Carbonate Minerals						Others				Cly	Qu
		Gyp	Anh	Hal	Plyh	Sylv	Kes	Then	Bloe	Sulph	Wavl	Ca	Dol	Ank	Sed	Tro	Car	Py	Hem	Ilm	Mag		
RAS GESAAREA AREA	7	-	-	-	-	-	-	-	-	-	-	6.2	2.5	-	-	-	-	-	2.5	-	-	81	-
	9	-	93	3.4	-	1.3	-	-	-	-	-	-	-	-	2.2	-	-	-	12.5	-	-	-	-
	12	-	12.5	-	-	-	-	-	-	-	-	-	3.1	56.6	-	-	-	12.5	-	-	-	2.8	-
	16	8.8	91.2	-	-	-	-	-	-	-	-	-	-	-	-	-	-	-	-	-	-	-	-
	21	-	69.4	-	-	-	16.2	-	-	-	-	-	-	-	-	-	-	-	-	2.4	11.6	-	-
	23	-	78.6	8.5	-	1.6	-	4.3	-	-	-	-	2.1	-	-	-	1.1	8.2	-	-	-	-	-
	27	2.6	-	-	-	-	-	-	-	-	-	-	-	55.5	-	4.9	-	1.5	-	-	-	6.9	-
	32	-	25.3	-	2.6	-	-	6.2	-	-	-	-	-	-	-	2.1	-	-	-	-	-	-	-
	36	-	82.3	-	-	-	-	-	-	-	-	7.9	17.6	-	-	-	-	-	-	-	-	-	-
	41	-	77.3	11.5	-	-	-	-	-	-	-	-	11.3	-	-	-	-	-	-	-	-	-	-
	45	-	64.5	-	-	-	-	-	4	-	-	-	-	-	-	2.5	-	6.5	-	-	-	-	-
	48	-	-	76.5	10.5	-	5.1	-	-	-	-	-	7.9	-	-	-	-	-	-	-	-	-	-
	54	-	88	8	-	-	-	-	-	-	-	-	-	-	-	-	-	2.1	-	-	-	-	-
	56	-	-	89.7	-	-	-	-	-	-	-	4.4	-	-	-	-	-	7.9	-	-	-	-	-
	69	-	77.7	-	-	-	-	-	-	-	-	-	15.6	-	-	-	-	6.7	-	-	-	-	-
	77	-	81.9	-	-	-	-	-	-	11.7	-	-	-	-	-	-	-	6.4	-	-	-	-	-
	84	-	81.7	-	-	-	-	-	-	-	-	8.2	-	-	-	-	-	5.8	-	-	-	-	4.3
	91	6.0	61.3	-	-	-	-	-	-	-	8.9	-	-	-	-	-	-	4.3	-	-	7.5	12.5	-
	95	-	93.6	-	-	-	-	-	-	-	-	-	-	-	-	-	-	6.4	-	-	-	-	-
	101	-	92.9	1.6	-	1.9	-	-	-	-	-	-	-	-	-	-	-	3.6	-	-	-	-	-
	104	1.6	80.1	13.2	-	-	-	-	-	-	-	-	-	-	-	-	-	5.1	-	-	-	-	-
	105	-	88.4	-	3.7	-	-	-	-	-	-	-	-	-	-	-	-	7.9	-	-	-	-	-
	110	-	88.4	-	-	-	-	-	-	-	-	-	11.6	-	-	-	-	-	-	-	-	-	-
	113	-	47.4	-	-	-	-	-	-	2.9	-	-	45.2	-	-	-	-	4.5	-	-	-	-	-

Gyp: Gypsum Anh: Anhydrite Ha: Halite Polh: Polyhalite Sylv: Sylvite Kes: Keserite Then: Thenardite
Bloe: Bloelite Sulph: Sulpher Wavl: Wavellite Ca: Calcite Dol: dolomite Ank: Ankerite Sed: Sederite
Tro: Trona Car: Carnalite Py: Pyrite Hem: Hematite Ilm: Illmenite Mag: Magnesite Cly: Clay Qu: Quartz

(Cont.) Table-3: SEMI-QUANTITATIVE OF XRD DATA FOR ANALYZED EVAPORITE CORE SAMPLES FROM THE STUDIED AREAS

Area	SNO.	Sulphate Minerals										Carbonate Minerals						Others				Cly	Qu
		Gyp	Anh	Hal	Polh	Sylv	Kes	Then	Bloe	Sulph	Wavl	Ca	Dol	Ank	Sed	Tro	Car	Py	Hem	Ilm	Mag		
SOUTH EAST ZEIT	119	50.5	1.4	1.4	-	17.7	-	-	-	-	1.2	-	-	-	-	1.2	-	2.5	-	-	-	-	16.2
	126	21.2	-	-	3.4	-	-	-	-	-	-	-	8.2	-	-	-	-	-	4.6	-	-	62.6	-
	133	-	61.7	-	-	-	-	-	-	-	-	7.4	-	-	-	-	-	5.1	3.5	-	-	22.3	-
RAS DIB AREA	141	12.5	11.2	-	-	-	-	-	-	-	-	36.8	12.5	-	-	-	-	3.9	-	-	-	-	11.8
	146	-	53.4	-	-	-	-	-	-	-	-	7.4	3.3	-	-	-	5.5	3.2	-	-	-	22.3	4.0
	157	-	5.7	61.6	-	-	-	-	-	-	-	13.6	-	-	-	-	-	6.0	-	-	-	-	13.1
	162	-	78.8	-	-	-	-	-	-	-	-	2.9	12.0	-	-	-	-	3.9	-	-	-	-	2.4
	167	-	75.1	-	-	-	-	-	-	-	-	2.5	-	-	-	11.8	-	1.8	-	-	-	8.8	-
	172	-	-	-	-	-	-	-	-	-	-	70.6	-	-	-	-	-	8.2	4.2	-	-	13.4	-
	177	-	78.6	-	-	-	-	-	-	-	-	-		-	-	-	-	-	-	-	-	-	-
	181	11.5	18.3	-	-	-	-	-	-	-	-	19.5	50.7	-	-	-	-	-	-	-	-	-	-
	183	-	6.8	-	-	-	-	-	-	-	-	1.8	-	-	-	-	-	-	-	-	-	-	-
	186	-	92.5	-	-	2.8	-	-	-	-	-	-	-	-	-	-	-	4.6	-	-	-	-	-
	188	12.4	4.9	-	1.5	-	-	-	-	-	-	15.5	-	-	-	-	-	2.4	-	-	-	-	-
	194	51.5	1.4	1.4	-	17.7	-	-	-	-	1.2	-	-	-	-	1.2	-	1.5	-	-	-	-	16.2
	199	8.8	91.2	-	-	-	-	-	-	-	-	-	-	-	-	-	-	-	-	-	-	-	-
	202	-	69.4	-	-	-	16.2	-	-	-	-	-	-	-	-	-	-	-	-	2.4	11.6	-	-
	205	-	78.6	8.5	-	1.6	-	4.3	-	-	-	-	2.1	-	-	-	1.1	8.2	-	-	-	-	-
	209	2.6	-	-	-	-	-	-	-	-	-	-	-	55.5	-	4.9	-	1.5	-	-	-	6.9	-
	213	-	25.3	-	2.6	-	-	6.2	-	-	-	-	-	-	-	2.1	-	-	-	-	-	-	-
	215	11.5	18.3	-	-	-	-	-	-	-	-	19.5	50.7	-	-	-	-	-	-	-	-	-	-
	216	-	25.3	-	2.6	-	-	6.2	-	-	-	-	-	-	-	2.1	-	-	-	-	-	-	-
	224	-	82.3	-	-	-	-	-	-	-	-	7.9	17.6	-	-	-	-	-	-	-	-	-	-
	227	-	77.3	11.5	-	-	-	-	-	-	-	-	11.3	-	-	-	-	-	-	-	-	-	-
	231	-	64.5	-	-	-	-	-	4	-	-	-	-	-	-	2.5	-	6.5	-	-	-	-	-

Gyp: Gypsum Anh: Anhydrite Ha: Halite Polh: Polyhalite Sylv: Sylvite Kes: Keserite Then: Thenardite
Bloe: Bloelite Sulph: Sulpher Wavl: Wavellite Ca: Calcite Dol: dolomite Ank: Ankerite Sed: Sederite
Tro: Trona Car: Carnalite Py: Pyrite Hem: Hematite Ilm: Illmenite Mag: Magnesite Cly: Clay Qu: Quartz

(Cont.) Table-3: SEMI-QUANTITATIVE OF XRD DATA FOR ANALYZED EVAPORITE CORE SAMPLES FROM THE STUDIED AREAS

Area	SNO.	Sulphate Minerals										Carbonate Minerals						Others				Cly	Qu
		Gyp	Anh	Hal	Polh	Sylv	Kes	Then	Bloe	Sulph	Wavl	Ca	Dol	Ank	Sed	Tro	Car	Py	Hem	Ilm	Mag		
SHAGAR AREA	251	-	61.7	-	-	-	-	-	-	-	-	7.4	-	-	-	-	-	5.1	3.5	-	-	22.3	-
	254	12.5	11.2	-	-	-	-	-	-	-	-	36.8	12.5	-	-	-	-	3.9	-	-	-	-	11.
	257	-	53.4	-	-	-	-	-	-	-	-	7.4	3.3	-	-	-	5.5	3.2	-	-	-	22.3	4.0
	259	-	5.7	61.6	-	-	-	-	-	-	-	13.6	-	-	-	-	-	6.0	-	-	-	-	13.
	262	-	78.8	-	-	-	-	-	-	-	-	2.9	12.0	-	-	-	-	3.9	-	-	-	-	2.4
GUBAL ISLAND	232	-	75.1	-	-	-	-	-	-	-	-	2.5	-	-	-	11.8	-	1.8	-	-	-	8.8	-
	236	-	-	-	-	-	-	-	-	-	-	70.6	-	-	-	-	-	8.2	4.2	-	-	13.4	-
	240	-	93.6	-	-	-	-	-	-	-	-	-	-	-	-	-	-	6.4	-	-	-	-	-
	241	-	92.9	1.6	-	1.9	-	-	-	-	-	-	-	-	-	-	-	3.6	-	-	-	-	-
	245	1.6	80.1	13.2	-	-	-	-	-	-	-	-	-	-	-	-	-	5.1	-	-	-	-	-
	250	-	88.4	-	3.7	-	-	-	-	-	-	-	-	-	-	-	-	7.9	-	-	-	-	-

Gyp: Gypsum Anh: Anhydrite Ha: Halite Polh: Polyhalite Sylv: Sylvite Kes: Keserite Then: Thenardite
Bloe: Bloelite Sulph: Sulpher Wavl: Wavellite Ca: Calcite Dol: dolomite Ank: Ankerite Sed: Sederite
Tro: Trona Car: Carnalite Py: Pyrite Hem: Hematite Ilm: Illmenite Mag: Magnesite Cly: Clay Qu: Quartz

Table -4: Melting temperatures of primary inclusions in Miocene Evaporite from different areas of study

SNO.	Area	Final melting temperature of ice (T°C) (TM)	Final melting temperature (T°C) (Te)	Salinity	Remarks
99	Ras Gemsa	-3.4 -3.5 -3.1 -3.5 -3.5 -3.0 -3.2 -3.4 -3.5 -3.1	-27.8 -35.0 -37.4 -31.1 -29.0 -27.3	3.4 to7.9	Data from a single crystal with primary fluid inclusions, single-phase (liquid), variable in size, trapping in growth zone
112		-3.1 -3.4 -3.1 -3.4 -3.5 -2.9 -3.7 -3.2 -3.0 -3.1 -2.9 -2.7 -2.6 -29 -3.1 -3.6 -3.1 -3.5 -2.8 -3.4 -3.3 -3.0 -3.4	-30.1 -34.1 -30.1 -34.1 -40.1 -39.8 -31.1 -35.7 -40.1 -39. -40.0 -39.9 -31.0 -35.6 -10.2 -39.8 -32.1 -35.7	1.4 to7.7 2.6 to 9.3	
116	Southeast Zeit	-3.1 -3.5 -3.4 -3.1 -3.1 -3.4 -3.1 -3.1 -2.9 -2.8 -3.1 -3.5 -3.1 -3.5 -3.1 -3.5 -3.4 -3.1 -3.2 -3.3 -3.2 -3.3 -3.0 -3.4 -3.1 -3.5 -3.4 -3.1 -2.9	-27.7 -25.1 -27.7 -25.1 -27.7 -25.1 -37.5 -31.2 -37.5 -31.2 -29.2 -27.4 -29.2 -27.4 -27.3 -29.1 -27.3 -29.2 -27.4 -29.2 -27.4	3.0 to8.9 3.4 to 7.8	Data collected from single crystal (gypsum) with primary single-phase (liquid) inclusions, variable in size, arrange in growth zone
139	Ras DIB	-3.3 -2.9 -3.1 -3.5 -3.6 -3.3 -3.1 -3.5 -3.6 -3.3 -2.9 -3.1 -3.5 -3.6	-28.8 -19.3 -29.3 -20.4 -21.3 -28.8 -19.3 -29.3 -20.4 -21.3	2.3 to 9.5	Data collected from single crystal (gypsum) with primary single-phase (liquid) inclusions, variable in size, arranged in parallel zone
168					Doesn't free, primary, single-phase (liquid) inclusions, air bubble increase in size with freezing between –145C° to –150C° indicate that its hydrocarbons.
169		-4.2 -4.0 -4.2 -4.0 -4.1 -4.2 -4.0 -4.3 -4.2 -4.2 -4.0	-32.2 -32.2 -35.1 -35.2 -32.3 -35.2 -32.1 -35.0	3.4 to 8.9	Data collected from single crystal (gypsum) with primary single-phase (liquid) inclusions which were very tiny and scattered allover crystals, variable in size, arrange in growth zone
196		-1.9 -1.8 -1.9 -1.8 -1.7 -1.9 -1.9 -1.8 -1.7 -1.9 -1.9 -1.8 -1.6 -1.5 -2.1 -2.2 -2.0 -2.3 -2.4 -2.1 -2.1 -2.0	-43.3 -44.9 -43.9 -43.7 -44.1 -43.3 -44.9 -43.9 -43.7 -44.1	2.3 to 7.7	Data collected from single crystal (gypsum) with primary single-phase (liquid) inclusions, variable in size, arrange in growth zone
251	Shagar	-16.6 -15.6 -16.6 -15.6 -14.7 -14.2 -14.7 -14.2 -14.7 -14.2 -14.7 -14.2 -14.6 -14.4 -14.5 -14.3 -14.5 -11.6 -11.4 -11.6 -11.4 -11.6 -11.4 -11.6 -11.4 -10.8 -9.3 -10.8 -9.3 -8.7 -8.5 -8.8 -8.6 -8.6 -8.7 -8.5 -8.4 -8.7	-29.5 -26.6 -29.5 -26.6 -25.7 -24.9 -26.6 -25.7 -24.9 -24.2 -23.6 -23.5 -23.5 -23.0 -23.4 -23.3 -23.2	1.9 to 16.2	Data collected from single crystal (gypsum) with primary single-phase (liquid) inclusions, variable in size, arrange in growth zone

(Cont.) Table -4: Melting temperatures of primary inclusions in Miocene Evaporite from different areas of study

SNO.	Area	Final melting temperature of ice (T°C) (TM)	Final melting temperature (T°C) (Te)	Salinity	Remarks
253	Shagar	-16.0 -15.3 -14.1 -11.7 -10.5 -9.1 -8.4	-30.1 -29.3 -25.6 -23.6 -23.4	3.4 to 10.7	Data collected from single crystal (gypsum) with primary single-phase (liquid) inclusions, variable in size, arrange in growth zone
232	Gubal Island	-2.8 -2.0 -2.2 -2.1 -3.3 -3.3 -3.7 -3.3 -3.7 -3.6 -3.5 -3.7 -2.8 -2.0 -2.2 -2.8 -2.0 -2.2 -3.7 -2.8 -2.0 -2.2 -2.8 -2.0 -2.2	-22.5 -22.8 -29.5 -29.1 -26.2 -26.4 -29.1 -26.2 -26.4 -29.1 -26.2 -26.4 -29.1 -26.2 -26.4	0.0 to 10.4	Data collected from single crystal (gypsum) with primary single-phase (liquid) inclusions, variable in size, arrange in growth zone
560	Esh El-Malaha	-2.3 -2.2 -2.5 -2.1 -2.7 -2.3 -2.2 -2.5 -2.1 -2.7 -2.3 -2.2 -2.5 -2.1 -2.7 -2.3 -2.2 -2.5 -2.1 -2.7	-31.5 -30.1 -31.6 -30.8 -31.2 -31.5 -30.1 -31.6 -31.5 -30.1 -31.6 -30.8 -31.2 -30.8	034 to 9.6	Data collected from a single crystal with primary single phase (liquid) inclusions which are arranged in zones parallel to each other and usually associated with solid inclusions trapping in direction to the growth of host crystal
560		-32.8 -33.0 -35.1 -35.6 -33.8	-50.5 -54.6 -60.5 -53.7 -51.6	3.4 to 11.6	Data collected from single crystal (Halite) associated with gypsum All fluid inclusions are single phase, arranged in growth zone and varying in size. At 50 5.0 C° to56.6C° and during melting inclusion become dark indicating formation a minerals
686		-32.8 -34.8 -34.3 -30.2	-48.3 -47.0 -46.4 -44.1 -45.5	3.5 to 9.3	Data collected from single crystal (Halite) associated with gypsum. All fluid inclusions are single phase, arranged in growth zone and varying in size. At 61.0C° and during melting inclusion become dark indicating formation a minerals

(Cont.) Table -4: Melting temperatures of primary inclusions in Miocene Evaporite from different areas of study

SNO.	Area	Final melting temperature of ice (T°C) (TM)	Final melting temperature (T°C) (Te)	Salinity	Remarks
741	Esh El-Malaha	-9.6 -6.4 -4.3 9.6 -6.4 -4.3 -3.7 -2.2 -1.5 -1.4 -1.3 -1.2 -3.7 -2.2 -1.5 -1.4 -1.3 -1.2	-32.6 -37.8 -32.4 -32.1 -32.0 -37.8 -44.3		Data collected from single crystal (gypsum) with primary single-phase (liquid) inclusions are in parallel zones. Brownish phase is formed at –82.6C°. Sometimes inclusions have two phase (liquid-solid) and three phase (liquid-solid-algal)
450	North Sinai	-23.5 -20.8 -25.0 -23.5 -20.8 -25.0 -24.0 -19.8 -19.1 -13.1 -14.4 -8.5 -6.6 -24.0 -19.8 -19.1 -13.1 -14.4 -8.5 -6.6	-43.1 -43.2 -42.9 -43.4 -43.5		Data collected from a single crystal with primary single phase (liquid) inclusions, which are arranged in zones of growth
738-39		-32.5 -31.5 -31.4 -31.0 -30.8 -30.3 -32.5 -31.5 -31.4 -31.0 -30.8 -30.3	-50.0 -45.3 -49.5 -54.7 -54.6		Data collected from a single crystal with primary, two phase (liquid-solid). Some filamentous algae and organic material observed in fluid inclusions. Darkness increase with warming freezing inclusions up to –65.5C° and transparency increase at –34.1C°

Table -5: Chemistry of different waters and stable phases calculated from the thermochemical-model of Spencer *et al* (1990)

Water Type	Temperature (T°C)	SPECIES CONCENTRATION (MOLALITY)						Phase in Equilibrium
		Na^+	K^+	Ca^{++}	Mg^{++}	Cl^-	$S04^{--}$	
Normal seawater	-1.9	0.485	0.0106	0.0094*	0.0551	0.5660	0.0292	Ice
Evaporite seawater (at gypsum saturation)	-7- -8	1.783	0.0390	0.0342	0.2026	2.0812	0.1071	Ice Mirabilite
Recycled seawater (seawater with dissolved gypsum)	-2- -3	0.485	0.0106	0.0315	0.0551	0.5660	0.0767	Ice

*0.00025 equivalent of Ca^{++} used in the precipitation of calcite.

Table –6: The Physical Properties And Hydrochemical Composition Of The Analyzed Collected Water Brine Samples At Different Depths From Hypersaline Pans And Solar Ponds Of Ras Shukeir Sabkha

Site	S.NO	Depth (m)	pH	Ec Mohs/ Cm	Rs Ohm-m	d Gm/ml	Sp.g	TDS	S	K^{+} ppm Meq %	Na^{+} ppm Meq %	Ca^{+2} ppm Meq %	Mg^{+2} ppm Meq %	Fe^{+2} ppm Meq %	Pb^{+2} ppm Meq %	Li^{+2} ppm Meq %	Sr^{+2} ppm Meq %	Cr^{+2} ppm Meq %	Cu^{+2} ppm Meq %	Zn^{+2} ppm Meq %	Cl ppm Meq %	$CO3^{-2}$ ppm Meq %	$HCO3^{-2}$ ppm Meq %	$SO4^{-2}$ ppm Meq %
Eastern hypersaline pan	1	0.0	6.5	0.0995	0.1005	1.0694	1.07518	124460	12000	4350 111.3 10.17	22794.2 995.4 53.27	4192 209.2 9.80	11440 17.2 26.74	0.01 0.0 0	0.02 0.0 0	0.08 0.0 0.00	13.4 0.3 0.03	0.002 0.0 0	0.003 0.0 0	0 0.0 0	75430.3 2127.8 88.6	Nil NIL NIL	163.8 2.7 0.2	9585.3 199.6 11.3
	2	0.25	6.0	0.092	0.1086	1.0505	1.05617	95190	90000	5360 137.1 5.48	61759.6 2696.9 63.11	3048 152.1 3.11	27667 12.5 28.27	0.01 0.0 0	0.02 0.0 0	0.10 0.0 0.00	25.7 0.6 0.03	0.002 0.0 0	0.003 0.0 0	0 0.0 0	198781.8 5607.4 97.1	Nil NIL NIL	119.7 2.0 0.1	5880.9 122.4 2.9
	3	0.50	6.0	0.084	0.1190	1.0392	1.4479	88050	88050	1579 40.4 5.24	20453.3 893.2 67.83	2362 117.9 7.83	5752 9.7 19.07	0.01 0.0 0	0.02 0.0 0	0.09 0.0 0.00	9.4 0.2 0.03	0.002 0.0 0	0.003 0.0 0	0 0.0 0	53363.6 1505.3 87.8	Nil NIL NIL	176.4 2.9 0.3	7250.7 151.0 11.9
	4	0.60	5.8	0.089	0.1020	1.0717	1.0775	122130	119000	1553 39.7 4.49	25151.7 1098.3 72.79	2325 116.0 6.73	5518 9.5 15.97	0.01 0.0 0	0.02 0.0 0	0.08 0.0 0.00	7.2 0.2 0.02	0.002 0.0 0	0.003 0.0 0	0 0.0 0	57690.9 1627.4 87.8	Nil NIL NIL	163.8 2.7 0.2	7817.1 162.8 11.9
Western hypersaline pan	5	0.0	5.5	0.098	0.1123	1.0457	1.0513	92060	87000	2005 51.3 6.31	19559.5 854.1 61.55	2931 146.3 9.22	7272 12.0 22.88	0.01 0.0 0	0.02 0.0 0	0.08 0.0 0.00	9.66 0.2 0.03	0.002 0.0 0	0.003 0.0 0	0 0.0 0	55793.9 1573.9 87.9	NIL NIL NIL	176.4 2.9 0.3	7533.9 156.9 11.9
	6	0.50	6.0	0.085	0.111	1.05817	1.0639	5269	1541	1030 26.3 48.05	605.6 26.4 28.25	204 10.2 9.52	1.9 0.2 0.09	12 0.6 0.56	6.2 0.1 0.29	0 0.0 0.00	0 0.0 0.00	23.8 1.4 1.11	120 6.9 5.60	140 4.3 6.53	933.9 26.3 29.88	305.4 10.18 9.77	621.1 10.18 19.87	1265.3 26.34 40.48
	7	0.75	6.5	0.099	0.1010	1.0639	1.0741	124450	120000	1815 46.4 6.01	19512.6 852.1 64.61	2381 118.8 7.88	6481 9.8 21.46	0.01 0.0 0	0.02 0.0 0	0.08 0.0 0.00	9.80 0.2 0.03	0.002 0.0 0	0.003 0.0 0	0 0.0 0	54145.5 1527.4 87.3	Nil NIL NIL	176.4 2.9 0.3	7682.1 159.9 12.4
	8	0.85	6.0	0.098	0.1015	1.07317	1.0789	122920	118000	2528 64.7 5.69	30592.6 1335.9 68.90	2796 139.5 6.30	8473 11.5 19.08	0.01 0.0 0	0.02 0.0 0	0.08 0.0 0.00	11.85 0.3 0.03	0.002 0.0 0	0.003 0.0 0	0 0.0 0	74497.0 2101.5 87.8	 NIL NIL	214.2 3.5 0.3	10163.2 211.6 12.0
	9	1.5	6.5	0.0995	0.1123	1.0732	1.0789	5291	1538	1028 26.3 47.39	604.5 26.4 27.86	204 10.2 9.40	1.4 0.1 0.06	12 0.6 0.55	15.6 0.2 0.72	0 0.0 0.00	0 0.0 0.00	23.8 1.4 1.10	200 11.5 9.22	80 2.4 3.69	932.1 26.3 29.86	305.4 10.2 9.78	621.1 10.2 19.90	1262.8 26.3 40.46
	10	2.25	6.5	0.092	0.111	1.0733	1.0794	5513	1548	1035 26.5 43.22	608.6 26.6 25.41	200 10.0 8.35	3.2 0.3 0.13	10 0.5 0.42	16 0.2 0.67	0 0.0 0.00	0 0.0 0.00	17.2 1.0 0.72	385 22.2 16.08	120 3.7 5.01	938.4 26.5 30.10	299.4 10.0 9.60	609.0 10.0 19.53	1271.4 26.5 40.77
	11	3.0	6.5	0.084	0.1010	1.07335	1.0798	5427	1556	1040 26.6 45.99	611.5 26.7 27.04	208 10.4 9.20	7.8 0.6 0.34	4 0.2 0.18	3.2 0.0 0.14	0 0.0 0.00	0 0.0 0.00	27 1.6 1.19	300 17.3 13.27	60 1.8 2.65	943.0 26.6 29.79	311.4 10.4 9.84	633.3 10.4 20.01	1277.5 26.6 40.36
	12	3.75	7.5	0.089	0.1015	1.07334	1.0871	5515	1576	1040 26.6 44.04	611.5 26.7 25.90	204 10.2 8.64	7.8 0.6 0.33	10 0.5 0.42	3.6 0.0 0.15	0 0.0 0.00	4 0.1 0.17	24.4 1.4 1.03	412 23.8 17.45	44 1.3 1.86	943.0 26.6 29.96	305.4 10.2 9.71	621.1 10.2 19.74	1277.5 26.6 40.59
	13	4.50	8.1	0.098	0.1123	1.0741	1.0878	5335	1571	1050 26.9 49.29	617.4 27.0 28.98	212 10.6 9.95	8 0.7 0.38	12 0.6 0.56	2.8 0.0 0.13	0 0.0 0.00	12 0.3 0.56	24 1.4 1.13	112 6.5 5.26	80 2.4 3.76	952.0 26.9 29.71	317.4 10.6 9.90	645.5 10.6 20.14	1289.8 26.9 40.25
	14	5.25	7.7	0.085	0.111	1.0742	1.0876	5297	1563	1045 26.7 49.68	614.5 26.8 29.21	212 10.6 10.08	7 0.6 0.33	12 0.6 0.57	1.8 0.0 0.09	0 0.0 0.00	8 0.2 0.38	13 0.8 0.62	100 5.8 4.75	90 2.8 4.28	947.5 26.7 29.66	317.4 10.6 9.94	645.5 10.6 20.21	1283.7 26.7 40.19

EC: Conductivity Rs: Resistivety d: density SP.G. : Specific gravity TDS: Total Dissolved Solid S: Salinity *Concentration in ppb

(Cont.) Table –6: The Physical Properties And Hydrochemical Composition Of The Analyzed Collected Water Brine Samples At Different Depths From Hypersaline Pans And Solar Ponds Of Ras Shukeir Sabkha

Site	S.No	Depth (m)	PH	Ec Mohs/ Cm	Rs0 Ohm-m	d Gm/ml	Sp.g	TDS	S	K^{+} ppm Meq %	Na^{+} ppm Meq %	Ca^{+2} ppm Meq %	Mg^{+2} ppm Meq %	Fe^{+2} ppm Meq %	Pb^{+2} ppm Meq %	Li^{+2} ppm Meq %	Sr^{+2} ppm Meq %	Cr^{+2} ppm Meq %	Cu^{+2} ppm Meq %	Zn^{+2} ppm Meq %	Cl ppm Meq %	$CO3^{-2}$ ppm Meq %	$HCO3^{-2}$ ppm Meq %	$SO4^{-2}$ ppm Meq %
Western hypersaline pan	15	6	8.6	0.099	0.1123	1.0741	1.0897	5379	1541	1030 26.3 46.07	605.6 26.4 27.09	208 10.4 9.30	8 0.7 0.36	12 0.6 0.54	1.2 0.0 0.05	0 0.0 0.00	8 0.2 0.36	11 0.6 0.49	252 14.5 11.27	100 3.1 4.47	933.9 26.3 29.71	311.4 10.4 9.91	633.3 10.4 20.14	1265.3 26.3 40.24
	16	6.50	6.7	0.0995	0.111	107432	1.08974	5566	1526	1020 26.1 41.43	599.8 26.2 24.36	204 10.2 8.29	8 0.7 0.32	10 0.5 0.41	3.2 0.0 0.13	0 0.0 0.00	8 0.2 0.32	8.8 0.5 0.36	480 27.7 19.50	120 3.7 4.87	924.8 26.1 29.79	305.4 10.2 9.84	621.1 10.2 20.01	1253.0 26.1 40.36
	17	7	7.8	0.092	0.1010	1.07417	1.09541	5585	1571	1050 26.9 43.44	617.4 27.0 25.54	204 10.2 8.44	5 0.4 0.21	30 1.6 1.24	4.2 0.0 0.17	0 0.0 0.00	8 0.2 0.33	8.4 0.5 0.35	400 23.1 16.55	90 2.8 3.72	952.0 26.9 30.05	305.4 10.2 9.64	621.1 10.2 19.60	1289.8 26.9 40.71
	18	7.5	7.9	0.092	0.1123	1.07432	1.09641	5346	1586	1060 27.1 48.75	623.3 27.2 28.67	200 10.0 9.20	3.2 0.3 0.15	40 2.1 1.84	7.8 0.1 0.36	0 0.0 0.00	0 0.0 0.00	20 1.2 0.92	160 9.2 7.36	60 1.8 2.76	961.1 27.1 30.30	299.4 10.0 9.44	609.0 10.0 19.20	1302.1 27.1 41.06
Smaller Saline pounds	19	0	6.5	0.088	0.1136	1.0493	1.0549	88610	81000	1785 45.7 5.93	19707.1 860.6 65.46	2312 115.4 7.68	6293 9.5 20.90	0.15 0 0	0.02 0 0	0.083 0.012 0.00	8.53 0.19 0.03	0.002 0	0.003 0	0 0	53703.0 1514.9 88.0	NIL NIL NIL	157.5 2.6 0.3	7156.4 149.0 11.7
Hypersaline pan	20	0	6.5	0.092	0.1086	1.0591	1.0648	95130	90000	2046 52.3 7.01	17748.8 775.1 60.85	2581 128.8 8.85	6783 10.6 23.25	0.15 0 0	0 0 0	0.083 0.012 0.00	9.74 0.22 0.03	0..002 0 0	0.003 0 0	0 0 0	57654.5 1626.4 87.9	NIL NIL NIL	210.6 3.5 0.3	7744.67 161.2 11.8
	21	0.15	6.0	0.084	0.119	1.0443	1.0499	84970	79000	1950 49.9 5.86	21498.9 938.8 64.57	2822 140.8 8.48	7014 11.6 21.07	0 0 0	0 0 0	0.083 0.012 0.00	10.06 0.23 0.03	0 0 0	0 0 0	0 0 0	51497.0 1452.7 86.9	NIL NIL NIL	144.9 2.4 0.2	7621.1 158.7 12.9
Hypersaline pan	22	0	6.0	0.091	0.1098	1.0594	1.0594	85010	77500	1842 47.1 5.74	20807.4 908.6 64.80	2668 133.1 8.31	6780 11.0 21.12	0 0 0	0 0 0	0.08212 0.012 0.00	10.52 0.24 0.03	0 0 0	0 0 0	0 0 0	51521.2 1453.3 86.8	NIL NIL NIL	144.9 2.4 0.2	7718.32 160.7 13.0
	23	0.15	6.5	0.088	0.1136	1.0542	1.05416	85950	78000	1945 49.7 6.84	16745.4 731.2 58.90	2808 140.1 9.88	6920 11.5 24.34	0 0 0	0 0 0	0.08258 0.012 0.00	9.92 0.23 0.03	0 0 0	0 0 0	0 0 0	52090.9 1469.4 87.4	NIL NIL NIL	163.8 2.7 0.3	7374 153.5 12.4

EC: Conductivity Rs: Resistivety d: density SP.G. : Specific gravity TDS: Total Dissolved Solid S: Salinity *Concentration in ppb

Table -7: Chemical composition of different cations(Na + K, Ca, Mg) and anions (Cl, SO4, HCO3 + CO3) fields of brine classification scheme proposed by Haride and Eugster,1970

Brine Type (cation)	No.of field	Brine type(anion)	No.of field
Na	1	Cl	1
Na-(Ca)	2	Cl-(SO4)	2
Na-(Ca)-Mg	3	Cl-(SO4)-(CO3)	3
Na-(Mg)	4	Cl-(CO3)	4
Na-Ca	5	Cl-SO4	5
Na-Ca-(Mg)	6	Cl-SO4-(CO3)	6
Na-Mg-(Ca)	7	Cl-CO3-(SO4)	7
Na-(Ca)-Mg	8	Cl-CO3	8
Na-Ca-Mg	9	Cl-SO4-CO3	9
Ca-(Na)	10	SO4-Cl	10
Ca-(Mg)-(Na)	11	SO4-(CO3)-(Cl)	11
Ca-Mg-(Na)	12	SO4-CO3-(Cl)	12
Mg-(Ca)-(Na)	13	CO3-(SO4)-(Cl)	13
Mg-(Na)	14	CO3-(Cl)	14
Ca	15	SO4	15
Ca-(Mg)	16	SO4-(CO3)	16
Ca-Mg	17	SO4-CO3	17
Mg-(Ca)	18	CO3-(SO4)	18
Mg	19	CO3	19

Table -8: :The brine samples from the study area and their corresponding field numbers and chemical composition.

Sn.O	Brine Type(cation)	No.of field	Brine type(anion)	No.of field
1	Na-(Ca)-Mg	3	Cl-(SO4)	2
2	Na-(Ca)-Mg	8	Cl-(SO4)	2
3	Na-(Mg)	4	Cl-(SO4)	2
4	Mg-Na-(Ca)	7	Cl-(SO4)	2
5	Mg-Na-(Ca)	7	Cl-(SO4)	2
6	Mg-Na-(Ca)	7	Cl-(SO4)	2
7	Mg-Na-(Ca)	7	Cl-(SO4)	2
8	Mg-Na-(Ca)	7	Cl-(SO4)	2
9	Mg-Na-(Ca)	7	Cl-(SO4)	2
10	Mg-Na-(Ca)	7	Cl-(SO4)	2
11	Mg-Na-(Ca)	7	Cl	1
12	Mg-Na-(Ca)	7	Cl-(SO4)	2
13	Mg-Na-(Ca)	7	Cl-(SO4)	2

Table-9 : The Major saline minerals of different brine types after Haride and Eugester,1970

Brine Type	*Saline minerals*	
Ca-Mg-Na-(k)-Cl	Antarcticite	CaCl2.6H2O
	Bischofite	MgCl2.6H2O
	Carnalite	KCl.MgCl2.6H2O
	Halite	NaCl
	Sylvite	KCl
	Tachyhydrite	CaCl2.2MgCl.12H2O
Na-(Ca)-SO4-Cl	Gypsum	CaSO4.2H2O
	Glauberite	CaSO4.NaSO4
	Halite	NaCL
	Mirabilite	NaSO4.10H2O
	Thenardite	NaSO4
Mg-Na-(Ca)-SO4-Cl	Bischofite	MgCl2.6H2O
	Bloedite	Na2SO4.MaSO4.4H2O
	Epsomite	MgSO4.7H2O
	Glauberite	CaSO4.NaSO4
	Gypsum	CaSO4.2H2O
	Halite	NaCl
	Hexahydrite	MgSO4.6H2O
	Kieserite	MgSO4.H2O
	Mirabilite	NaSO4.10H2O
	Thenardite	NaSO4
Na-CO3-Cl	Halite	NaCL
	Nahcolite	NaHCO3
	Natron	Na2CO3.10H2O
	Thermonatrite	Na2CO3.H2O
	trona	NaHCO.NaCO3.2H2O
Na-CO3SO4-Cl	Brukeite	Na2CO3.2Na2SO4
	Halite	NaCL
	Mirabilite	NaSO4.10H2O
	Nahcolite	NaHCO3
	Natron	Na2CO3.10H2O
	Thenardite	NaSO4

Table-10 : The TOC content and Rocky Eval pyrolysis results of analysed samples

Well Name	SAMPLE ID	ID depth(m)	TOC wt%	S1 mg/g	S2 mg/g	S3 mg/g	Tmax degC	S2/S3 QI	S2/TOC HI	S3/TOC OI	S1/(S1+S2) PI	K(S1+S PC
Ras Gemsa Area												
Gs-89-02	1	39.3	0.04	0.02	0.27	0.06	425	4.5	675	75	0.06	0.02
Gs-89-02	4	48.6	0.01	0	0	0	430	0	0	80		0.00
Gs-89-02	5	49	0.03	0.03	0.04	0.39	341	0.1	133	53	0.39	0.01
Gs-89-02	7	75.7	1.9	1.04	0	1	434	0	0	10	1	0.09
Gs-89-02	9	106.3	0.02	0	0	0	326	0	0	90		0.00
Gs-89-02	11	88.3	0.41	2.21	1.35	0.62	404	2.2	329	7	0.62	0.30
Gs-89-02	12	131.1	0.03	0.16	0.02	0.86	422	0.0	67	133	0.86	0.01
Gs-89-02	18	182.3	0.81	1.53	1.54	0.5	412	3.1	190	12	0.5	0.25
Gs-89-02	21	221.6	0.83	0.58	1.18	0.33	421	3.6	142	6	0.33	0.15
Gs-89-02	25	356.3	0.01	0.01	0	1	351	0	0	50	1	0.00
Gs-89-02	27	370.2	2.18	0.4	3.88	0.09	426	43.1	178	4	0.09	0.36
Gs-89-03	32	89.7	0.01	0	0	0.06	352	0	0	52	0	0.00
Gs-89-03	33	102.5	0.06	0.04	0.05	0	340		83	44	0.44	0.01
Gs-89-03	36	157.9	1.8	3.52	5.2	0.39	415	13.3	289	2	0.4	0.72
Gs-89-03	38	203.1	0.01	0	0	1	608	0	0	69	0	0.00
Gs-89-03	40	219.8	1.18	1.38	1.6	0	416		136	10	0.46	0.25
Gs-89-03	41	234.6	0.05	0.23	0.18	0.62	396	0.3	360	84	0.55	0.03
Gs-89-03	48	277	0.02	0	0	0.86	423	0	0	83	1	0.00
Gs-89-03	50	295.1	0.03									
Gs-89-03	51	333.5	0.21									
Gs-89-03	53	338.7	0.12									
Gs-89-03	55	405.45	0.27	0.02	0.02	0.12	274	0.2	7	44	0.50	0.00
Gs-89-03	56	405.2	1.35	0.78	7.82	0.48	430	16.3	579	36	0.09	0.71
												0.00
Gs-89-04	57	95.6	0.37	0.48	0.90	0.12	401	7.5	243	32	0.35	0.11
Gs-89-04	60	121.3	0.25									
Gs-89-04	62	135.7	0.22									
Gs-89-04	64	244.6	0.08									
Gs-89-04	65	246.3	0.44	0.01	0.00	0.12	223	0	0	27	1.00	0.00
Gs-89-04	67	268.5	0.29	0.01	0.00	0.02	265	0	0	7	1.00	0.00
Gs-89-04	70	284.2	2.18	0.13	0.56	0.09	342	6.2	26	4	0.19	0.06
Gs-89-04	71	316	0.32	0.02	0.00	0.02	216	0	0	6	1.00	0.00
Gs-89-04	72	316	5.95	0.07	0.57	0.14	455	4.1	10	2	0.11	0.05
Gs-89-05	34	56.5	0.28	0.17	0.77	0.20	413	3.9	275	71	0.18	0.08
Gs-89-05	77	81.5	0.36	0.93	0.93	0.12	380	7.8	258	33	0.50	0.15
Gs-89-05	80	109.8	0.25	0.75	0.98	0.04	392	24.5	392	16	0.43	0.14
Gs-89-05	82	118.2	0.78	0.05	0.00	0.04	262	0	0	5	1.00	0.00
Gs-89-05	86	155.3	0.39	0.09	0.32	0.06	263	5.3	82	15	0.22	0.03
Gs-89-05	88	208	0.61	1.21	1.64	0.00	415		269	0	0.42	0.24
Gs-89-05	91	234.7	2.63	1.56	11.66	0.31	413	37.6	443	12	0.12	1.10
Gs-89-05	95	249.6	0.28	0.06	0.00	0.07	338	0	0	25	1.00	0.00
Gs-89-05	97	269.5	0.59	0.01	0.04	0.22	268	0.2	7	37	0.20	0.00
Gs-89-06	99	46	0.04									0.00
Gs-89-06	103	99.2	0.80	0.03	0.03	0.01	424	3	4	1	0.50	0.00
Gs-89-06	105	111.3	0.32	0.22	0.14	0.08	341	1.8	44	25	0.61	0.03
Gs-89-06	108	117.6	0.32	0.11	0.03	0.07	244	0.4	9	22	0.79	0.01
Gs-89-06	110	160	0.42	0.02	0.00	0.01	215	0	0	2	1.00	0.00
Gs-89-06	112	203.2	0.10									0.00

Table-10 : The TOC content and Rocky Eval pyrolysis results of analysed samples

Well Name	SAMPLE ID	depth(m)	TOC wt%	S1 mg/g	S2 mg/g	S3 mg/g	Tmax degC	S2/S3 QI	S2/TOC HI	S3/TOC OI	S1/(S1+S2) PI	K(S1+S PC
Gs-89-06	114	211.8	0.56	5.78	10.34	0.14	424	73.9	1846	25	0.36	1.34
Gs-89-06	116	250.8	2.64	1.29	1.37	0.02	401	68.5	52	1	0.48	0.22
uth East Zeit Area												
Gs-89-07	119	56.1	0.17									
Gs-89-07	121	73.8	0.11									
Gs-89-07	126	87.2	2.19	0.01	0.00	0.07	284	0	0	3	1.00	0.0
Gs-89-07	127	98	0.11									0.0
Gs-89-07	130	101.5	3.01	0.43	0.69	0.11	371	6.3	23	4	0.38	0.1
Gs-89-07	132	131	0.10									
Gs-89-07	133	158.6	0.11									
Gs-89-07	134	174.4	0.08									
Ras Dib Area												
Gs-89-08	136	76.4	0.12									
Gs-89-08	138	81.5	0.07									
Gs-89-08	140	89.3	1.00	0.79	3.79	0.26	395	14.6	379	26	0.17	0.4
Gs-89-08	142	96.1	0.15									
Gs-89-08	144	102.8	0.06									
Gs-89-08	145	120.1	2.44	0.77	13.66	0.41	420	33.3	560	17	0.05	1.2
Gs-89-08	146	123	0.33	0.35	1.55	0.13	336	11.9	470	39	0.18	0.2
Gs-89-08	148	162.7	0.17									
Gs-89-08	150	179.5	0.09									
Gs-89-08	151	204.6	0.16									
Gs-89-08	154	225	0.09									
Gs-89-08	156	237.2	0.08									
Gs-89-08	157	238.6	0.55	0.24	1.54	0.43	350	3.6	280	78	0.13	0.1
Gs-89-09	160	40.1	0.29	0.21	1.09	0.06	304	18.2	376	21	0.16	0.1
Gs-89-09	163	47.1	0.11									
Gs-89-09	168	52.4	0.80	0.73	4.47	0.05	409	89.4	559	6	0.14	0.4
Gs-89-09	169	67.9	2.40	3.32	12.48	0.62	400	20.1	520	26	0.21	1.3
Gs-89-09	170	73.6	0.59	0.51	2.77	0.06	414	46.2	469	10	0.16	0.3
Gs-89-09	174	96.6	0.26	0.14	0.72	0.34	380	2.1	277	131	0.16	0.1
Gs-89-09	177	112	0.15									
Gs-89-09	179	119.1	0.05									
Gs-89-09	180	120.2	0.06									
Gs-89-09	182	129.1	0.95	0.04	0.08	.0.05	252	1.6	8	5	0.33	0.0
												0.0
Gs-89-10	184	40.8	0.69	0.06	0.06	0.00	427		9	3	0.50	0.0
Gs-89-10	186	116.6	0.17									
Gs-89-11	187	24.1	1.19	0.05	0.17	0.00	325		14	5	0.23	0.0
Gs-89-11	192	56.6	0.14									
Gs-89-11	194	68.3	0.11									
Gs-89-11	195	70.6	0.21	0.27	0.95	0.00	274		452	75	0.22	0.1
Gs-89-11	196	71.2	0.10									
Gs-89-11	197	82.2	0.08									
Gs-89-11	199	97.6	2.41	0.17	0.45	0.00	274		19	7	0.27	0.1
Gs-89-11	200	134	0.05									
Gs-89-11	201	136.4	0.07									
Gs-89-12	203	68.2	2.38	0.18	0.50	0.00	248		21	0	0.26	0.1

Table-10 : The TOC content and Rocky Eval pyrolysis results of analysed samples

Well Name	SAMPLE ID	ID depth(m)	TOC wt%	S1 mg/g	S2 mg/g	S3 mg/g	Tmax degC	S2/S3 QI	S2/TOC HI	S3/TOC OI	S1/(S1+S2) PI	K(S1+S PC
Gs-89-12	205	74.6	0.30	0.05	0.12	0.05	218	2.4	40	17	0.29	0.0
Gs-89-12	206	88.9	0.12									
Gs-89-12	208	126.6	0.23									
Gs-89-12	210	215.8	0.10									
Gs-89-13	213	52.8	1.62	0.20	0.10	0.17	274	0.6	6	10	0.67	0.02
Gs-89-13	213	53.2	0.11									
Gs-89-13	215	100.8	0.08									
Gs-89-14	216	49	0.12									
Gs-89-14	218	67.8	0.09									
Gs-89-14	24	84.8	1.76	0.34	7.18	1.05	421	6.8	408	60	0.05	0.62
Gs-89-14	223	102	0.08									
Gs-89-14	225	131.1	0.06									
Gs-89-14	226	153.2	0.11									
Gs-89-14	228	78/178.1	0.37	0.08	0.18	0.00	264		49	0	0.31	0.02
Gs-89-14	230	188.1	0.20	0.04	0.11	0.00	218		55	0	0.27	0.01
Shagar Area												
Gs-90-15A	251	150.7	0.39	0.09	0.13	0.00	213		33	5	0.41	0.02
Gs-90-15A	252	185.6	0.13									
Gs-90-15A	254	223.7	0.17									
Gs-90-15A	255	237.2	0.39	0.11	0.05	0.00	213		13	4	0.69	0.01
Gs-90-15A	257	256.2	0.23									
Gs-90-16	259	175.2	0.25	0.17	0.39	0.00	220		156	60	0.30	0.05
Gs-90-16	260	199.2	0.12									
Gs-90-16	261	256.1	0.07									
Gubal Island Area												
Gs-89-17	233	8.3	0.04									
Gs-89-17	234	25.9	0.09									
Gs-89-17	235	35	0.54	0.41	0.99	0.21	428	4.7	183	39	0.29	0.12
Gs-89-17	237	58	0.95	0.14	0.16	0.14	326	1.1	17	15	0.47	0.02
Gs-89-17	238	70	0.18									
Gs-89-17	240	313.7	0.64	0.13	0.15	0.05	219	3	23	8	0.46	0.02
Gs-89-18	241	179.8	0.19									
Gs-89-18	242	207.3	0.12									
Gs-89-18	244	220	0.02									
Gs-89-18	245	249.7	0.14	0.30	0.89	0.01	275	89	636	7	0.25	0.10
Gs-89-18	248	282	0.14									
Gs-89-18	250	336.9	0.06									
Ras El Esh Area												
DH7	663.0	664.0	0.31	0.42	0.60	0.70	292	0.9	194	226	0.41	0.08
DH7	664.0	665.0	0.26									
DH3R	686.0	687.0	0.12									
DH3R	689.0	690.0	0.21	0.01	0.00	0.35	219	0	75	167	1.00	0.00

Table-10 : The TOC content and Rocky Eval pyrolysis results of analysed samples

Well Name	SAMPLE ID	ID depth(m)	TOC wt%	S1 mg/g	S2 mg/g	S3 mg/g	Tmax degC	S2/S3 QI	S2/TOC HI	S3/TOC OI	S1/(S1+S2) PI	K(S1+S2 PC
DH3R	705.0	706.0	0.06									
DH3R	724.0	725.7	0.82	0.02	0.00	0.31	252	0	15	38	1.00	0.00
DH3R	730.0		0.24									
DH3R	738.0	739.9	0.39	0.02	0.00	0.22	219	0	23	56	1.00	0.00
DH3R	739.0	741.0	0.20									
DH3R	741.0	742.0	0.07									
N. Sinai Area												
88-15	429.0	431.0	0.13									
88-15	431.0	434.0	0.11									
88-26	447.5	450.4	0.13	0.08	0.18	0.06	429	3	138	46	0.31	0.02
88-34	496.0	498.7	0.13									
88-34	506.0	508.9	0.11									
88-44	578.0		0.26	0.09	0.18	0.52	322	0.3	69	200	0.33	0.02
88-44	580.0	583.2	0.08									
88-44	585.0		0.14									
88-44	592.0		0.06									
88-44	592.0	595.0	0.09									
Ras Shukeir Area												
C#1	:L1		2.25	7.63	11.60	0.67	432	17.3	516	30	0.40	1.60
	L2		0.34	0.60	0.94	1.63	439	1	276	170	0.39	0.13
C#3	L3		0.16									
	L4		0.34	0.31	0.45	0.53	348	0.8	132	156	0.41	0.06
C#4	L5		2.3	7.5	10.6	0.65	435	16.3	416	150	0.41	1.50
	L6		0.08									
C#5	L7		0.34	0.31	0.45	0.53	348	0.8	140	160	0.41	0.06
C#6	L8		2.35	7.66	12.30	0.67	439	18.4	514	30	0.39	1.66
	L9		0.81	1.53	3.54	0.50	412	7.1	190	12	0.40	0.42
Trench	L10		2.44	1.38	13.66	0.41	420	33.3	540	30	0.05	1.25
	L11		1.5	3.32	4.47	0.05	409	89.4	559	40	0.39	0.65

Table-11: Infrared spectroscopic data For Kerogen from subsurface evaporite samples of the study areas.

Area	Well No.	SNO.	Depth (m)	TOC%	IR-analysis for Kerogen					
					A	C	R_0%	HP	W	M
RAS GEMSA	Gs-89-03	56	405.2	1.35	0.56	0.47	0.39	7.69	1638	2923.6
	Gs-89-04	70	280.9	2.18	0.71	0.65	0.28	15.48	1634.9	2923.1
	Gs-89-04	72	316	5.95	0.93	0.86	0.3	55.3	1633.4	2924.2
	Gs-89-05	82	118.2	0.78	0.75	0.50	0.36	5.85	1641.3	2925.5
	Gs-89-05	91	234.7	2.63	0.62	0.51	0.38	16.3	1633.9	2923.1
	Gs-89-06	103	99.2	0.80	0.73	0.52	0.37	5.84	1641.3	2925.4
Ras Dib	Gs-89-08	140	89.3	1.0	0.65	0.53	0.36	6.43	1630.8	2922.6
	Gs-89-08	145	120.1	2.44	0.67	0.68	0.29	18.54	1633.6	2923.3
	Gs-89-09	169	67.9	2.4	0.88	0.82	0.45	21.12	1634	2923.3
	Gs-89-10	184	40.8	0.69	0.75	0.53	0.4	5.17	1628.6	2924.5
	Gs-89-11	187	24.1	1.19	0.75	0.52	0.4	5.17	1638.6	2924.5
	Gs-89-11	199	97.6	2.41	0.75	0.61	0.3	18.07	1639.7	2923.3
Gubal Island	Gs-89-17	237	58	0.95	0.77	0.59	0.27	7.22	1634.6	2923.3
	Gs-89-18	240	313.7	0.64	0.72	0.55	0.28	4.1	1630.2	2923.4
Shagar	Gs-90-15A	255	237.2	0.11	0.70	0.65	0.28	0.77	1633	2924.1
	Gs-90-16	259	175.2	0.65	0.52	0.29	0.29	1.12	1633	2922.5
Esh El - Malaha	DH7	-	663-4	0.31	0.75	0.53	0.27	2.4	1633.1	2922.3
	DH3R	-	725.7	0.82	0.74	0.61	0.27	6.1	1633.1	2924.1

TOC%: Total organic carbon%
A: A-Factor
C: C-Factor
M: maximum wave number (cm^{-1})

R_0%: Vitrinite Reflectance
HP: A-Factor x TOC% x 10
W: minimum wave number (cm^{-1})

Table-12 : Gas Chromatograph Data For The Analyzed Extracts Of Evaporite Core Samples From The Study Areas

Area	Well NO.	SNO.	Depth (m)	Bitumen Analysis		
				Pr/Ph	Pr/n-C17	Ph/n-C18
Ras Gemsa	Gs-89-03	56	405.2	0.89	0.63	0.77
	Gs-89-05	91	234.7	0.69	0.62	0.83
	Gs-89-06	114	211.8	0.45	0.28	0.41
Ras Dib	Gs-89-08	145	120.1	0.49	0.71	1.93
	Gs-89-09	168	52.4	0.50	0.71	1.17
	Gs-89-10	169	67.9	0.56	0.93	1.51
	Gs-89-14	24	84.8	0.56	0.61	1.5
Gubal Island	Gs-89-17	245	249.7	0.35	0.65	1.41
	Gs-89-18	258	175.2	0.38	0.71	1.5
Shagar	Gs-90-15A	255	237.2	0.5	0.71	1.17
Esh El-Malaha	Dh7	-	663-994	0.13	1.25	5.49

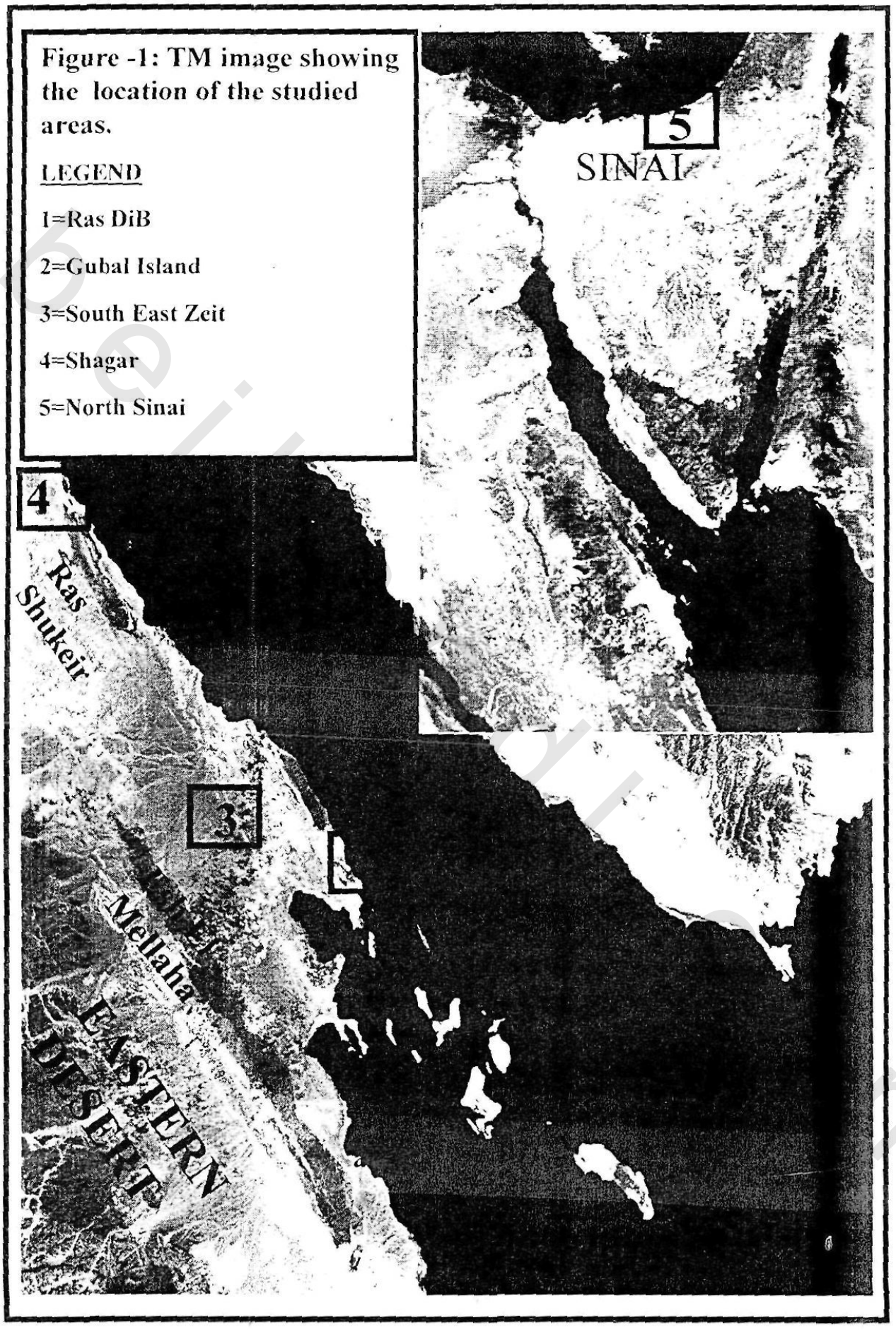
Figure -1: TM image showing the location of the studied areas.
LEGEND
1=Ras DiB
2=Gubal Island
3=South East Zeit
4=Shagar
5=North Sinai
5
SINAI
4
Ras Shukeir
3
Mellaha
EASTERN DESERT

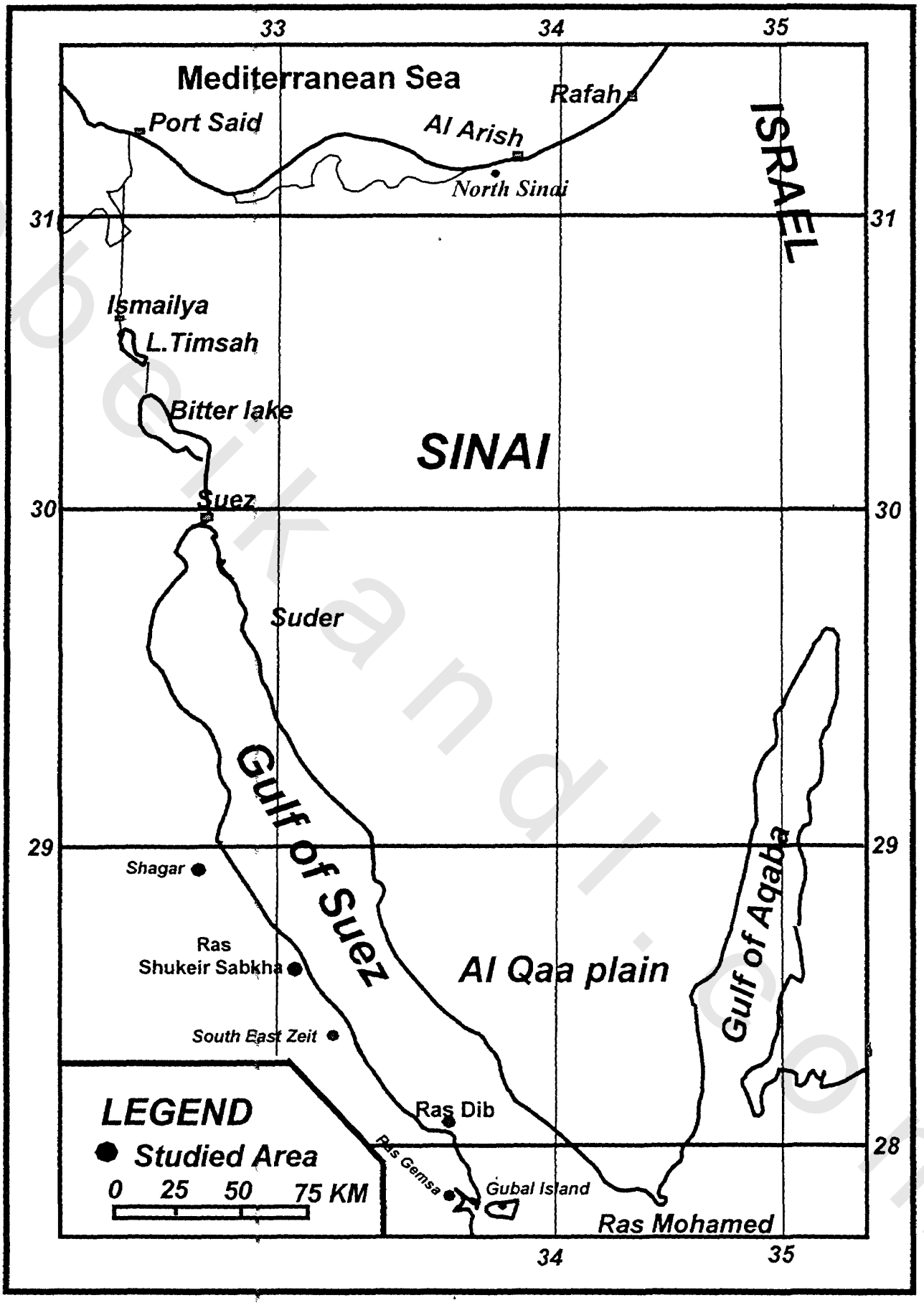

Figure -2 : The Location map of the studied areas according to their geographic location

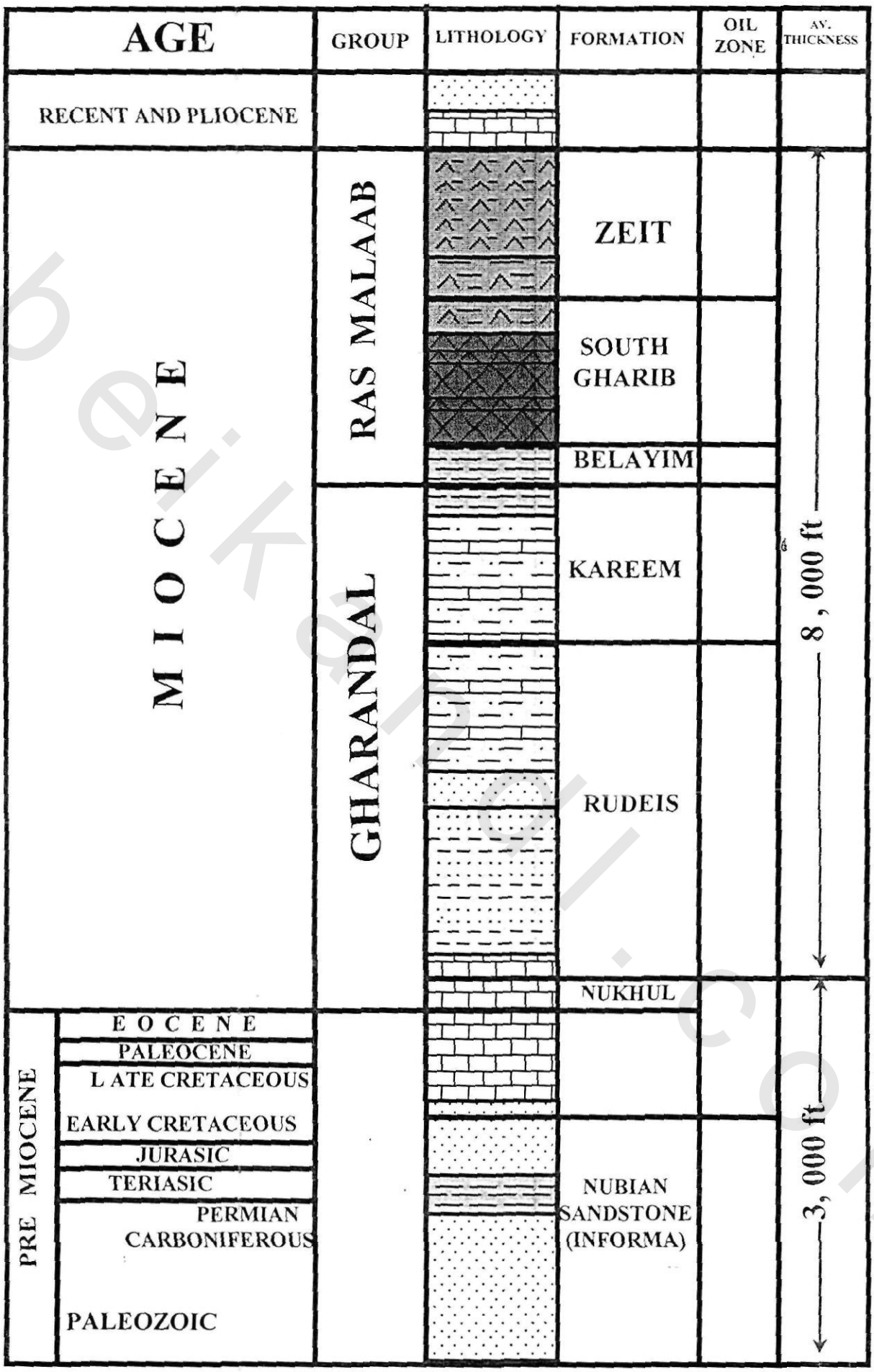

Figure-3 : Generalized stratigraphic section of sediments in the Gulf of Suez after abdine, 1979.

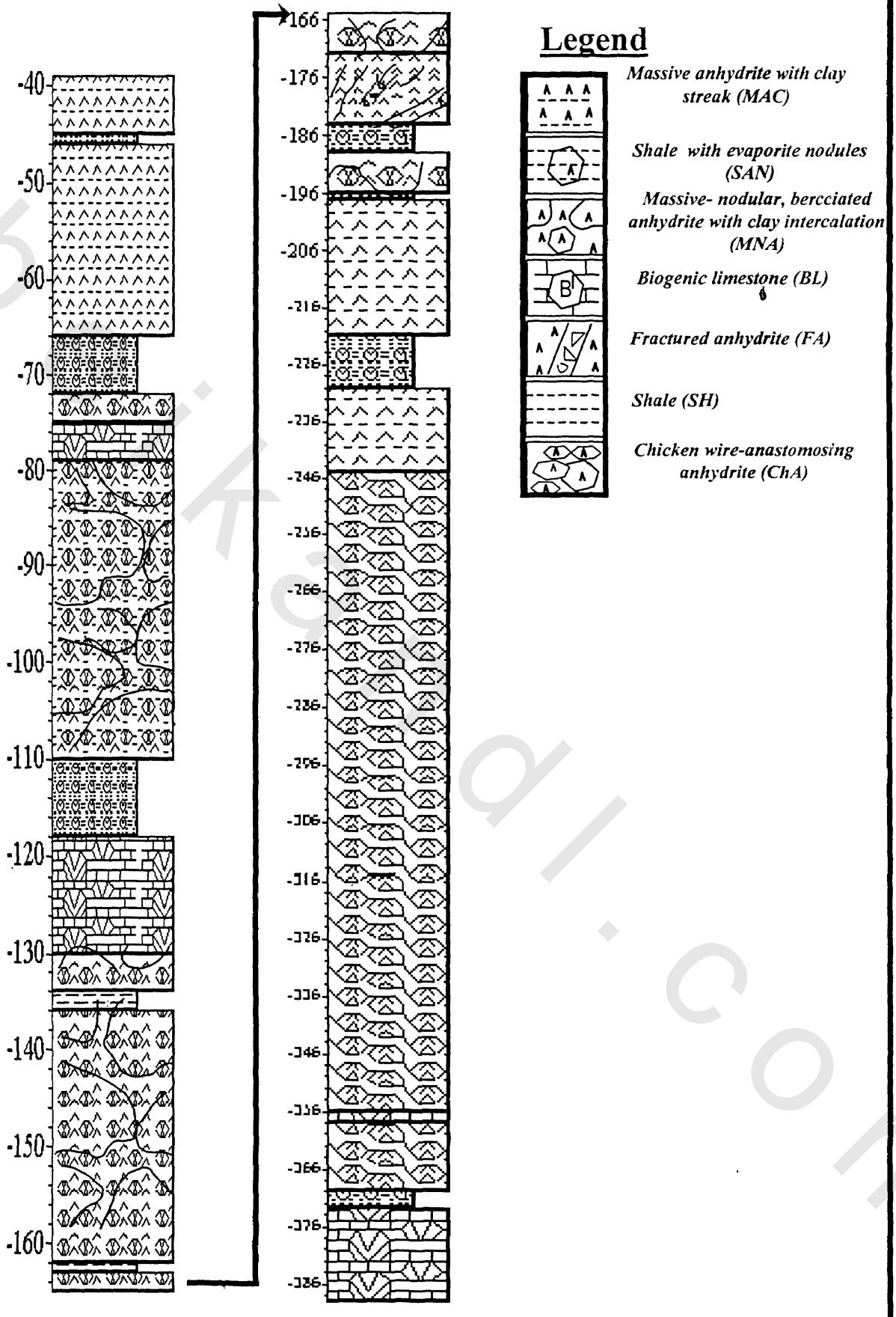

Figure -4: The stratigraphic sequence and associated facies of Ras Gemsa area (Gs-89-02 well)

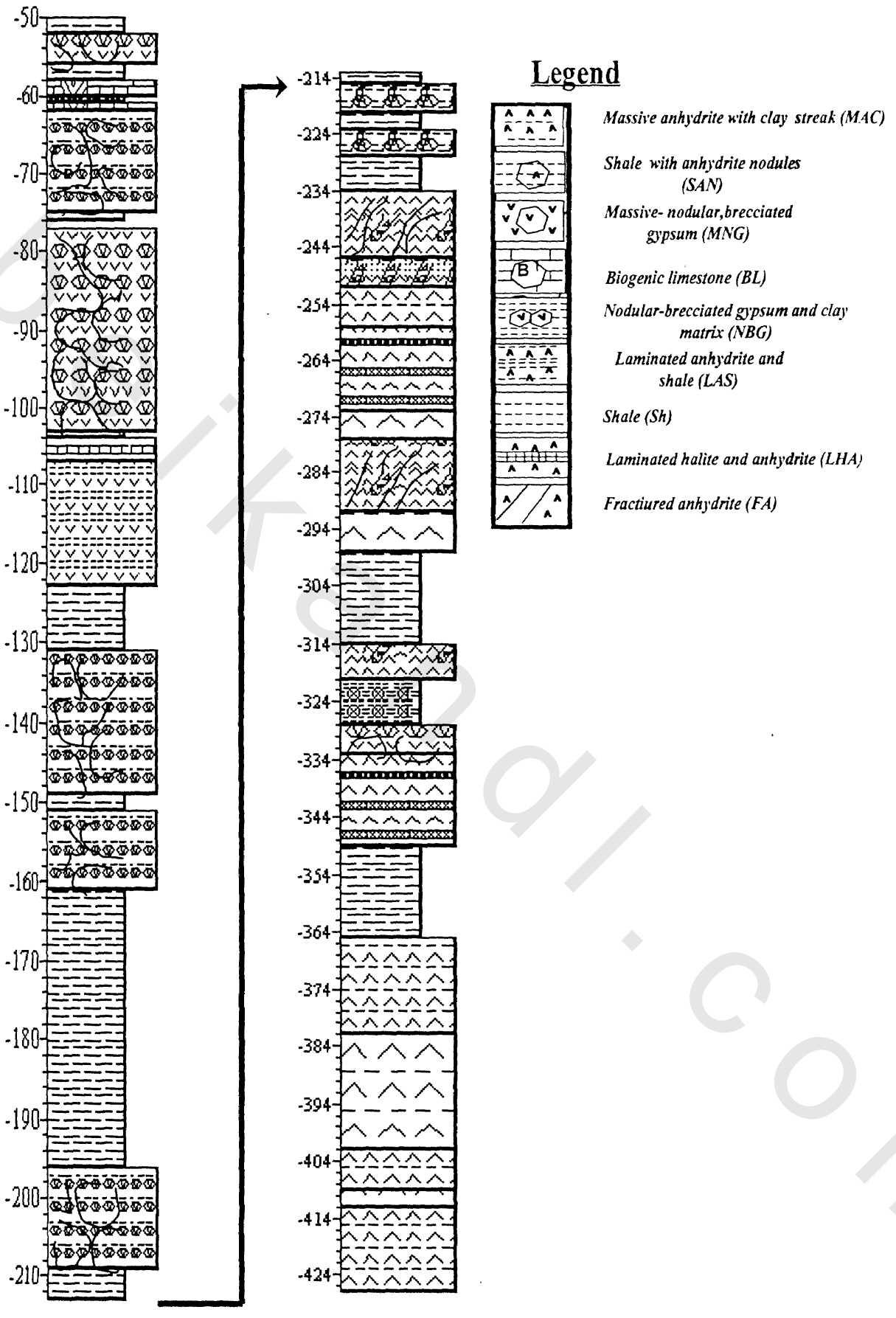

Figure -5 : The stratigraphic sequence and associated facies of Ras Gemsa area (Gs-89-03 well)

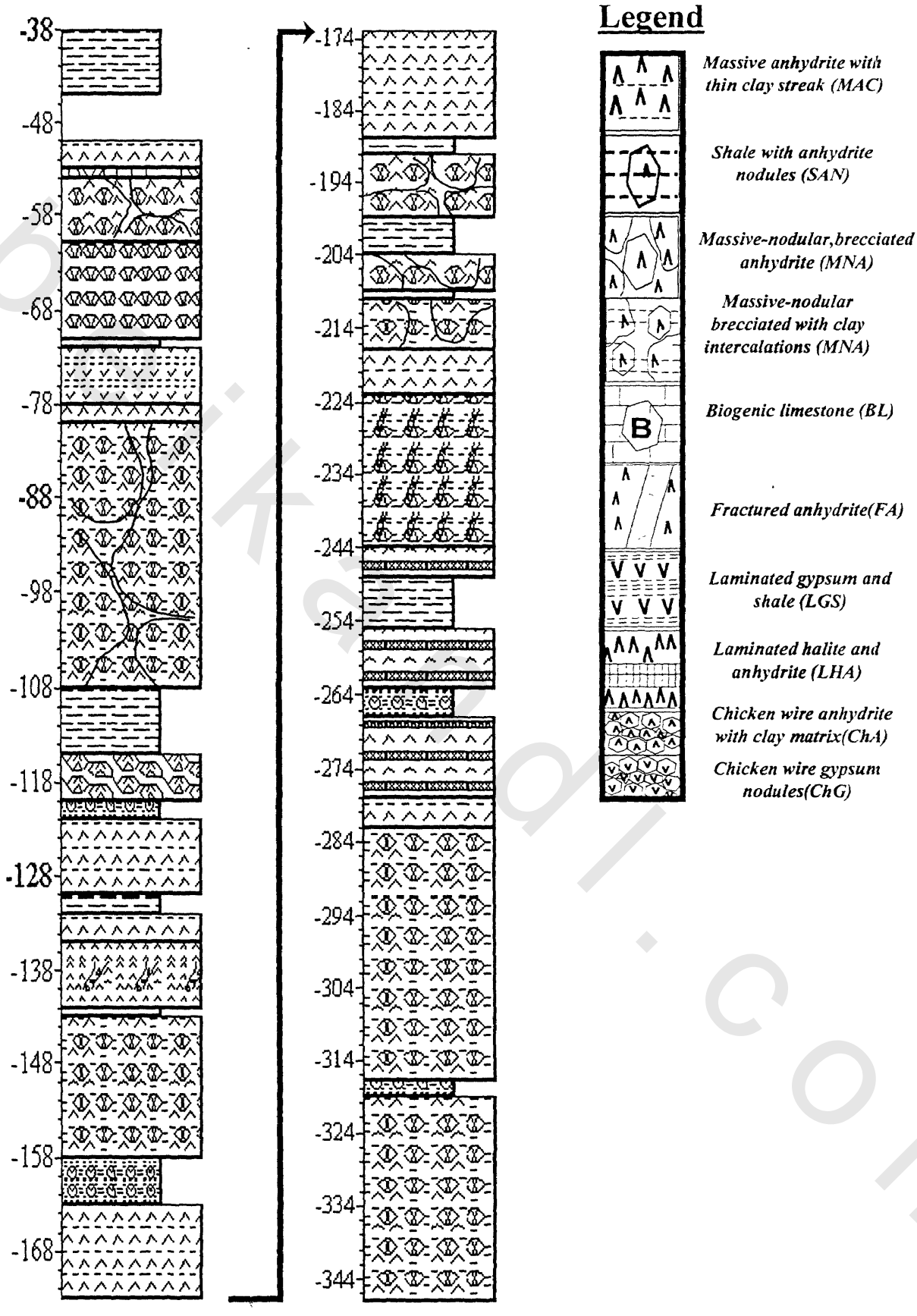

Figure-6 : The stratigraphic sequence and associated facies of Ras Gemsa area (Gs-89-04 well)

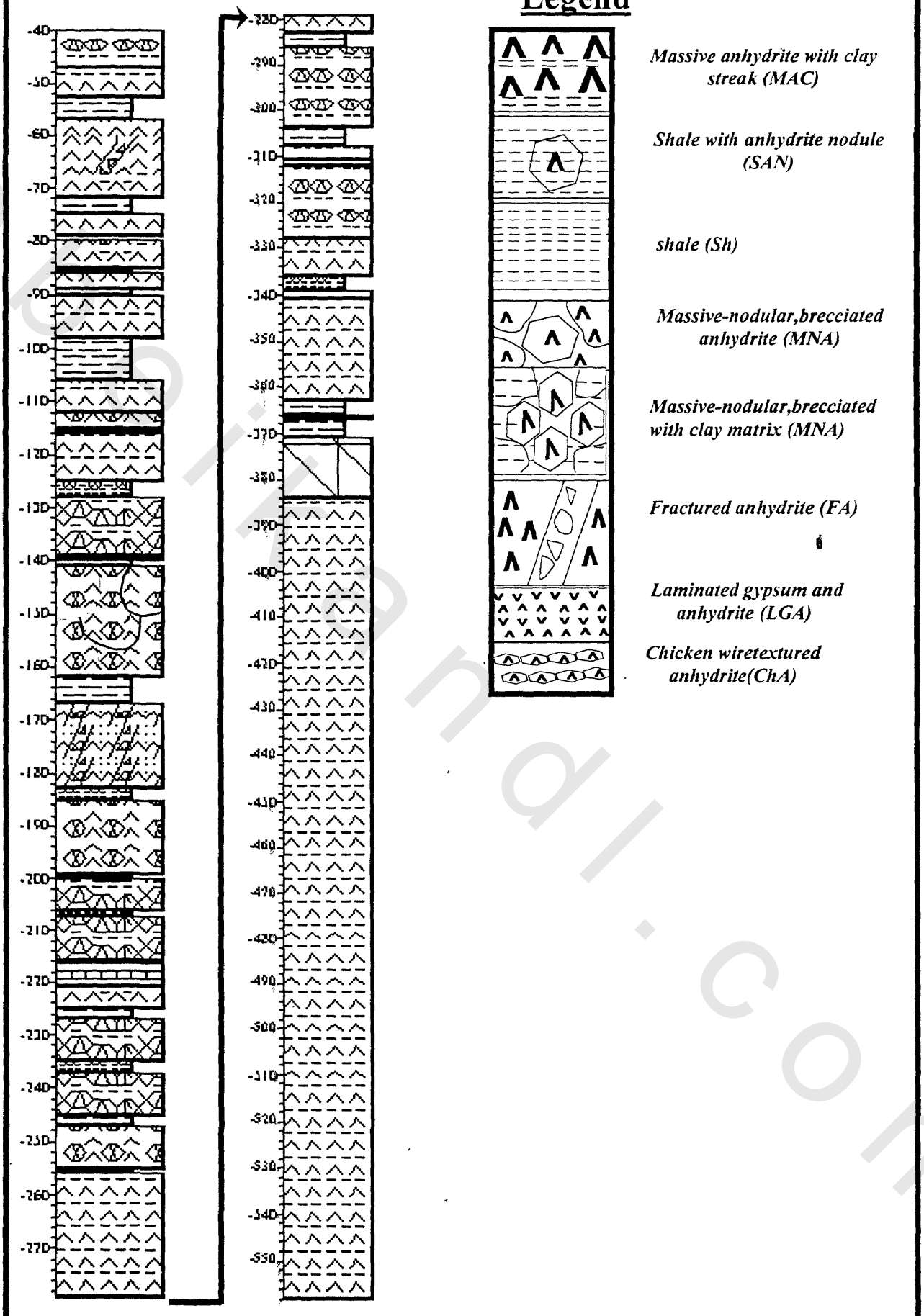

Figure-7: The stratigraphic sequence and associated facies of Ras Gemsa area (Gs-89-05 well)

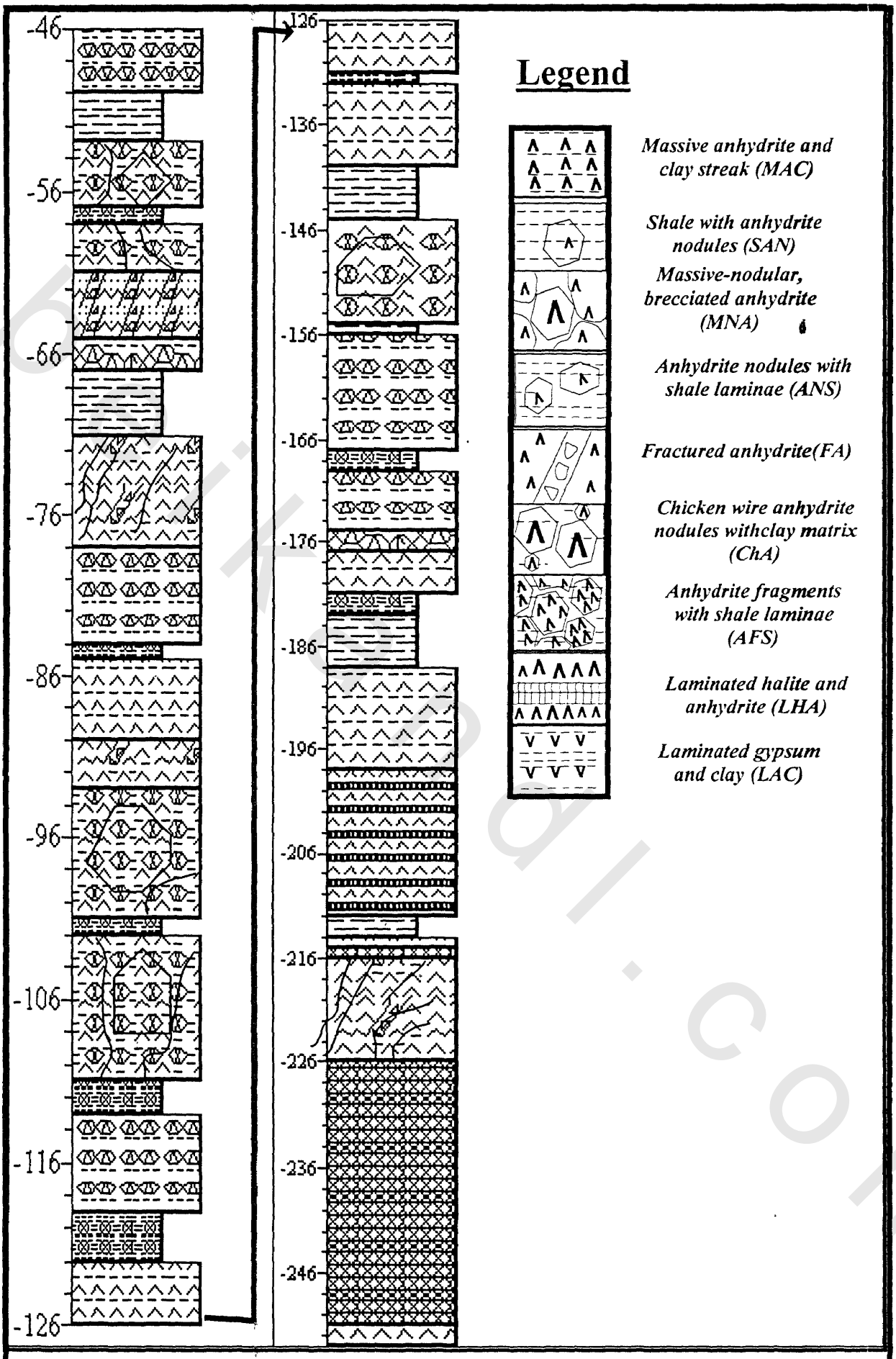

Figure-8 : The stratigraphic sequence and associated facies of Ras Gemsa area (Gs-89-06well)

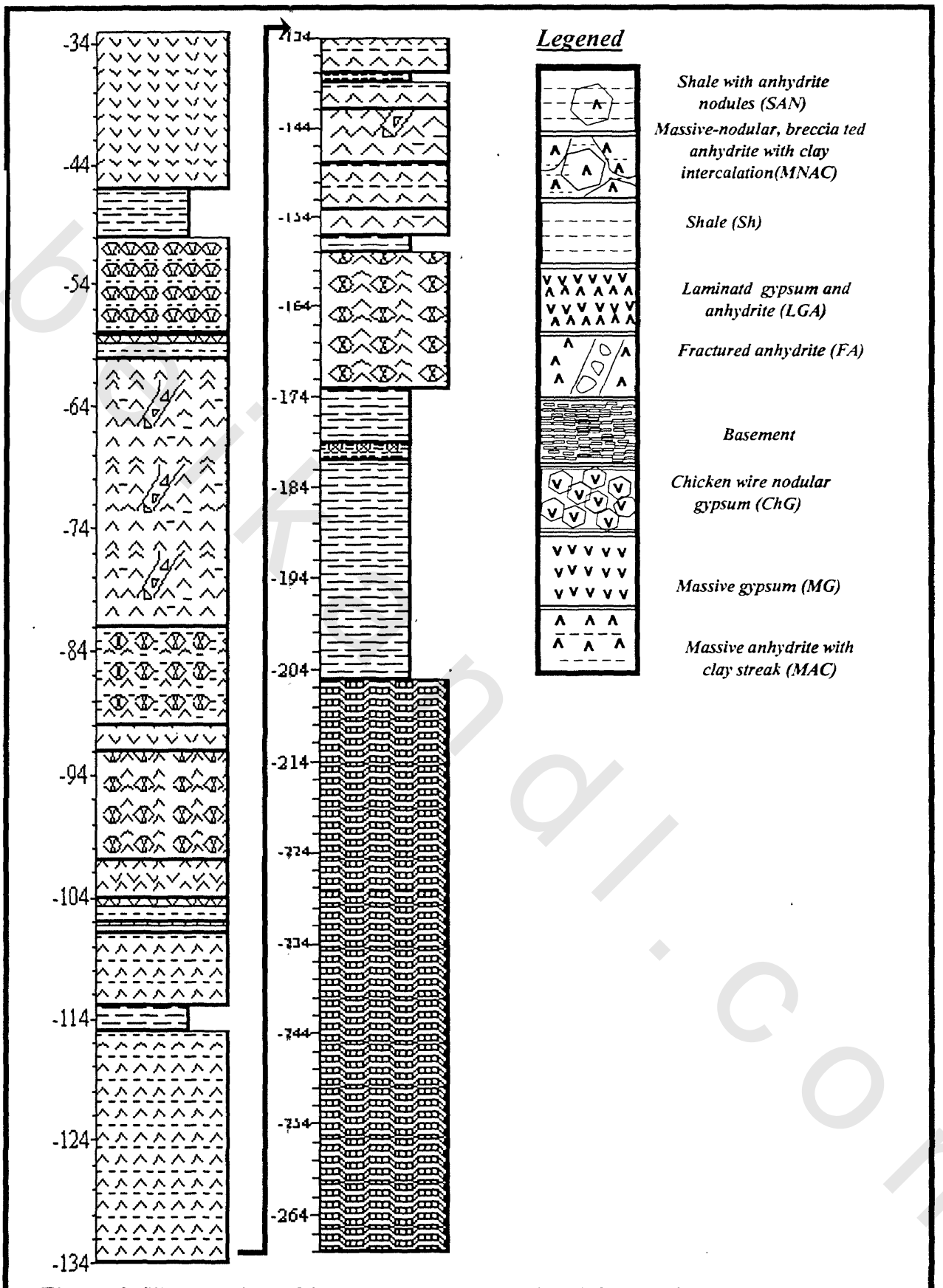

Figure-9: The stratigraphic sequence and associated facies of South East Zeit area (Gs-89-07 well)

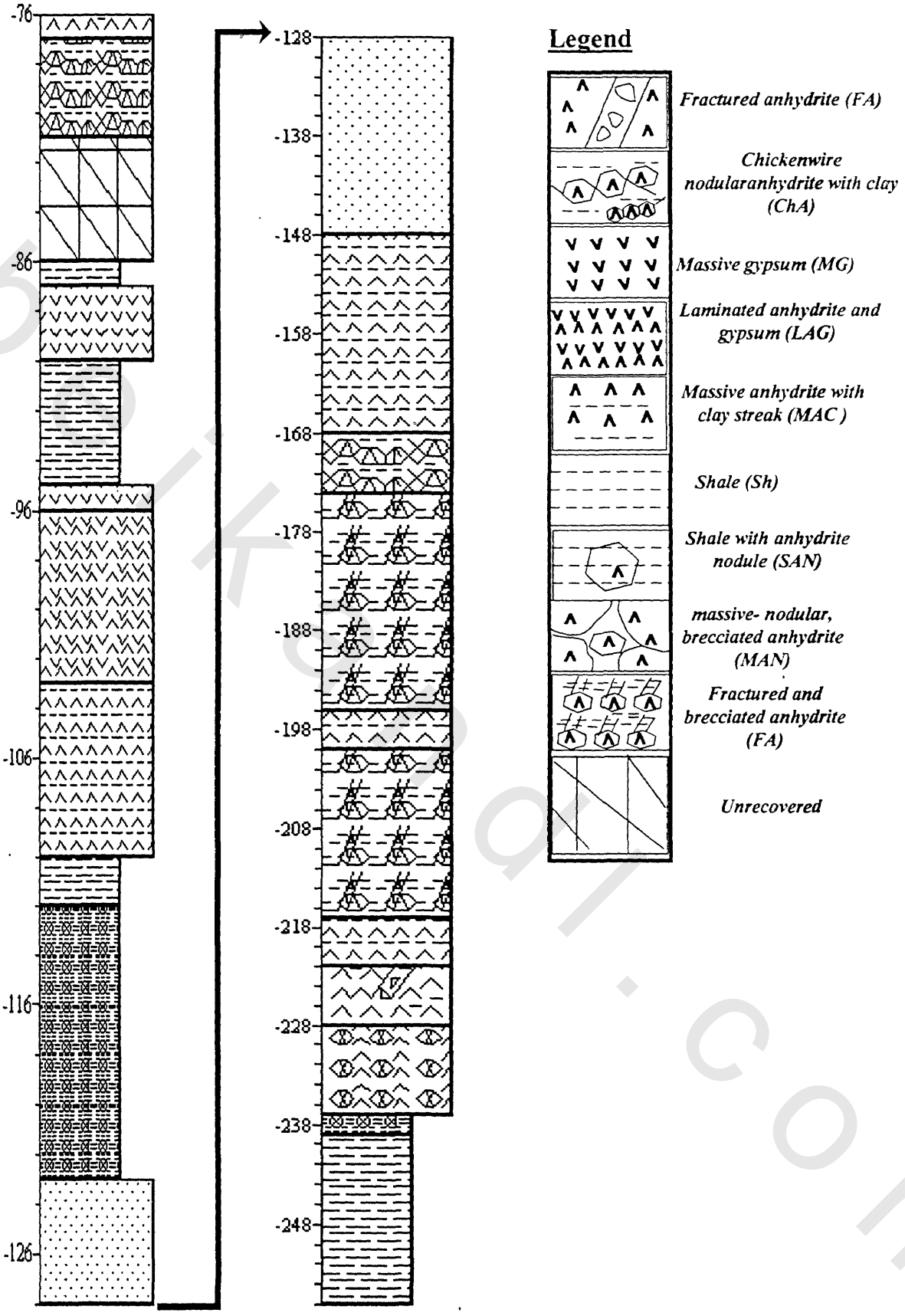

Figure-10 : The stratigraphic sequence and associated facies of Ras Dib area (Gs-89-08 well)

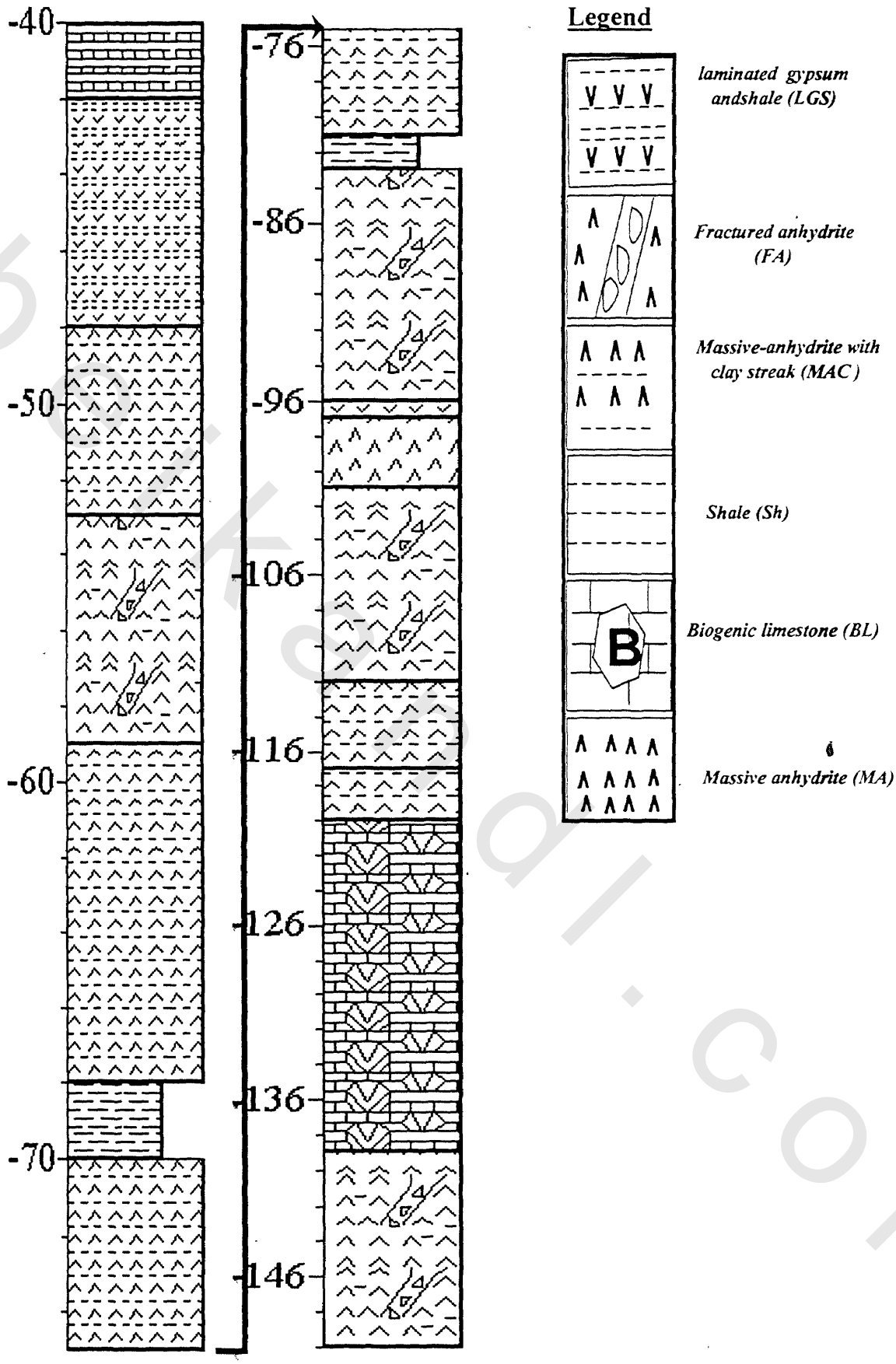

Figure-11:The stratigraphic sequence and associated facies of Ras Dib (Gs-89-09 well)

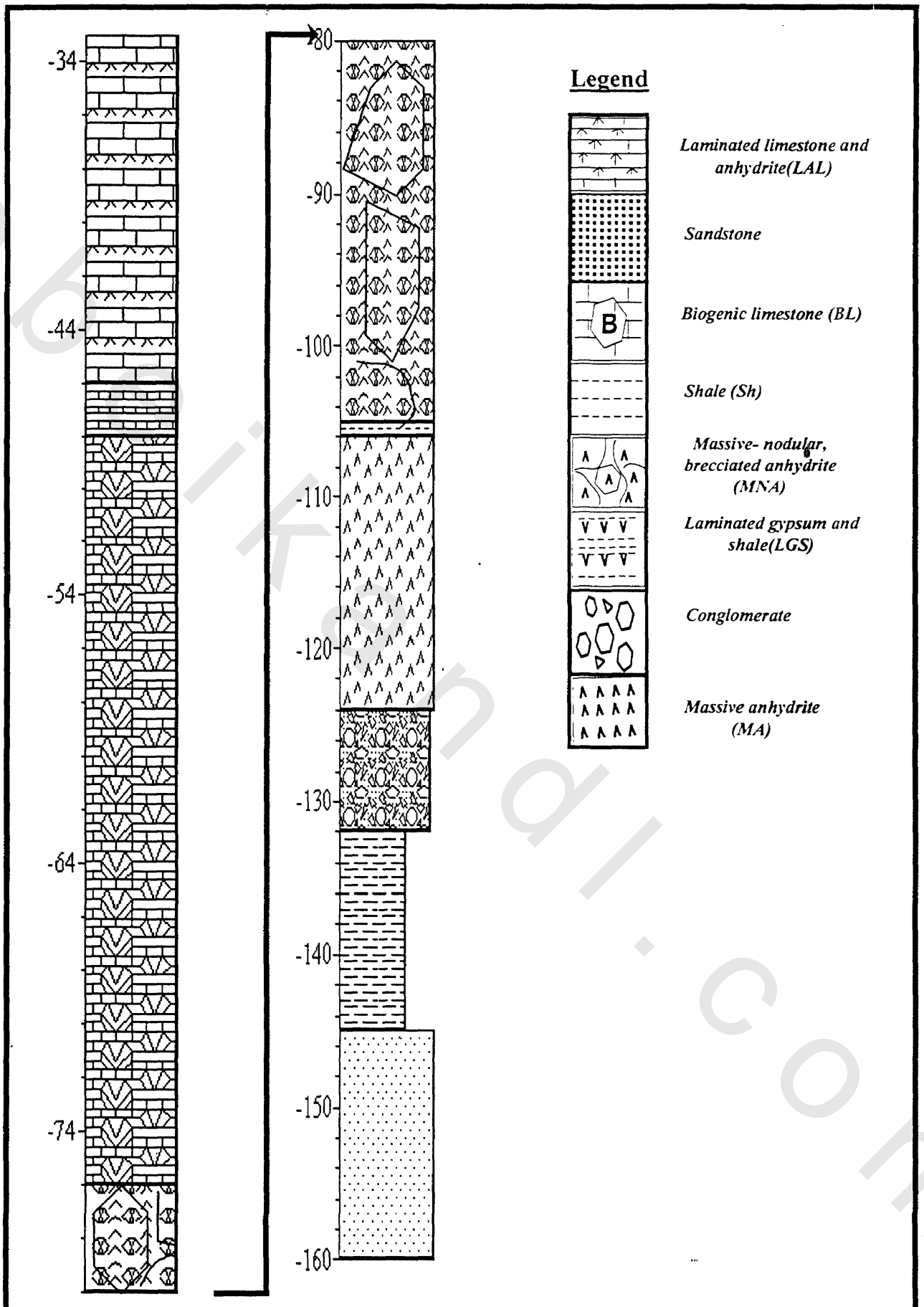

Figure-12: The stratigraphic sequence and associated facies of Ras Dib area Gs-89-10 well

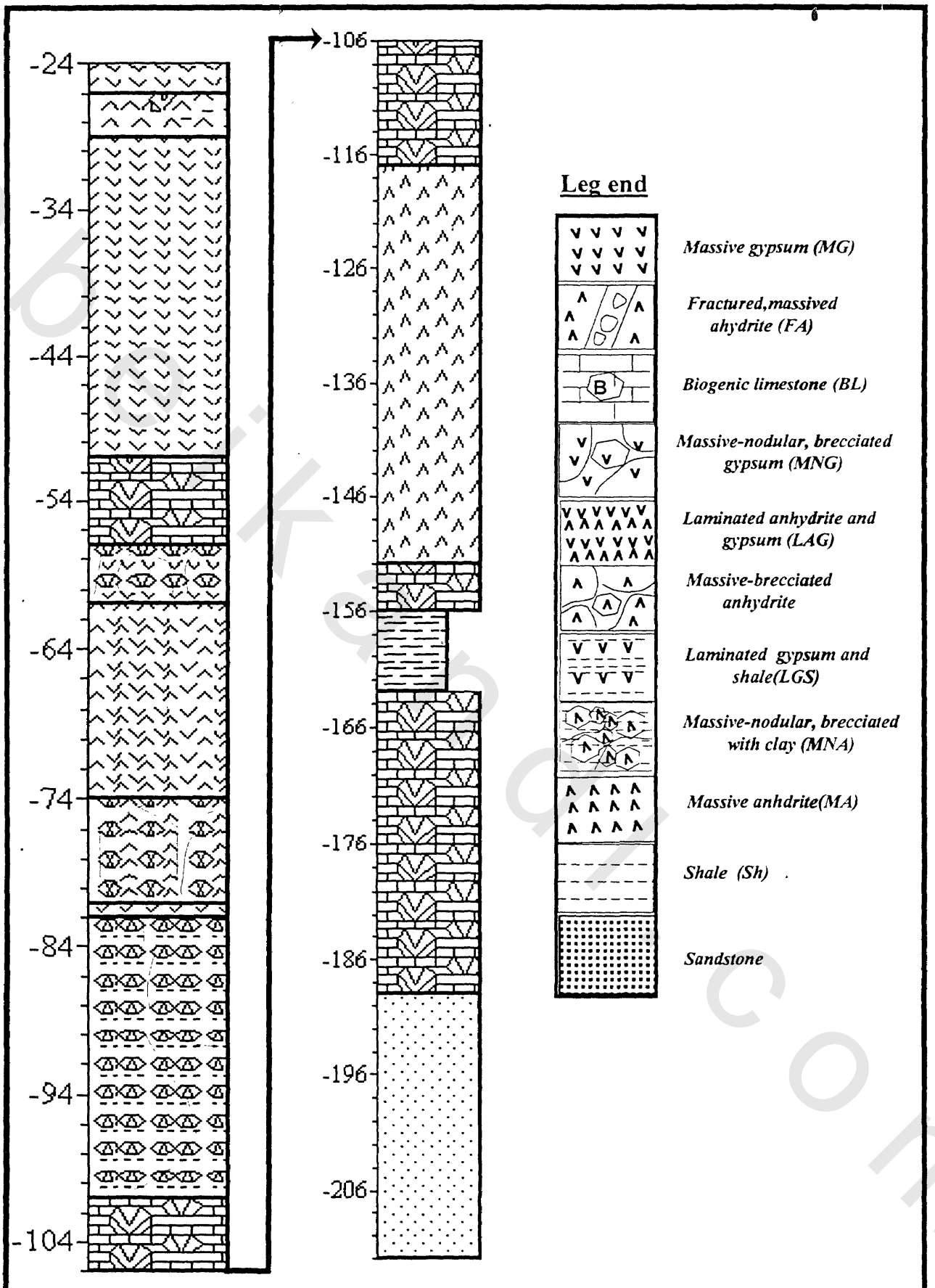

Figure-13 : The stratigraphic sequence and associated facies of Ras Dib area (Gs-89-11 well)

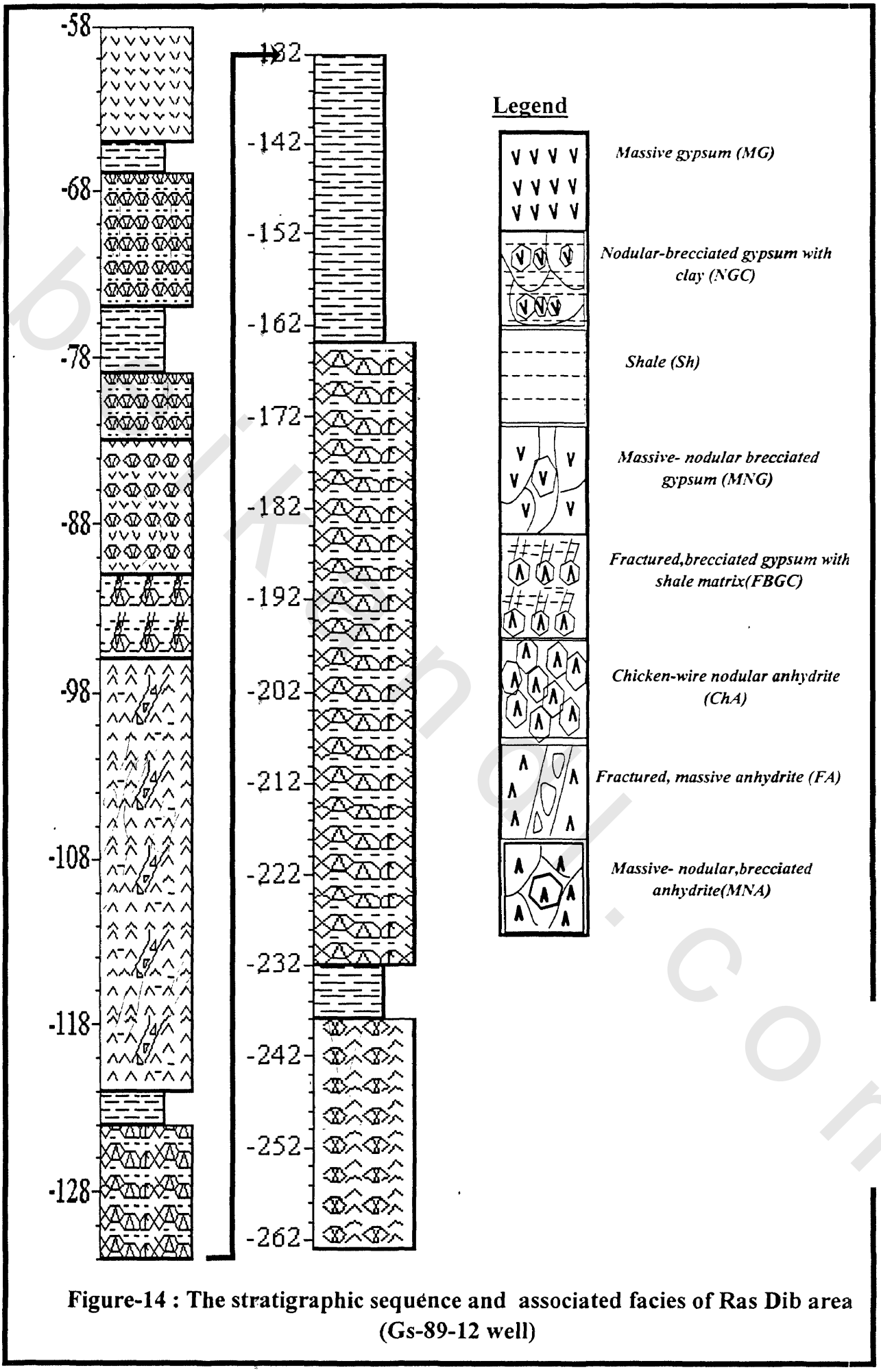

Figure-14 : The stratigraphic sequence and associated facies of Ras Dib area (Gs-89-12 well)

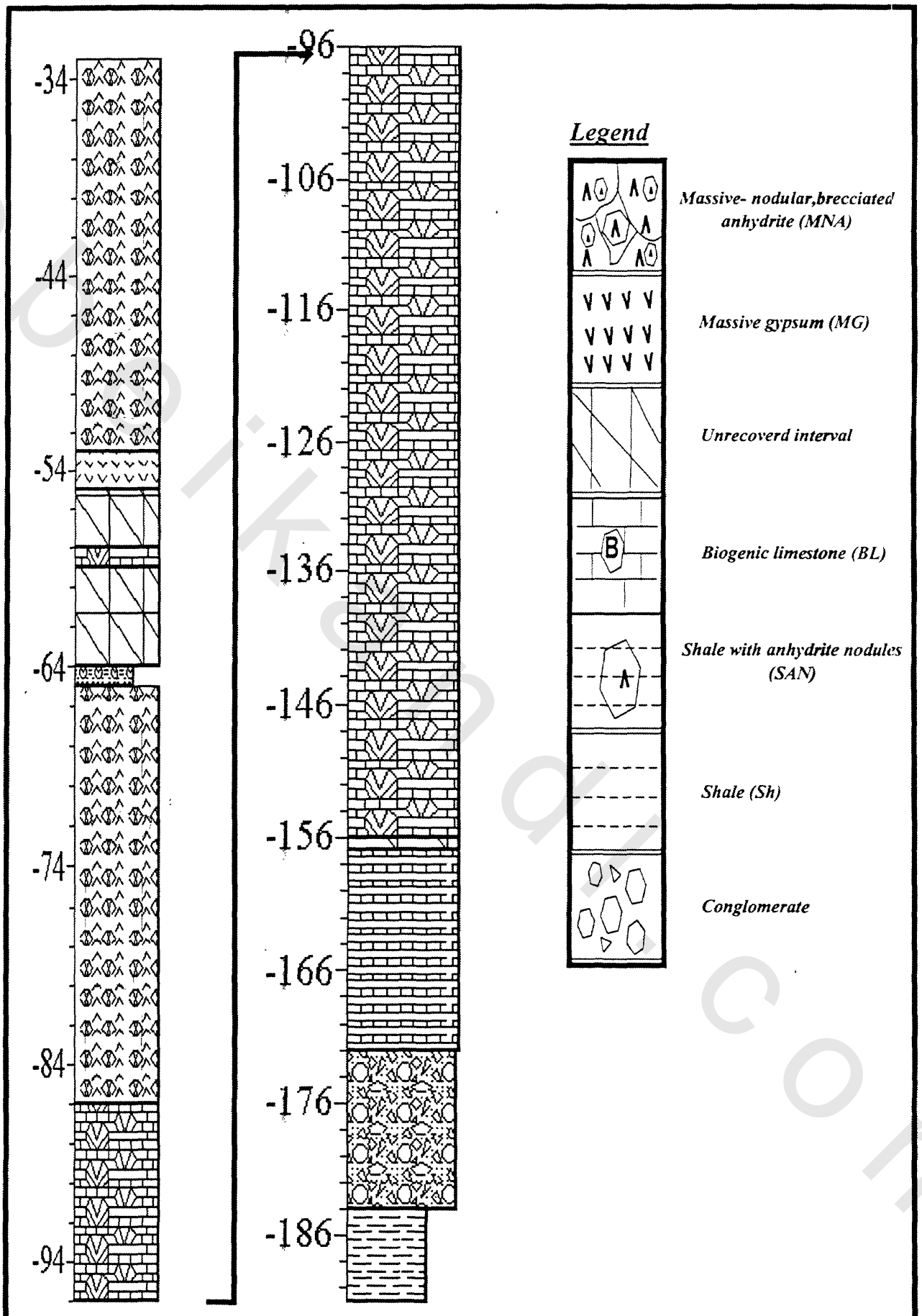

Figure-15 : The stratigraphic sequence and associated facies of Ras Dib area (Gs-89-13 well)

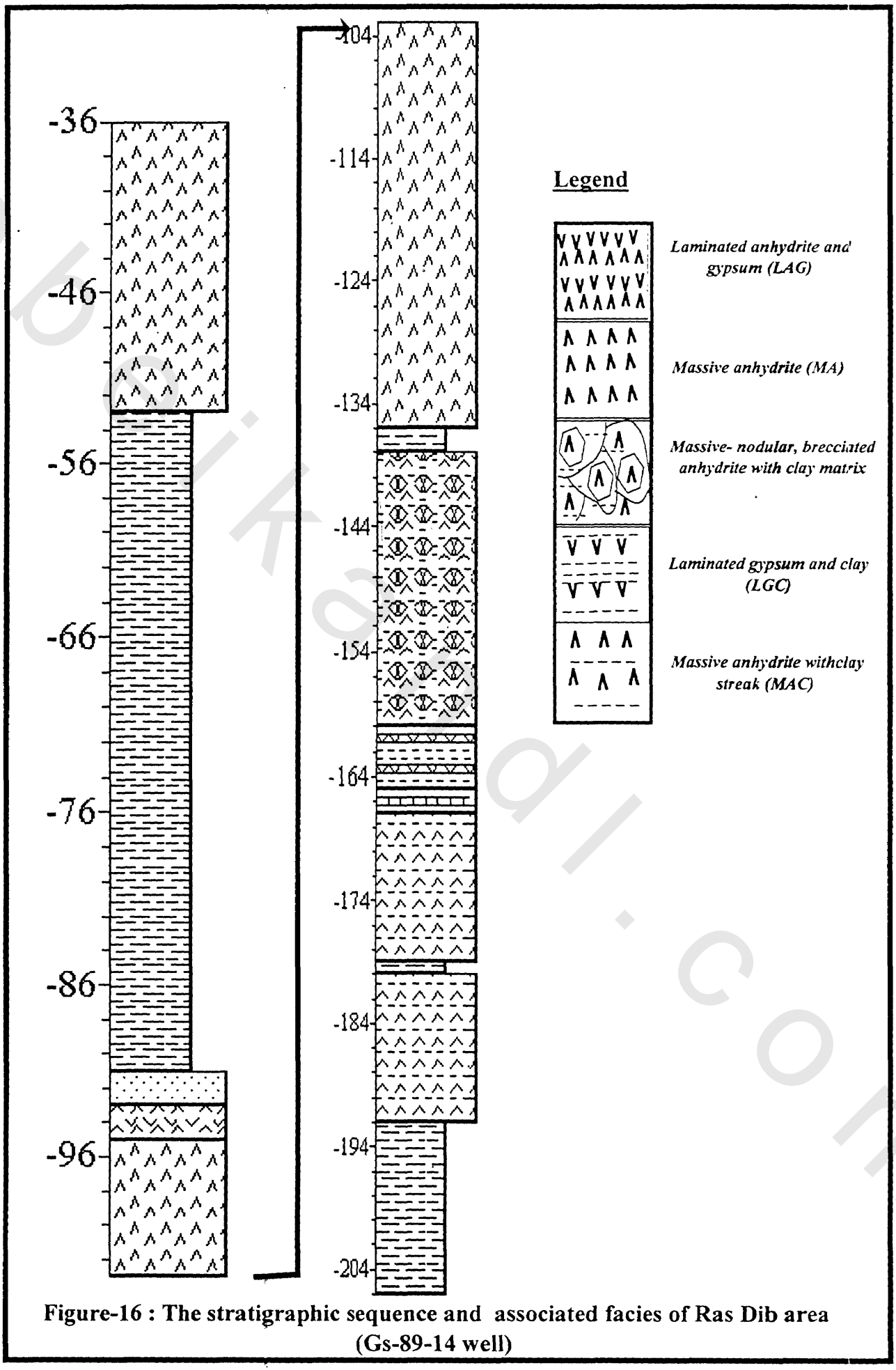

Figure-16 : The stratigraphic sequence and associated facies of Ras Dib area (Gs-89-14 well)

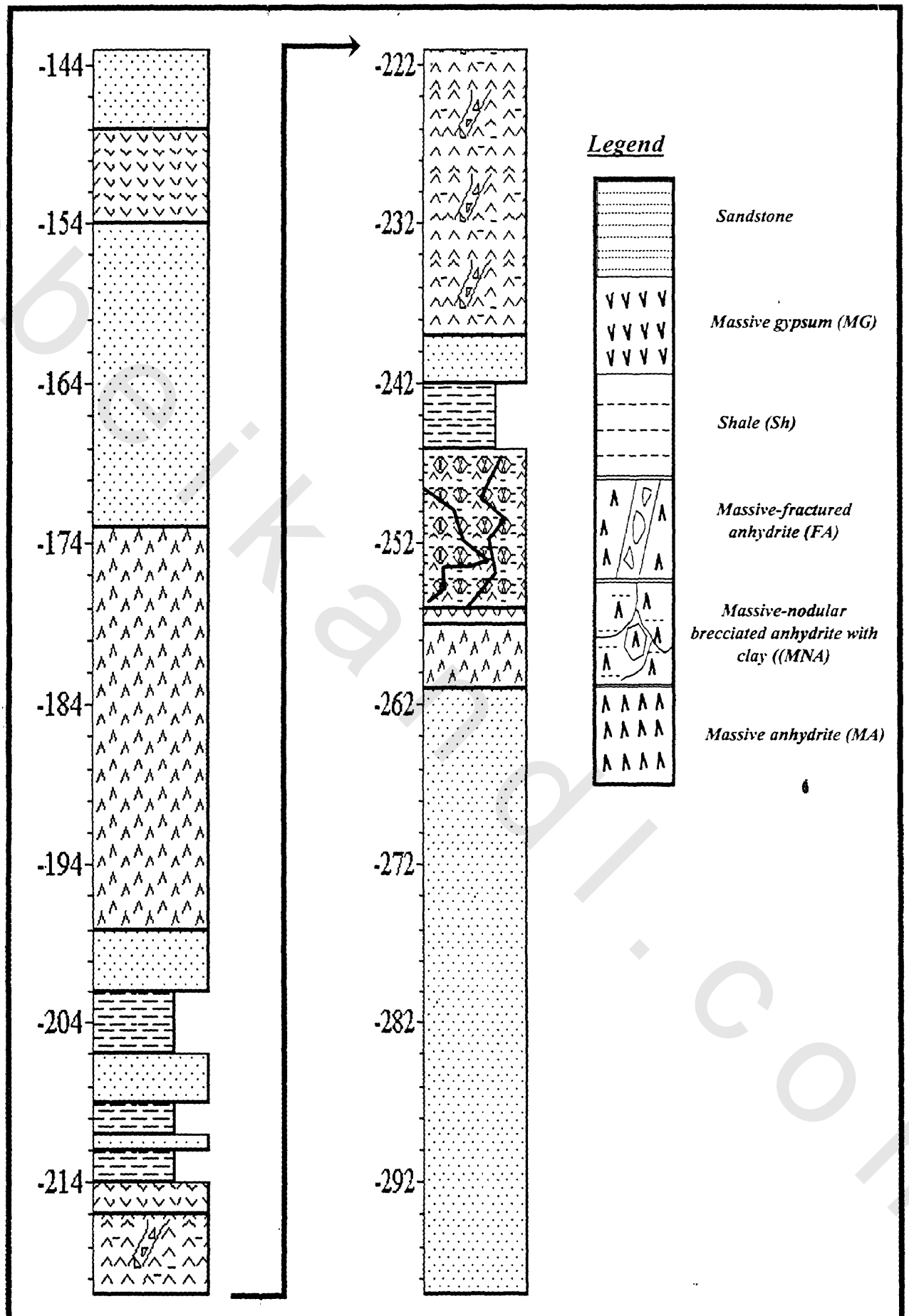

Figure-17: The stratigraphic sequence and associated Facies of Shagar area (Gs-90-15A well)

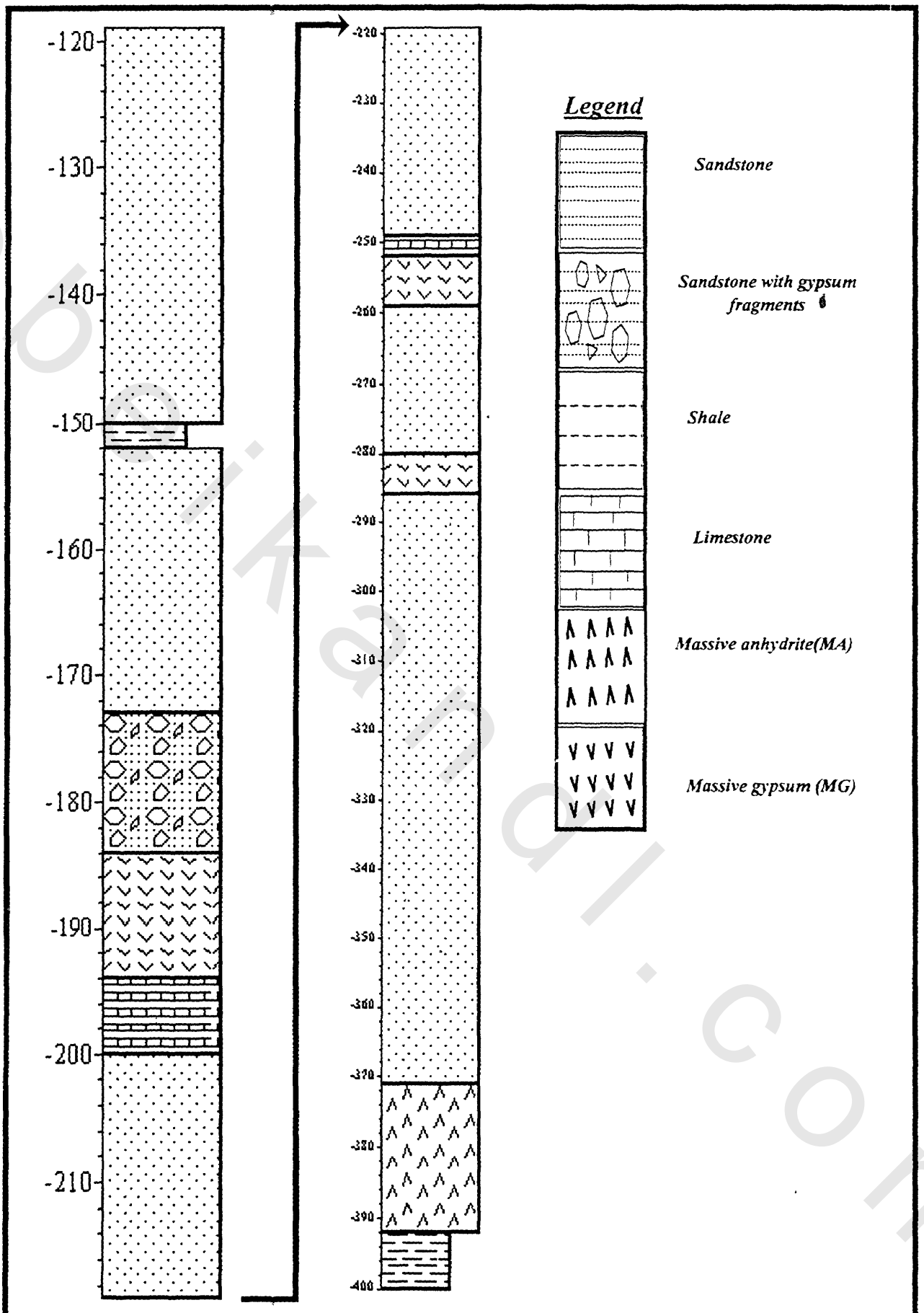

Figure-18: The stratigraphic sequence and associated Facies of Shagar area (Gs-90-16 well)

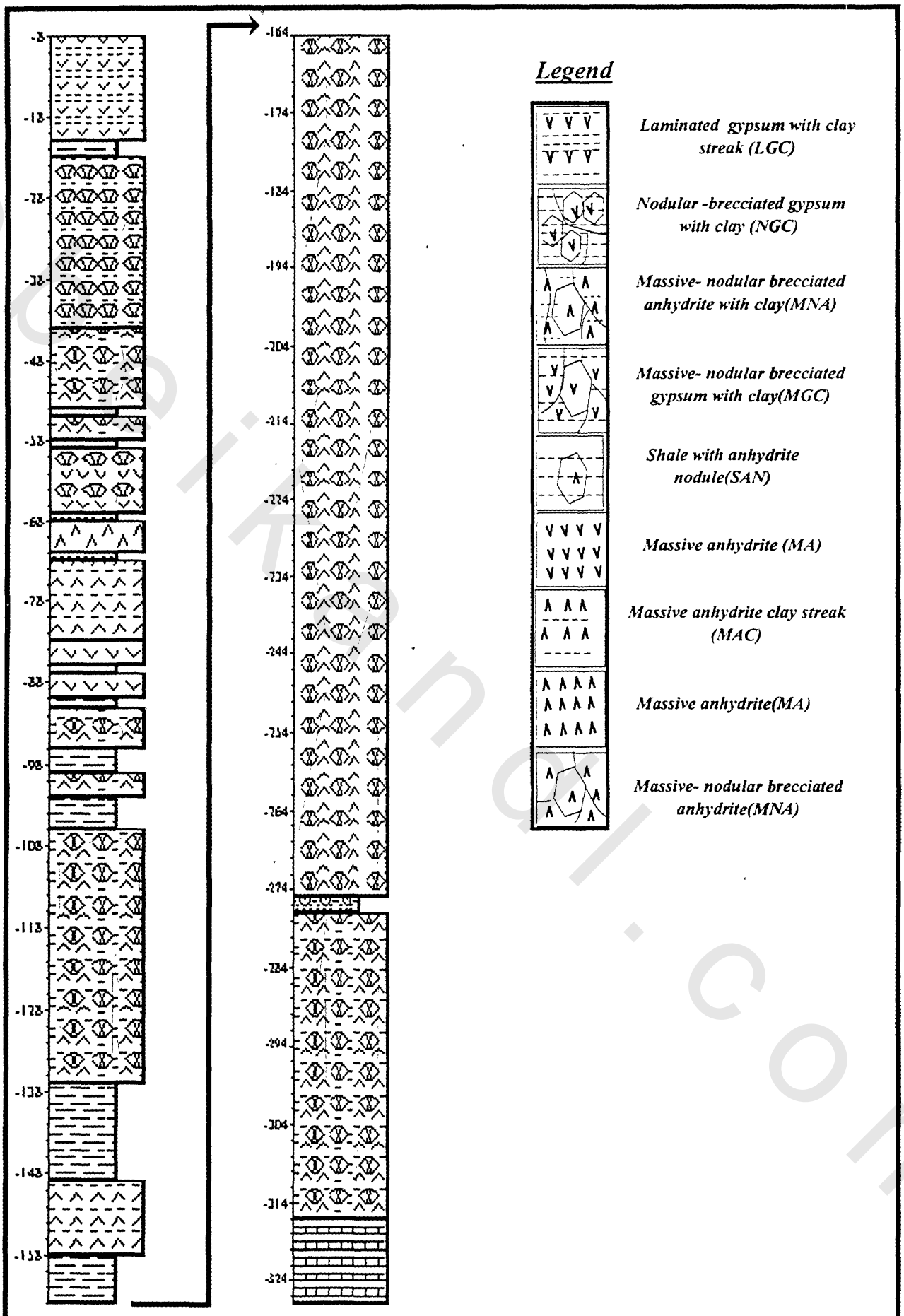

Figure -19:The stratigraphic sequence and associated facies of Gubal Island (Gs-89-17 well)

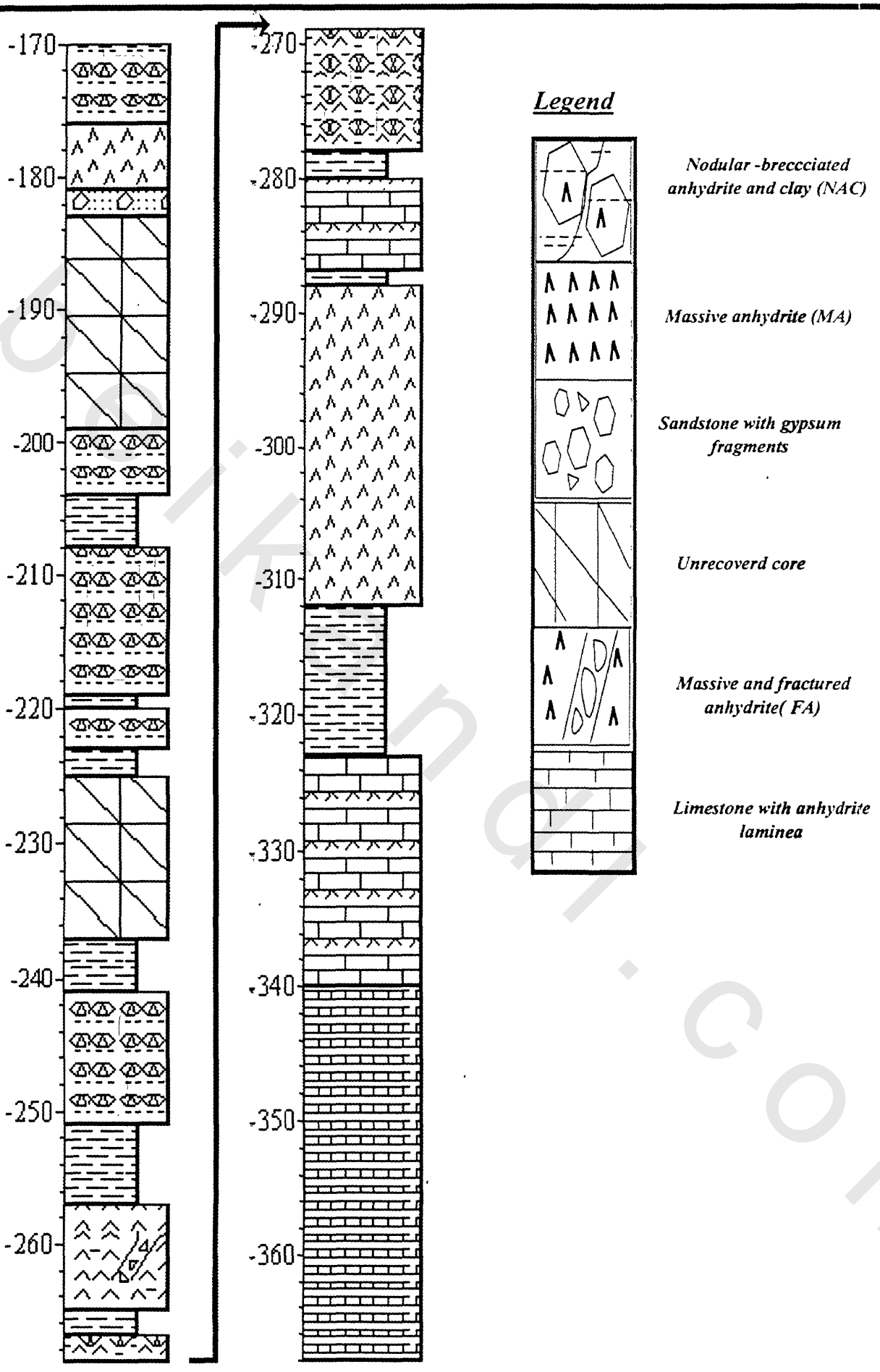

Figure-20: The stratigraphic sequence and associated facies of Gubal Island (Gs-89-18 well)

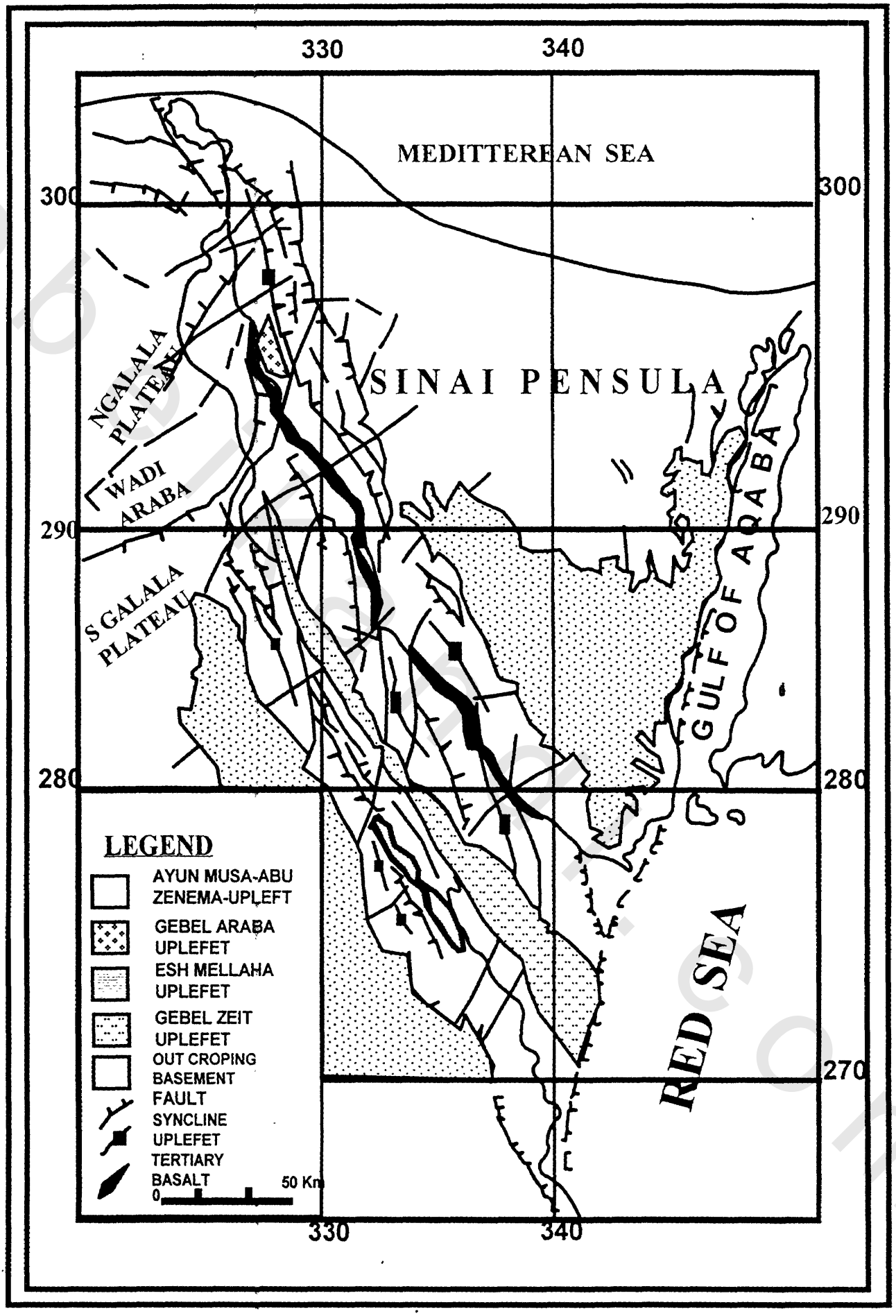

Figure -21: The Overall structure Configuration Of The Gulf Of Suez (After Bayoumi, 1983).

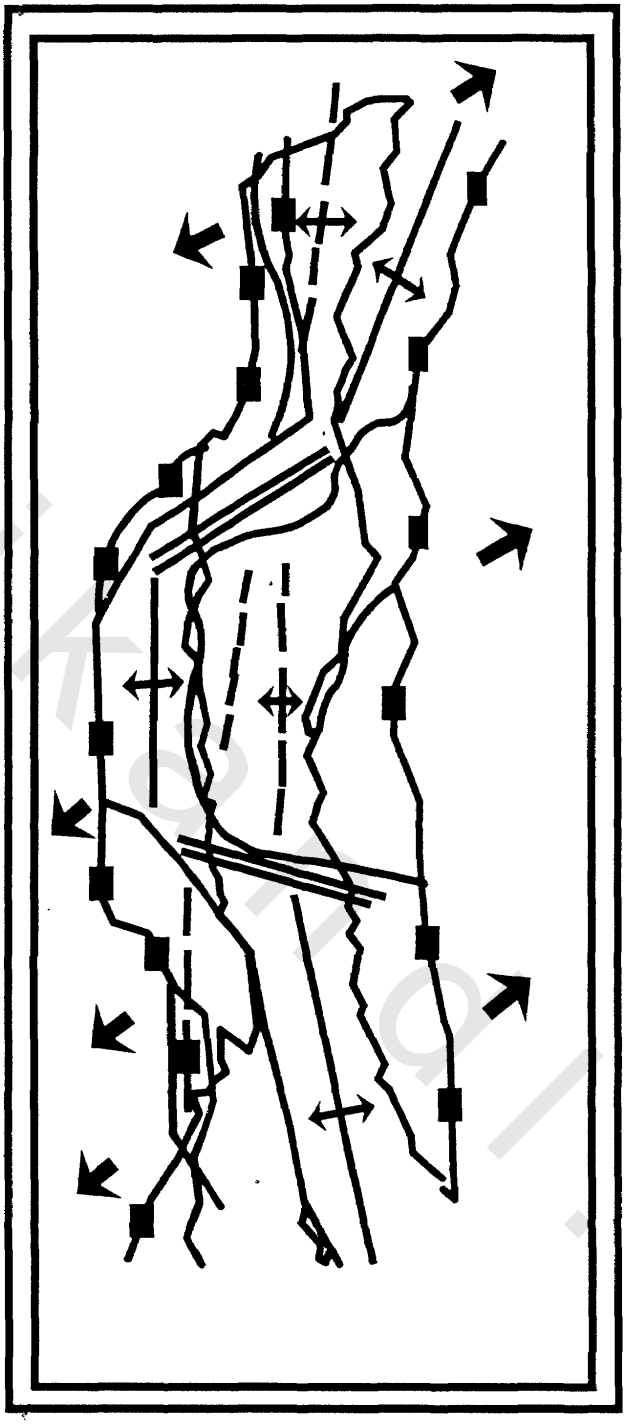

LEGEND

REGIONAL EXTENSION

ACCOMODATION ZONE

INITIAL RIFT AXIX
(Oligocene-Early Miocene)

AXIS OF LATER RIFT
(Middle Miocene- Recent)

Figure-22 : Gulf of Suez Rift Tectonics (After Mesherf, 1990)

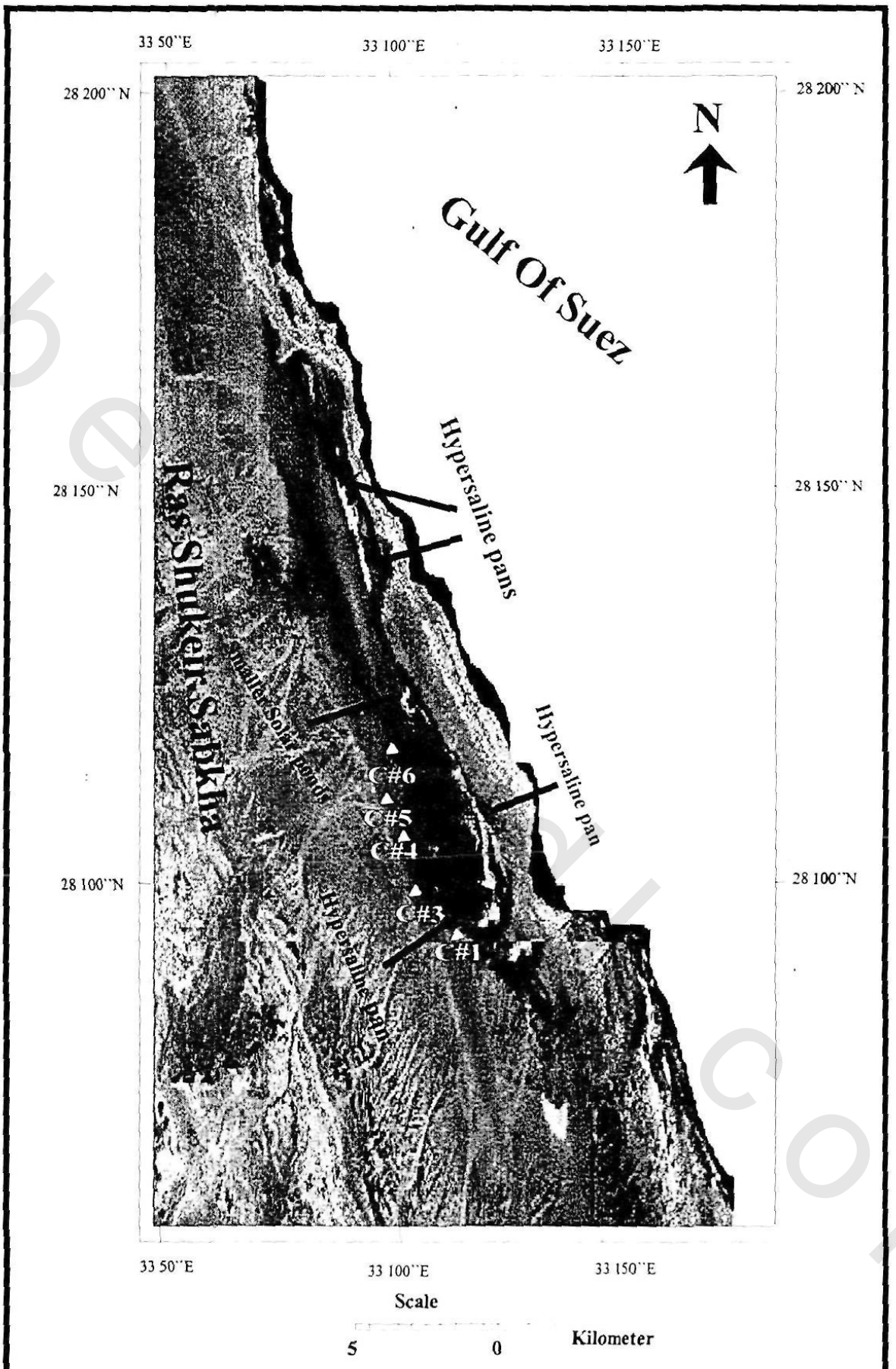

Figure-23 : Mosaic of processed TM satellite image of Ras Shukeir area, applying bands 3,4,7.

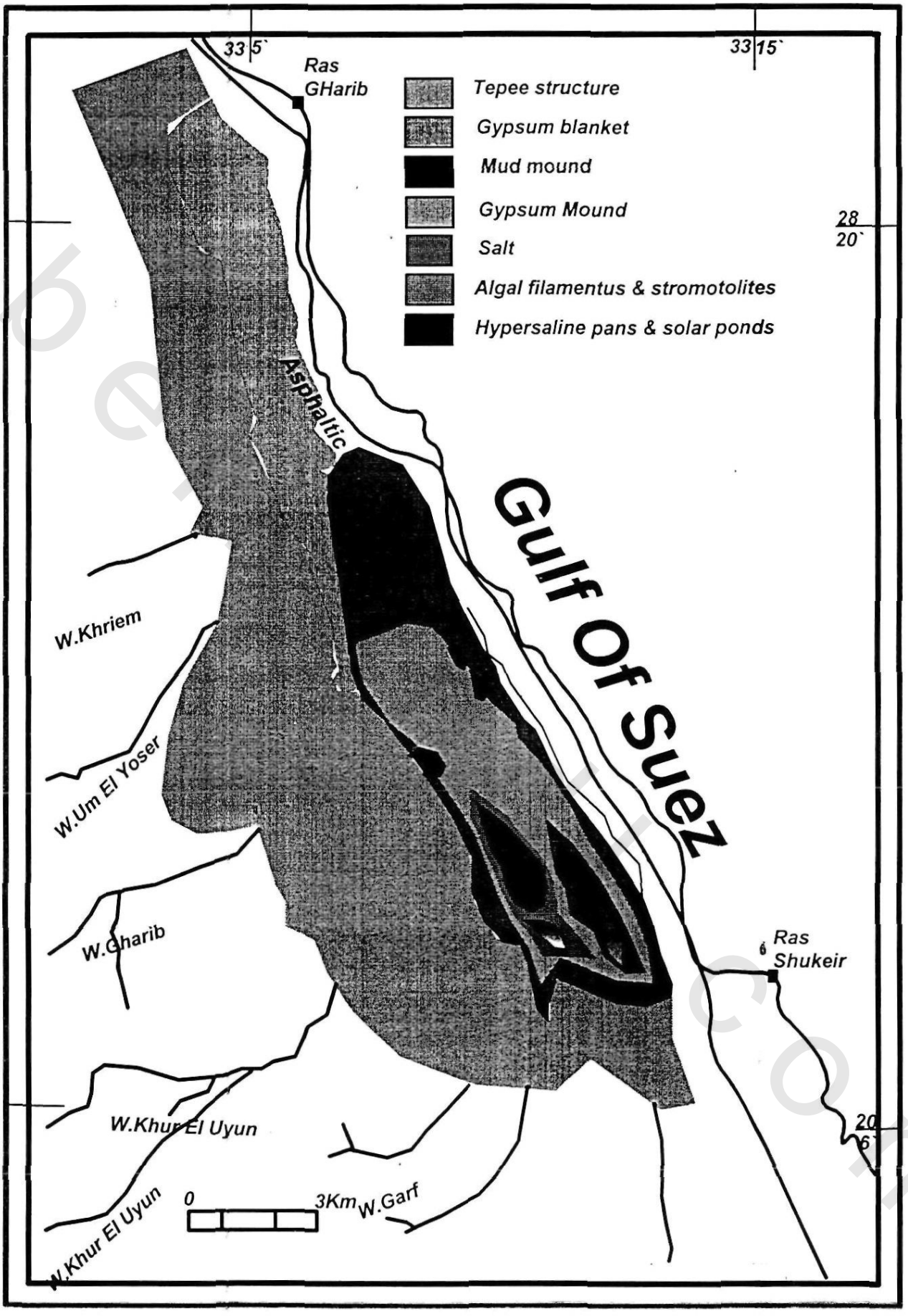

Figure-24B : Sketch showing encountered facies in Ras Shukeir recent sabkha and hypersaline pans

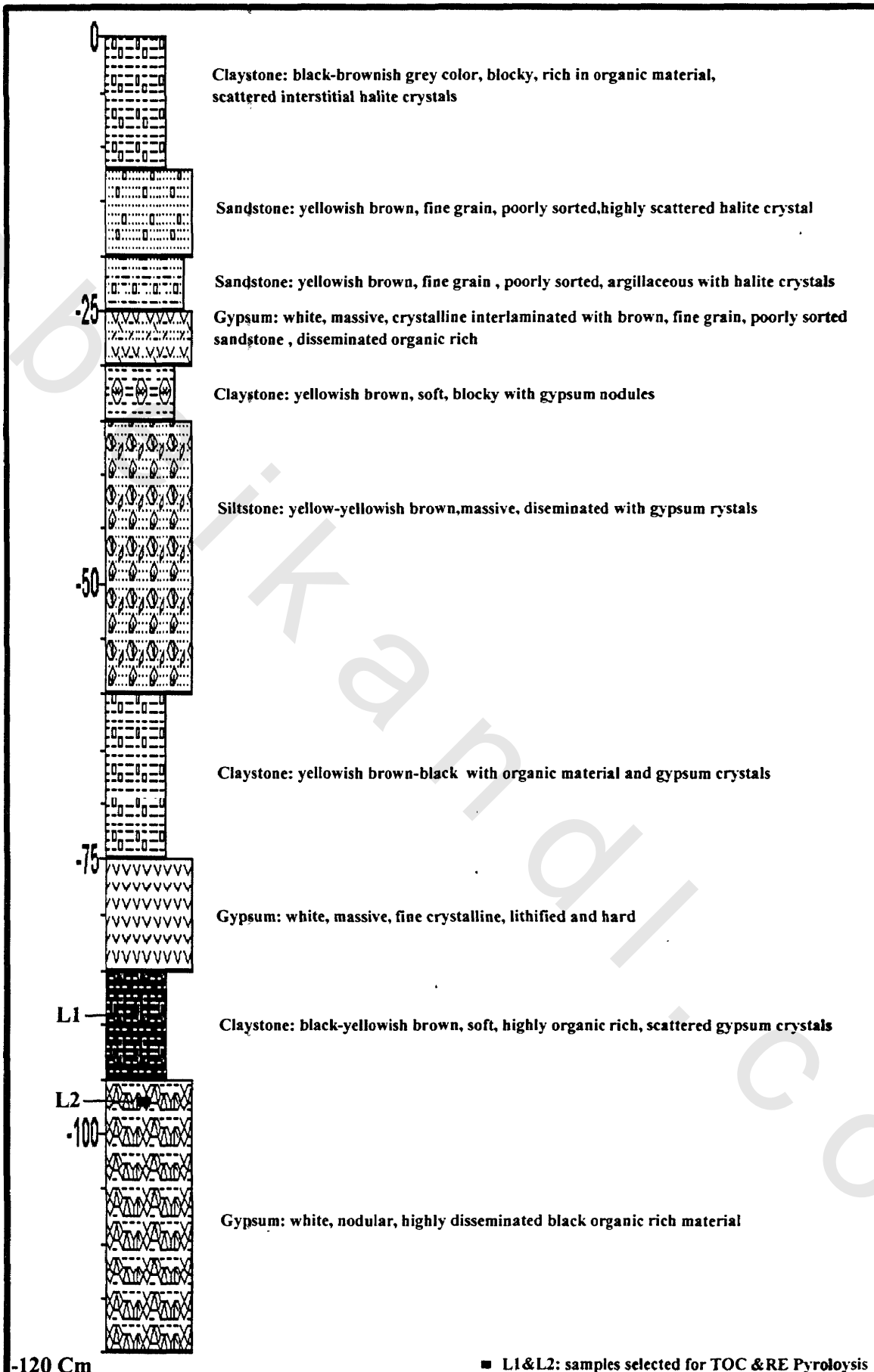

Figure-25A:Stratigraphic sequence and associated facies for C#1, Ras Shukeir sabkha

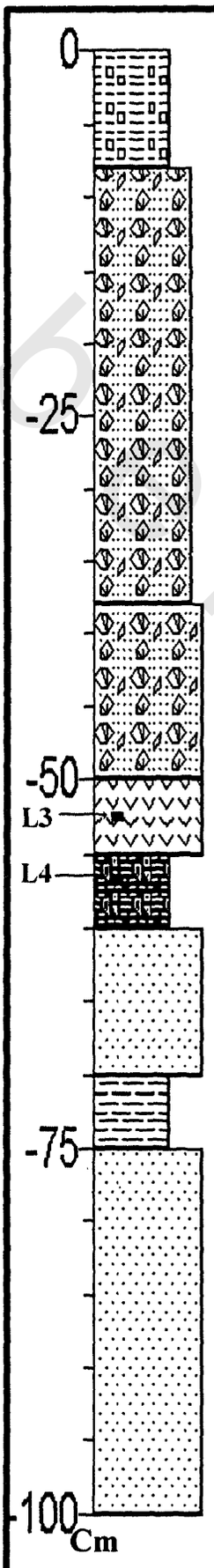

Claystone: brownish yeloow, blocky, soft with disseminated halite crystals

Sandstone : brownish yellow, medium grain, moderately sorted, fraible with scattered gypsum crstals and nodules

Sandstone : brownish yellow, Coarse grain, moderately sorted, fraible with scattered gypsum crstals and nodules

Gypsum: white , fine-sand size crystalline, massive, hard

Sapproplic mud: green,greyish, soft, muddy, highly organic rich, vicous, organic ouder

sandstone: grey,gryish green,very fine, moderatlely sorted, massive.

Claystone: grey, greenish grey, spft friable

Sandstone: grey, fine -medium grain, moderately sorted , shell fragments

■ L3&4 : Samples selected for TOC &RE pyrolysis

Figure-25 B:Stratigraphic sequence and associated facies for C#3, Ras Shukeir sabkha

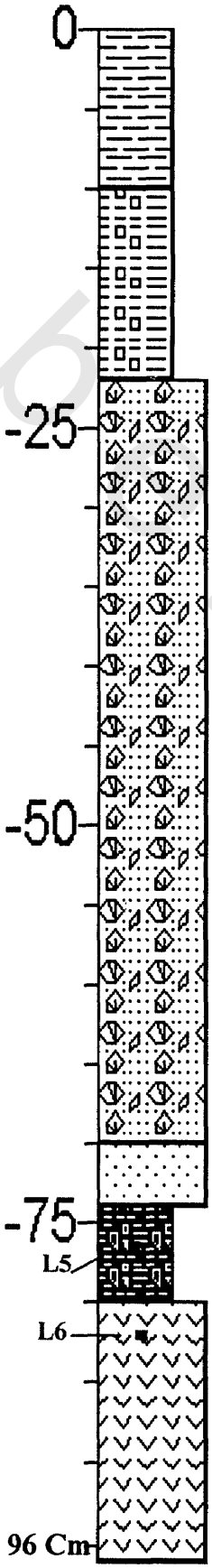

Claystone: black-brownish grey, blocky, soft, rich in organic material

Claystone : yellowis brown, soft with disseminated gypsum and halite crystals

Sandstone:yellowish brown,fine-medium grain size, moderately sorted, massive, with scattered gypsum crystals

Sandstone:yellow, finr grain,moderatley sorted, massive, friable

Sapproplic mud: greenish grey, soft, highly organic richness, muddy

Gysum: white, fine -medium sand size crystalline, massive, fraible.

■ L5&6 : Samples selected for TOC &RE pyrolysis

Figure-25C: Stratigraphic sequence and associated facies for C#4, Ras Shukeir sabkha

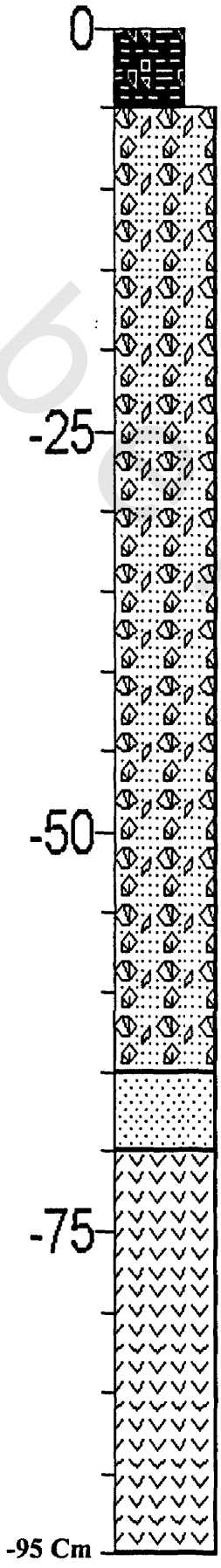

Clatstone:yellowish brown-black,blocky, soft, rich in organic material

Sandstone: brownish yellow, fine-medium size, moderately sorted, argillaceous with disseminated gypsum crystals

Siltstone: yellowish brown, soft, fine silt size, massive, argillaceous

Gypsum: white, fine-medium sand size crystals, massive with black orgainc disseminated material

Figure-25D:Stratigraphic sequence and associated facies for C#5, Ras Shukeir sabkha

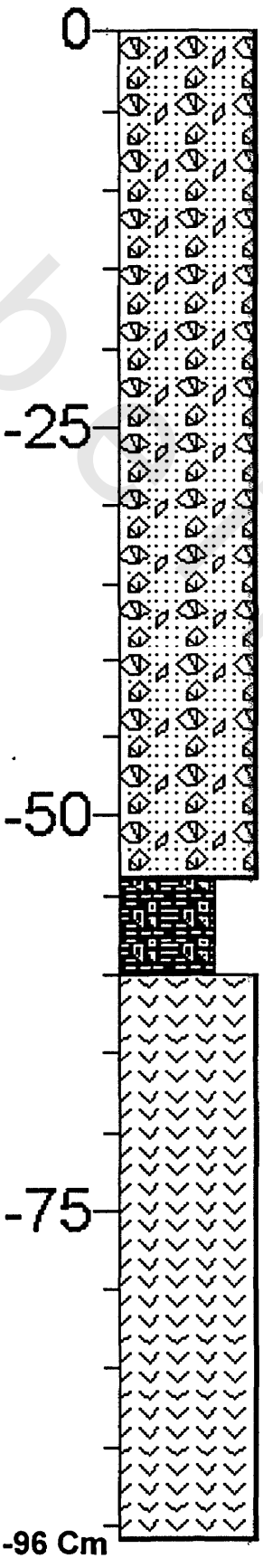

Sandstone: brownish yellow, fine-medium, poorly sorted,gypsum disseminated

Claystone : greenish grey, soft, highly organic rich and scattered gypsum crystals

Gypsum: white, fine crystalline, massive

Figure-25E Stratigraphic sequence and associated facies for C#6, Ras Shukeir sabkha

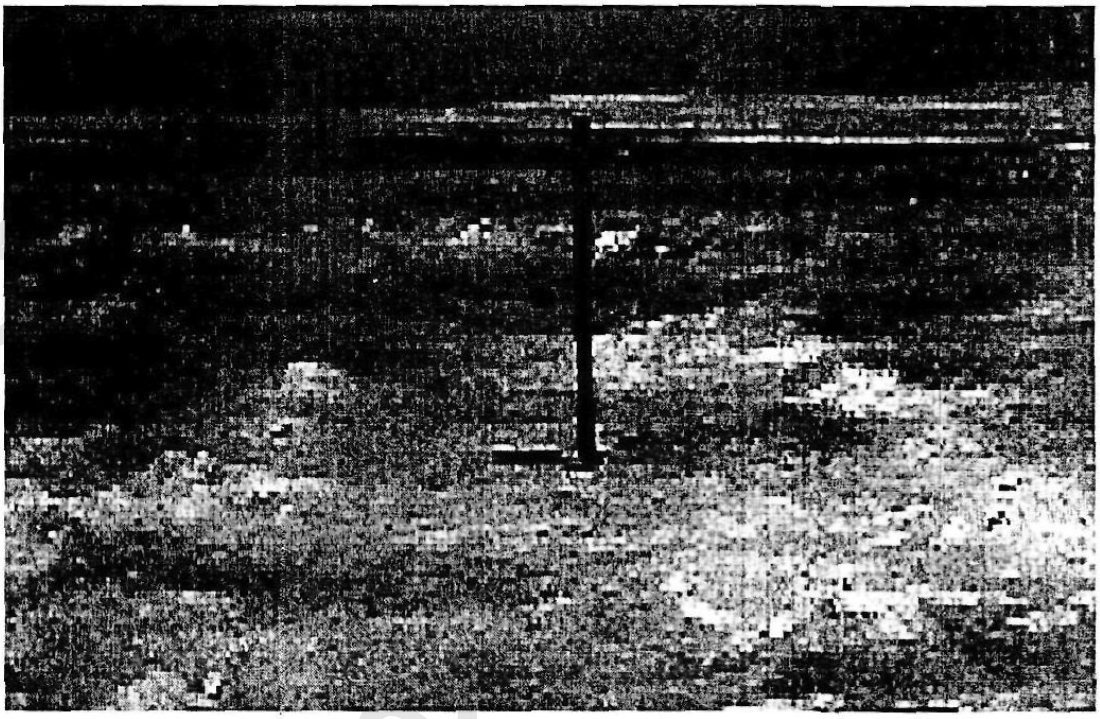

Figure –24A : *Photomicrograph showing Eastern hypersaline pan.* Notice different elevation due to saturation caused by slope

Figure -26: Photomicrograph shows the Tepee structure completely cover the outer margin Zone of the sabkha (zone-I)

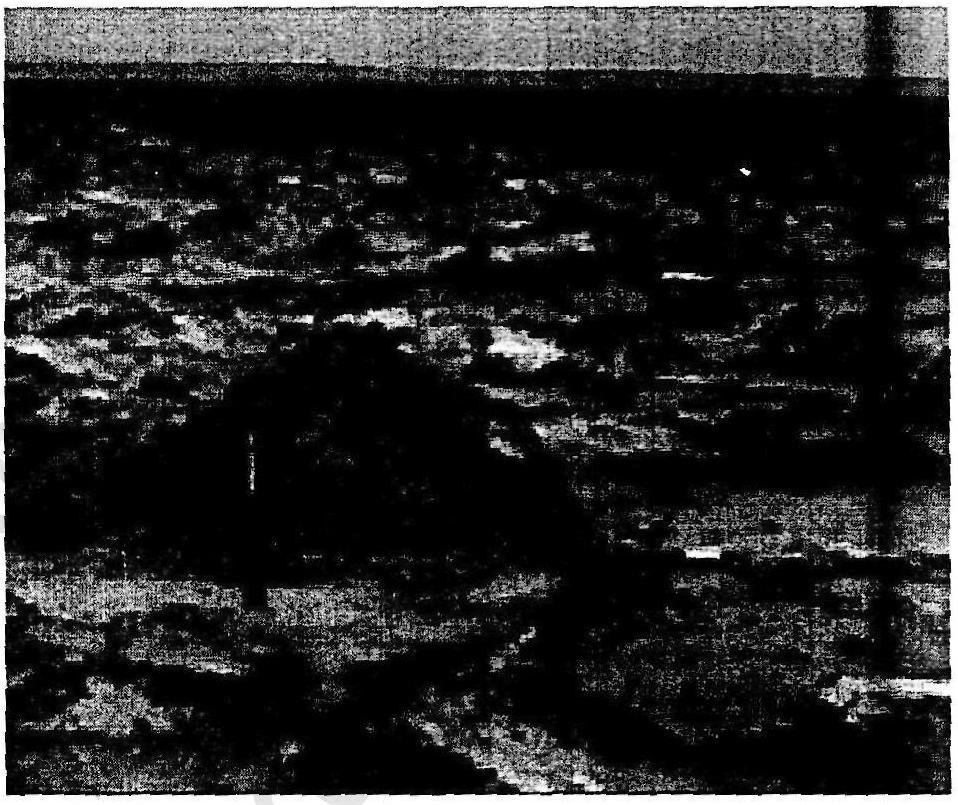

Figure-27 : Photomicrograph showing Tepee structure front rough crusting with hard veneer of crystalline salt. Topography located at the outer zone with hard veneer

Figure-28: Photomicrograph showing Halophyta surrounded the small seasonal saline hypersaline ponds in intermediate zone

Figure –29 : Photomicrograph showing gypsum mounds that cover most of the intermediate central zone at Ras Shukeir sabkha

Figure-30 : Photomicrograph showing the disc or circular shape of gypsum mounds with open crest due to pressure and gas escape.

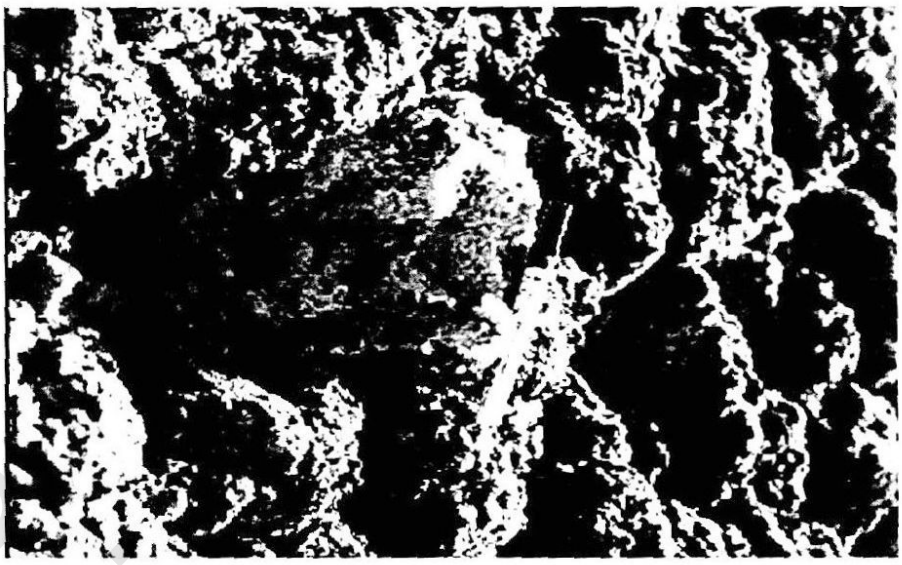

Figure-31: Photomicrograph showing radiating growth of gypsum starting from center . Notice the green coloration due to algae.

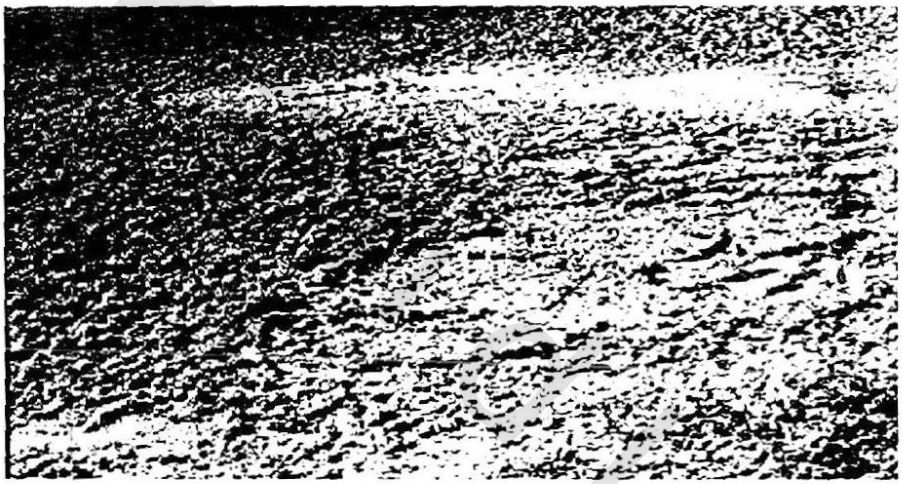

Figure-32: Photomicrograph showing the mud mound which cover the marginal of the hypersaline pans at the intermediate zone

Figure-33: Photomicrograph showing the solar pans field with tomato soap color brine due to flourishing of green algae

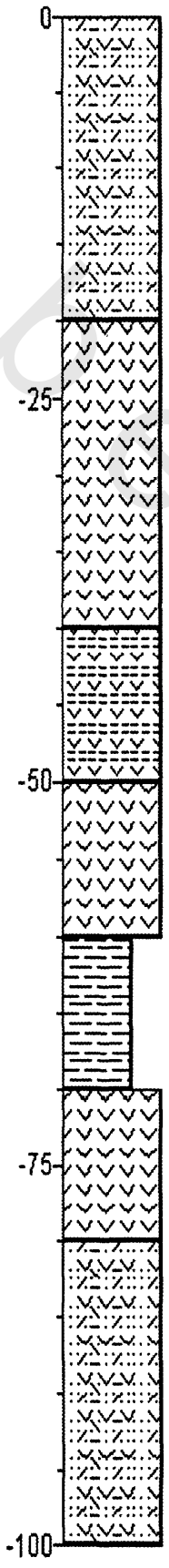

Sandstone: yellow, fine grain, will sorted, friable with gypsum crystals and scattered grganic materials

Gypsum: white, hard crystalline.

Laminated sand and algal filamintus with massive gypsum

Sandy gypsum with algal filamintus

Claystone: green-grey, wet with algal filamintus

Gysum : pure crystalline , white

Gysum : silt to fine crystals with dark clay and algal filamintus

Figure-34: Stratigraphic sequence and associated facies forTrench, Ras Shukeir sabkha

Figure - 35: Flow Chart Represent The Applied Technique Of The Present Work

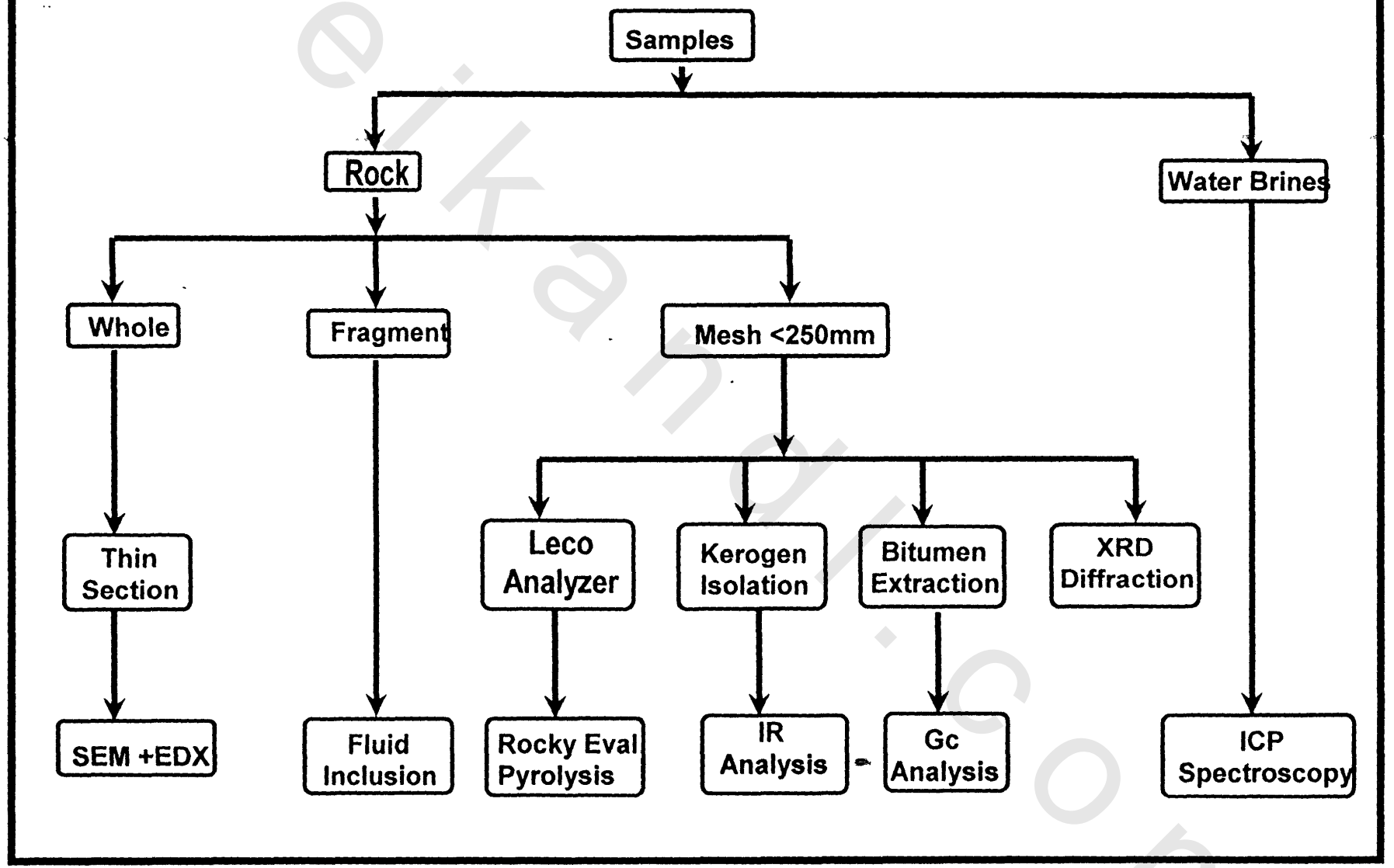

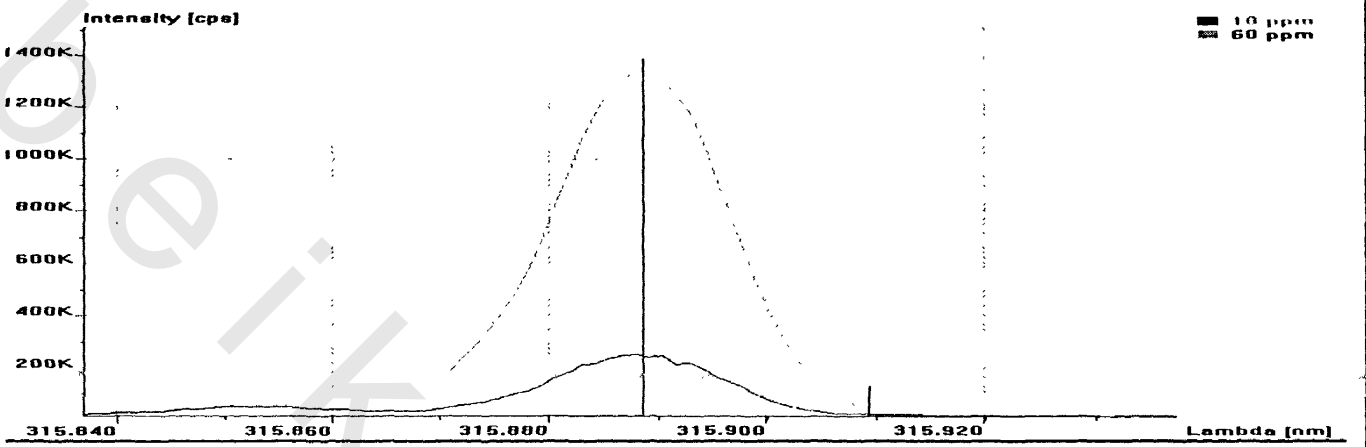

Figure -36: Scanning of calcium line with two different calcium standards.

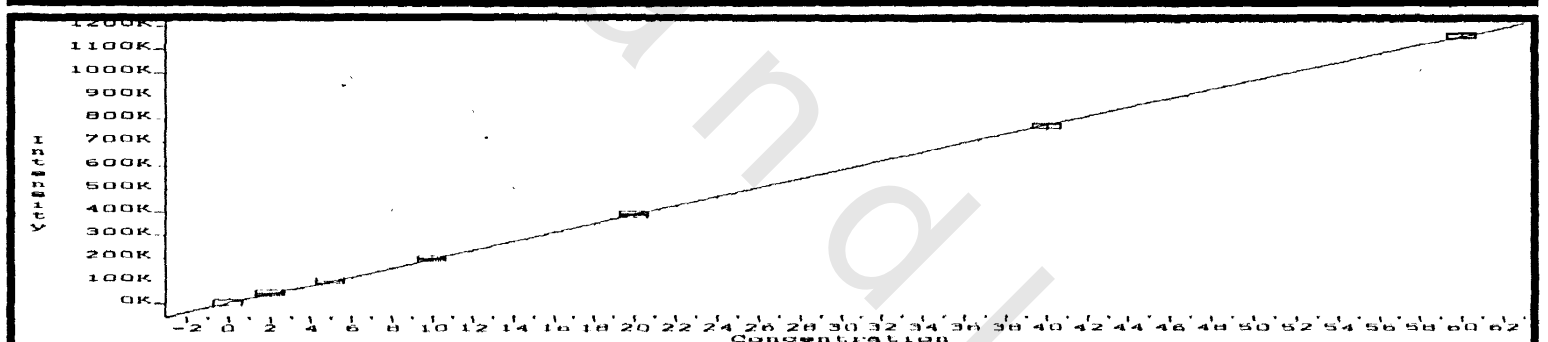

BEC :	0.88688	Range :	0.0035506 - 72.0000	A0 : -0.1130	
DL :	0.0035506	Unit :	ppm	A1 : 0.000051884	
Std.error :	0.22807	Weighting :	Manual	A2 : 0.0	
Corr.coef. :	1.0000			A3 : 0.0	

Standard	Weight	Intensity	Cert.conc.	Calc.conc.	Diff.	Rel. diff.
W-98-blank	20	1977	0.0	-0.01045	-0.01045	-
W-98-2 ppm	1.0	44555	2.00000	2.19866	0.19866	9.93280%
W-98- 5 ppm	1.0	101373	5.00000	5.14660	0.14660	2.93192%
W-98- 10 PPM	1.0	197011	10.0000	10.1086	0.10863	1.08633%
W-98- 20 PPM	1.0	385052	20.0000	19.8649	-0.1351	-0.6755%
W-98- 40 PPM	1.0	766575	40.0000	39.6597	-0.3403	-0.8507%
W-98- 60 PPM	1.0	1163055	60.0000	60.2306	0.23057	0.38429%

Figure -37: Calibration curve of the method of determination of calcium ion concentration

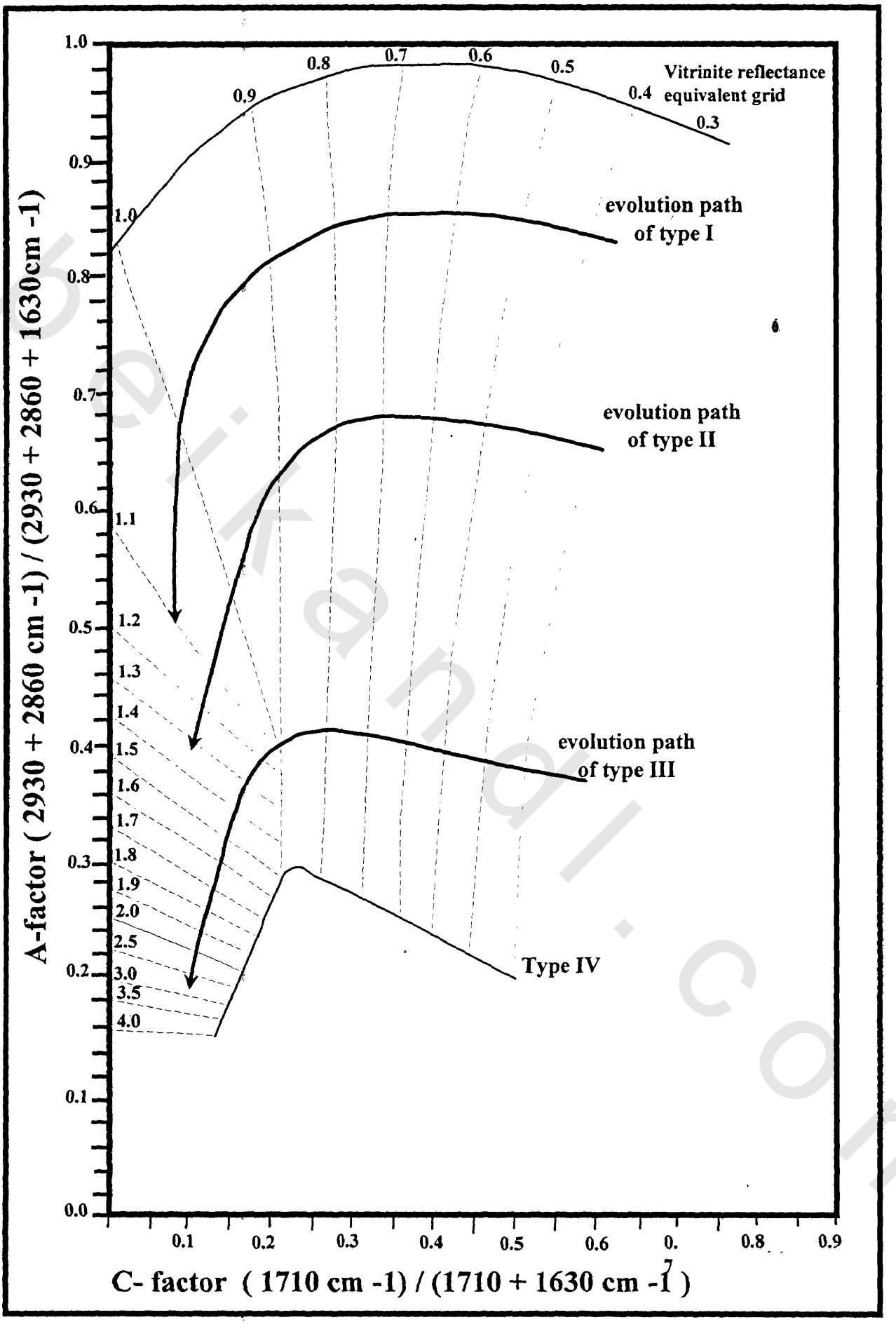

Figure-38 : Infrared modified diagram

PLATE-1

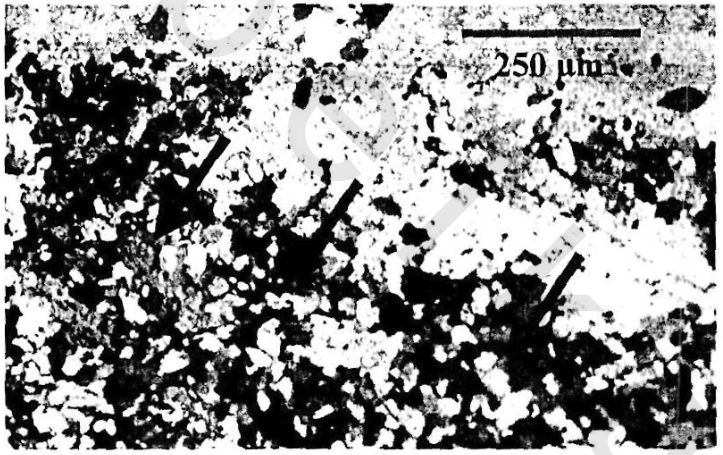

Figure-A: Photomicrograph showing a part of large, irregular xenotopic gypsum that brecciated and disintegrated into microcrystalline secondary gypsum. Nicols Crossed (N.C.).

Figure-C: Photomicrograph showing a disintegrated part of felty prismatic granular gypsum into microcrystalline secondary gypsum and anhydrite (arrows), (N.C.).

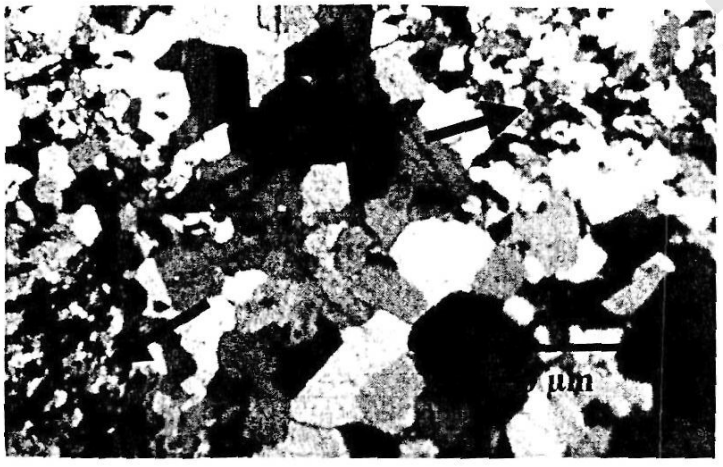

Figure-B: Photomicrograph showing disintegrated and transformed prismatic granular gypsum into microcrystalline secondary gypsum aggregates (arrows), (N.C.).

Figure-D: Photomicrograph showing a thin part of intercrystalline clays enriched in black,opaque organic matter (arrows) , (N.C.) .

PLATE-2

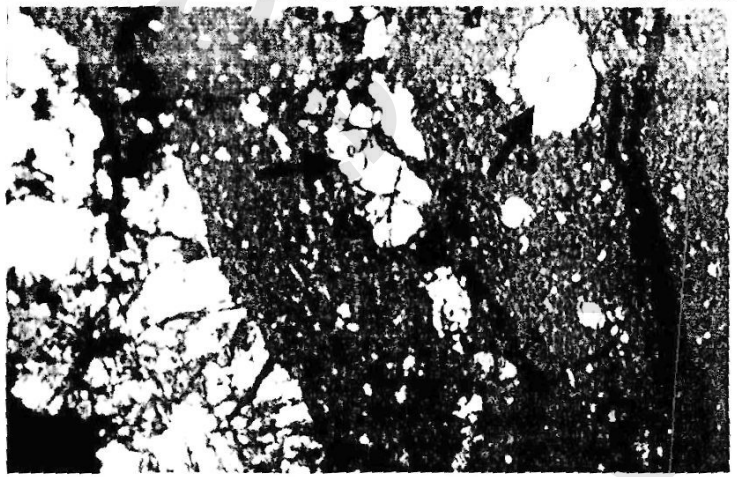

Figure-A: Photomicrograph displaying a part thin clay streaks enriched in black,opaque organic matter and enclosed nodular pattern of composite gypsum (arrows) , (N.C.).

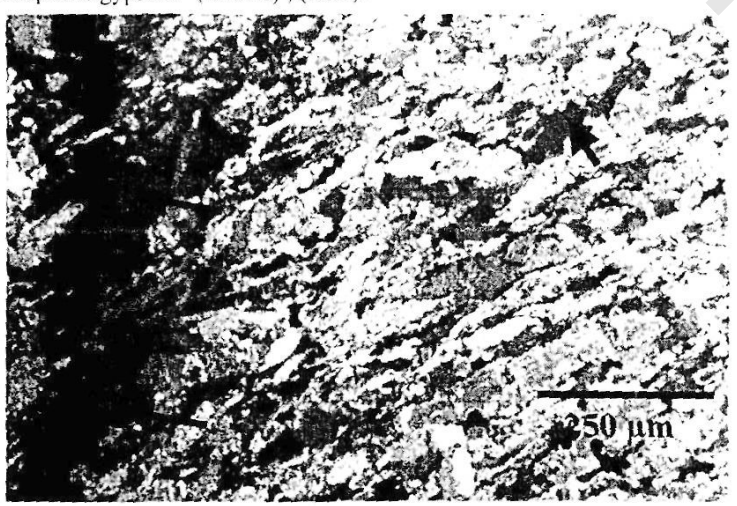

Figure-B: Photomicrograph displaying a part of thin intercrystalline clay streaks enriched in black,opaque organic matter (arrows) , (N.C.).

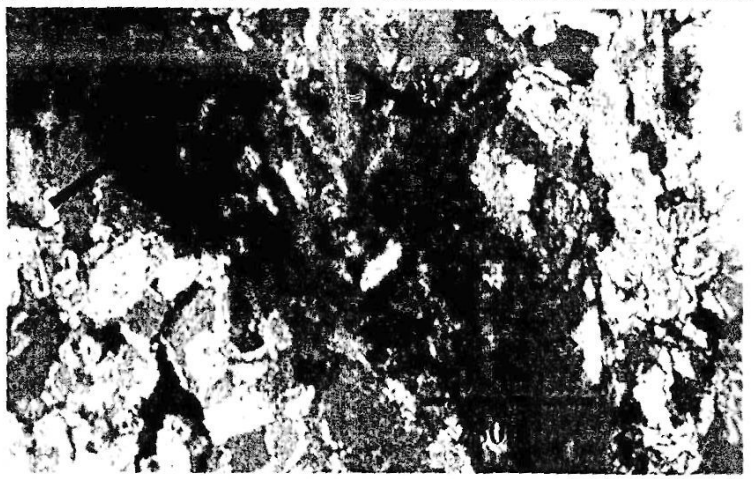

Figure-C: Photomicrograph displaying a part of thin intercrystalline clay streaks enriched in black,opaque organic matter (arrows) , (N.C.).

Figure-D: Photomicrograph showing large swallow-tail gypsum refilled small fractured in anhydrite (arrows), (N.C.).

PLATE-3

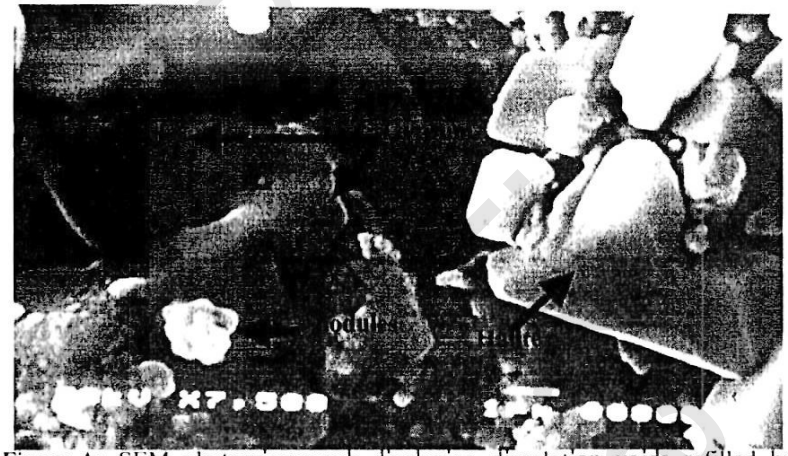

Figure-A: SEM photomicrograph displaying dissolution voids refilled by deformed secondary prismatic gypsum due to pressure growth, which partly transformed into fine nodular gypsum/anhydrite (white arrows) as well as the halite (yellow arrow)

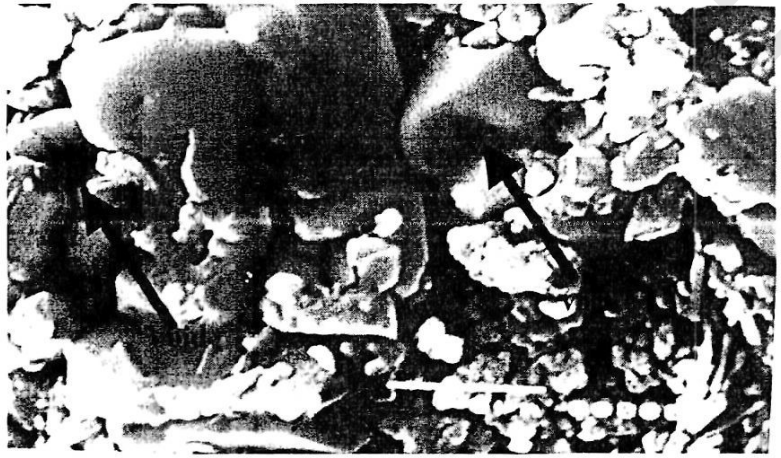

Figure-B: SEM photomicrograph showing micro-dissolution voids refilled by deformed and etched (small voids) secondary prismatic gypsum due to pressure growth, which partly transformed into fine nodular gypsum/anhydrite

Figure-C: Photomicrograph showing felty, epigenetic anhydrite of stellate texture that brecciated (arrows) into microcrystalline anhydrite aggregates, (N. C).

Figure-D: Photomicrograph showing pesudomorph gypsum now anhydrite forming nodule corroded at periphery embedded in carbonate host sediments, (N. C).

PLATE-4

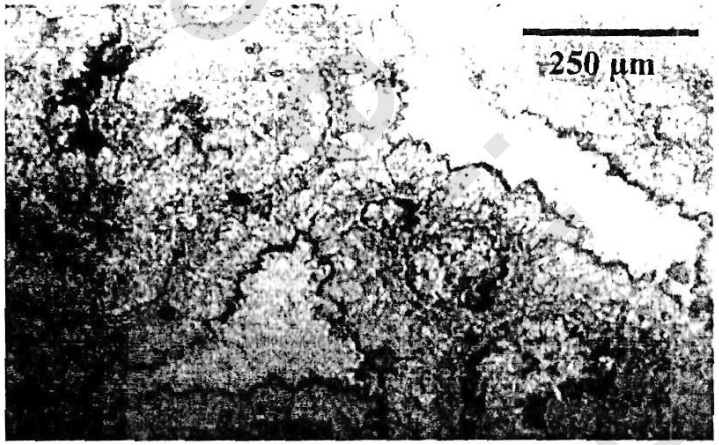

Figure-A: *Photomicrograph showing pesudomorph bioclast of different* types replaced and embedded in carbonate sediments, (N. C).

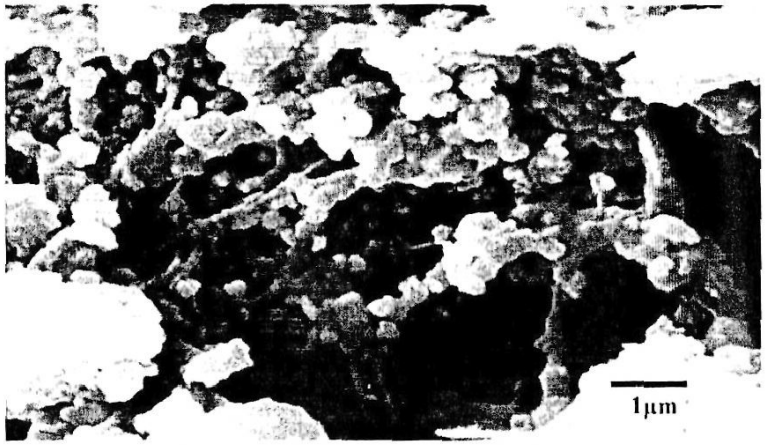

Figure-C : *SEM photomicrograph displaying the detailed structure of the* stromatolites (algae) completely replaced by anhydrite

Figure-B: Photomicrograph showing pesudomorph bioclast of different types replaced by fibrous gypsum and embedded in carbonate sediments, (N. C).

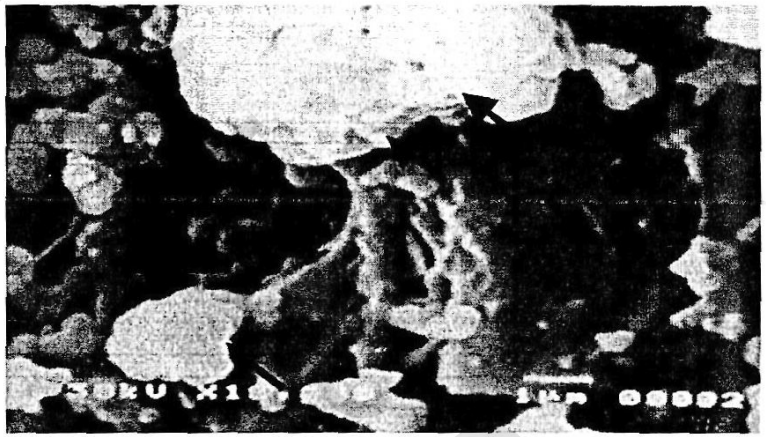

Figure-D : SEM photomicrograph displaying microbial matt (arrows) and algal matt embedded in Biogenic limestone.

PLATE-5

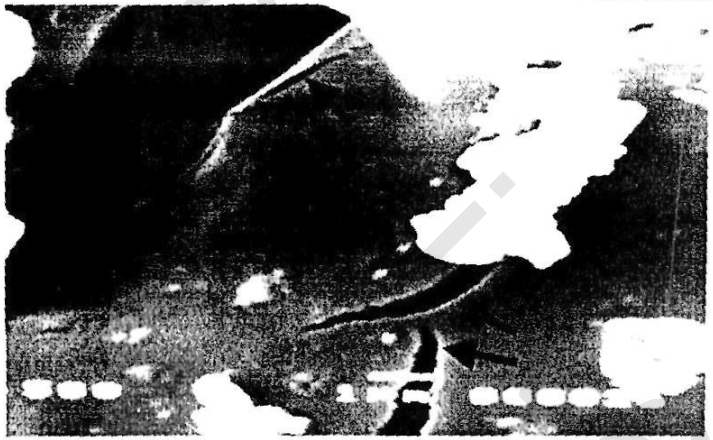

Figure-A : SEM photomicrograph displaying rupturing (arrows) of biocapsule with cavoli structure due to biogas escaping in the Biogenic limestone facies.

Figure-C: Photomicrograph showing a part of anhydrite nodule composed of step stair (white arrows) anhydrite crystals in crystalline carbonate that partly corroded it (yellow arrows) , (N. C).

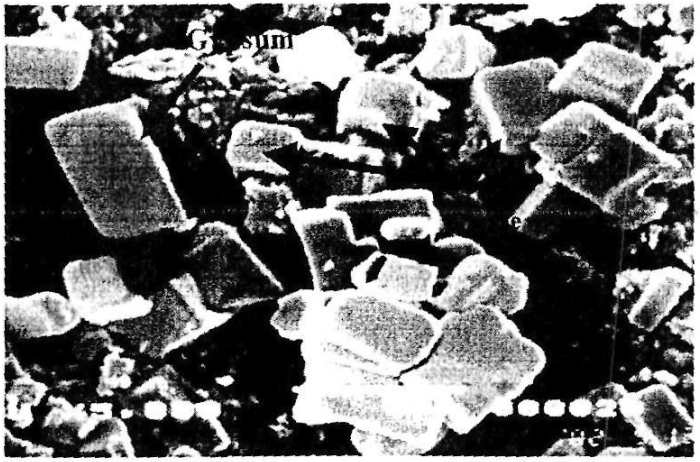

Figure-B : SEM photomicrograph displaying halite crystals replacing anhydrite as well as prismatic gypsum (arrows)

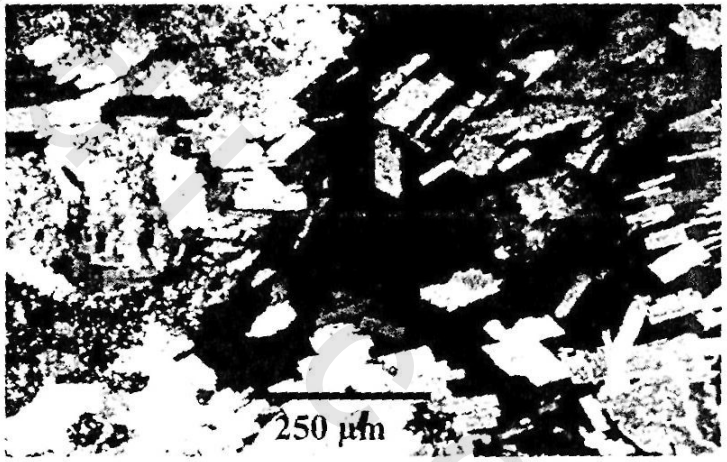

Figure-D: Photomicrograph showing a part of anhydrite nodule composed of anhydrite streaks with sweeping color and floating textured due to compression stress, (N. C).

PLATE-6

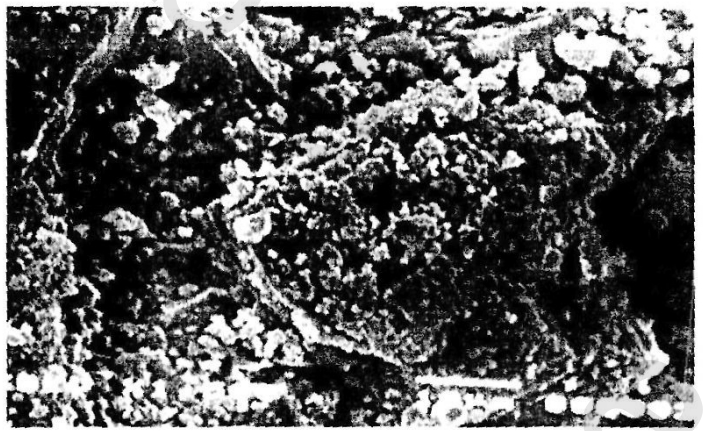

Figure-A: SEM photo showing anhydrite nodules displaying packed textured composed of very fine grained

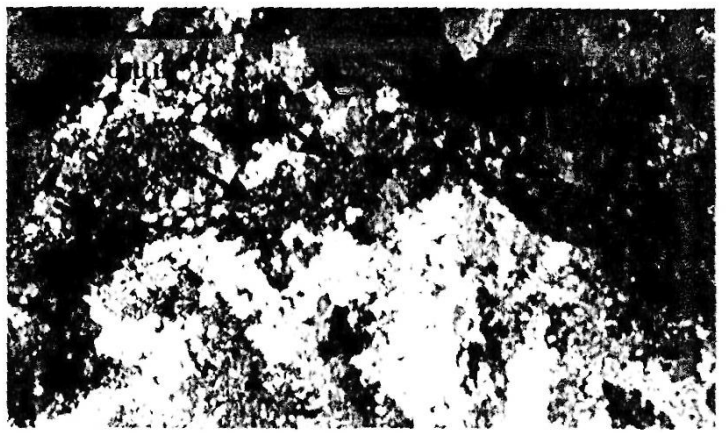

Figure-C: Photomicrograph showing a part of anhydrite nodule composed of amebiode gypsum pesudomorph with clays rich in organic that outline their shape (arrows) , (N. C).

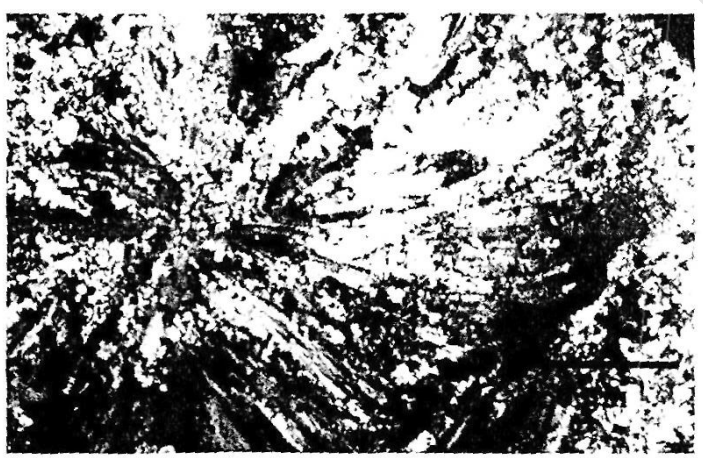

Figure-B : Photomicrograph showing anhydrite nodules mainly composed of felty epigenetic anhydrite with radial arrangement forming the stellate structure embedded in microcrystalline anhydrite lathes, (N. C).

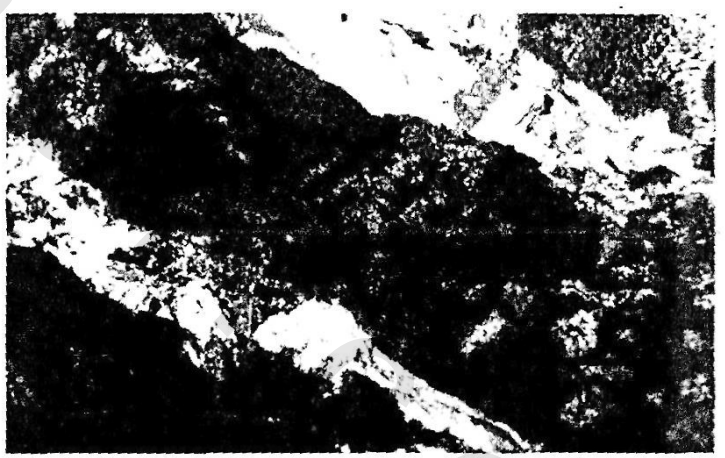

Figure-D: Photomicrograph showing the clay host evaporite enriched in dense, black and opaque organic material, (N. C).

PLATE-7

Figure-A: SEM photo showing a creeping structure displayed by anhydrite crystal (arrows) due to intense deformation resulted in compression stress

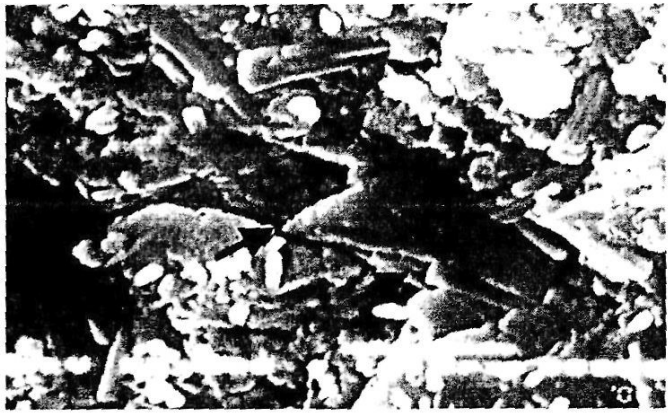

Figure-B: SEM photo showing a micro fracturing displayed by anhydrite crystal (arrows) due to intense deformation resulted in compression stress

Figure-C: SEM photomicrograph displaying the algal filamentus glue together forming algal matt and frambiodal pyrite embedded in evaporite

Figure-D: SEM photo showing the spheroid-shape of microbial matt and the pyrite rhombs embedded and replaced the anhydrite

PLATE-8

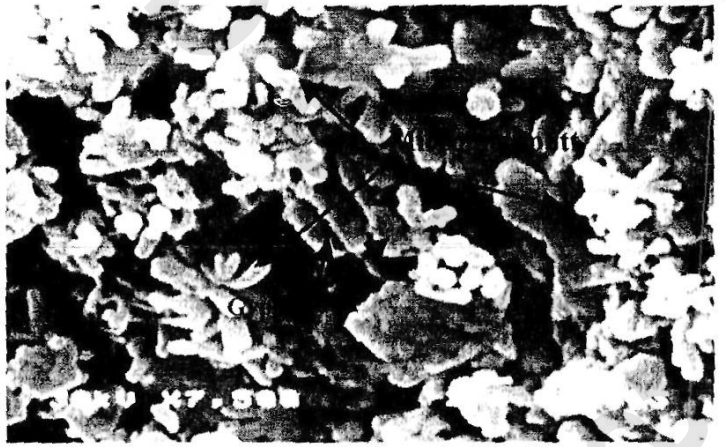

Figure-A: SEM photo micrograph displaying the rode shaped of the microbial matt enriched anhydrite in association with prismatic secondary gypsum that replace anhydrite

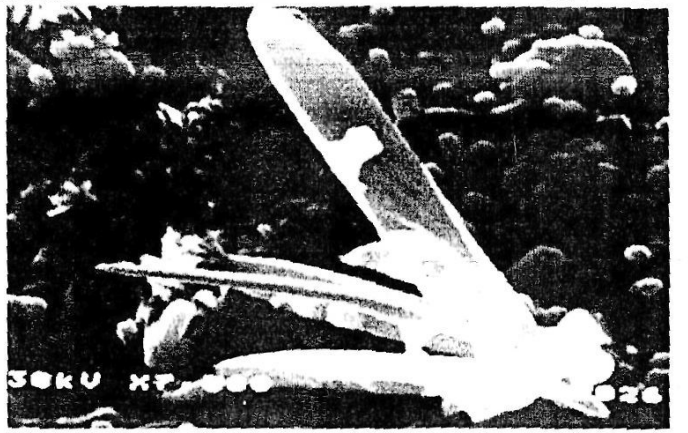

Figure-C: SEM photomicrograpoh showing lenticular gypsum in association with microbial matt embedded in anhydrite

Figure-B: SEM photo micrograph displaying the bio mineralized bio-capsule embedded in anhydrite sediments

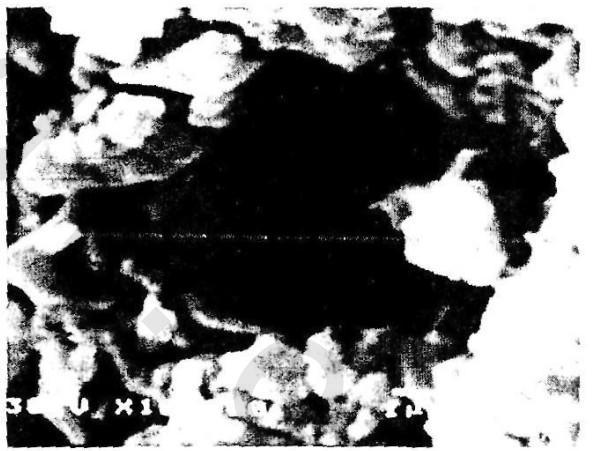

Figure-D: SEM photomicrograph showing irregular steep shaped voids , which believed to be due to the dissolutions of pre-existing halite that replaced former anhydrite.

PLATE-9

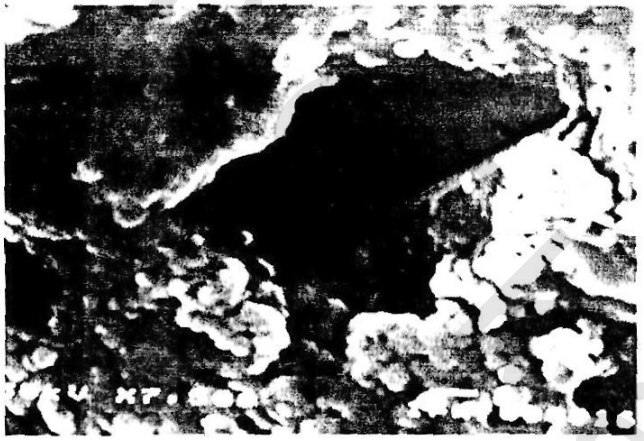

Figure-A: SEM photo showing square steep shaped voids , which believed to be due to the dissolutions of pre-existing halite that replaced former anhydrite.

Figure-C: Photomicrograph showing a part of anhydrite nodule composed of swallow-tail gypsum pesudomorph in association with microcrystalline anhydrite laminae and dark, opaque and dense organic rich material occupying the intercrystalline spaces, (N. C).

Figure-B: SEM photo showing a part of halite hopper replacing and displacing anhydrite NB the microbial matt upper left.

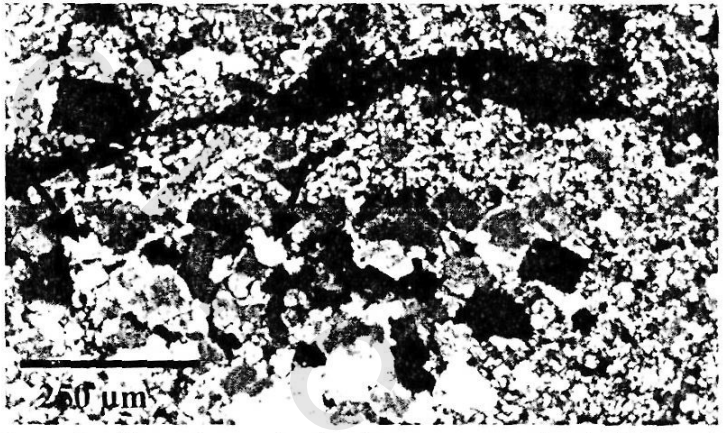

Figure-D: Photomicrograph showing a part of anhydrite nodule composed of xenotopic anhydrite granular engulfed gypsum relics(arrows) in association with microcrystalline anhydrite laminae and dark, opaque and dense organic rich material occupying the interlamination, (N. C)..

PLATE-10

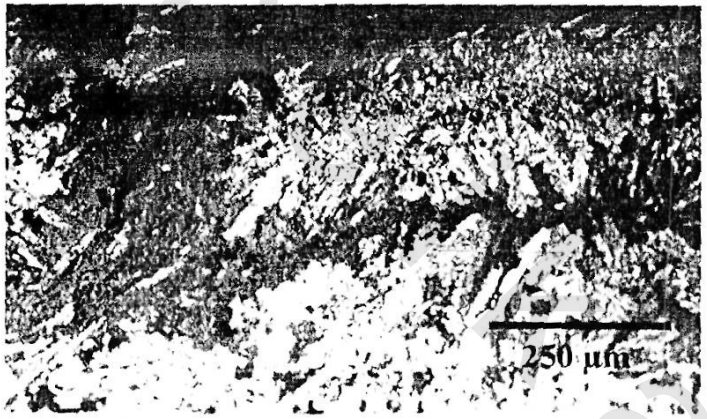

Figure-A: Photomicrograph showing elongated and coalesced anhydrite nodules composed of felty epigenetic anhydrite crystals engulfed gypsum and clay streaks enriched in dense, opaque organic material , (N. C).

Figure-C: SEM photo showing the dissolution of enclosed gypsum crystal along the old cleavage and lenticular gypsum filled voids (arrows)

Figure-B: Photomicrograph showing a part of anhydrite nodule composed of fibrous anhydrite crystals engulfed gypsum and bioclast completely replaced by carbonates (arrows) , (N. C)..

Figure-D: SEM photo showing the dissolution and disintegration into fine grained anhydrite (arrows) of enclosed gypsum crystal along the old cleavage

PLATE-II

Figure-A: Close-up view displaying the brecciation and disintegration of selenite at the periphery

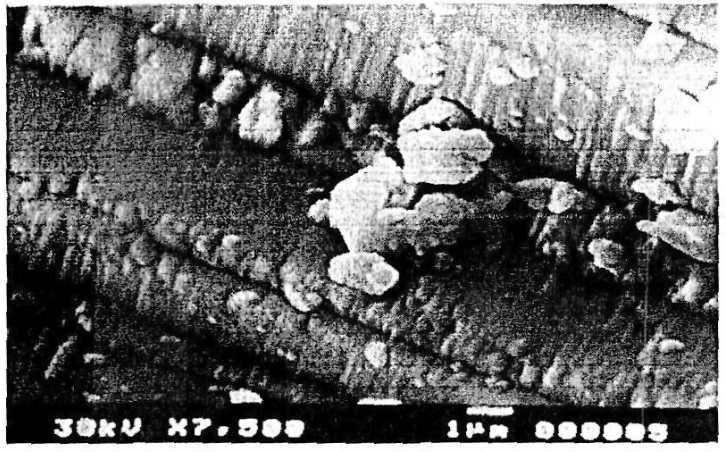

Figure-B: Close-up view displaying the brecciation and disintegration of selenite along the cleavage

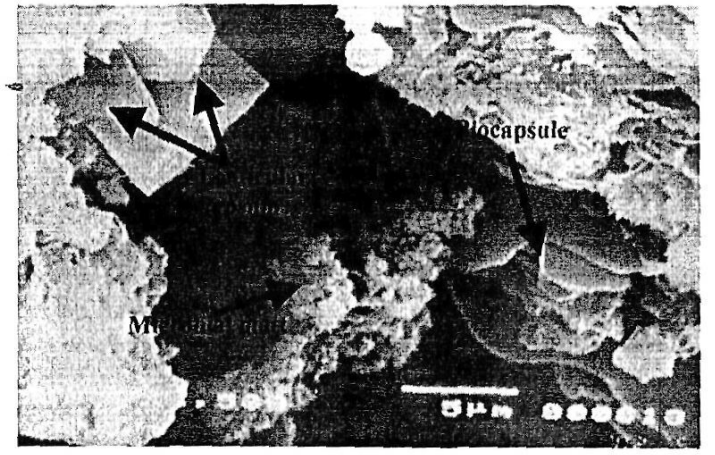

Figure-C: SEM photomicrograph showing the microbial matt and biocapsule in association with lenticular gypsum embedded in anhydrite.

Figure-D : SEM photo showing the algal remain embedded in anhydrite.

PIATE-12

Figure-A: SEM photomicrograph showing algal matt entrapped by fine grained anhydrite

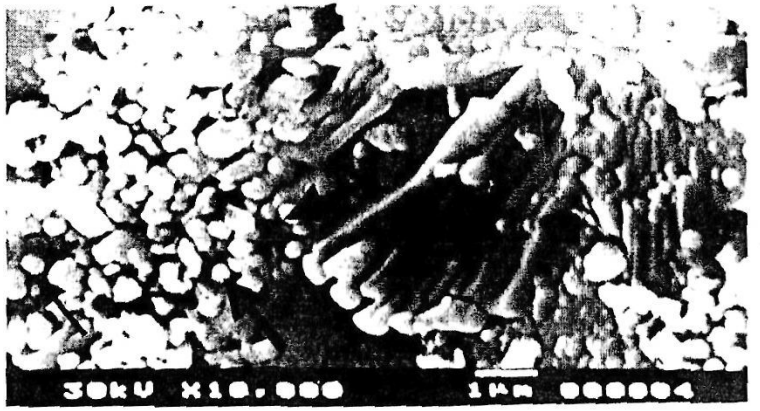

Figure-C: SEM photomicrograph showing fibrous, straight and aligned gypsum of domal structure brecciated into fine anhydrite and mineralized fine spheroid –shaped microbial matt(arrows) embedded in anhydrite

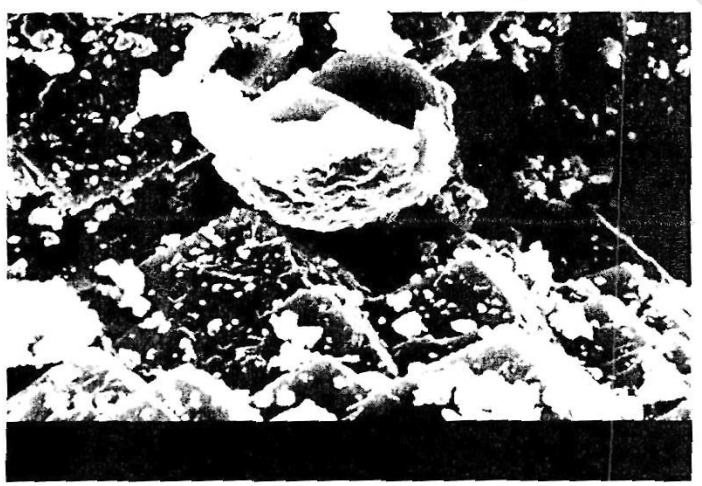

Figure-B: SEM photomicrograph showing creeping structure of the idiotopic prismatic gypsum transformed into fine anhydrite and biocapsule retaining some original textured of the organisms.

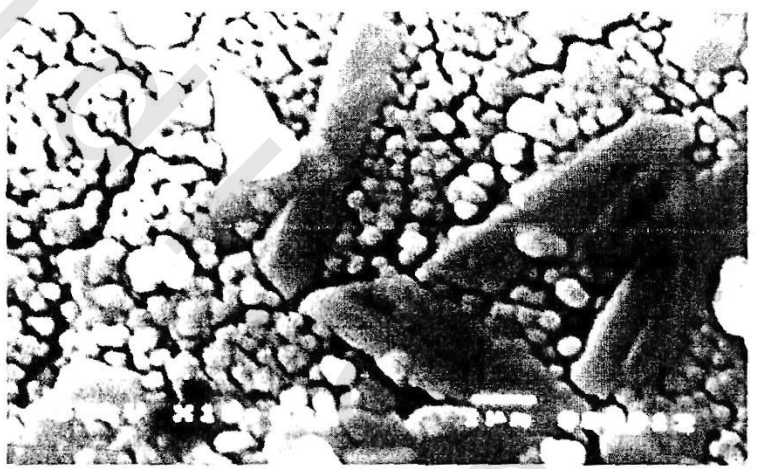

Figured-D : SEM photomicrograph displaying prismatic secondary gypsum replacing fine grained anhydrite nodules

PIATE-13

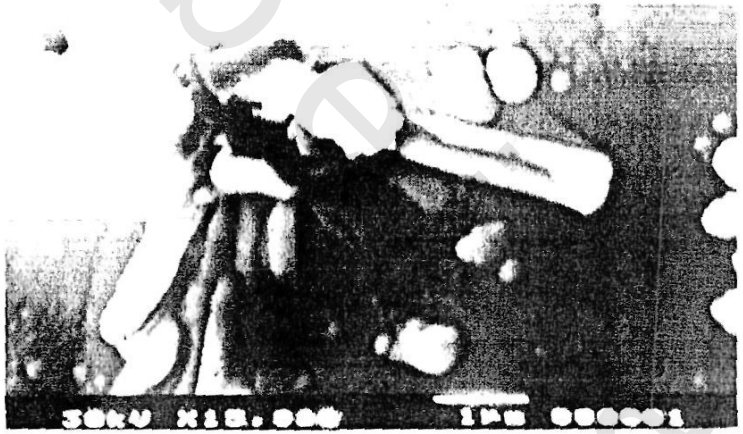

Figure-A: SEM photo displaying irregular dissolution vugs of anhydrite refilled by idiotopic prismatic secondary gypsum and fine secondary anhydrite

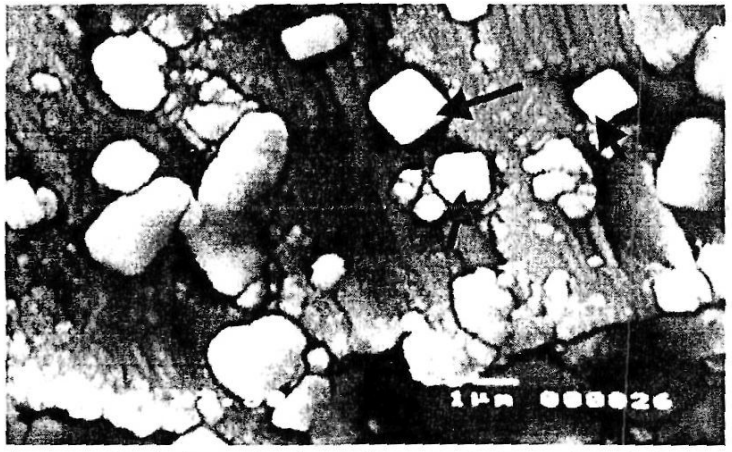

Figure-B: SEM photo showing halite crystals (arrows) replacing and displacing the anhydrite after gypsum indicating the pre-existing the hypersaline conditions

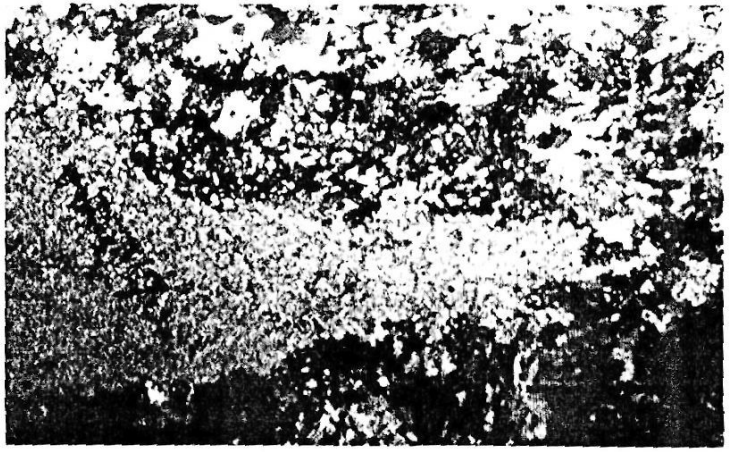

Figure-C: Photomicrograph showing a part of stressed, deformed idiotopic prismatic gypsum nodules and squeezed clays due to effect of deformation stress, (N.C.).

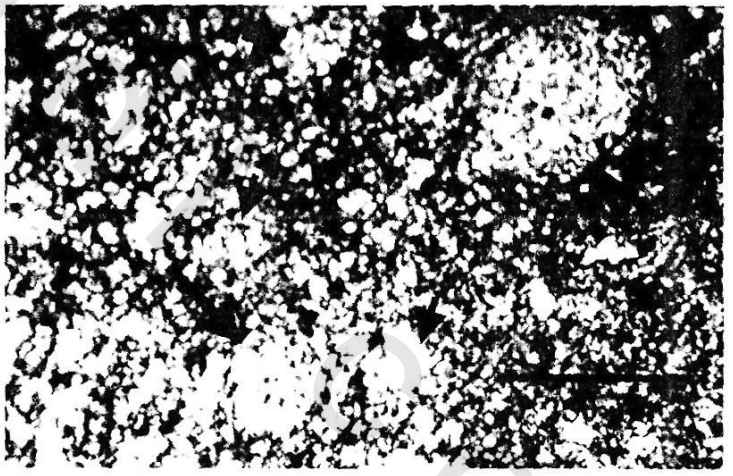

Figure-D: Photomicrograph showing rounded, scattered small gypsum nodules floating in clay which rich in opaque, black and dense organic material, (N.C.)..

PIATE-14

Figure-A: Photomicrograph showing swallow-tail gypsum crystal brecciated and disintegrated into fine granular aggregates secondary gypsum, (N.C.).

Figure-C: Photomicrograph showing gypsum nodules composed of fibrous , radially oriented gypsum forming stellate textured with dark black clay with organic rich material, (N.C.).

Figure-B: Photomicrograph showing nodular laminated gypsum with black, clays rich in organic matter, (N.C.).

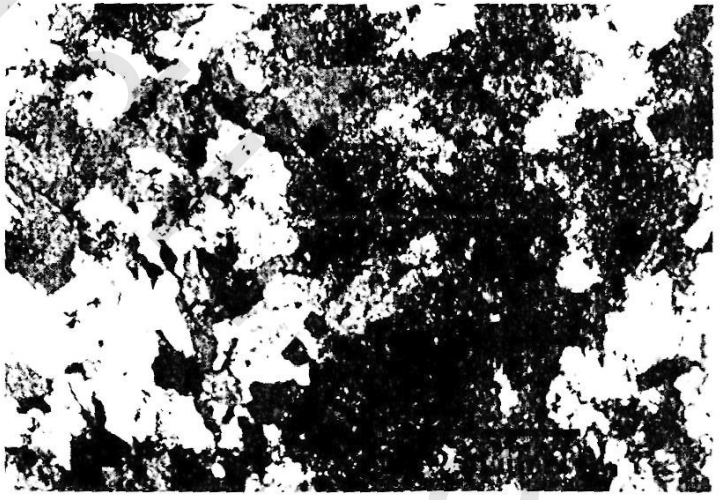

Figure-D: Photomicrograph displaying xenotopic granular gypsum engulfed dense and opaque organic rich material (arrows) , (N.C.).

PIATE-15

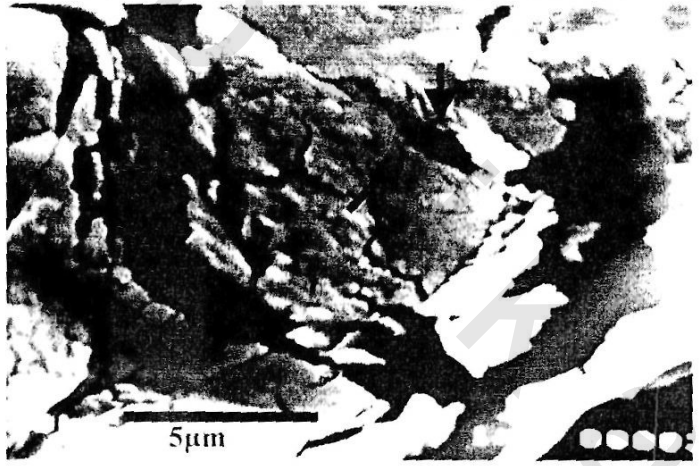

Figure-A: SEM photomicrograph showing cavoli-texture of biocapsule with rupturing the apex (arrows) due to biogas escaping in gypsum

Figure-C: SEM photomicrograph displaying microfolding deformation featured of prismatic gypsum due to deformation stress.

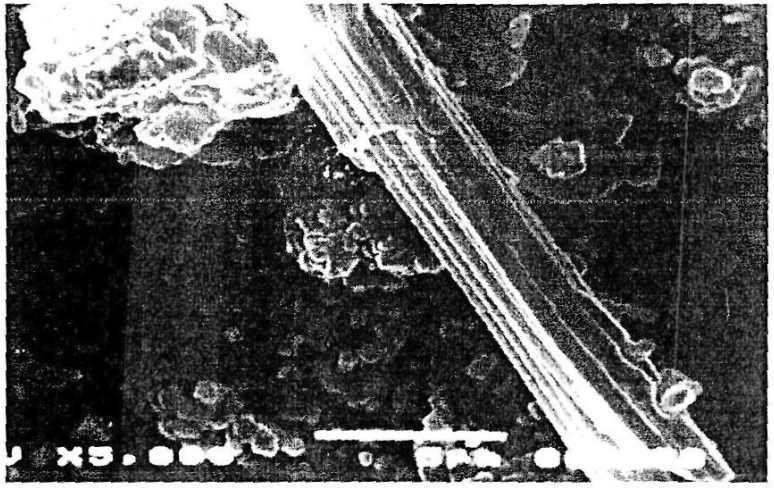

Figure-B: SEM photomicrograph showing mineralized algal remains (algal matt) in association with microbial matt embedded in gypsum

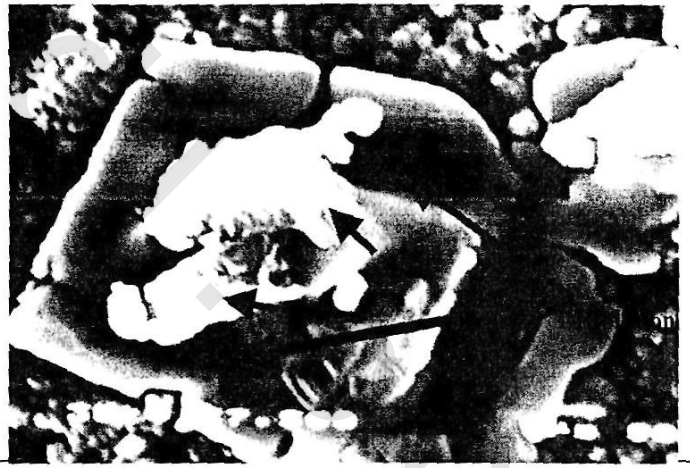

Figure-D: SEM photomicrograph showing a large idiotopic prismatic gypsum crystal fill vugs and etched by dissolution followed by recrystallization secondary generation (arrows)

PIATE-16

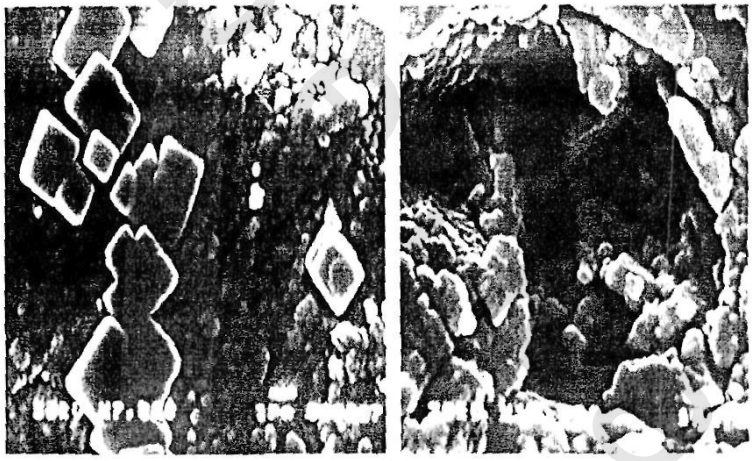

Figure-A: SEM photomicrograph displaying halite raft replace fine grained gypsum nodules and irregular step shaped voids resulted from dissolution of pre-existing halite

Figure-C: Photomicrograph showing randomly oriented , straight anhydrite crystals of massive textured engulfed some gypsum relics and dense, opaque organic rich material (arrows), (N.C.).

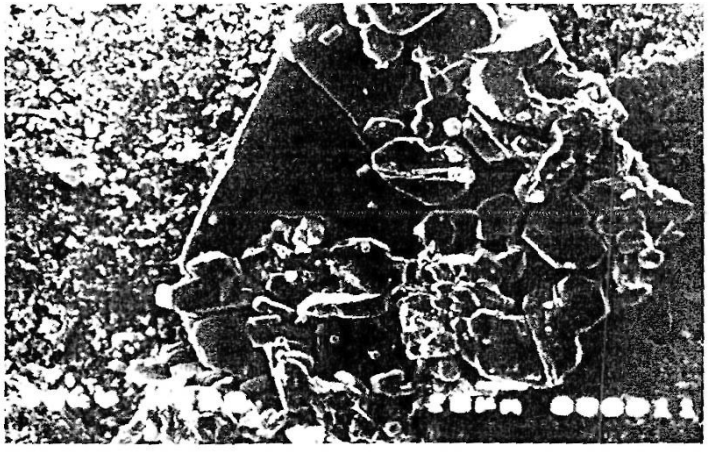

Figure-B: SEM photomicrograph displaying calcite xenomorphic textured completely replace the pre-existing evaporite nodules

Figure-D: Photomicrograph showing a part of contorted and convoluted pattern displayed by massive, felty epigenetic anhydrite enclosed clay rich in organic matter (arrows), (N.C.).

Figure-A: Photomicrograph unfilled fractured in a massive textured of felty anhydrite (arrows)), (N.C.).

Figure-C: Photomicrograph showing a part of deformed , wavy laminated felty anhydrite and thin laminae made of black, opaque and dense organic rich lamina , (N.C.).

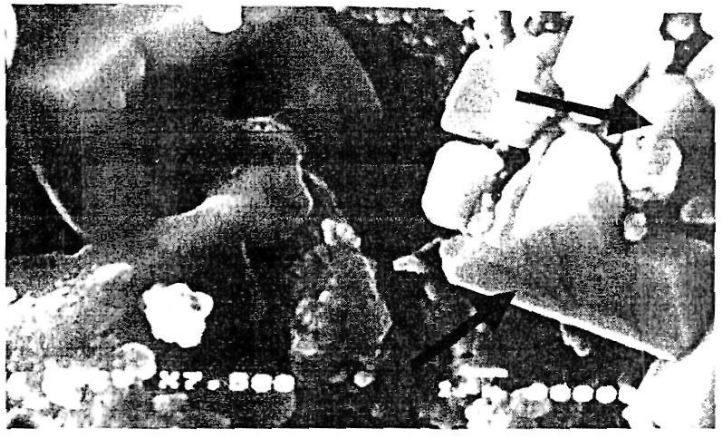

Figure-B: SEM photomicrograph showing a large idiotopic prismatic gypsum and deformed halite due to pressure growth (arrows).

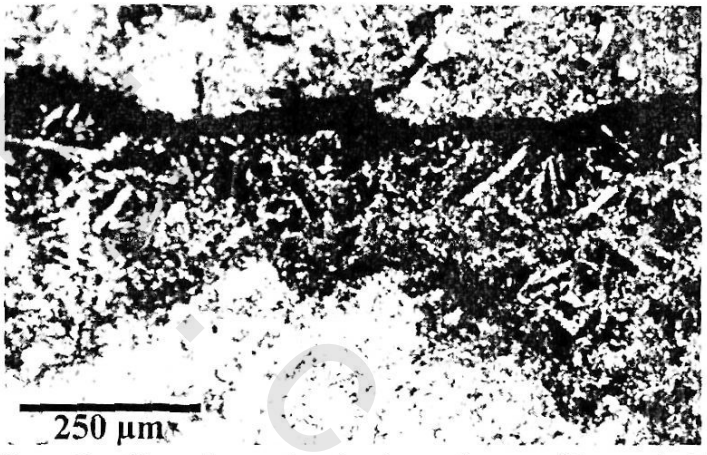

Figure-D: Photomicrograph showing microcrystalline anhydrite interlaminated with black, opaque and dense organic rich lamina engulfed fibrous gypsum crystals , (N.C.).

PIATE-18

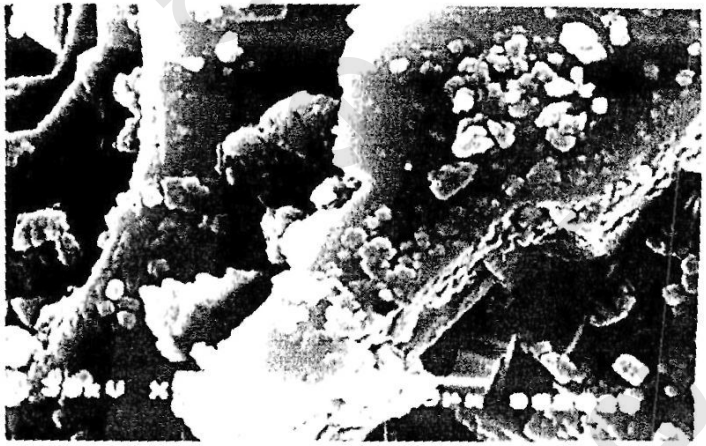

Figure-A: Closed up view displaying the enclosed gypsum by dense lamina that brecciated into fine sub-euhedral anhydrite

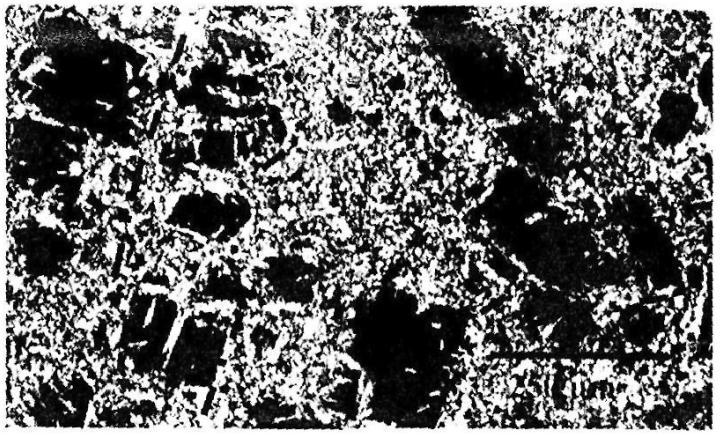

Figure-C: Photomicrograph showing irregular lamination of felty epigenetic anhydrite engulfed gypsum relics and halite, (N.C.).

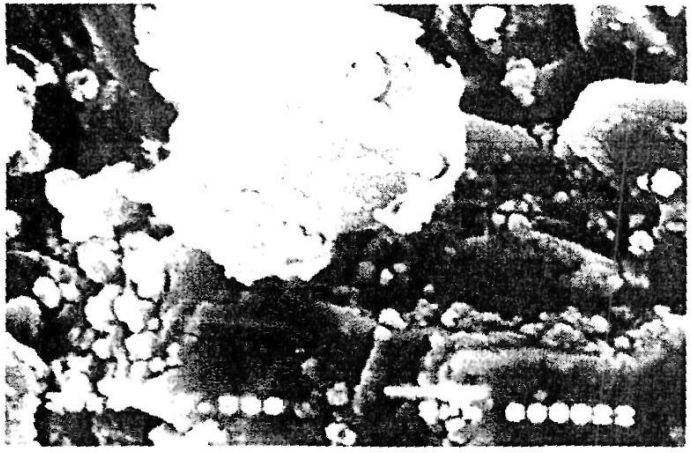

Figure-B: Closed up view displaying the enclosed biocapsule that enclosed by evaporite sediments.

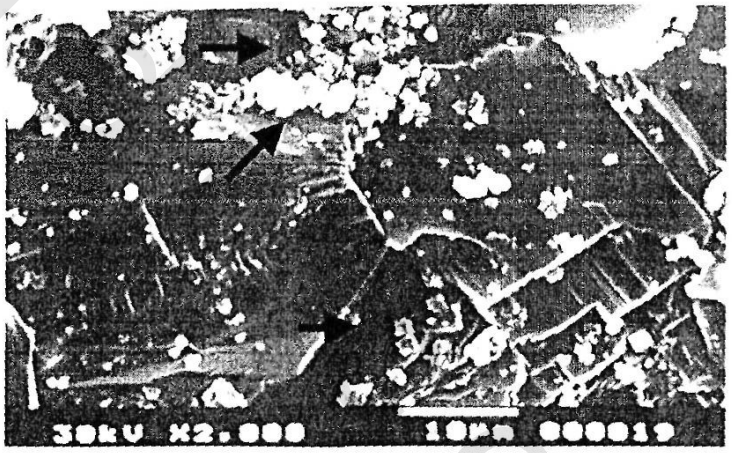

Figure-D: Close-up view displaying the enclosed gypsum relics and crystals that brecciated and disintegrated into euhedral anhydrite (arrows)

PIATE-19

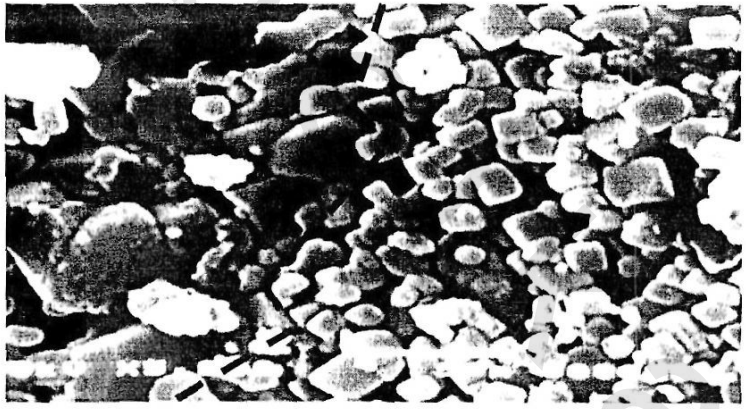

Figure-A: SEM photomicrograph showing a part of prismatic anhydrite laminae and halite cumulate laminae

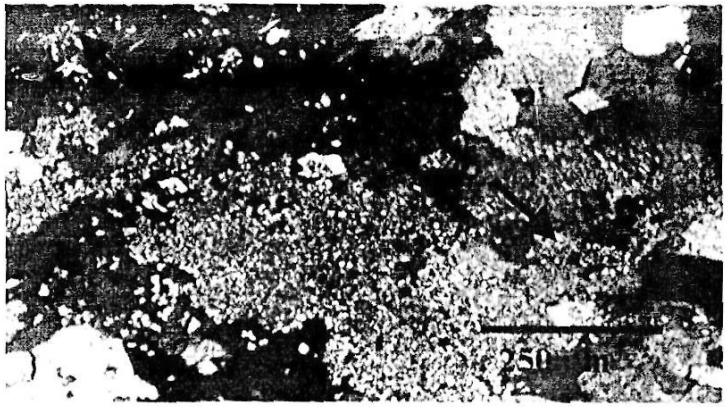

Figure-C: Photomicrograph large , interlocked, xenotopic granular gypsum crystals of slkenside texture enclosing lime mud carbonates, which partly corroded gypsum (arrows), (N.C.).

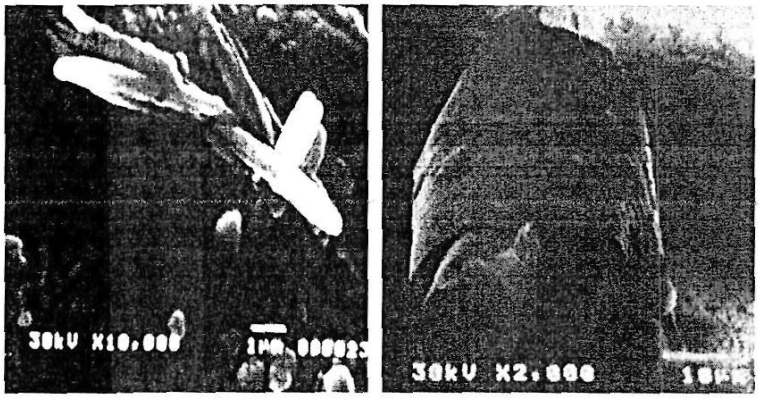

Figure-D: Close-up views displays lenticular gypsum (left) and biocapsule (right) embedded in anhydrite sediments

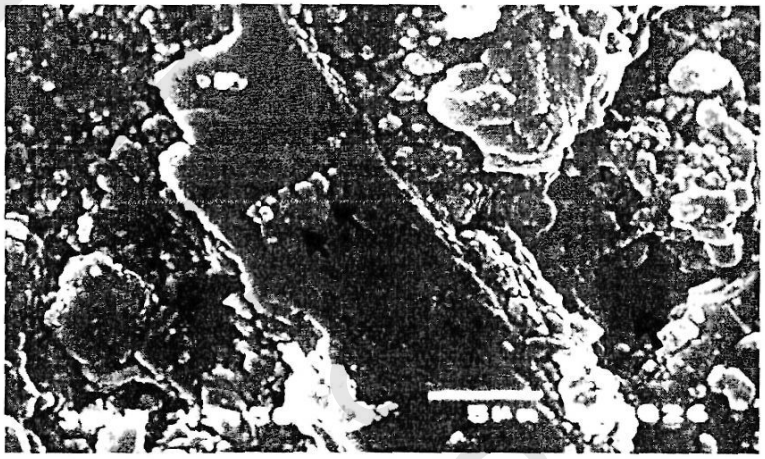

Figure-D: SEM photomicrograph showing coalesced nodules in association with idiotopic gypsum which disintegrated into sub-euhedral secondary gypsum (arrows) . NB. Step shaped voids , which probably due to dissolution of pre-existing halite.

PIATE-20

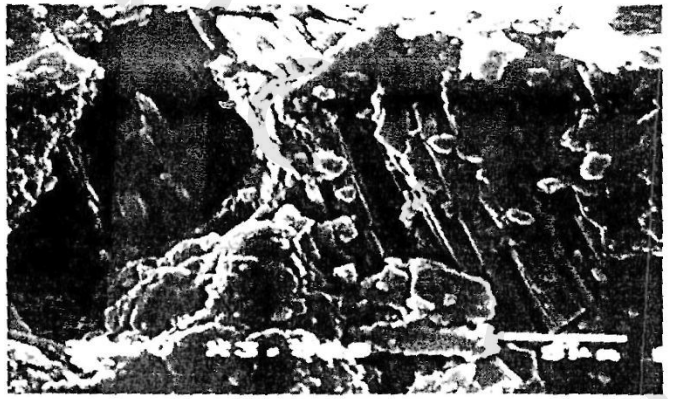

Figure-A: Close-up view showing a selenite (gypsum) crystal disintegrated into secondary gypsum along the cleavage and dissolution voids (Left)

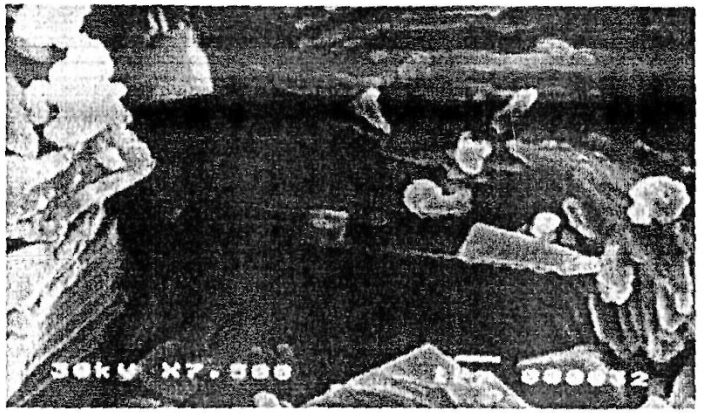

Figure-C: SEM photomicrograph showing the ductile behavior of gypsum that displaying folding textured due to compaction deformation process and dissolution along the old cleavage

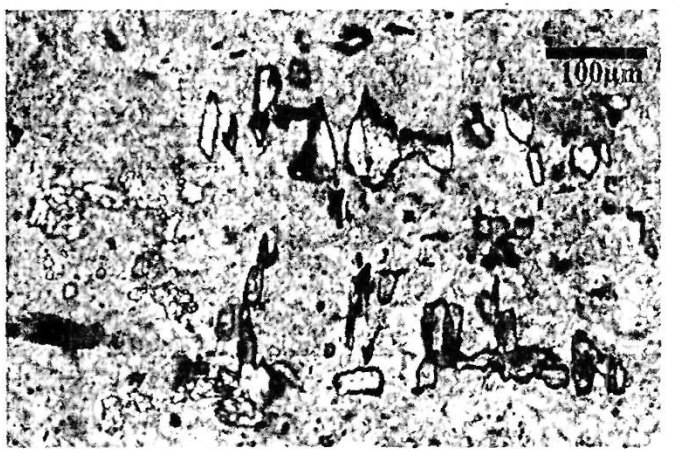

Figure-B: Photomicrograph displaying different size and shape of solid and liquid inclusions in xenotopic gypsum, (N.C.).

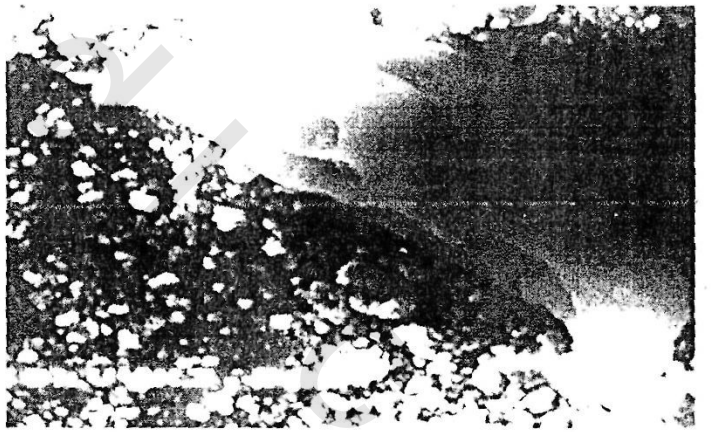

Figure-D: Close-up view showing bio-mineralized organic ghost of the algal filamentus and leafs embedded in gypsum

PIATE-21

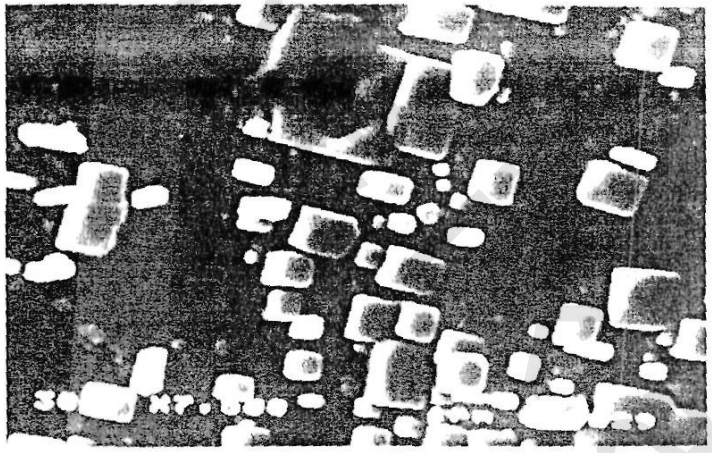

Figure-A: Close-up photomicrograph displaying halite crystals displaying *different size , which replacing the gypsum . NB. The rode-shape of the* microbial matt embedded in gypsum

Figure-C: Photomicrograph showing a part of fracture in anhydrite, which filled by fibrous, straight secondary gypsum that vertically oriented up on the *wall of the fracture*, (N.C.).

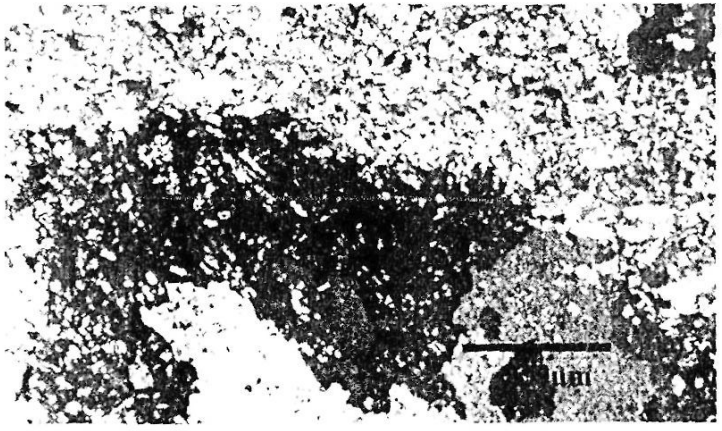

Figure-B: Thin section photomicrograph showing felty epigenetic anhydrite rehyderated into interlocked xenotopic secondary gypsum , *which contain relics of anhydrite indicating their epigenetic origin*, (N.C).

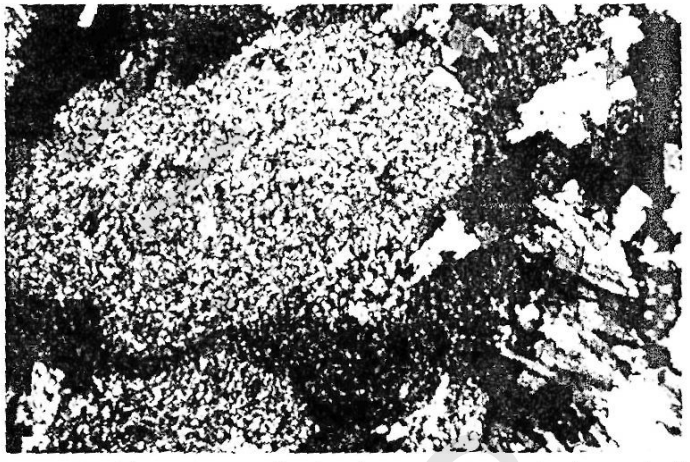

Figure-D: Photomicrograph showing a part of closely packed *anhydrite nodules that floating in clay matrix rich in organic* material, (N.C.).

PIATE-22

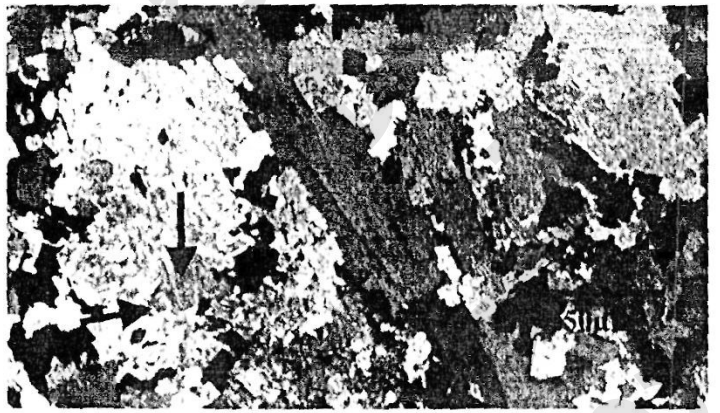

Figure-A: Photomicrograph showing a part of anhydrite nodule composed of xenotopic anhydrite granules that enclosed a gypsum relics (arrows), (N.C.).

Figure-B: Photomicrograph show anhydrite brecciated and rehyderated into microcrystalline gypsum and carbonate crystalline carbonates engulfed opaque organic material, (N.C.).

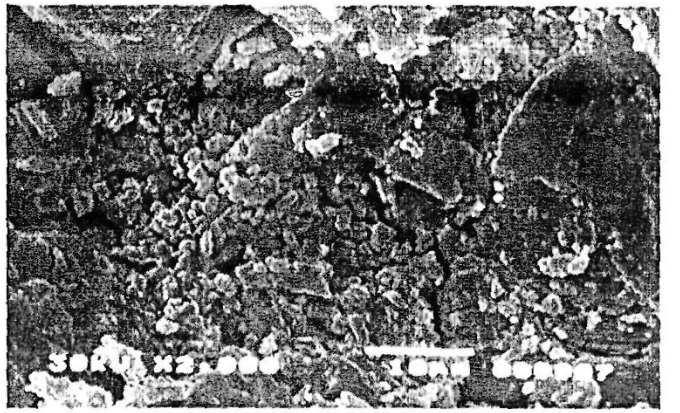

Figure-C: Close-up view showing the brecciation and rehydration of anhydrite into fine sub-euhedral secondary gypsum as indicated by minor cracking due to the difference in ionic radii.

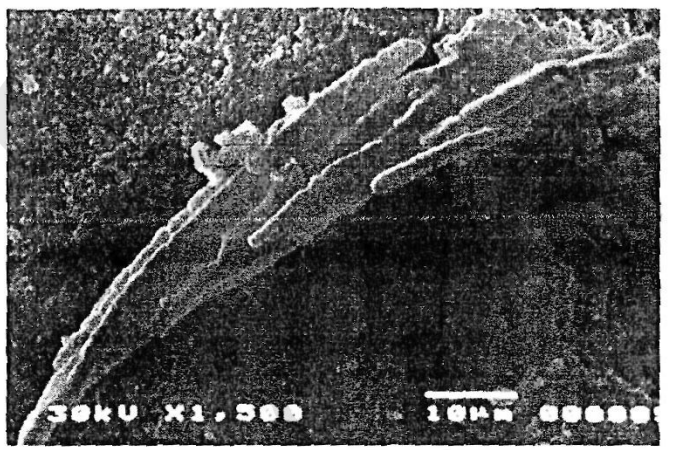

Figure-D: Close-up view showing bio-mineralized algal remains embedded in anhydrite

PLATE-24

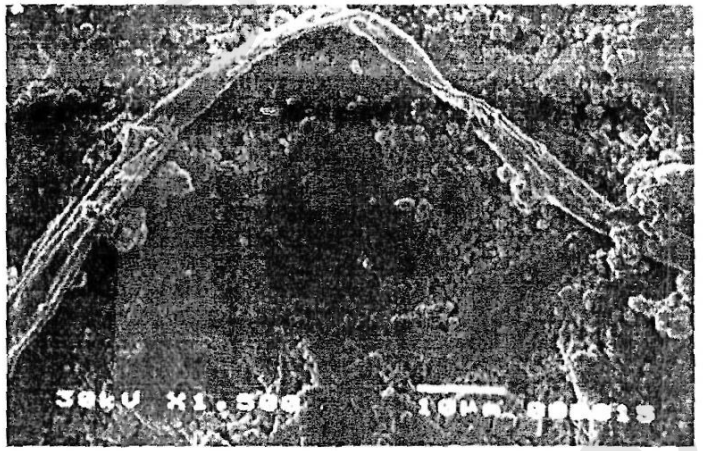

Figure-A: SEM photomicrograph showing the detailed structure of the algae that embedded in anhydrite.

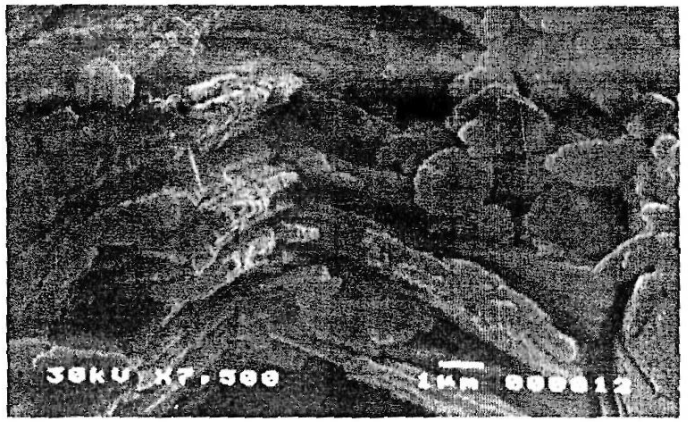

Figure-C: Close-up showing the deformation ruptured and brittles character of gypsum cased by compaction stress.

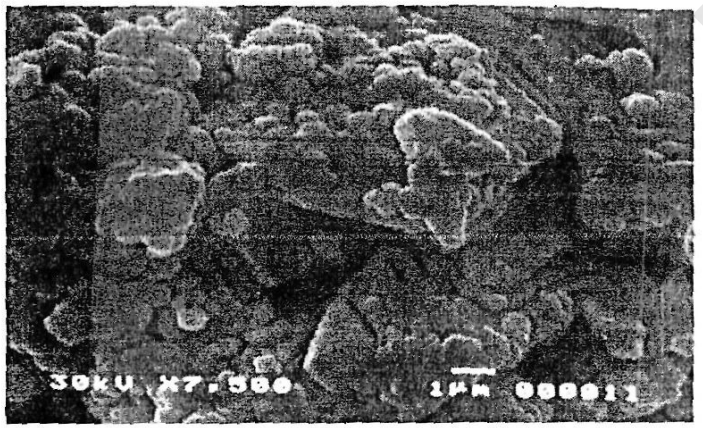

Figure-B: SEM photomicrograph displaying the microfolding and convolute texture of gypsum due to intensive deformation and voids as a result of dissolutions.

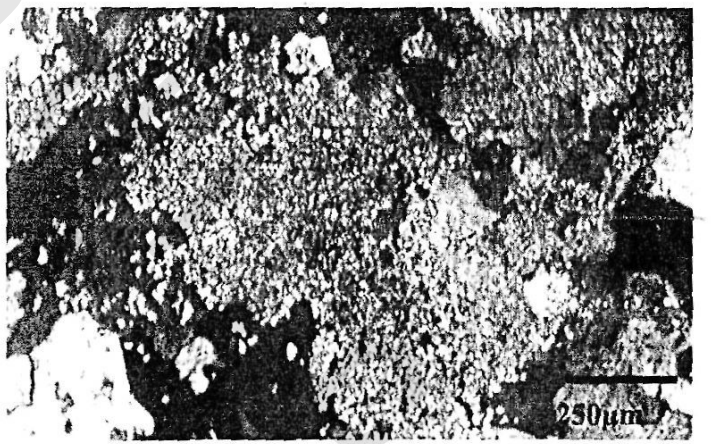

Figure-D: Photomicrograph large, interlocked, xenotopic granular gypsum crystals of slkenside texture enclosing lime mud carbonates, which partly corroded gypsum, (N.C.).

PIATE-25

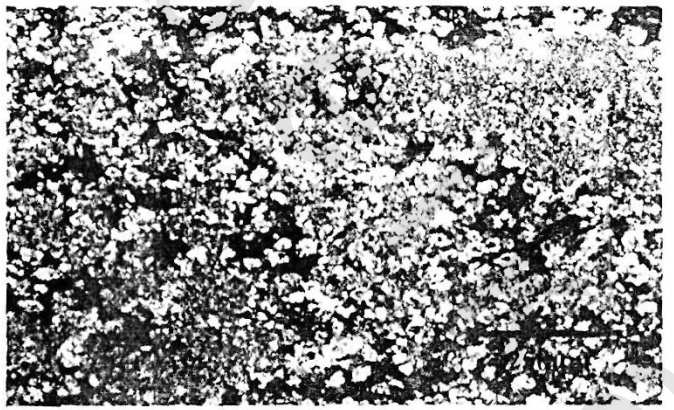

Figure-A: Photomicrograph showing the intensive placement of gypsum by crystalline carbonate, (N.C.).

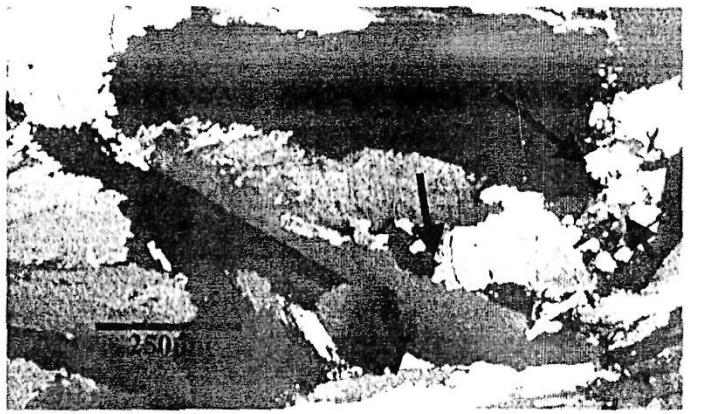

Figure-C: Photomicrograph showing a part of swallow-tail gypsum pesudomorph now anhydrite that brecciated and fragmented resulted in microcrystallization (arrows), (N.C.).

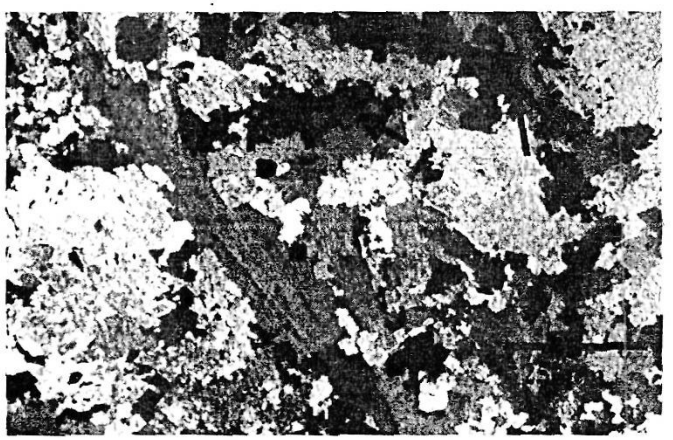

Figure-B: Photomicrograph showing xenotopic anhydrite contain a fracture filled by cloudy swallow tail secondary gypsum crystal and black clay streaks (arrows), (N.C.).

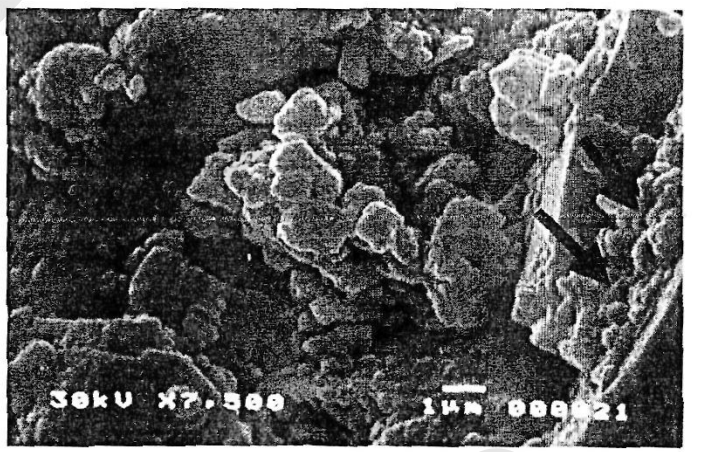

Figure-D: SEM photomicrograph displaying a rounded and folded gypsum nodules completely replaced by anhydrite and voids due to ionic radii difference as well as disintegration of swallow tail along the old cleavage (arrows)

PLATE-26

Figure-A: Photomicrograph showing felty, prismatic anhydrite enclosed gypsum crystals and marl spots rich in opaque organic material (arrows), (N.C.).

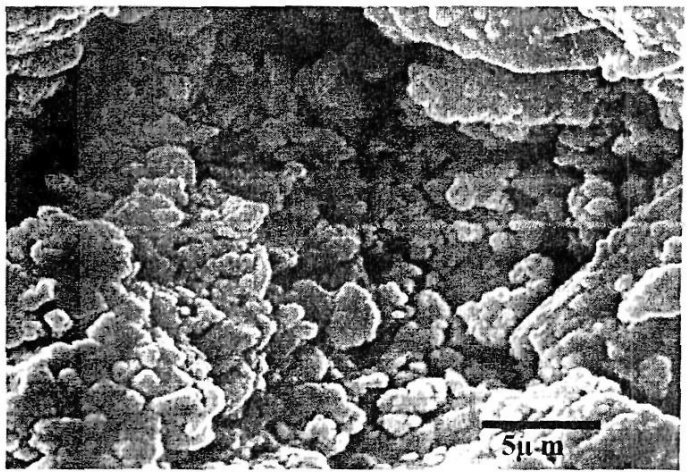

Figure-B: SEM photomicrograph displaying the complete alteration and disintegration of gypsum into anhydrite resulted in porosity due to ionic radii difference

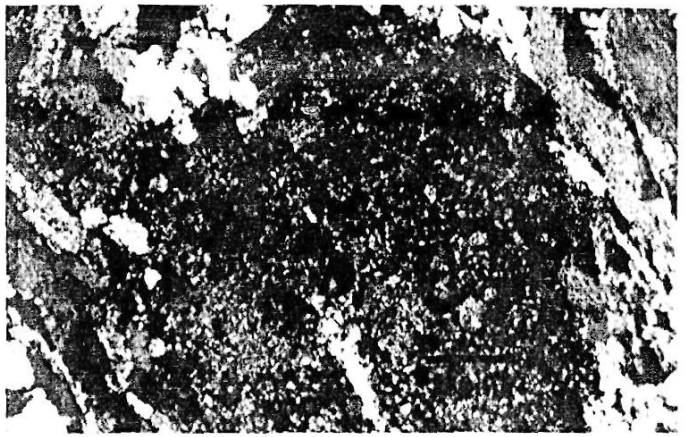

Figure-C: Photomicrograph showing the clay was rich in organic material and partly replaced by crystalline carbonate, (N.C.).

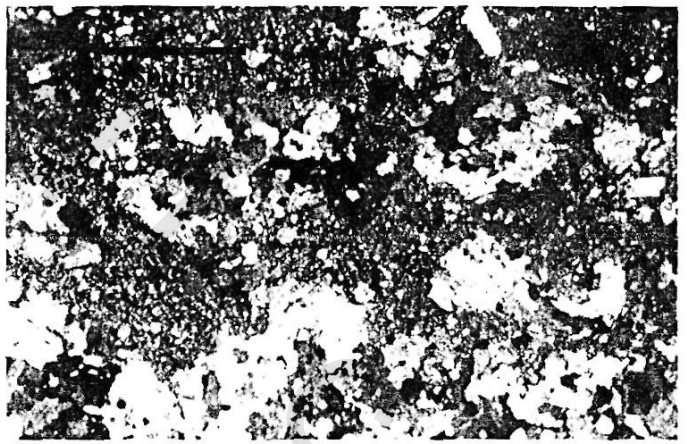

Figure-D: Photomicrograph showing the small isolated gypsum nodules hosted by clays that altered to crystalline carbonate, (N.C.).

PIATE-27

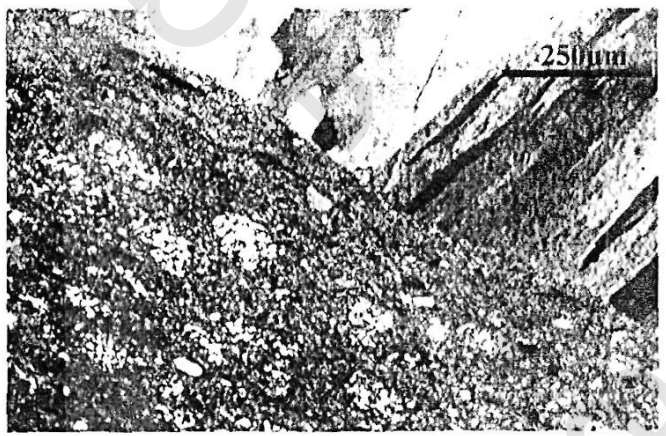

Figure-A: Photomicrograph showing a part of felty, fibrous gypsum fill fracture in evaporite sediments, (N.C.).

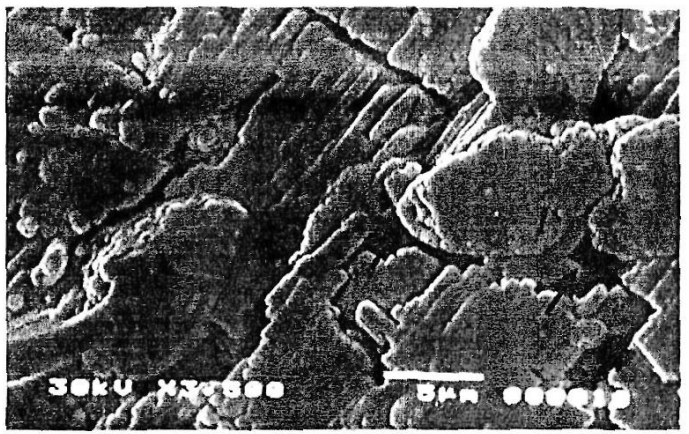

Figure-C: SEM photomicrograph showing a selenite crystal displayed a sign of deformation and dissolution (arrows) along the cleavage

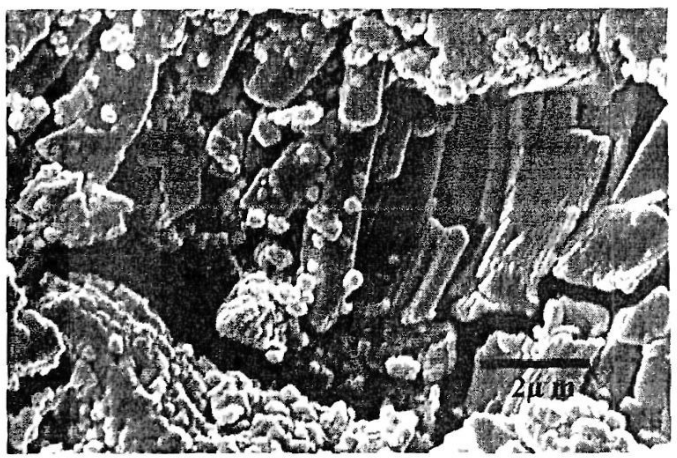

Figure-B: SEM photomicrograph displaying the fracture in massive anhydrite filled by straight , felty gypsum , which vertically oriented up on the fracture wall.

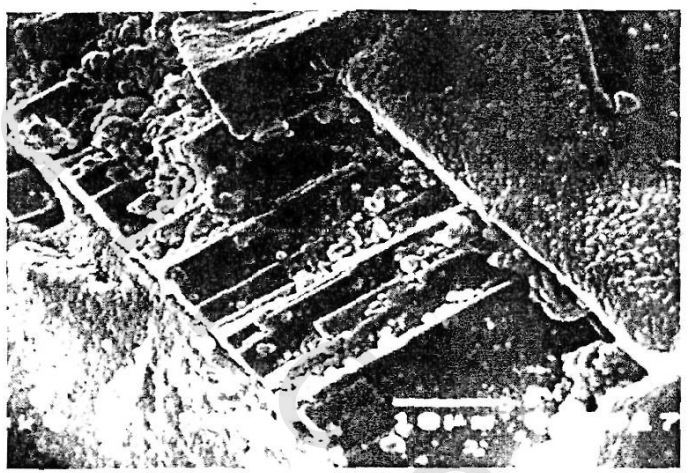

Figure-D: Close-up view showing a selenite fill fracture in anhydrite and display a sign of deformation due to compaction stress.

PLATE-28

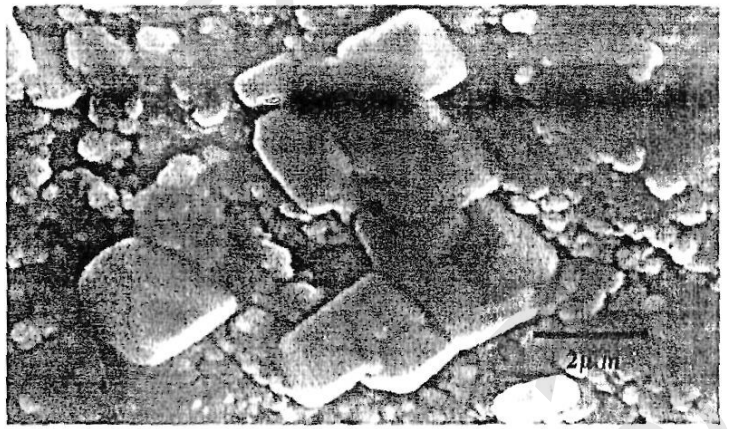

Figure-A: SEM photomicrograph showing deformed prismatic secondary gypsum due to pressure growth in massive anhydrite.

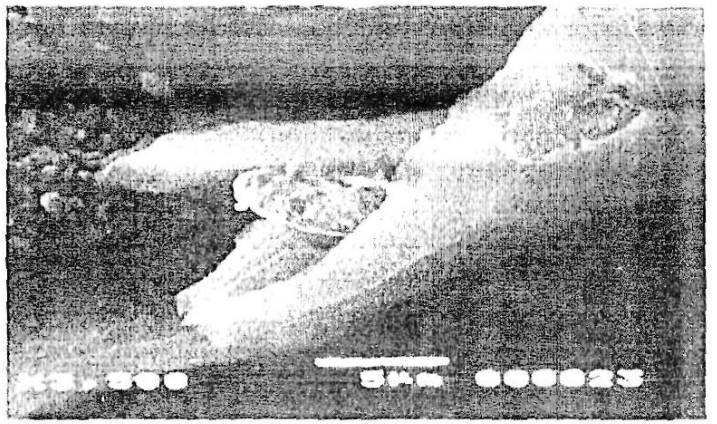

Figure-C: SEM photomicrograph micrograph showing the bio-mineralized algal retaining some original detailed of the organisms embedded in anhydrite

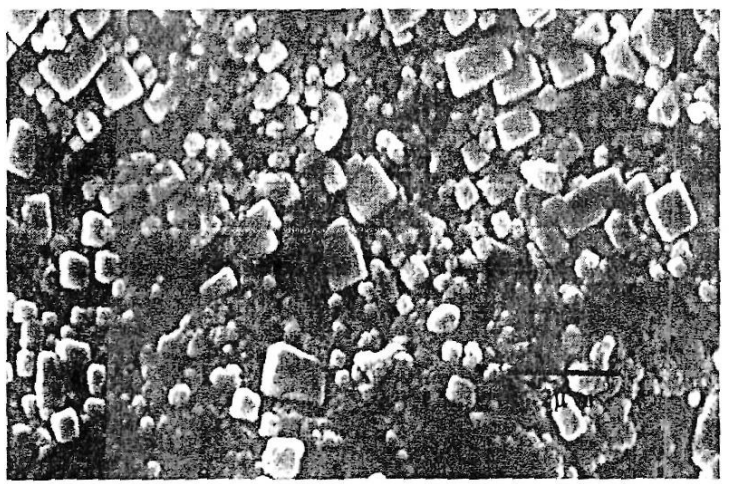

Figure-B: SEM photomicrograph displaying halite crystals replace and displace the anhydrite

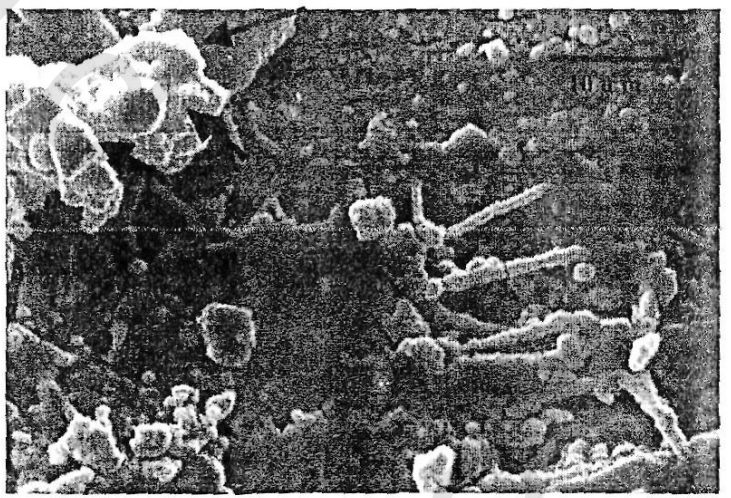

Figure-D: SEM photomicrograph showing the bio-mineralized algal matt as well as the microbial matt (Arrows) embedded in anhydrite

PIATE-29

Figure-A: SEM photomicrograph showing the bio-mineralized biocapsule retaining some original detailed of the organisms embedded in anhydrite

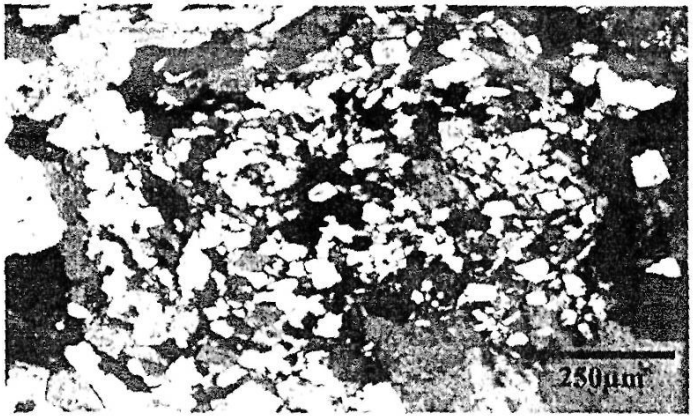

Figure-C: Photomicrograph showing a anhydrite nodule composed of xenotopic prism in association of anhydrite granules, (N.C.).

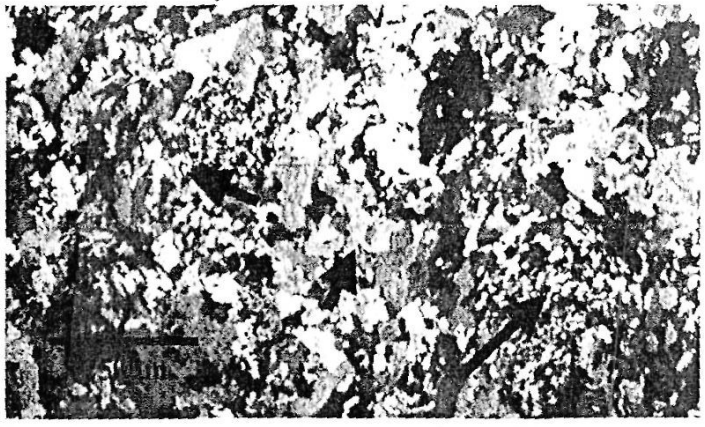

Figure-B: photomicrograph showing anhydrite nodules composed of microcrystalline anhydrite aggregates engulfed gypsum relics (arrows) in association with xenotopic anhydrite lathes, (N.C.).

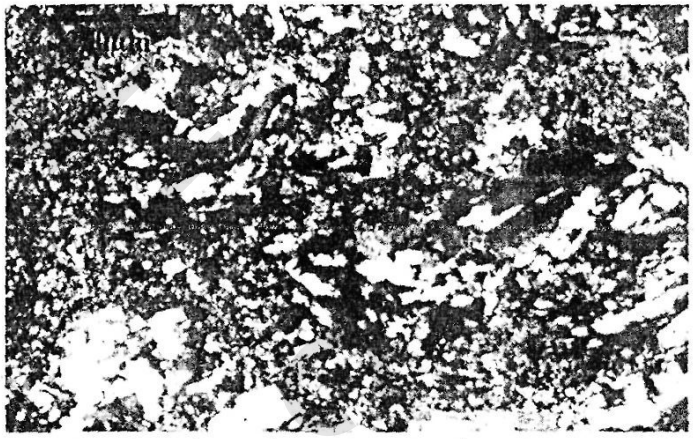

Figure-D : Photomicrograph showing anhydrite nodule composed of felty crystals displayed sweeping color character hosted by crystalline carbonate enriched in black and opaque organic rich materials, (C.N.).

PIATE-30

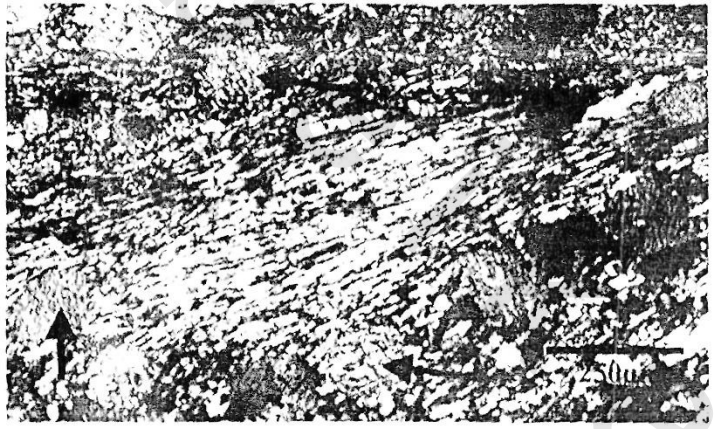

Figure-A: Photomicrograph showing aligned, fibrous, anhydrite of sweeping character replacing algal remains and calcite xenomorphic texture replace the former evaporite nodules(arrows), (N.C.).

Figure-B: Photomicrograph showing calcite xenomorphic texture replace and corroded the former evaporite nodules(arrows), (N.C.).

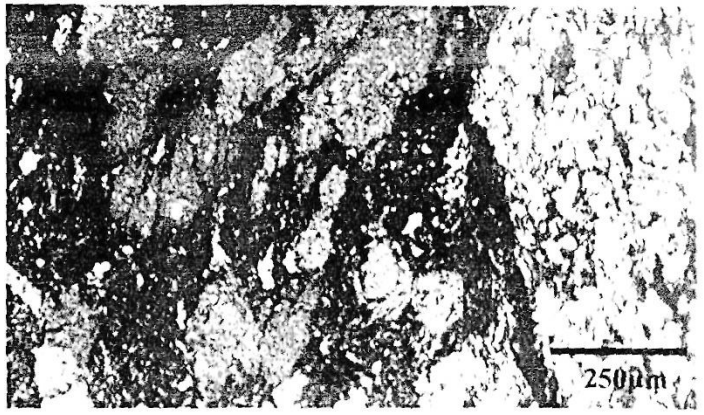

Figure-C: Photomicrograph showing dissected and elongated gypsum nodules floating in clays rich in organic material and interlaminated with dense massive anhydrite laminae of sweeping color, (N.C.).

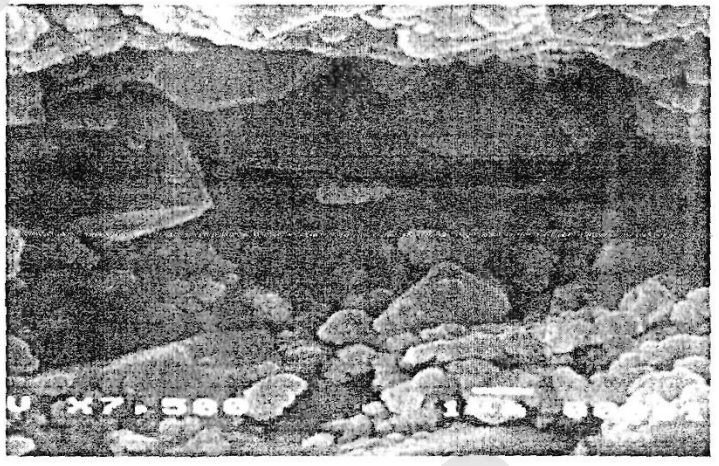

Figure-D: SEM photomicrograph showing fine grained anhydrite is interlaminated with idiotopic prismatic gypsum.

PIATE-31

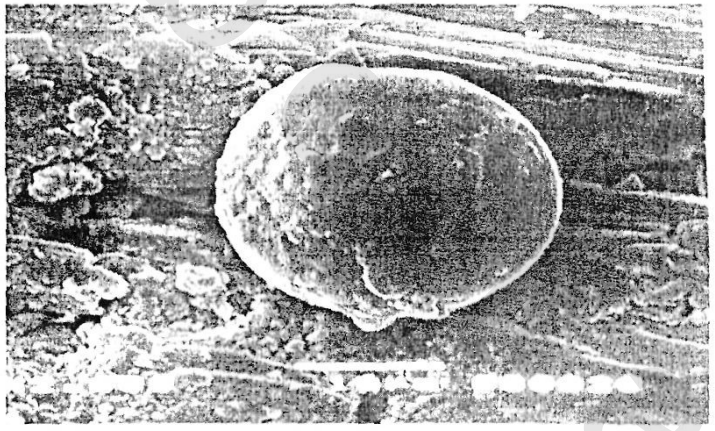

Figure-A: SEM photomicrograph showing bio-mineralized biocapsule that retain the external feature of the original organism embedded in evaporite sediments

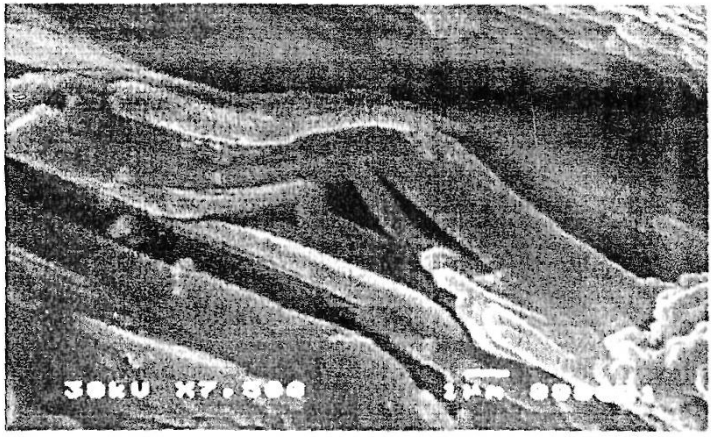

Figure-C: SEM photomicrograph displaying a large selenite that filled voids show a sign of deformation and ductile character due to compaction deformation.

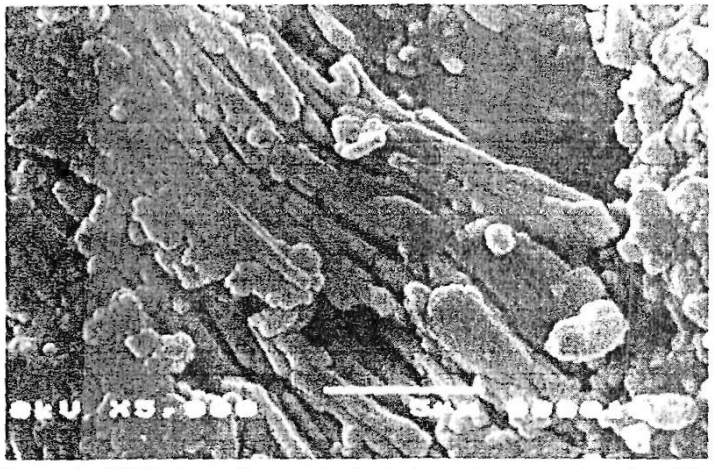

Figure-D: SEM photomicrograph displaying a large selenite that filled voids show a sign of deformation and ductile character due to compaction deformation.

Figure-D: Photomicrograph showing small anhydrite nodules ,which made of xenotopic crystals, are floating in microcrystalline evaporite lathes partly corroded by carbonate, (N.C.).

PIATE-32

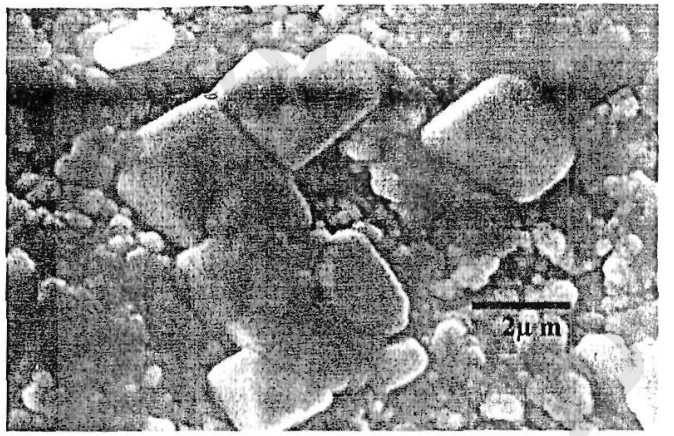

Figure-A: SEM photomicrograph showing deformed prismatic secondary gypsum due to pressure growth in massive anhydrite.

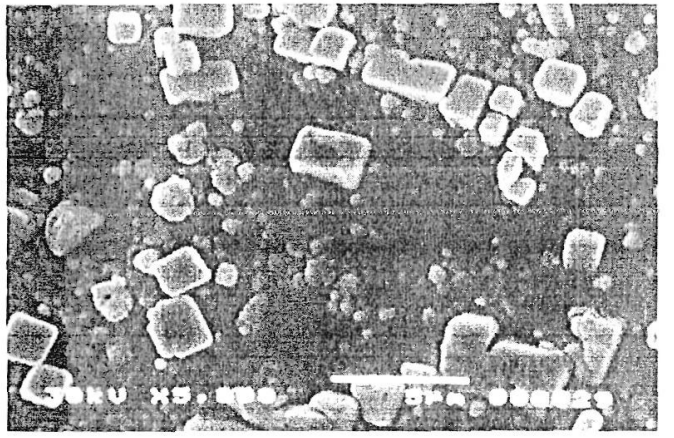

Figure-B: Close-up displaying halite crystals displaying different size , which replacing the gypsum suggesting the hypersaline condition of the depositional regime.

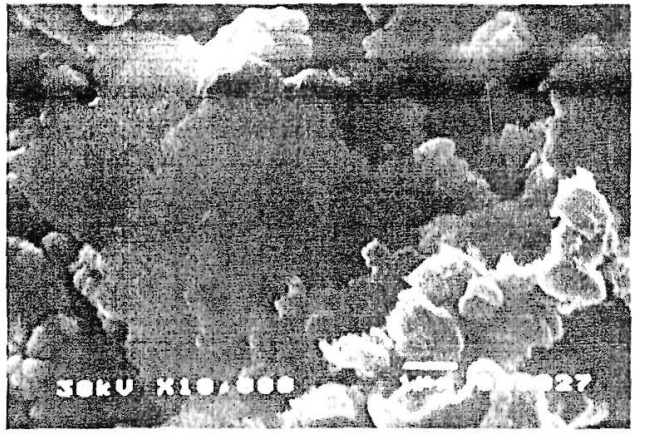

Figure-C: SEM photomicrograph show the microbial matt embedded in evaporite nodule

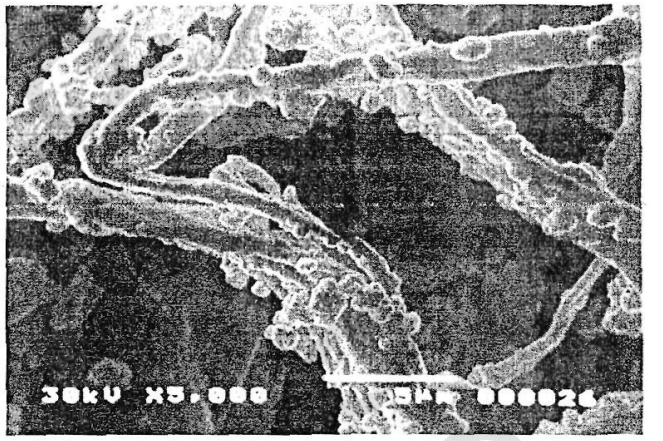

Figure-D: Close-up view show the detailed structure of algae embedded in the evaporite nodule.

PIATE-33

Figure-A: Photomicrograph showing a part of small isolated anhydrite nodule floating in microcrystalline gypsum forming lathes. NB. The dense, opaque and black organic rich material occupying the intercrystalline spaces(arrows), (N.C.).

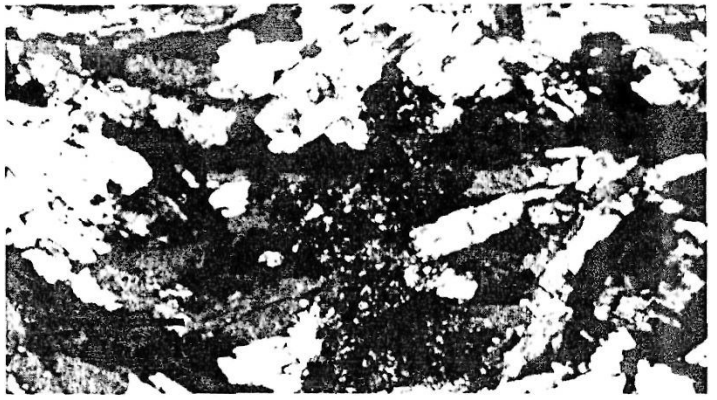

Figure-C: Photomicrograph showing xenotopic anhydrite of sweeping color character engulfed crystalline carbonates in association with black,dense organic rich, (N.C.).

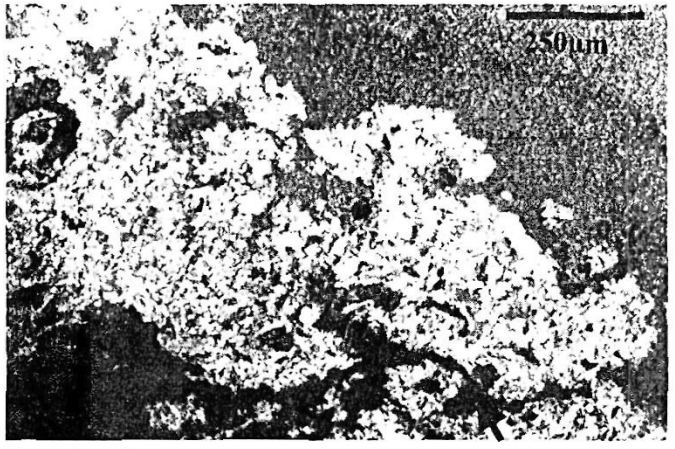

Figure-B: Photomicrograph showing a part of small packed anhydrite nodule floating carbonate mud forming the host sediments. NB. The dense, opaque and black organic rich material occupying the intercrystalline spaces(arrows) , (N.C.).

Figure-D : Photomicrograph displaying xenotopic anhydrite and the narrow fractures filled by swallow-tail secondary gypsum , (N.C.).

PIATE-34

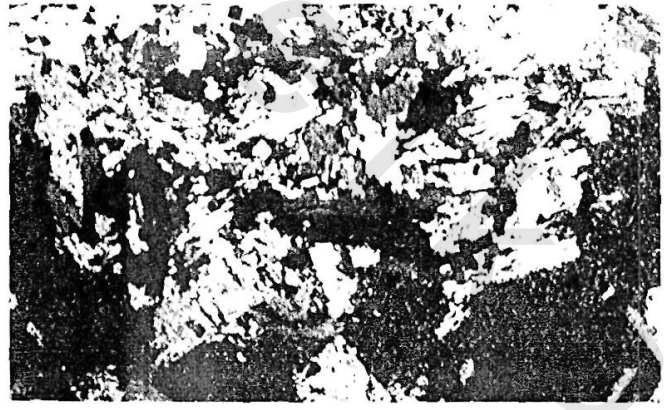

Figure-A: Photomicrograph showing felty, straight , prismatic gypsum / anhydrite that interlaminated with clays , which partly corroded by carbonate and rich in dense and black organic rich materials, (N.C.).

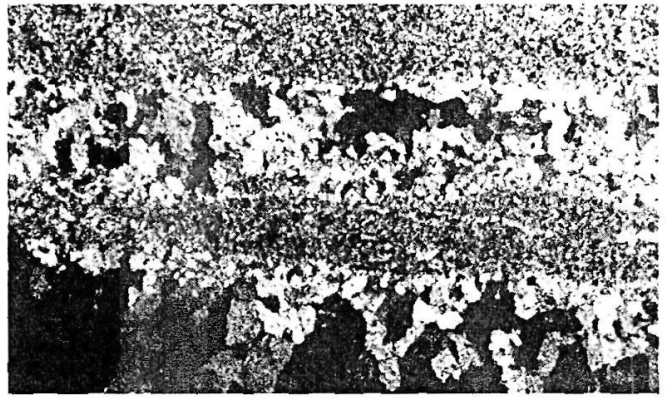

Figure-B: Photomicrograph showing a part of veins filled by felty, straight gypsum in lime mud carbonates , (N.C.).

Figure-C: Photomicrograph showing a part of large irregular , cloudy xenotopic gypsum crystals contains solid inclusions (anhydrite) and engulfed dark, opaque organic rich material, (N.C.).

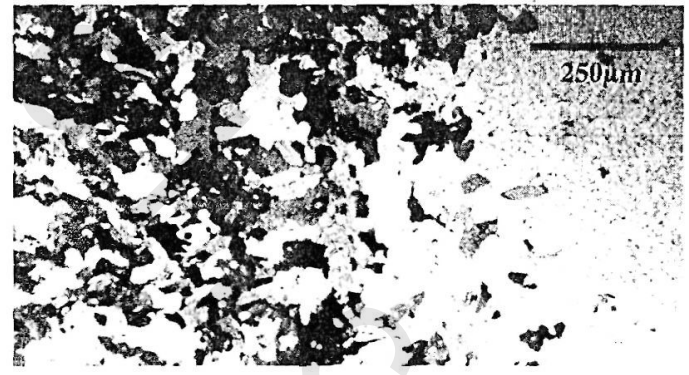

Figure-D: Photomicrograph showing a part of large irregular , cloudy xenotopic gypsum crystal disintegrated into fine crystalline secondary gypsum , (C.N.).

PIATE-35

Figure-A: Photomicrograph showing the clay streaks enriched in black, dense and opaque organic matter, (N.C.).

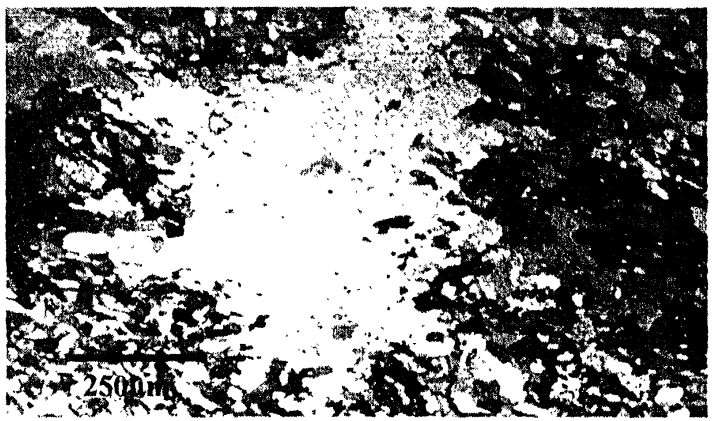

Figure-C: Photomicrograph shows a large , cloudy, irregular boundaries gypsum crystal that forming nodule, floating into xenotopic granular gypsum lathes, (N.C.).

Figure-B: Photomicrograph shows amebiode secondary gypsum fill vugs in anhydrite , (N.C.).

Figure-D: Photomicrograph showing large, xenotopic, agglutinated gypsum crystals brecciated and disintegrated into secondary felty anhydrite with directional strain due to compaction stress , (N.C.).

PLATE-36

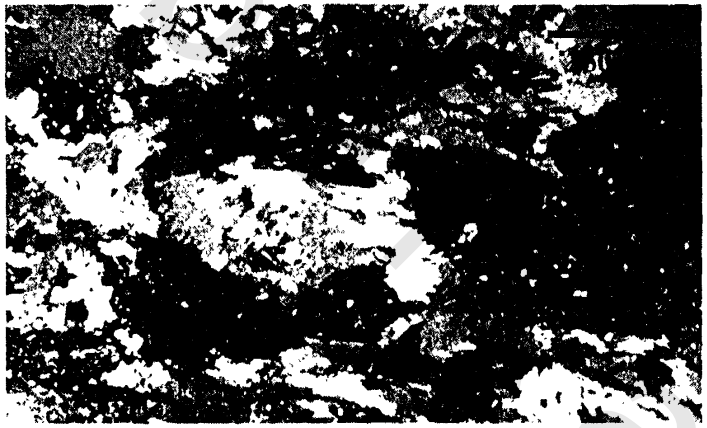

Figure-A: Photomicrograph showing intermixed , brecciated xenotopic gypsum that partly altered into anhydrite due to rotational strain with compaction that led to admixture of terrigenic material rich in organic rich material to interfere with brecciated gypsum form interlocked pattern, (N.C.).

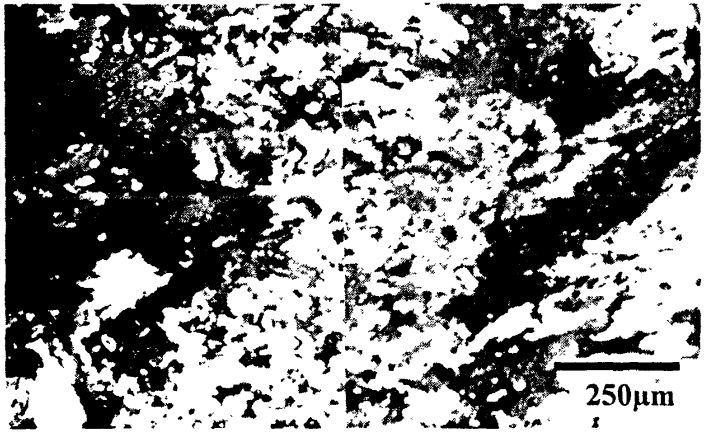

Figure-B: Photomicrograph showing xenotopic agglutinated gypsum crystals brecciated into felty anhydrite display an sweep color due to the strain effect enclosed clay streaks rich in organic matter due rotational strain and compaction, (N.C.).

Figure-C: SEM photomicrograph displaying the detailed structure of gypsum nodule that show sign of folded deformation , dissolution and transformation into anhydrite with clear sign of forming larger composite nodules due to rotational stress

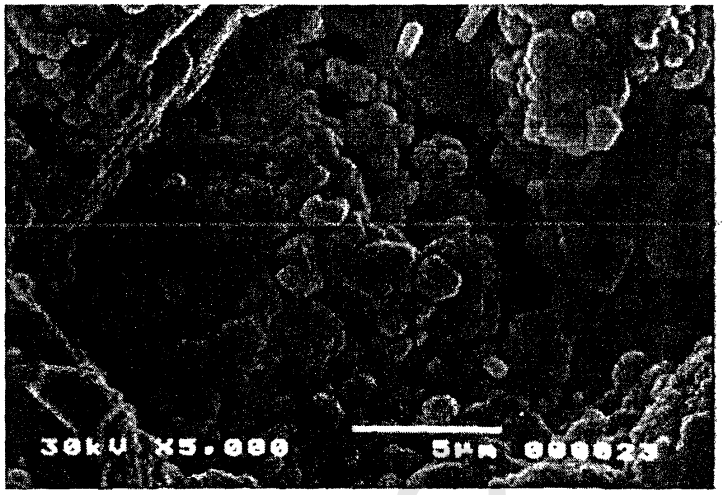

Figure-D: SEM photomicrograph the replacement of gypsum nodules by fine anhydrite resulted in an increasing of porosity due to ionic difference radii

PIATE-37

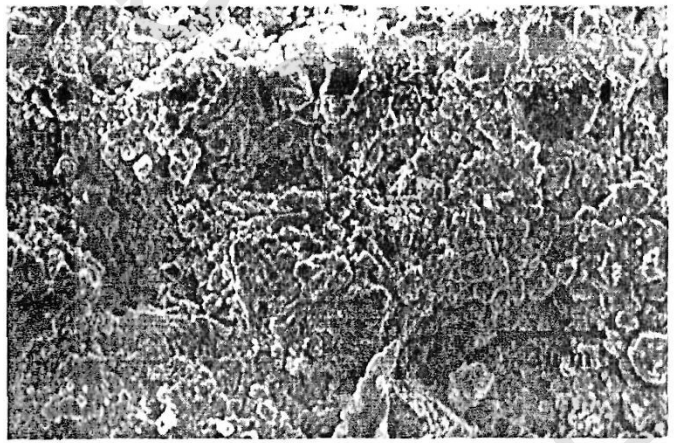

Figure-A: SEM photomicrograph displaying compact fabric of nodular texture style displayed by fine grained gypsum aggregates .

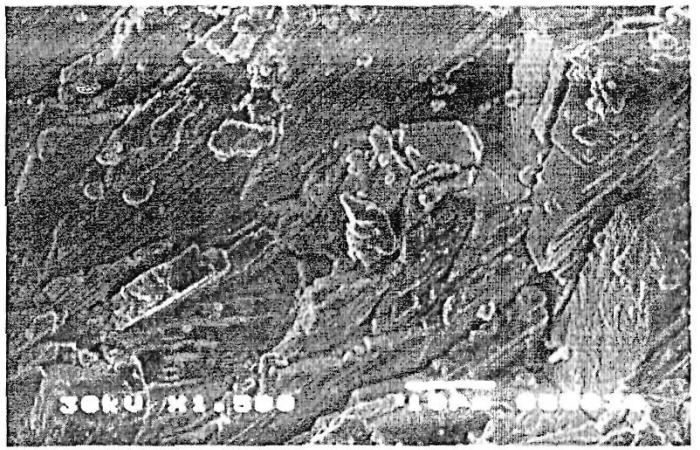

Figure-C: SEM photomicrograph showing gypsum crystal have been grown in multidirectional directions due to compaction.

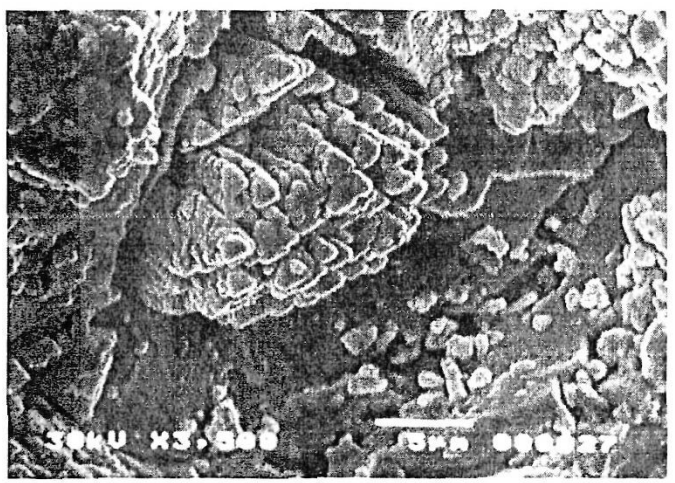

Figure-B: SEM photomicrograph showing bundle (compressed) prismatic secondary anhydrite after gypsum due to deformation stress

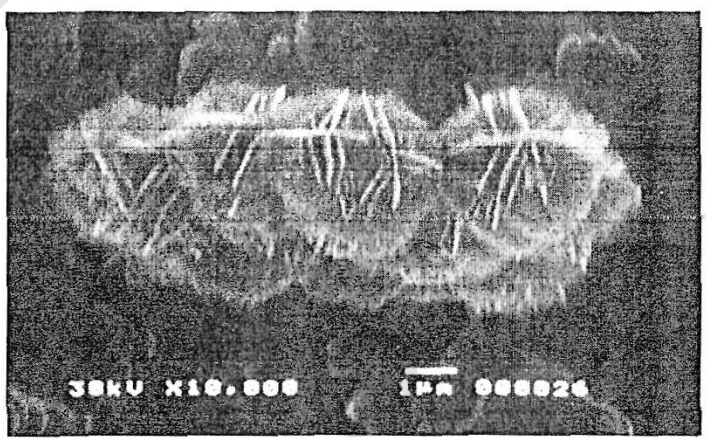

Figure-D: SEM photomicrograph showing the composite lenticular anhydrite as a bio-product of biocapsule embedded in gypsum

PIATE-38

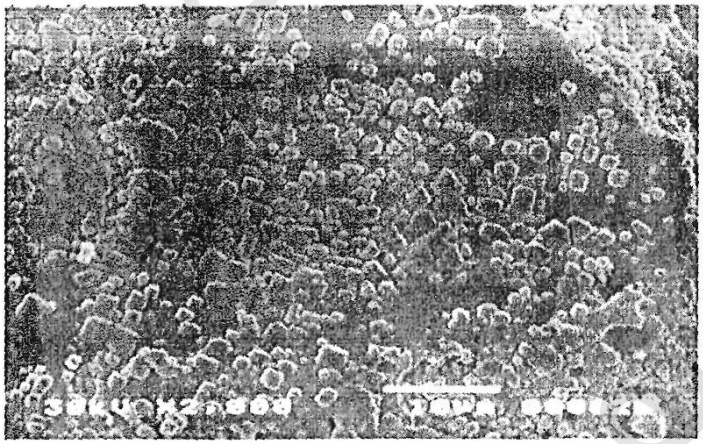

Figure-A: SEM photomicrograph showing the extensive replacement of gypsum by halite crystals of different sizes.

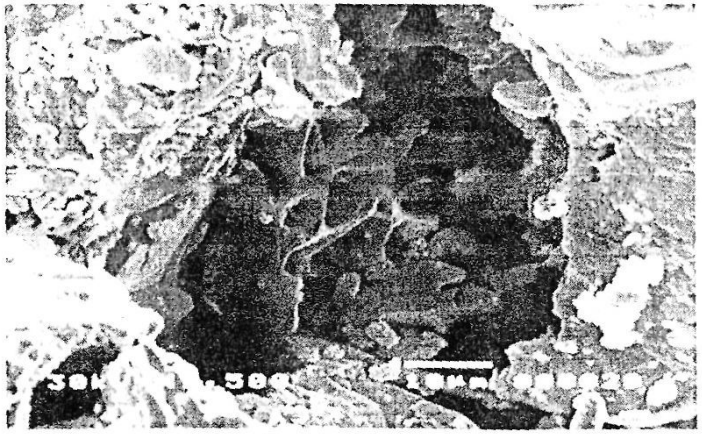

Figure-B: Close-up view the dissolution pattern of gypsum resulted from alteration of gypsum into anhydrite led to increasing the porosity

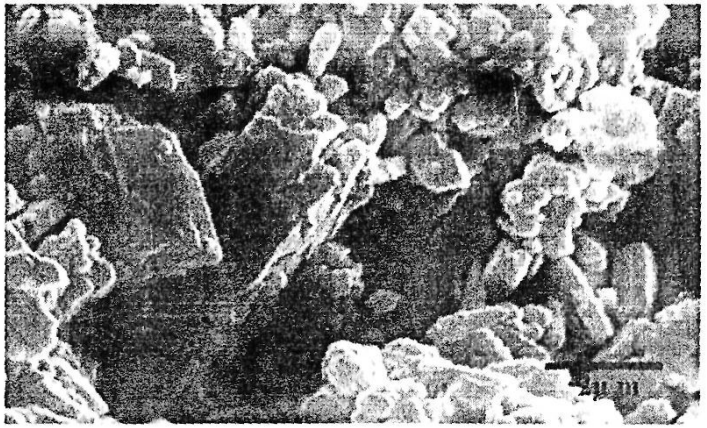

Figure-C: SEM photomicrograph representing the alteration steps between gypsum and anhydrite , which replace the first former. NB. Pattern displayed at the periphery part left cracks representing voids due to ionic radii.

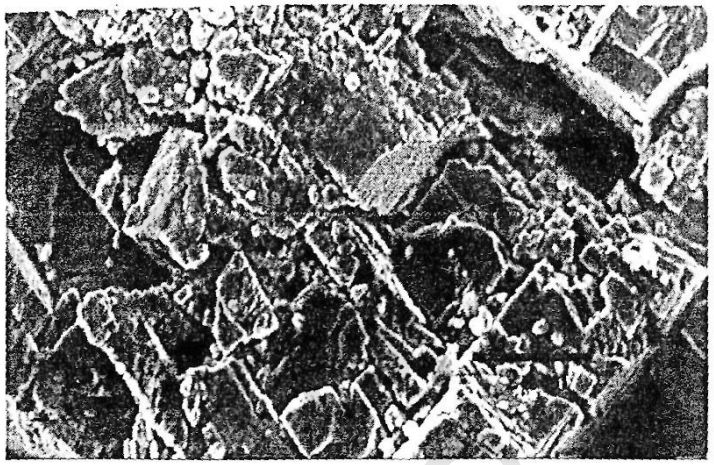

Figure-D: SEM photomicrograph showing the brecciation pattern that displayed by halite due to cubic intersection pattern

PIATE-39

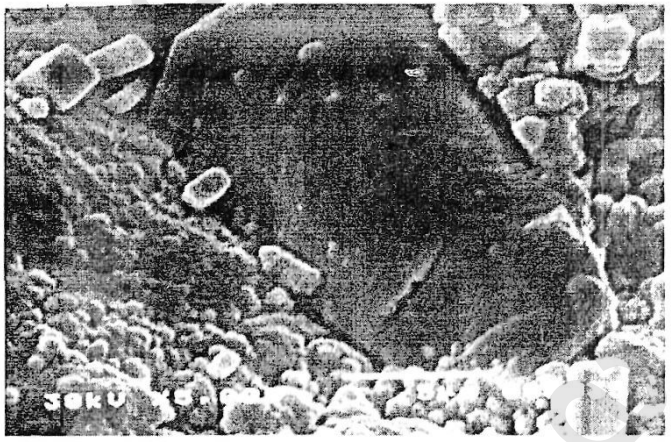

Figure- A: SEM photomicrograph displayed a large secondary gypsum filling cavity in evaporite and small replacive halite crystals

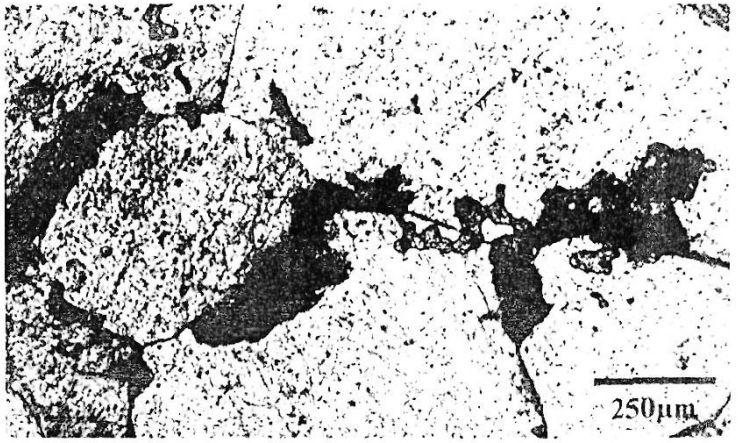

Figure-C: Photomicrograph showing the black, opaque organic rich material enclosed by the interlocked anhydrite crystals. Plane Polarized Light (P.L.L.)

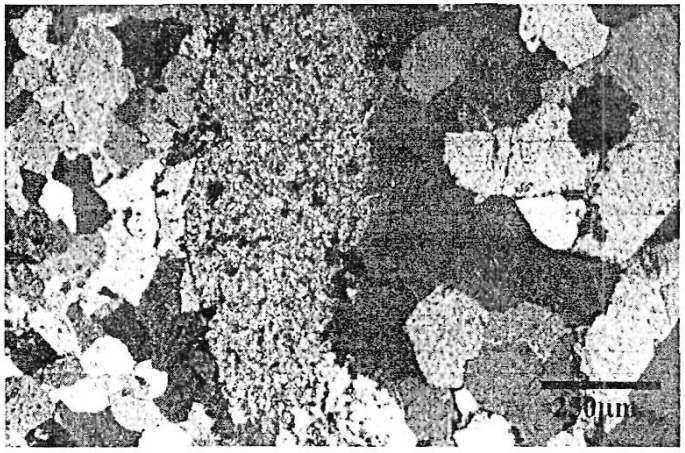

Figure-B: Photomicrograph showing gypsum pesudomorph of equigranular sized particles displaying interlocked textured (foam Textured), which alternating with micritic sized terrigenic material rich in organic matter. (N.C.).

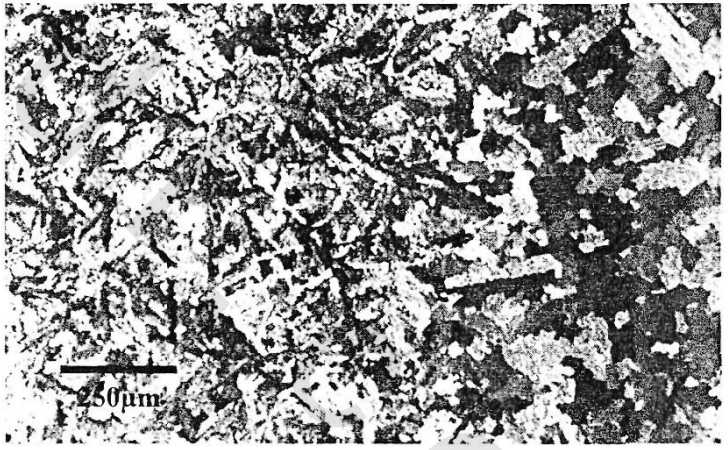

Figure-D: Photomicrograph showing xenotopic , prismatic anhydrite brecciated into felty epigenetic anhydrite with sweeping color character, (N.C.).

PIATE-40

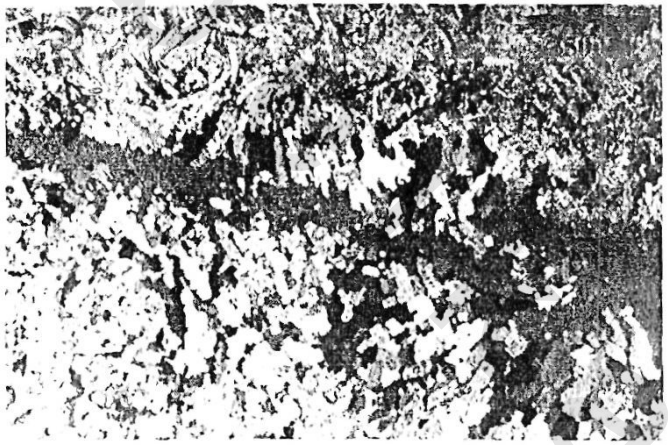

Figure-A: Photomicrograph the terrigenous material rich in organic matter occupying the inter spaces, (N.C.).

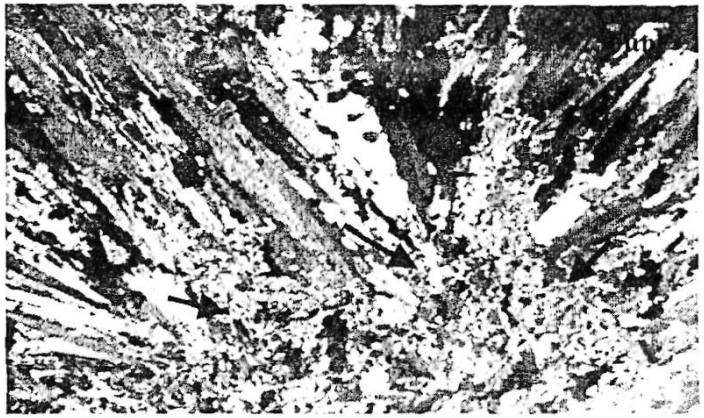

Figure-C: Photomicrograph showing the radial arrangement of fibrous anhydrite crystals that forming stellate structure. NB: the brecciation into crystalline aggregates (arrows) , (N.C.).

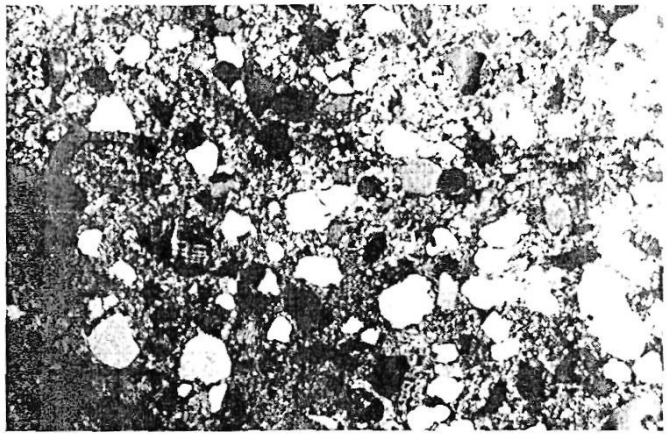

Figure-B: Photomicrograph showing pesudomorph gypsarenite now anhydrite composed of sand size, angular, poorly sorted gypsum, quartz, feldspars and rock fragments embedded in microsparite matrix, (N.C.).

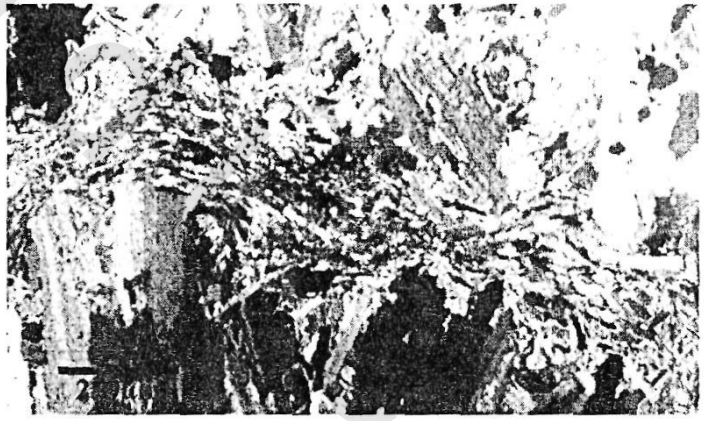

Figure-D: Photomicrograph showing a part of stellate structure of anhydrite fibrous crystals and aligned fibrous anhydrite lath that displayed a crenulated and wavy layer , (N.C.).

PIATE-41

Figure-A: Photomicrograph showing the dense, black and opaque organic rich material enclosed in intercrystalline spaces, (N.C.).

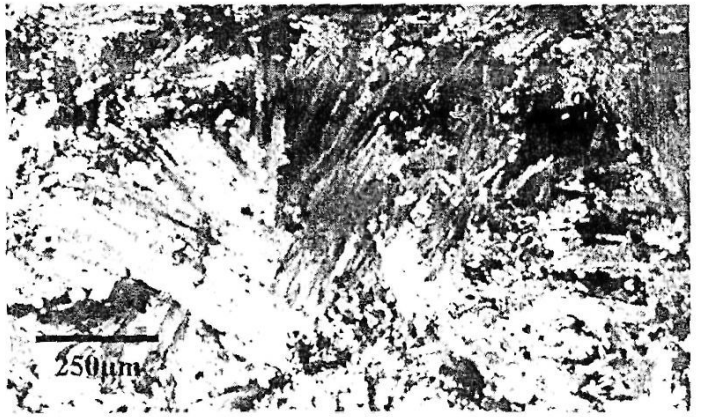

Figure-C: Photomicrograph showing swallow-tail secondary gypsum fill vugs in anhydrite, (N.C.).

Figure-B: Photomicrograph showing prismatic anhydrite with gypsum crystals grade up into microcrystalline anhydrite of sweeping color engulfed gypsum relics , (N.C.).

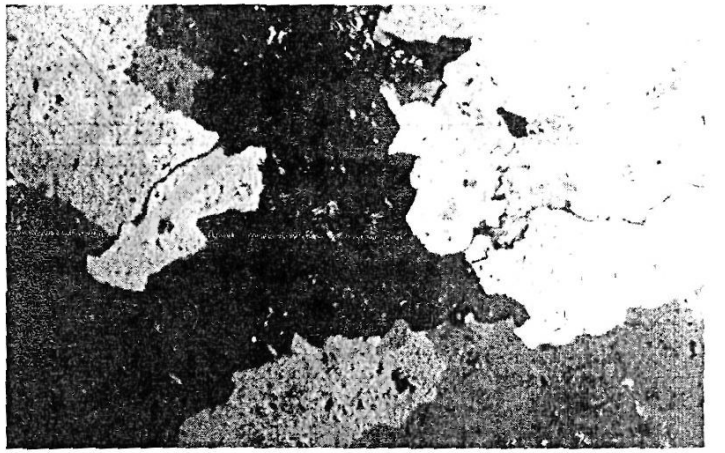

Figure-D: Photomicrograph showing a large, inter;locked, xenotopic gypsum crystals of slkenside textured enclosed anhydrite relics which indicating their epigenetic origin , (N.C.).

PIATE-42

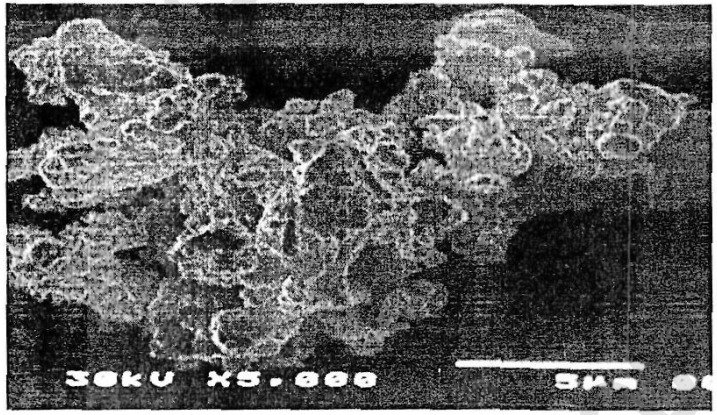

Figure-A: SEM photomicrograph displaying bio-mineralized microbial matt embedded in gypsum

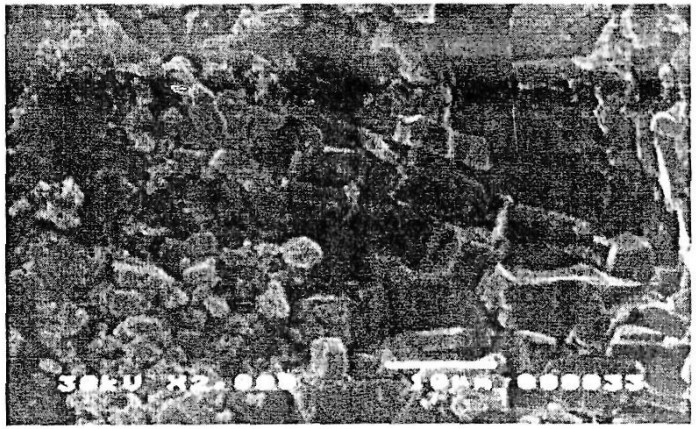

Figure-C: SEM photomicrograph showing the brecciated pattern that displayed by prismatic gypsum crystals due to compaction stress

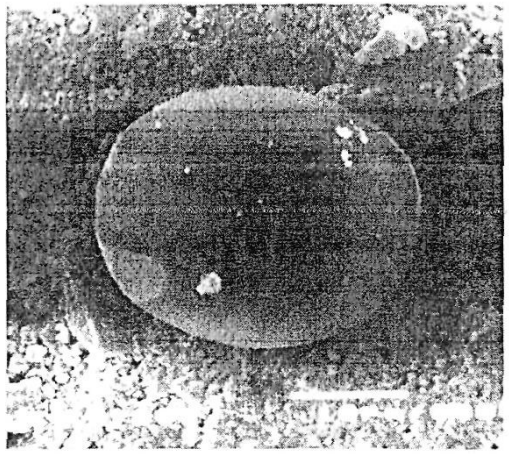

Figure-B: SEM photomicrograph showing the bio-mineralized biocapsule embedded in gypsum sediments

Figure-D: Photomicrograph showing xenotopic agglutinated gypsum *brecciated into fibrous*, felty anhydrite of sweeping color due to compression strain, (N.C.).

PIATE-43

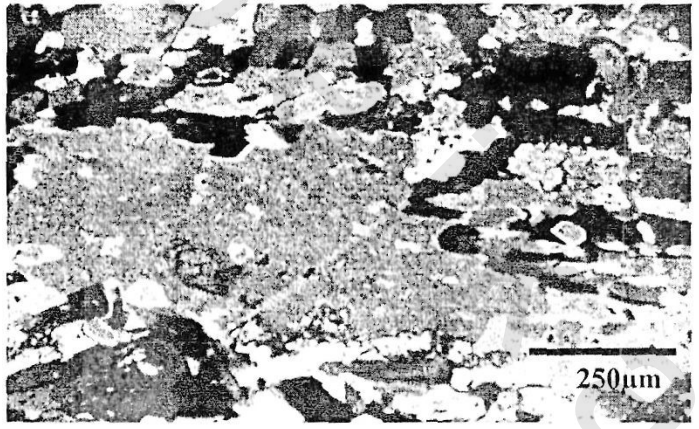

Figure-A: Photomicrograph showing irregular corroded gypsum pesudomorph fill fracture in prismatic anhydrite, (N.C.).

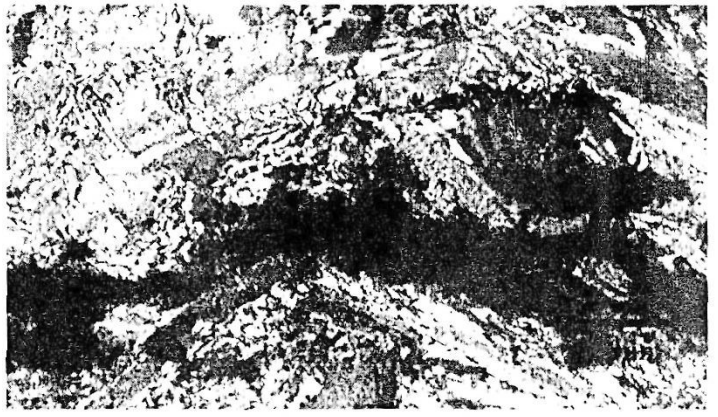

Figure-C: Photomicrograph showing the black, opaque and dense organic matter occupying the inter crystalline spaces of anhydrite prisms crystals, (N.C.).

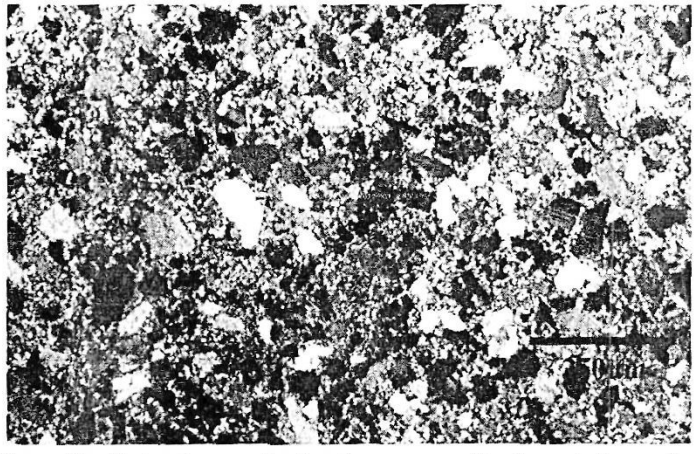

Figure-B: Photomicrograph showing gypsarenite formed from -fine sand size , angular, poorly sorted gypsum , quartz and feldspars floated *in microsparite cement, (N.C.).*

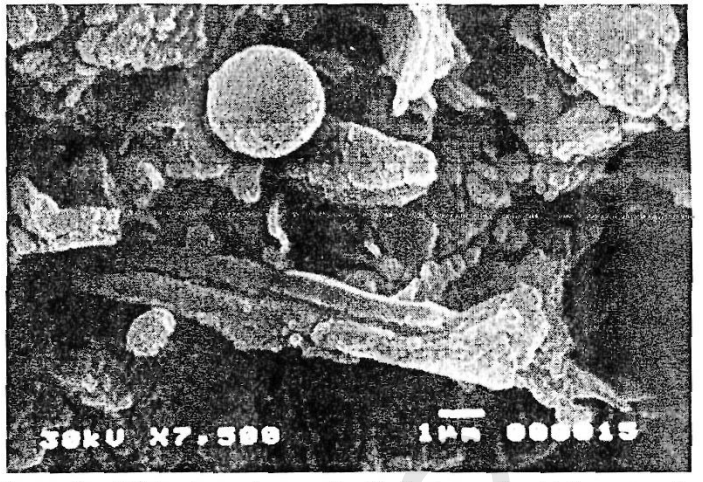

Figure-D: *SEM photomicrograph displaying microbial matt of* spheroid-shaped and mineralized algae embedded in anhydrite sediments

PIATE-44

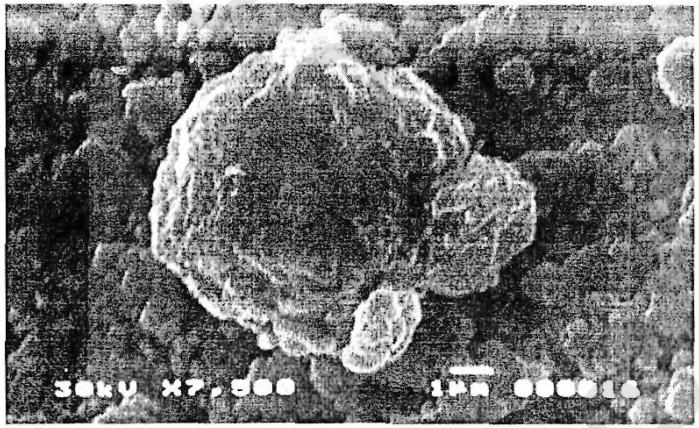

Figure-A: SEM photomicrograph showing bio-mineralized biocapsule embedded in anhydrite

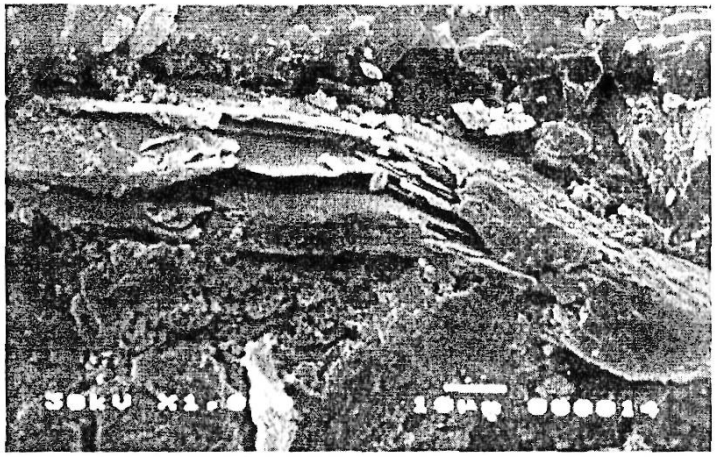

Figure-C: SEM photomicrograph displaying a small veins filled by xenotopic selenite crystal

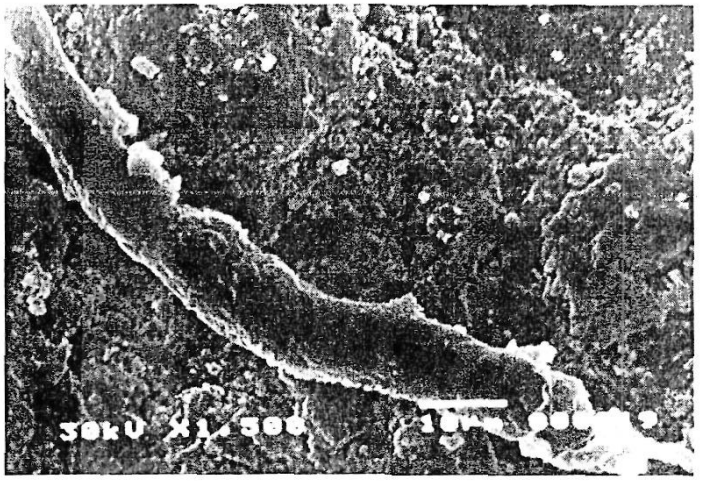

Figure-B: SEM photomicrograph showing bio-mineralized algae embedded in anhydrite

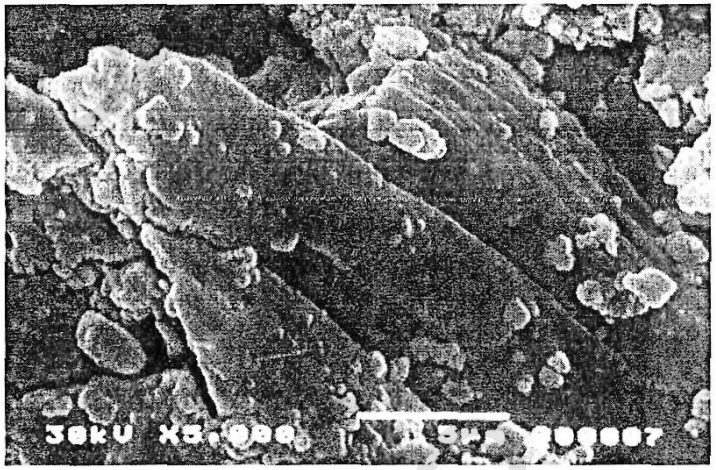

Figure-D: SEM photomicrograph displaying a small vugs filled by xenotopic selenite crystal displaying disintegration into fine anhydrite.

PIATE-45

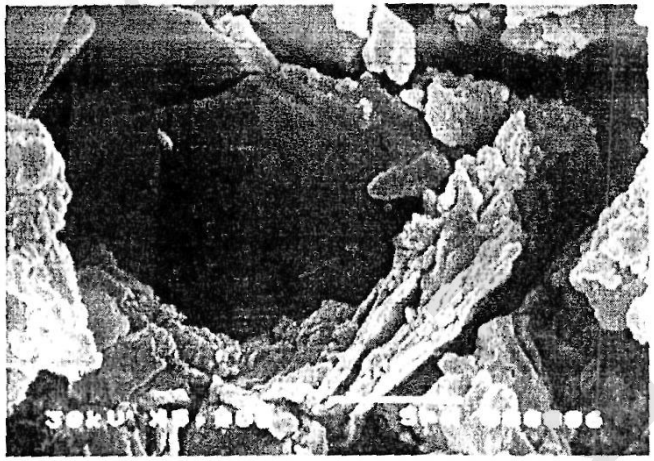

Figure-A: SEM photomicrograph showing bio-mineralized molds of ruptured apex fill vugs in gypsum crystals.

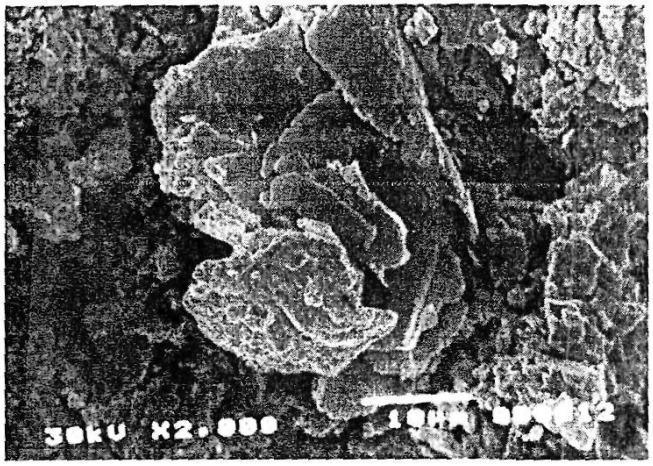

Figure-B: SEM photomicrograph showing bio-mineralized organic remains embedded in gypsum sediments

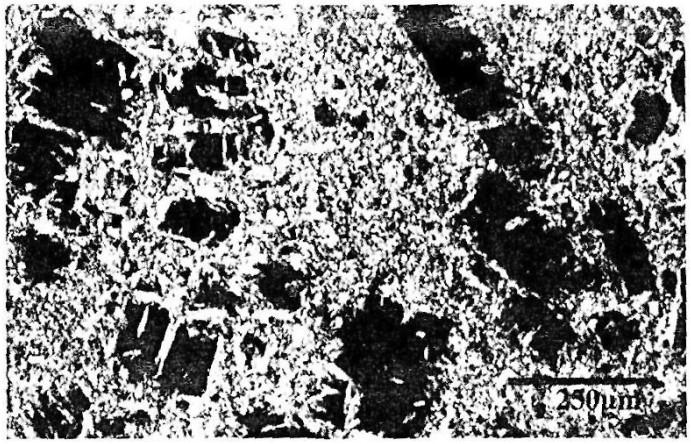

Figure-C: Photomicrograph showing irregular, step shaped of unfilled molds after halite dissolution in non-oriented felty epigenetic anhydrite, (N.C.).

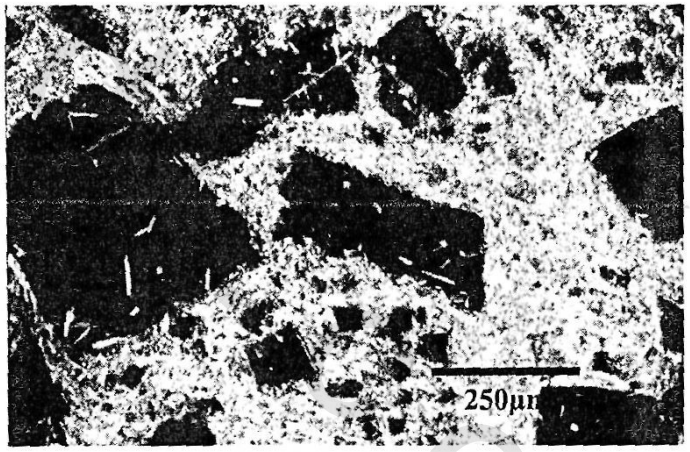

Figure-D: Photomicrograph showing irregular, step shaped of unfilled molds after halite dissolution in non-oriented felty epigenetic anhydrite, (N.C.).

PIATE-46

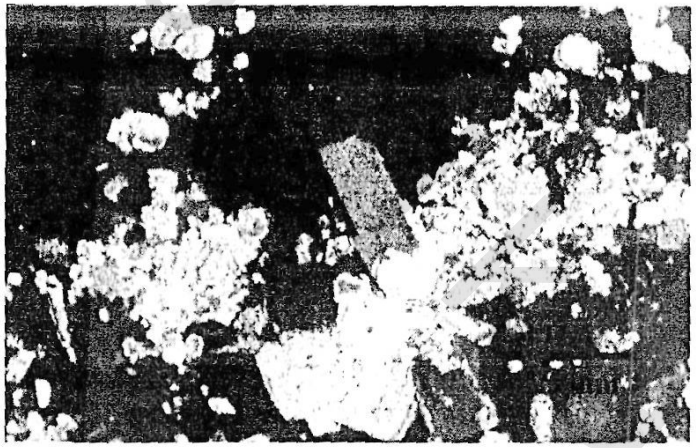

Figure-A: Photomicrograph showing xenotopic anhydrite granule engulfed gypsum prismatic crystals. (N.C.).

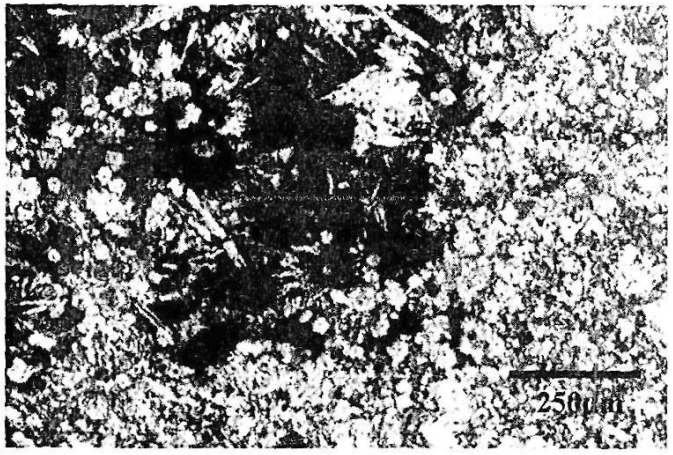

Figure-B: Photomicrograph showing randomly oriented fibrous gypsum partly corroded by xenomorphic calcite textured . (N.C.).

Figure-C: Photomicrograph showing the unfilled mold after dissolution of the pre-existing halite raft in anhydrite sediments, (C.N.).

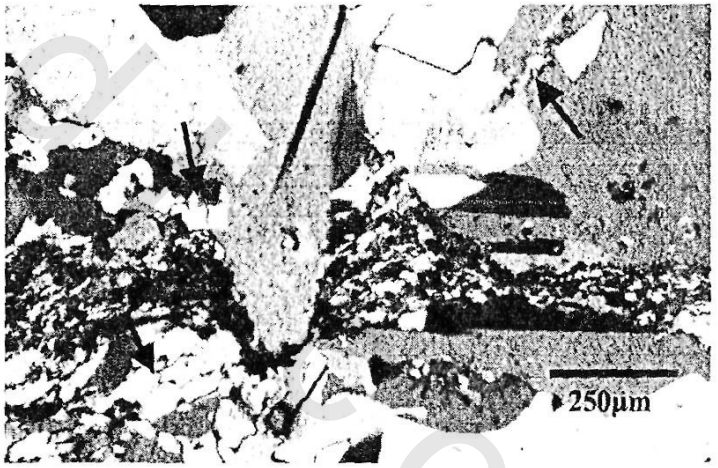

Figure-D: Photomicrograph representing the deformation features as brecciated and disintegration of large gypsum pesudomorph now anhydrite crystal into microcrystalline secondary gypsum aggregates (arrows), (N.C.).

PIATE-47

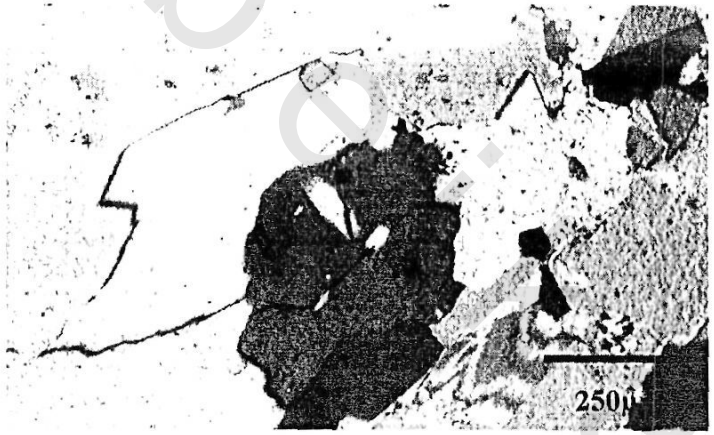

Figure-A: Photomicrograph showing large, interlocked gypsum pesudomorph gypsum displaying the irregular and deformed boundaries due to pressure growth, (N.C.).

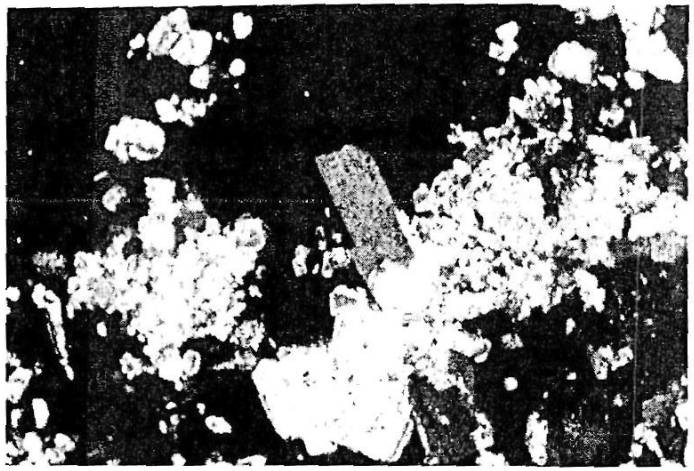

Figure-B: Photomicrograph showing xenotopic anhydrite engulfed prismatic gypsum relics with void mold probably due to the dissolution of pre-existing halite , (N.C.).

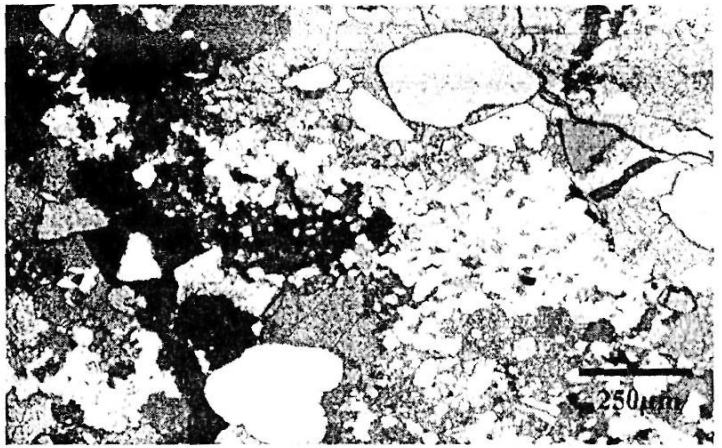

Figure-C: Photomicrograph showing the black, opaque and dense organic rich material occupied the intercrystalline spaces of anhydrite. NB: The sand size, angular terrigenous clast (quartz)draped in anhydrite, (N.C.).

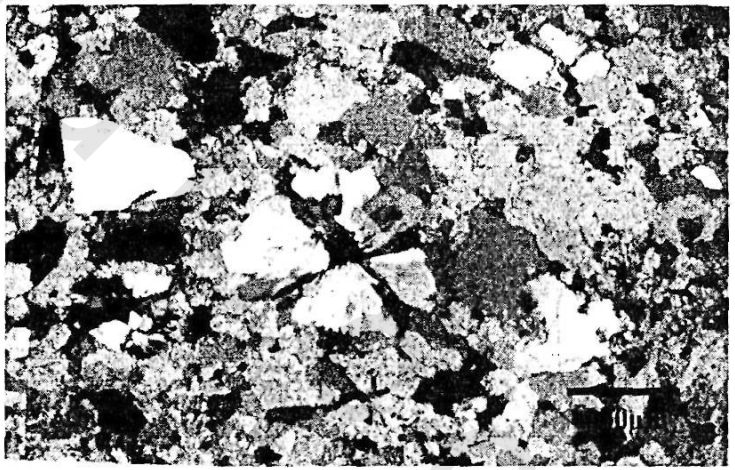

Figure-D: Photomicrograph showing amebiode secondary gypsum filled vugs and terrigenous clast which indicating uplifting and land input , (N.C.).

PIATE-48

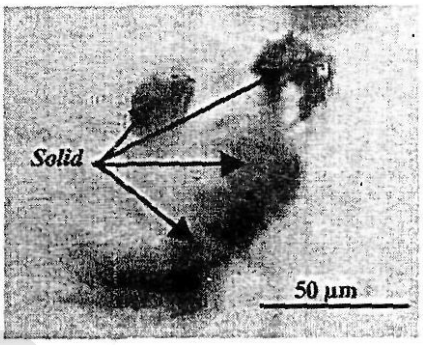

Figure 1A: Dark, organic solid inclusions of rounded shape in gypsum crystal

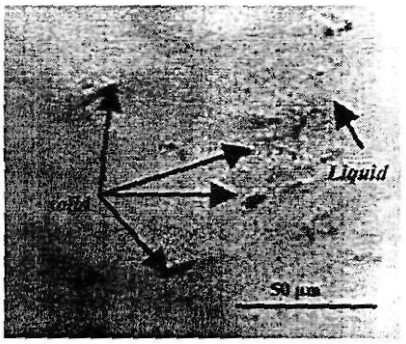

Figure -1B: Black,solid,organic residue inclusion with liquid hydrocarbon in anhydrite

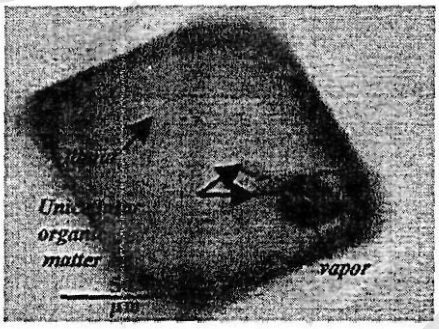

Figure -2: Solid,unicellular organic matter (cyanobacteria) with vapor and liquid inclusions

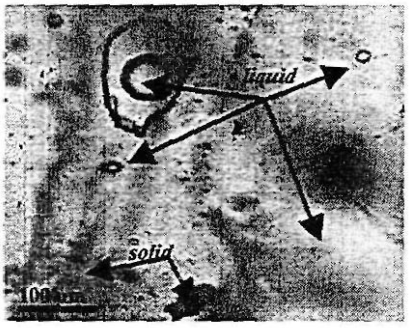

Figure-1C: Liquid hydrocarbon inclusion filled cavity and black organic matter solid inclusion in gypsum crystal

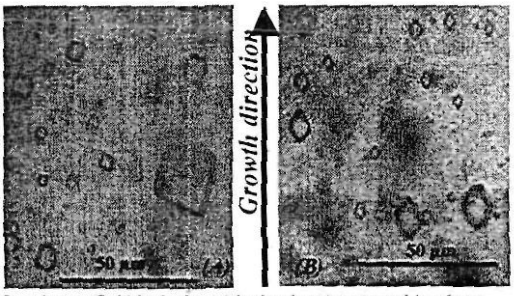

Figure -3: primary fluid inclusions (single-phase) arranged in plane parallel to the growth direction of host crystals. The inclusions are different in size (a&B) and become brown during the melting indicating the formation of a minerals (b)

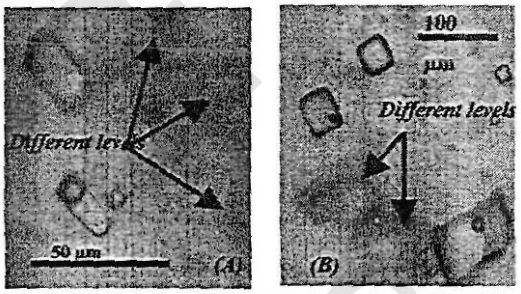

Figure-4: single phase (liquid) inclusions with negative form.NB: the inclusions at different levels within the host crystal and the vapor formed artificially freezing

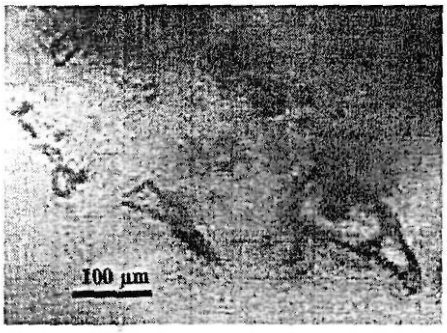

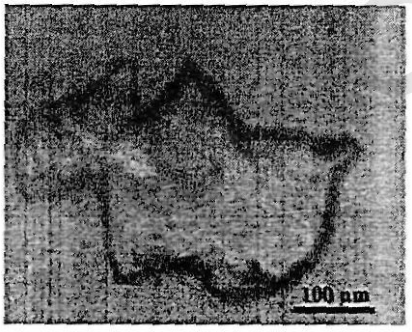

Figure-5: Cavity filed with liquid Inclusions (single- phase) (A&B) and hydrocarbons (A)

PIATE-49

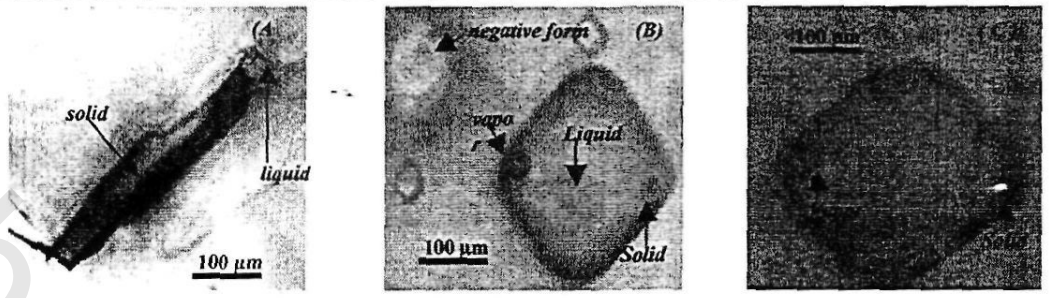

Figure-6: Two-phase(Liquid-solid) inclusions. Vapor bubble produced artificially by freezing.The liquid phase is hydrocarbon in (A).The solid is mineral in (B&C). Polarized light and crossnicols

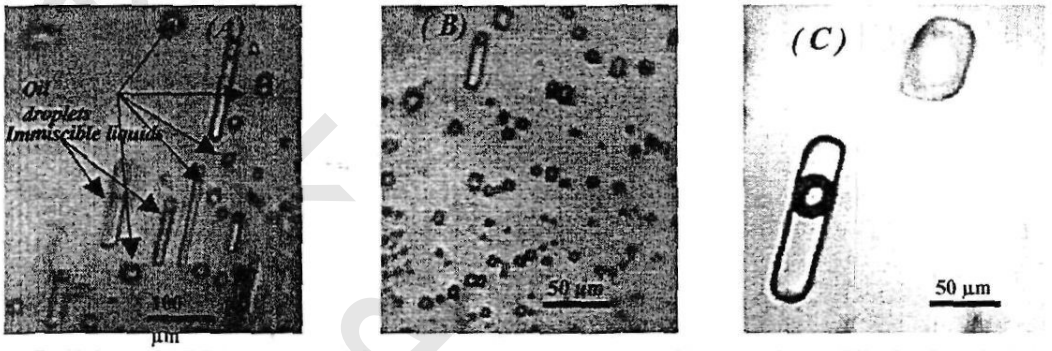

Figure-7: Oriented oil (single-phase) inclusions in gypsum (A) and in anhydrite (B) with immiscible two liquids , probably hydrocarbon,and brines (A&C). Ultraviolet light

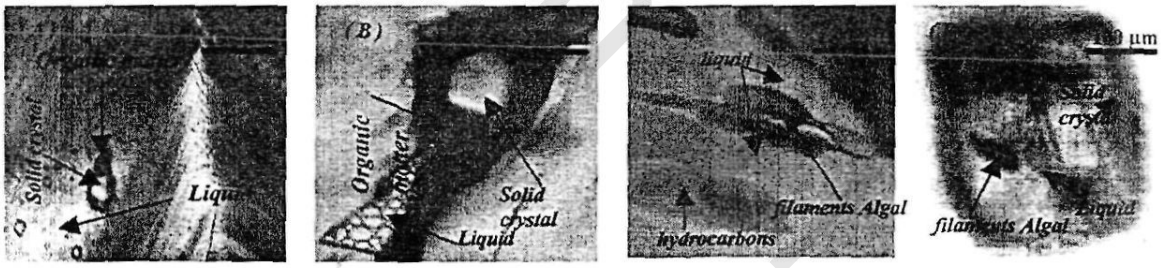

Figure-8: Three-phase (liquid-algal filamentous or organic matter-solid crystal) inclusions parallel to the growth direction of host crystals

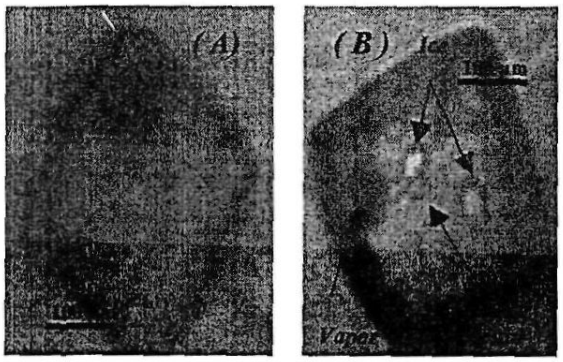

Figure-9: Dark brownish color of fluid inclusions (A) and stretched and irregular shape of the vapor bubble up on freezing the fluid inclusions. Temperature range from -61C to –81C

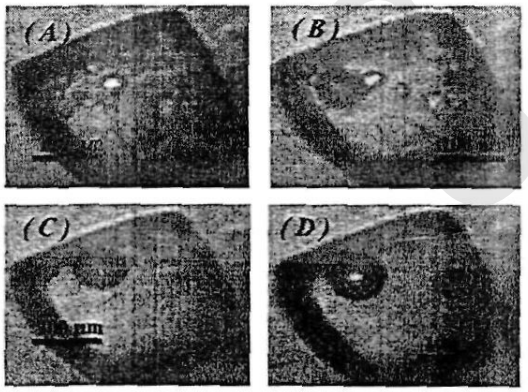

Figure-10: Sequence of melting point behavior of primary fluid inclusion. Vapor bubble increase and ice crystal decrease in size with slight movement of vapor bubble

Figure -39: Comparison of the final melting temperature of ice in primary fluid inclusions of evaporite with the calculated melting temperature of ice from the thermochemical model of Spencer et al, 1990 A=fresh water saturated with Calcium sulfate, B=normal sea water , C=recycled seawater saturated with gypsum derived from dissolution, and D=seawater evaporated to gypsum saturation.

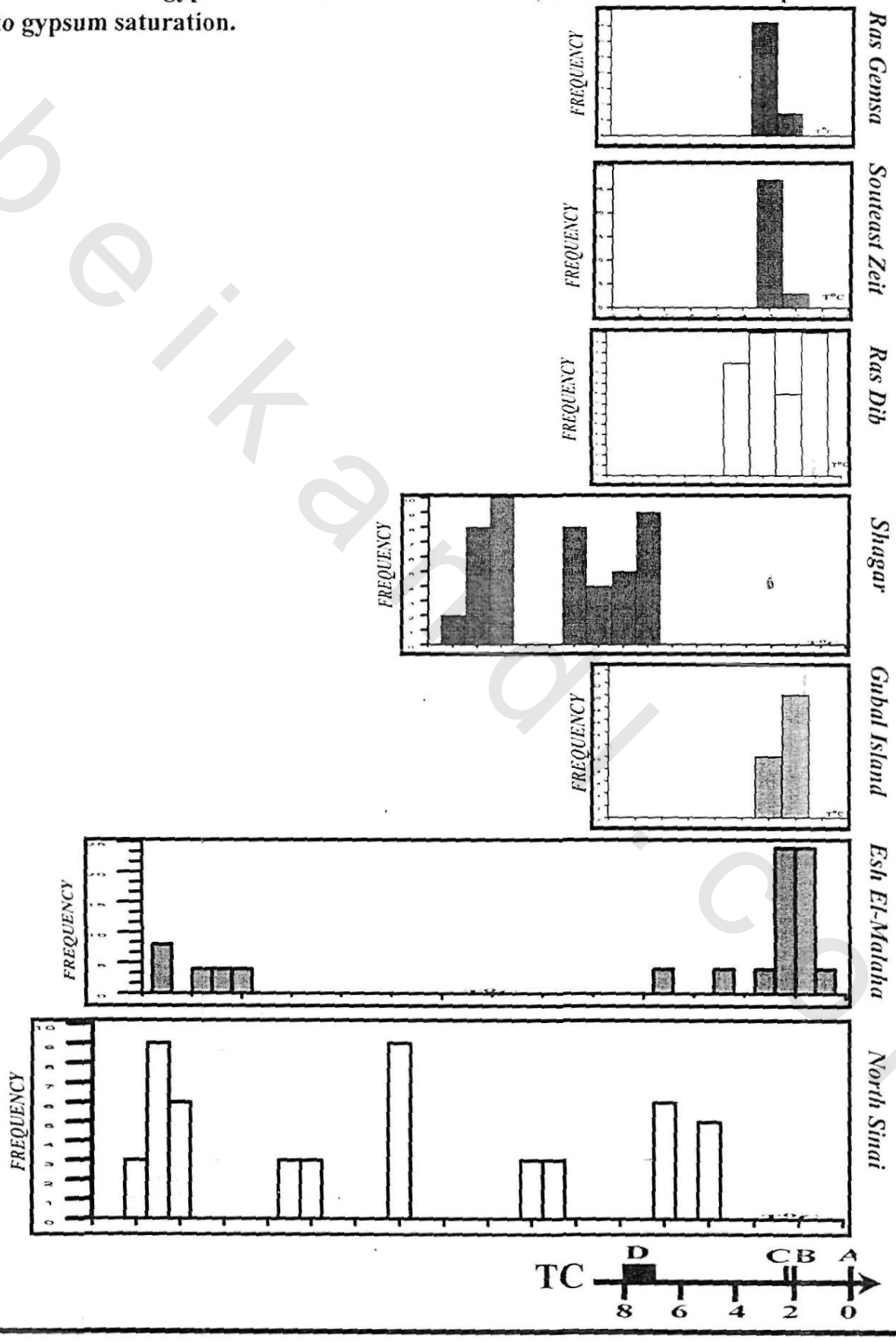

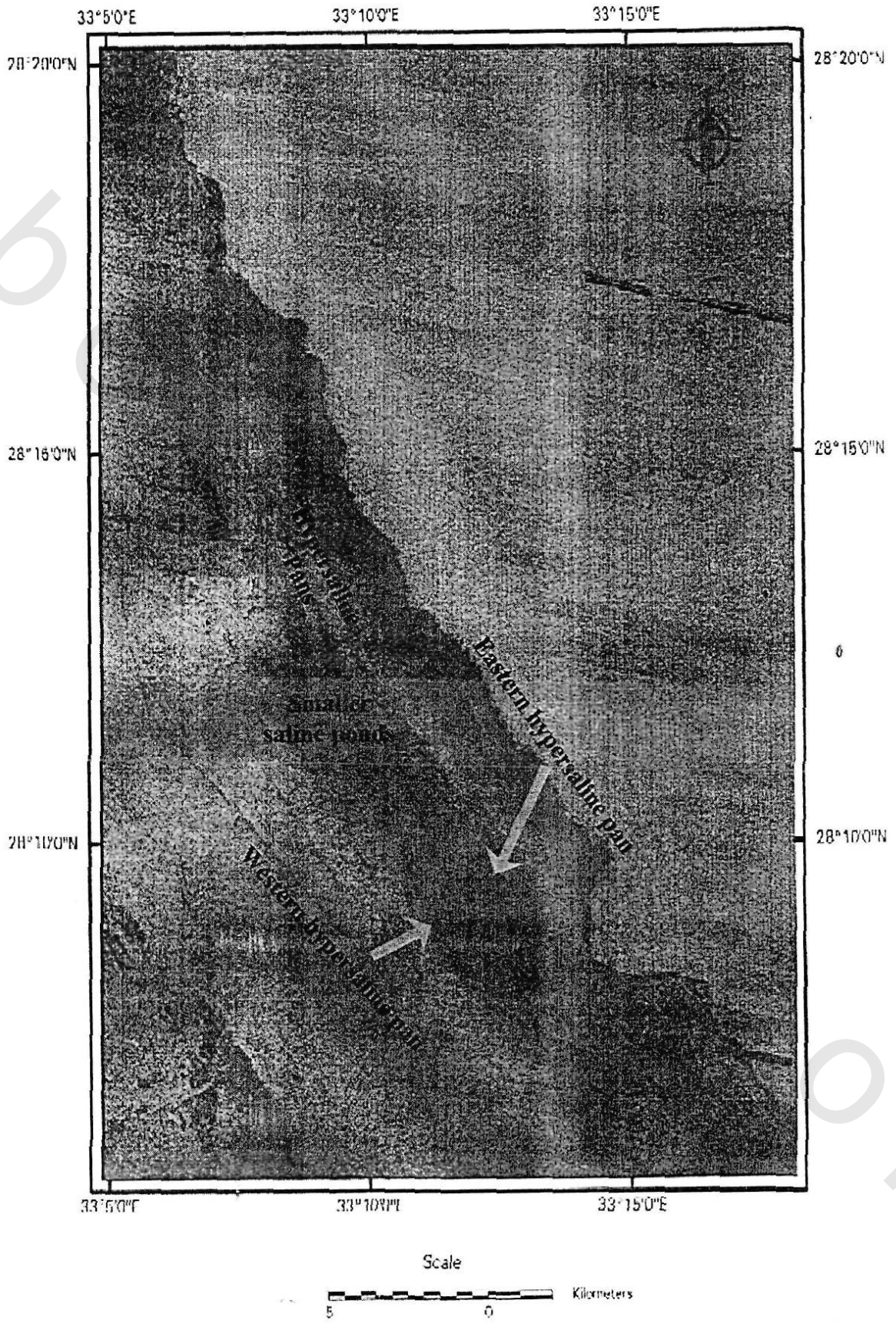

Figure -40 : The thermal analysis maps of principal component 7.4.1 in R.G.B for Ras Shukeir coastal sabkha, 2003

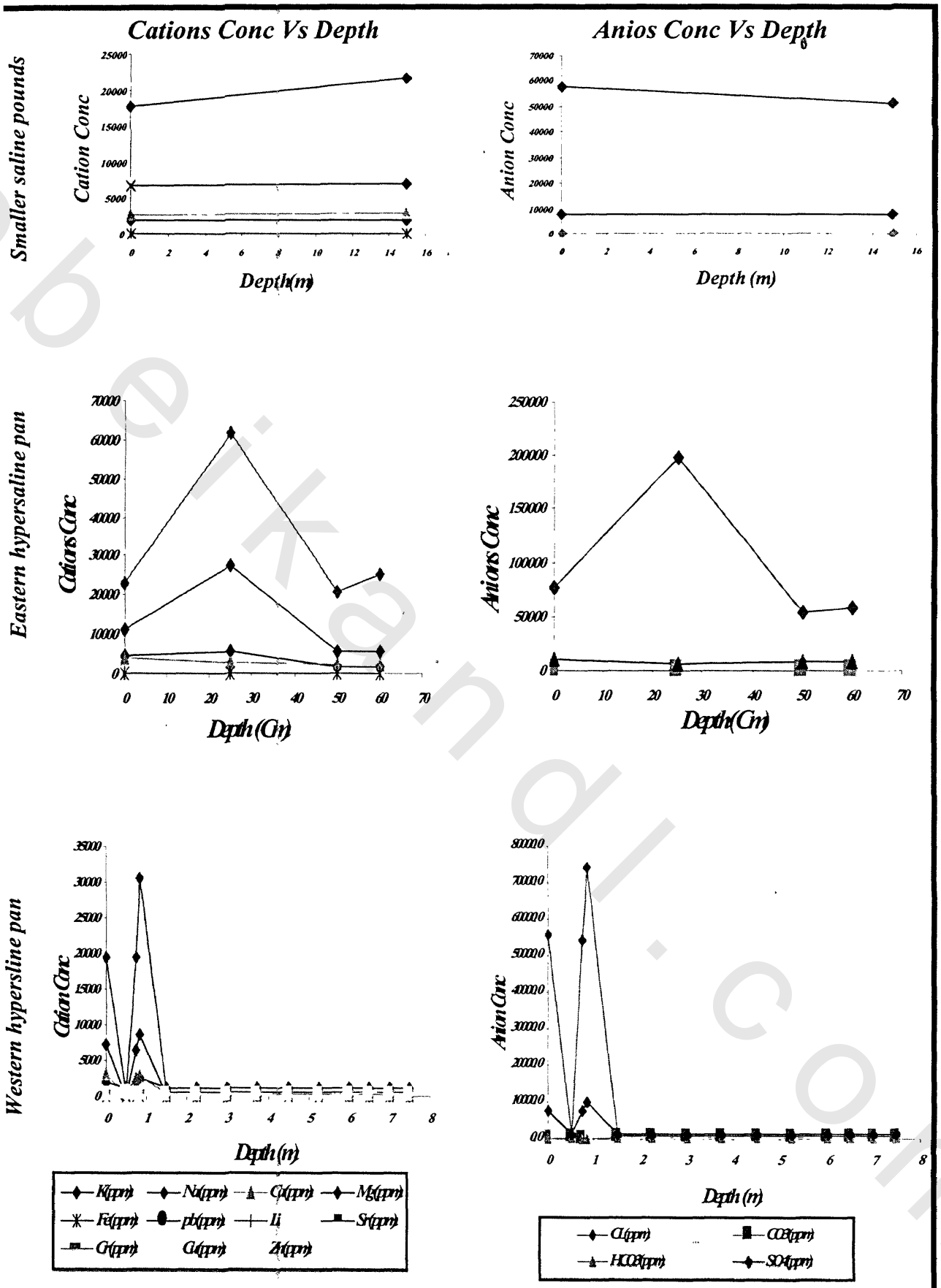

Figure.-41: The vertical Distribution of Hydrochemical Composition of brine Samples from The study Area displaying existence of layering within the water body

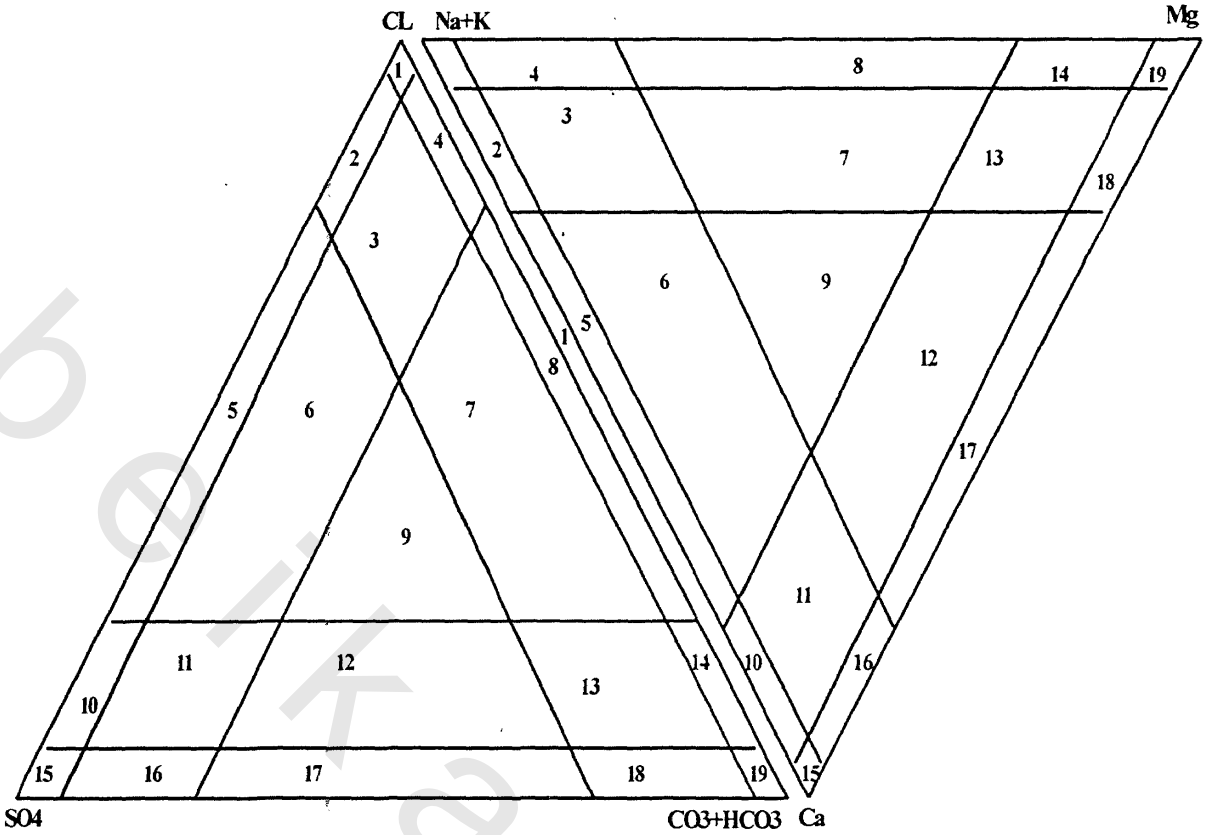

Figure -42: Brine classification scheme proposed by Haride and Eugster,1970

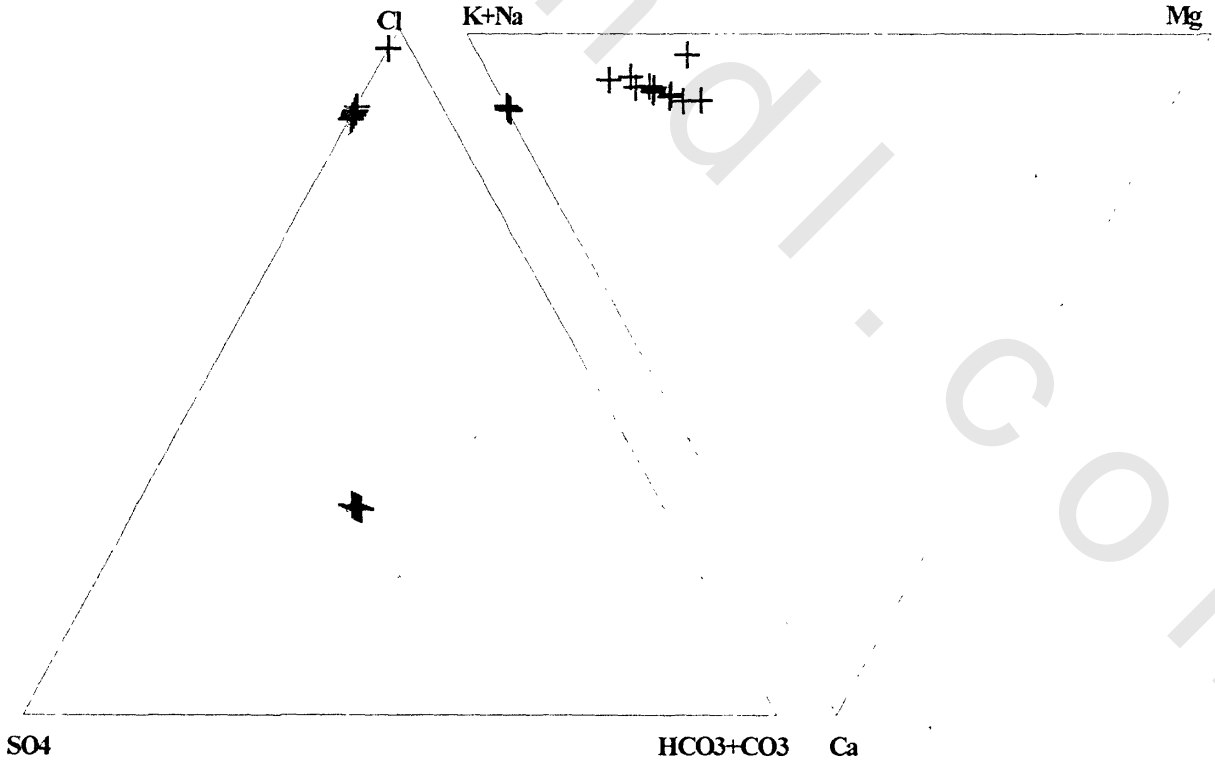

Figyre-43: Composition plot of analyzed brine samples from the study area according to Haride and Eugster,1970

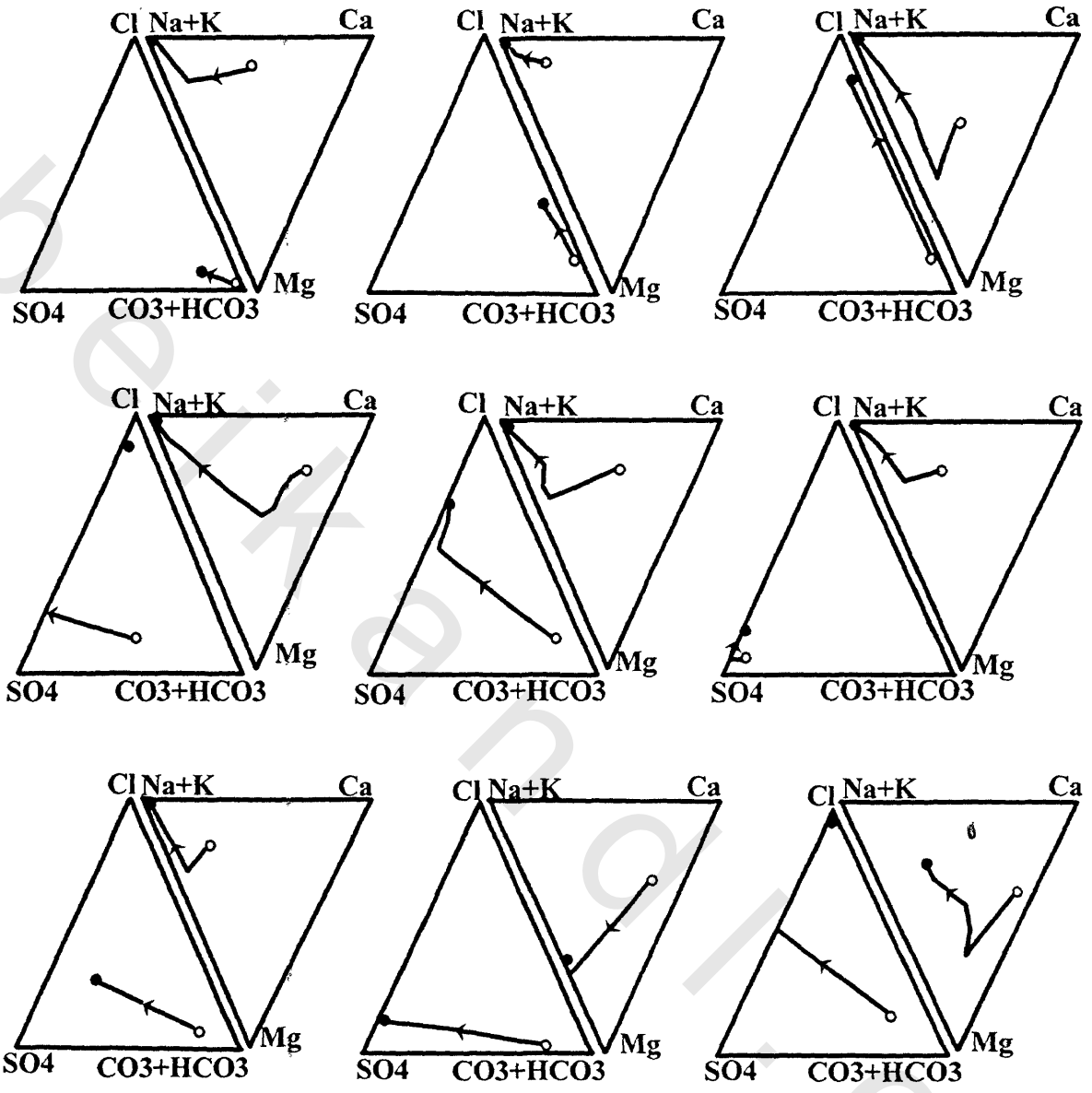

Figure-44: Individual calculated evaporation paths, open circles are dilute waters and solid circles are brines at an ionic strength 5 a:Sierra Nevada Springs(Feth *et al.*,1964 and Garrels and Mackenzie,,1967); b: rhyolite water W 1.2; c: basalt water W 2.9; d: shale water W5.5; e: average North American river water (Livingstone,1963);f: shale water W5.6, g: Deep Springs Lake, California, Bog-Mound Spring (Jones, 1965); h: quartzite water W 9.5; i: sandstone Water W4.4 (all water from White *et al.*,1963). In mole percent.

Figure-45: Modified Van Krevelen diagram for analysed samples from Ras Shukeir area

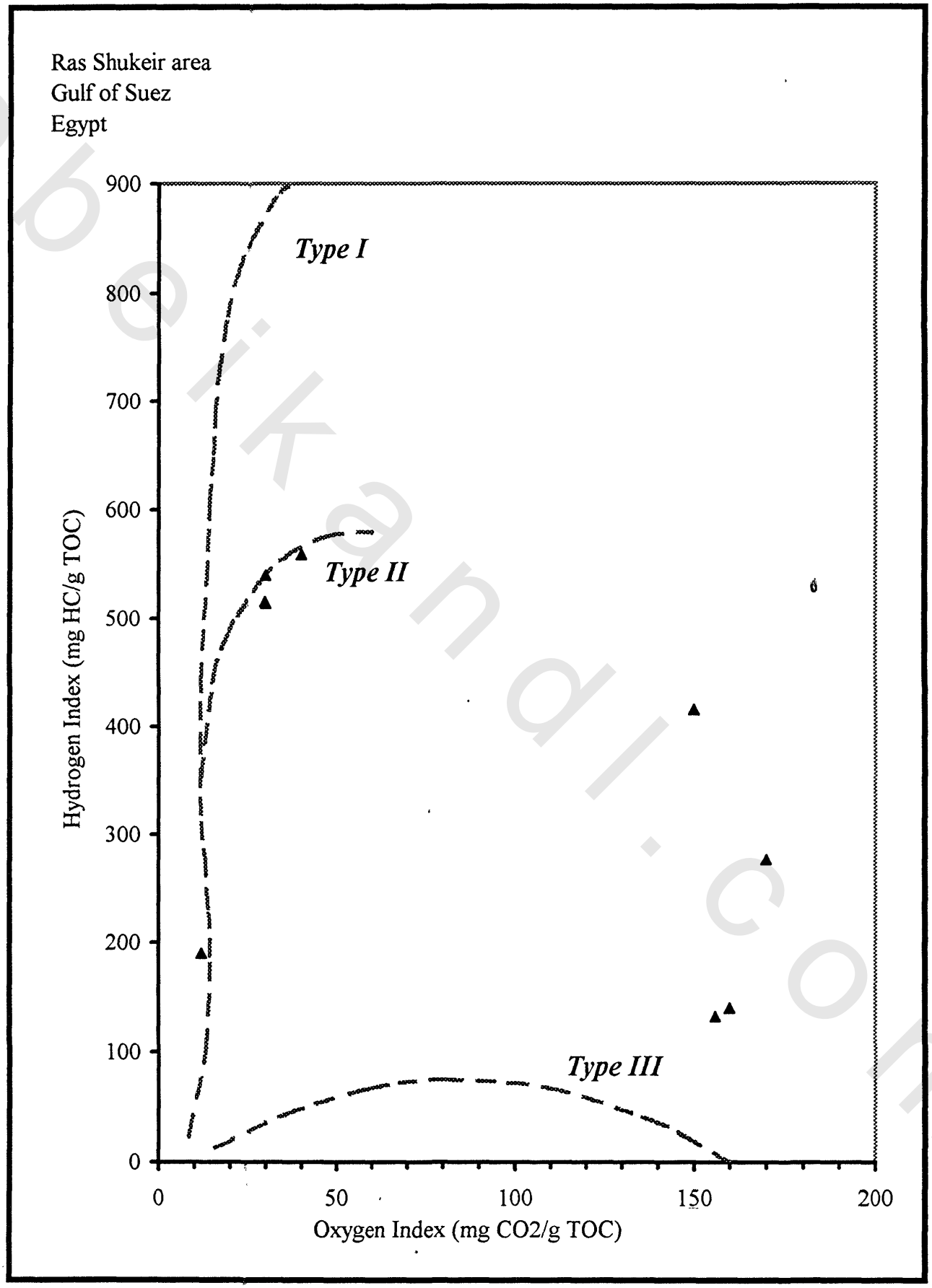

Figure-46: Modified Van Krevelen diagram for analysed samples from Ras Gemsa, Gulf of Suez, Eygpt

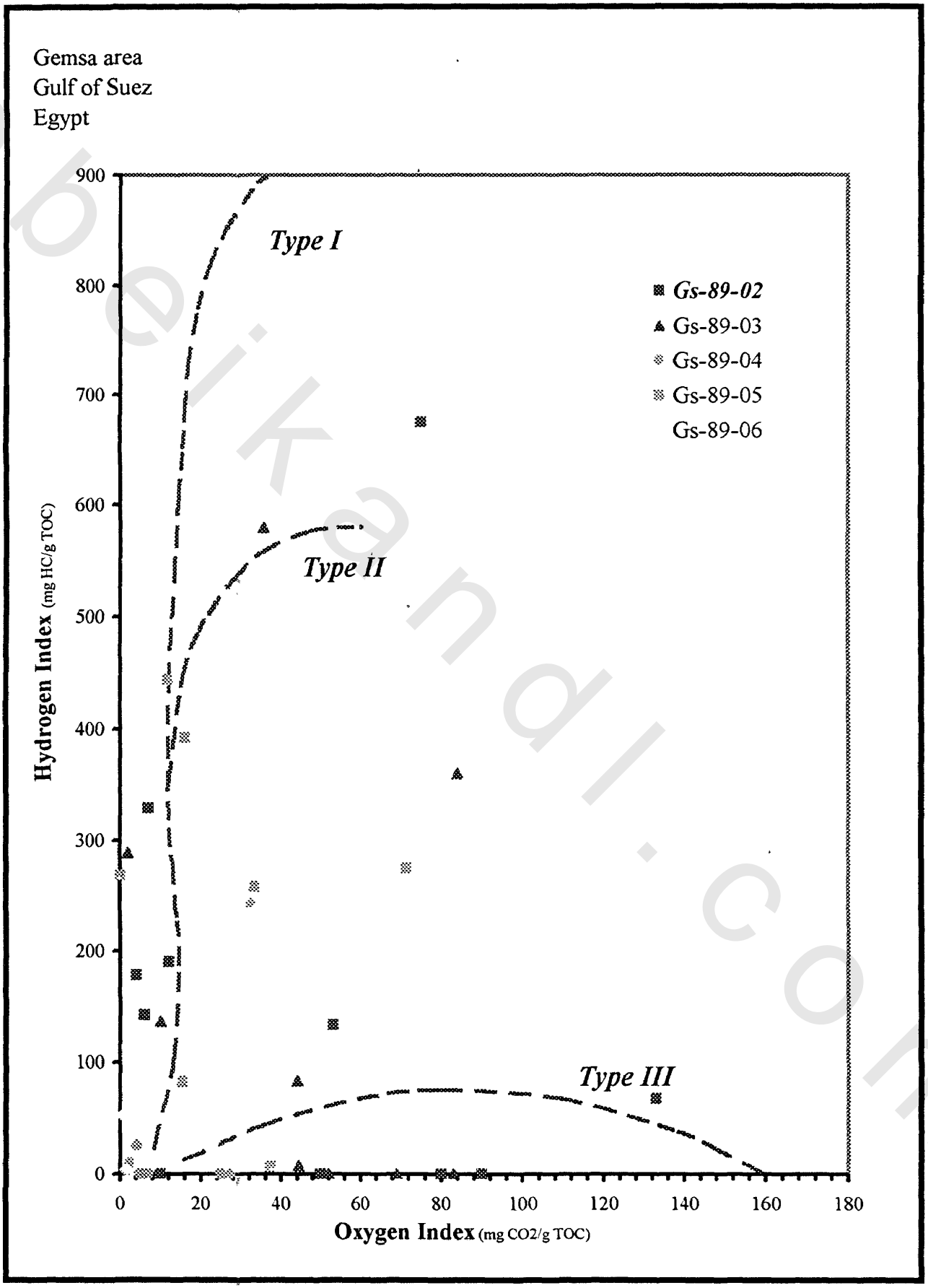

Figure- 47 : Infrared modified diagram for the investigated evaporite core samples from Ras Gemsa Area

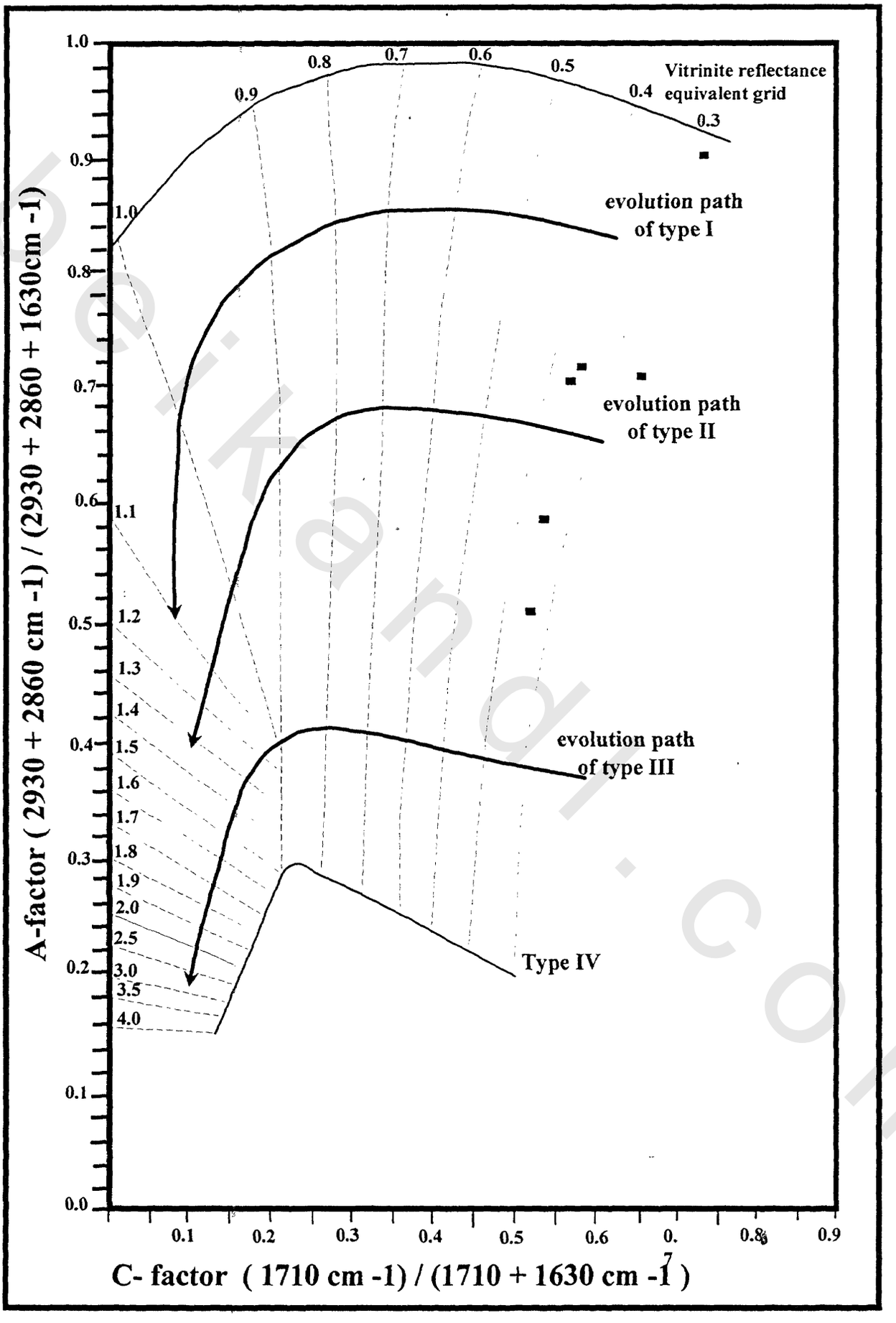

Figure-48: GC diagrams for the extracts of subsurface evaporite core samples from Ras Gemsa area

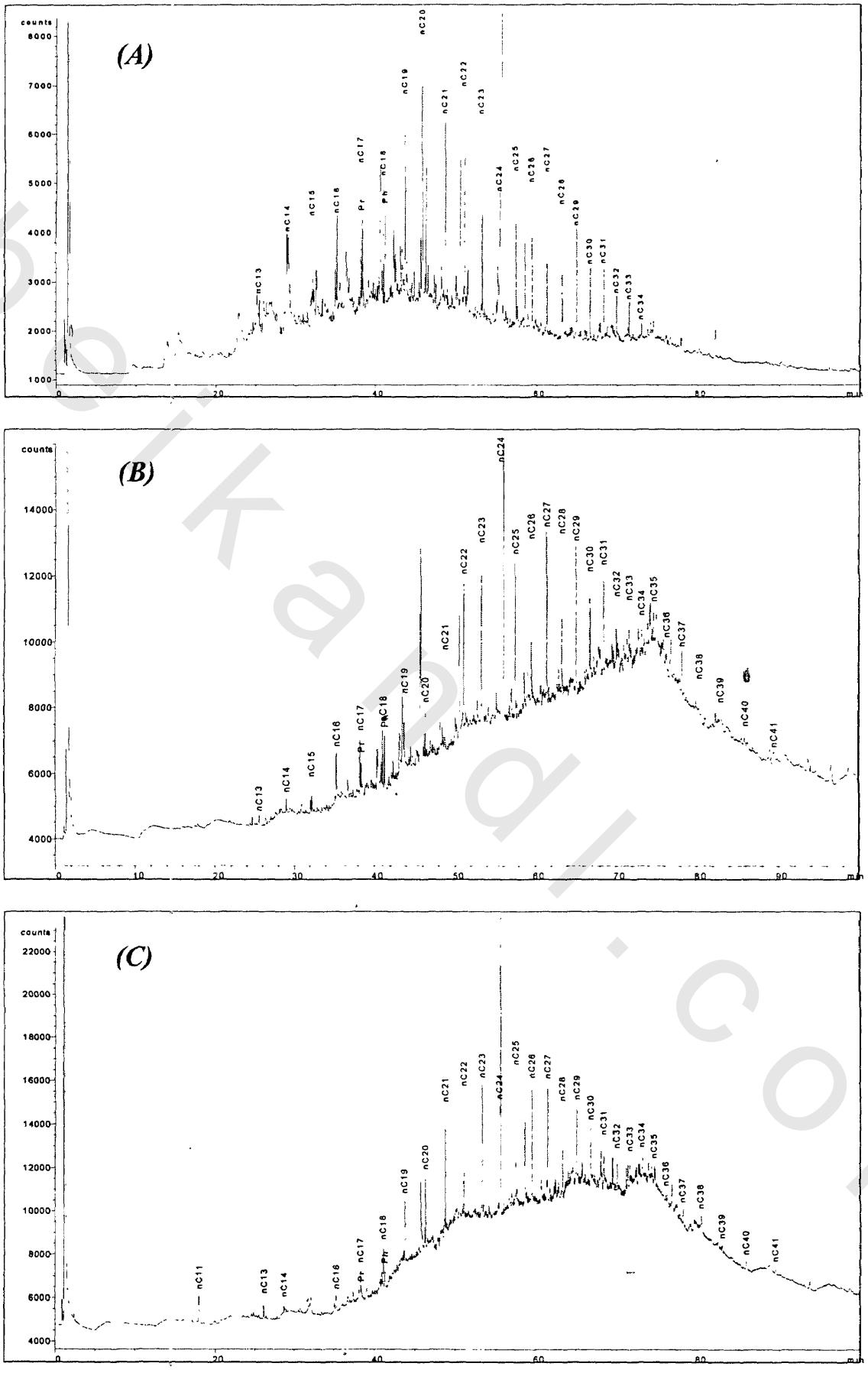

The n-alkane patterns show the unimodal distribution at A &B and n-alkane bulge between C21 to C32 at (B&C)

Figure -49

GEOCHEMICAL LOG

Area name : Ras Gemsa

Well Name : GS-89-03

Start Depth : 89.7 M
End Depth : 405.45 M
Plot Scale 1 : 2500

Country : EGYPT

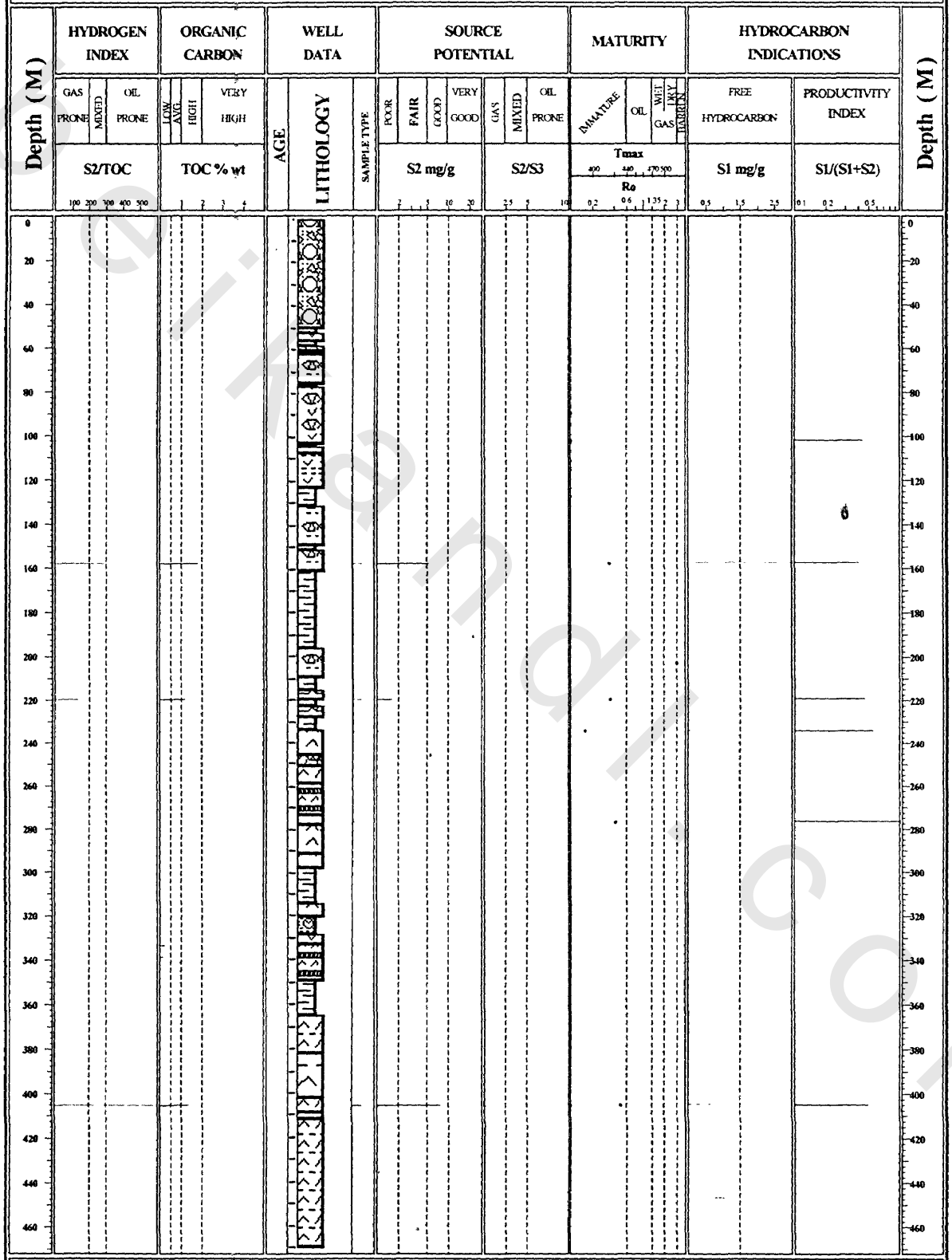

S1 HC already in rock
S2 HC from Kerogen Pyrolysis
S3 CO2 from Kerogen Pyrolysis

Sample Type	Symbol	Line Type	Tmax
Cuttings		———	•
Sidewall		- - - -	*
Core		----------	o

Ro ◆
VL *

TOC cut off .0 %
S2 cut off .0 %

Figure -50

GEOCHEMICAL LOG

Area Name: Ras Gemsa

Well Name : Gs-89-04

Start Depth : 95.6 M
End Depth : 316 M
Plot Scale 1 : 2000

Country . EGYPT

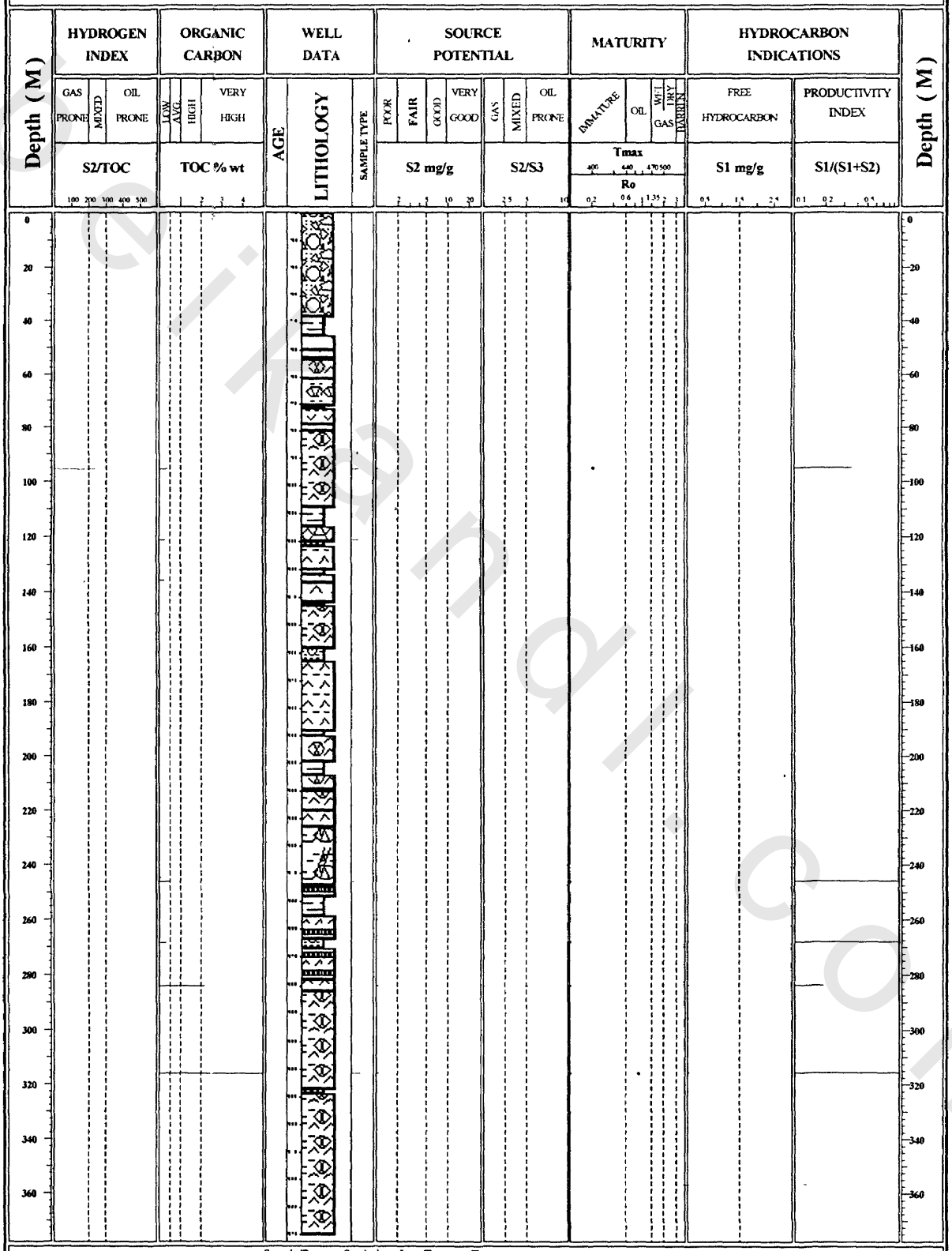

S1 HC already in rock
S2 . HC from Kerogen Pyrolysis
S3 CO2 from Kerogen Pyrolysis

Sample Type	Symbol	Line Type	Tmax
Cuttings		———	•
Sidewall		- - - -	♦
Core		.....	o

Ro ◆
VL ×

TOC cut off : 0 %
S2 cut off : 0 %

Figure-51

GEOCHEMICAL LOG

Area Name : Ras Gemsa **Well Name : Gs-89-05**

Start Depth : 56.5 M
End Depth 269 5 M
Plot Scale 1 2000

Country : EGYPT

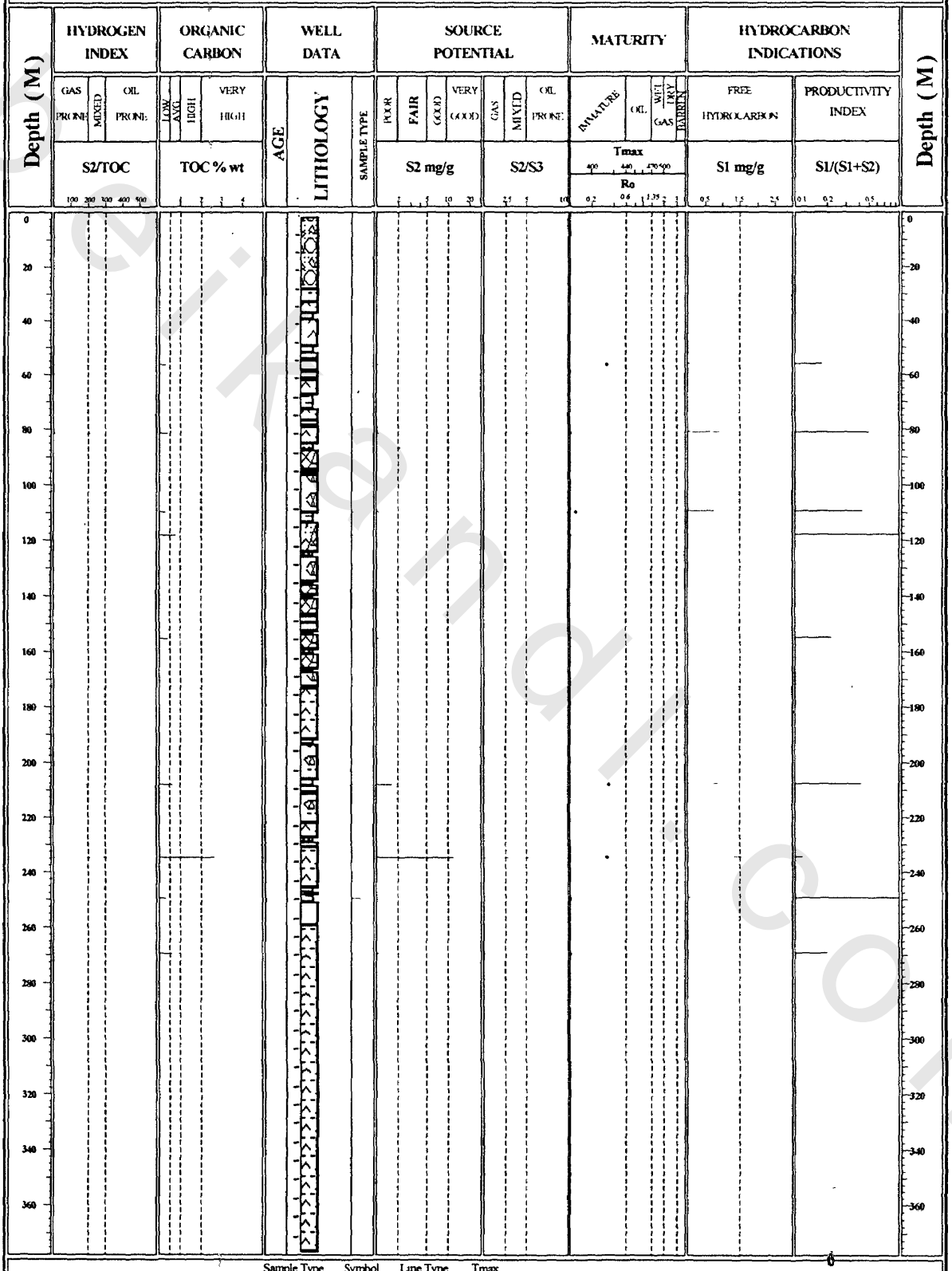

S1 HC already in rock
S2 HC from Kerogen Pyrolysis
S3 CO2 from Kerogen Pyrolysis

Sample Type: Cuttings, Sidewall, Core
Symbol
Line Type
Tmax
Ro ◆
VL *

TOC cut off 0 %
S2 cut off 0 %

Figure -52

GEOCHEMICAL LOG

Area Name : Ras Gemsa **Well Name :** Gs-89-06

Start Depth . 46 FT
End Depth : 250.8 FT
Plot Scale 1 : 1000

Country · EGYPT

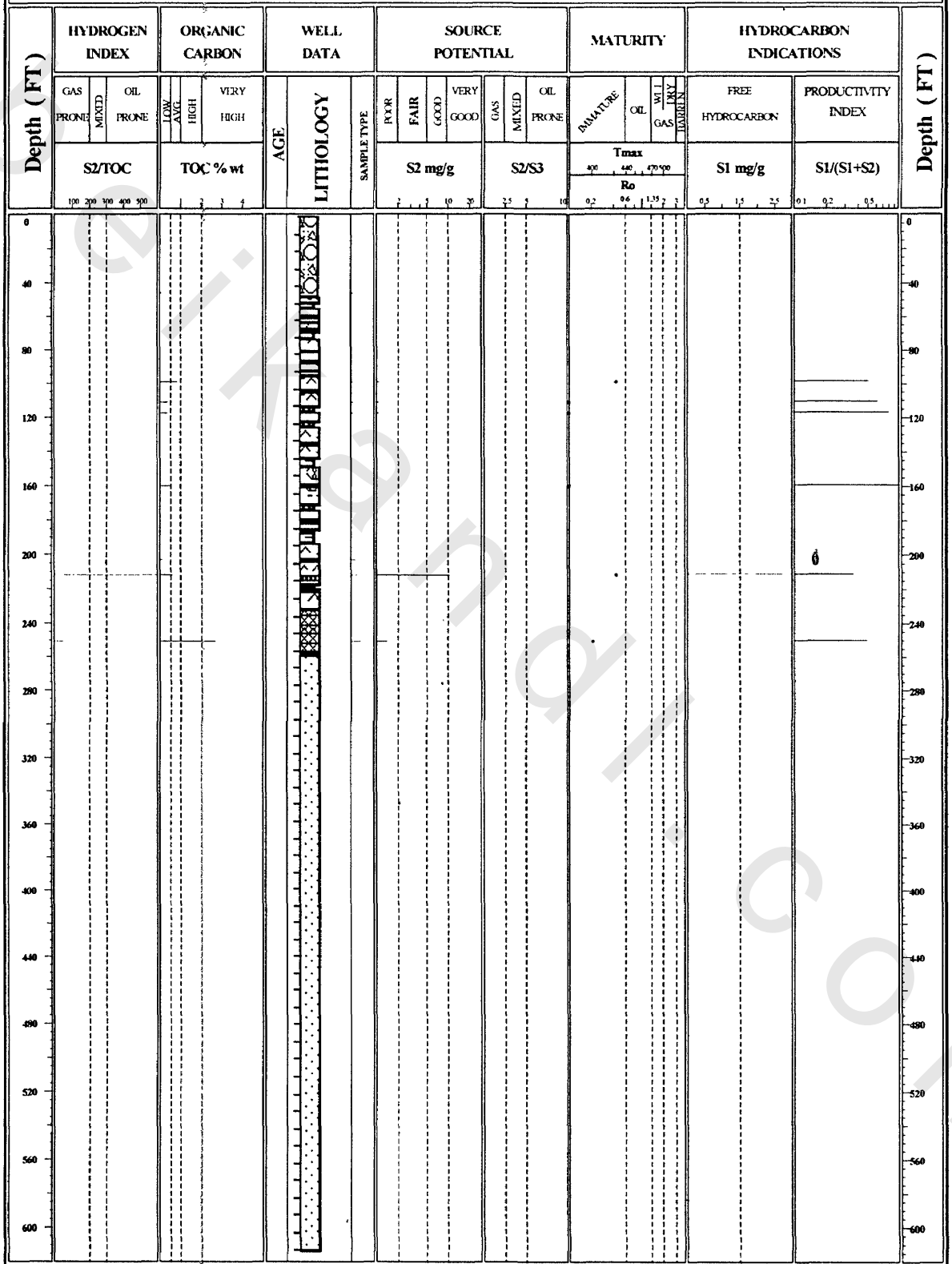

S1 HC already in rock
S2 HC from Kerogen Pyrolysis
S3 CO2 from Kerogen Pyrolysis

Sample Type	Symbol	Line Type	Tmax
Cuttings		———	+
Sidewall		- - -	•
Core		.....	o

Ro ◆
VL *

TOC cut off · 0 %
S2 cut off . 0 %

Figure-53: Modified Van Krevelen diagram for analyzed samples from South East Zeit

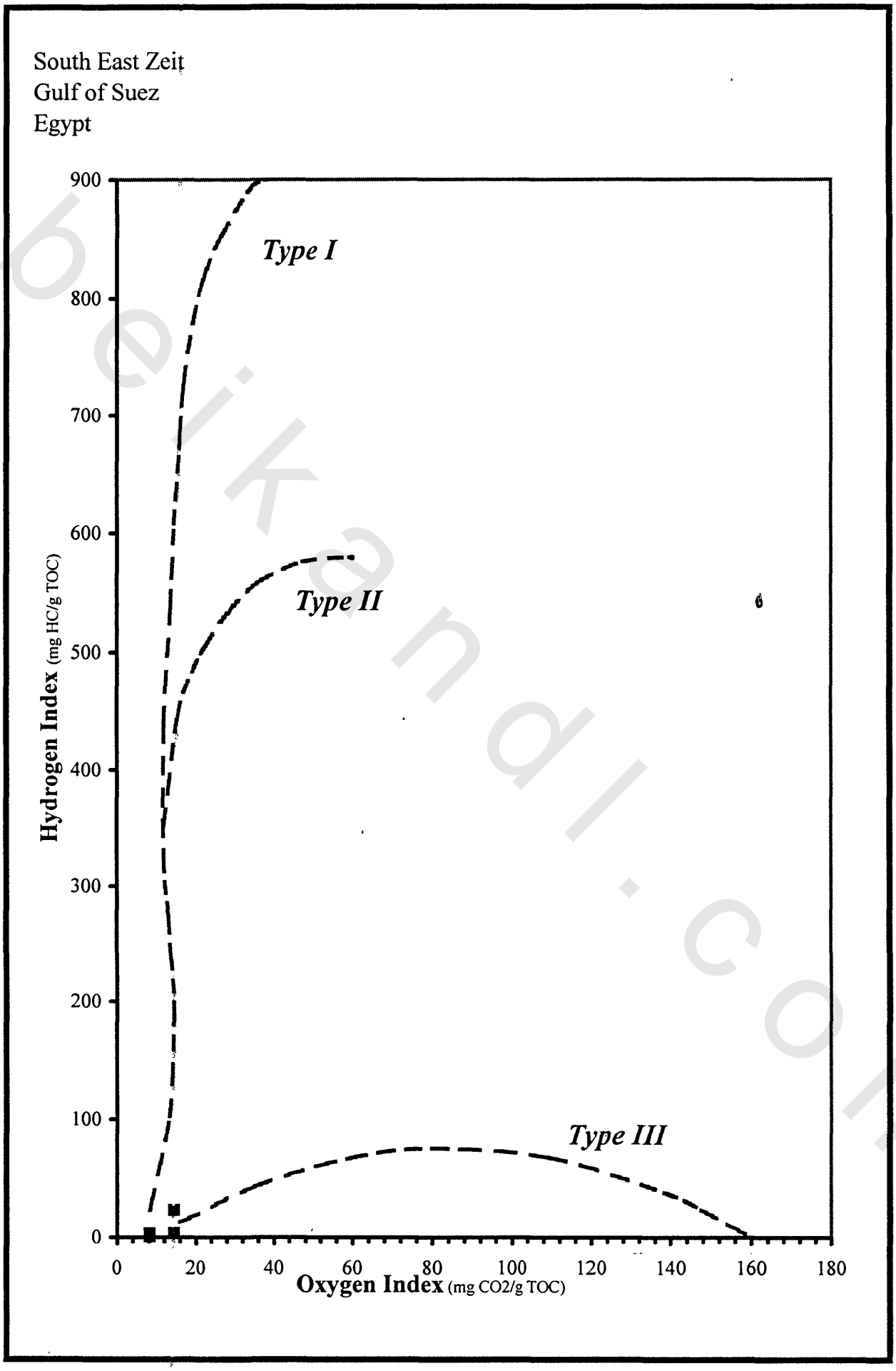

Figure -54

GEOCHEMICAL LOG

Area Name : South East Zeit

Well Name : GS-89-07

Start Depth : 56.1 M
End Depth : 174.4 M
Plot Scale 1 : 1000

Country . EGYPT

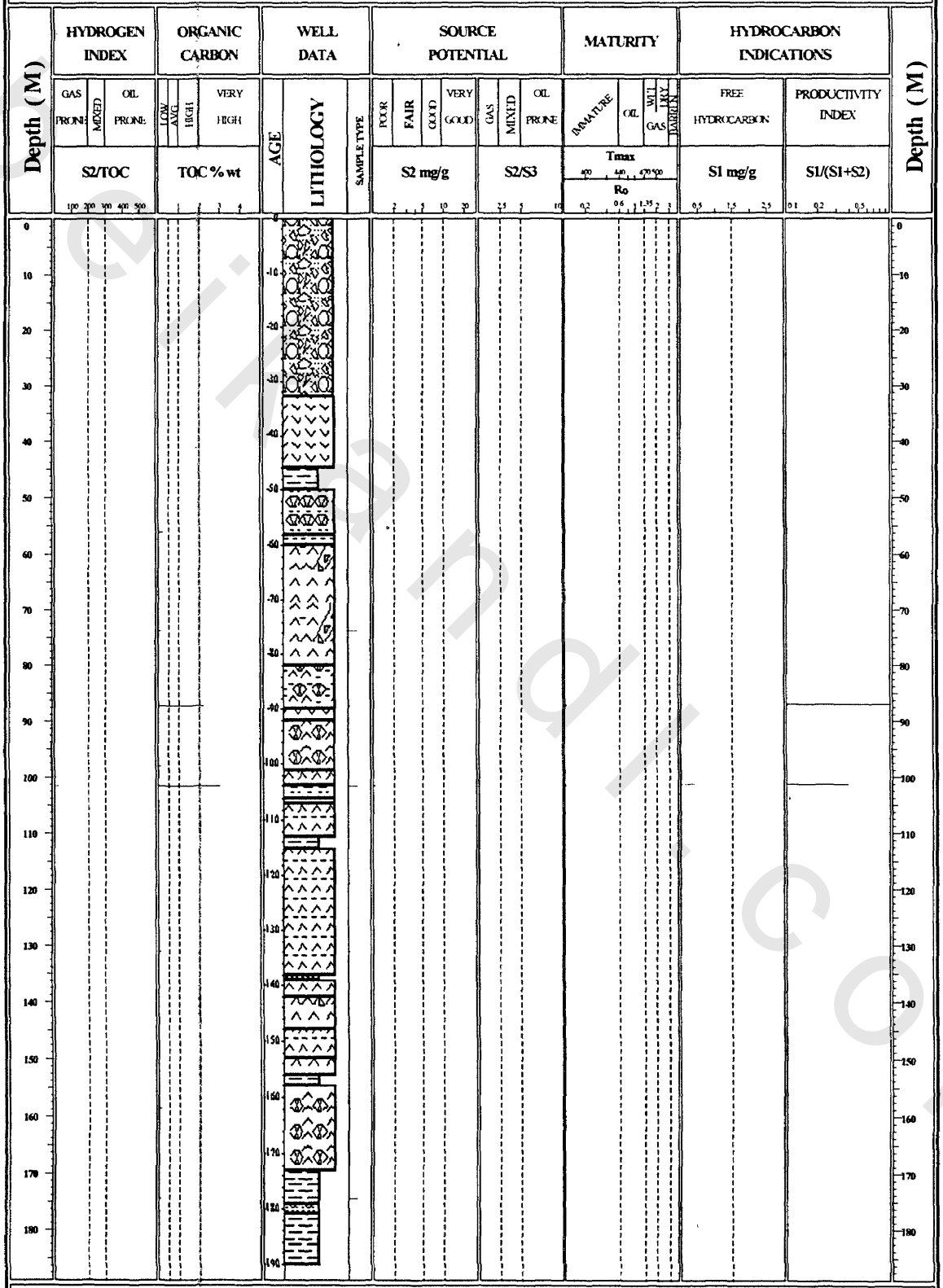

S1 : HC already in rock
S2 . HC from Kerogen Pyrolysis
S3 CO2 from Kerogen Pyrolysis

Sample Type	Symbol	Line Type	Tmax
Cuttings			•
Sidewall			♦
Core			o

Ro ◆
VL *

TOC cut off : 0 %
S2 cut off : 0 %

Figure-55 : Infrared modified diagram for the investigated evaporite core samples from Ras Dib area

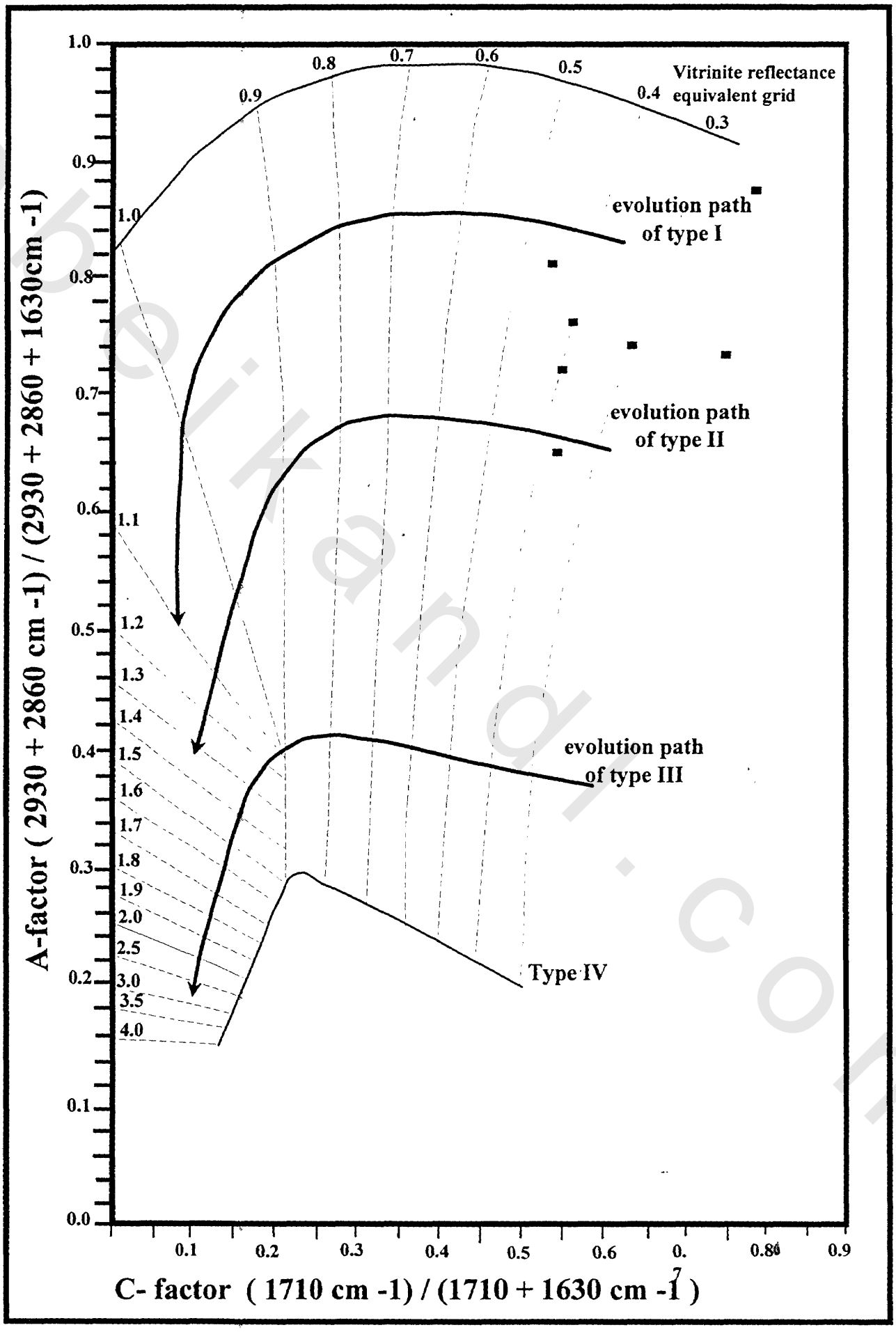

Figure-56: Modified Van Krevelen diagram for analysed samples from Ras Dib area, Gluf of Suez

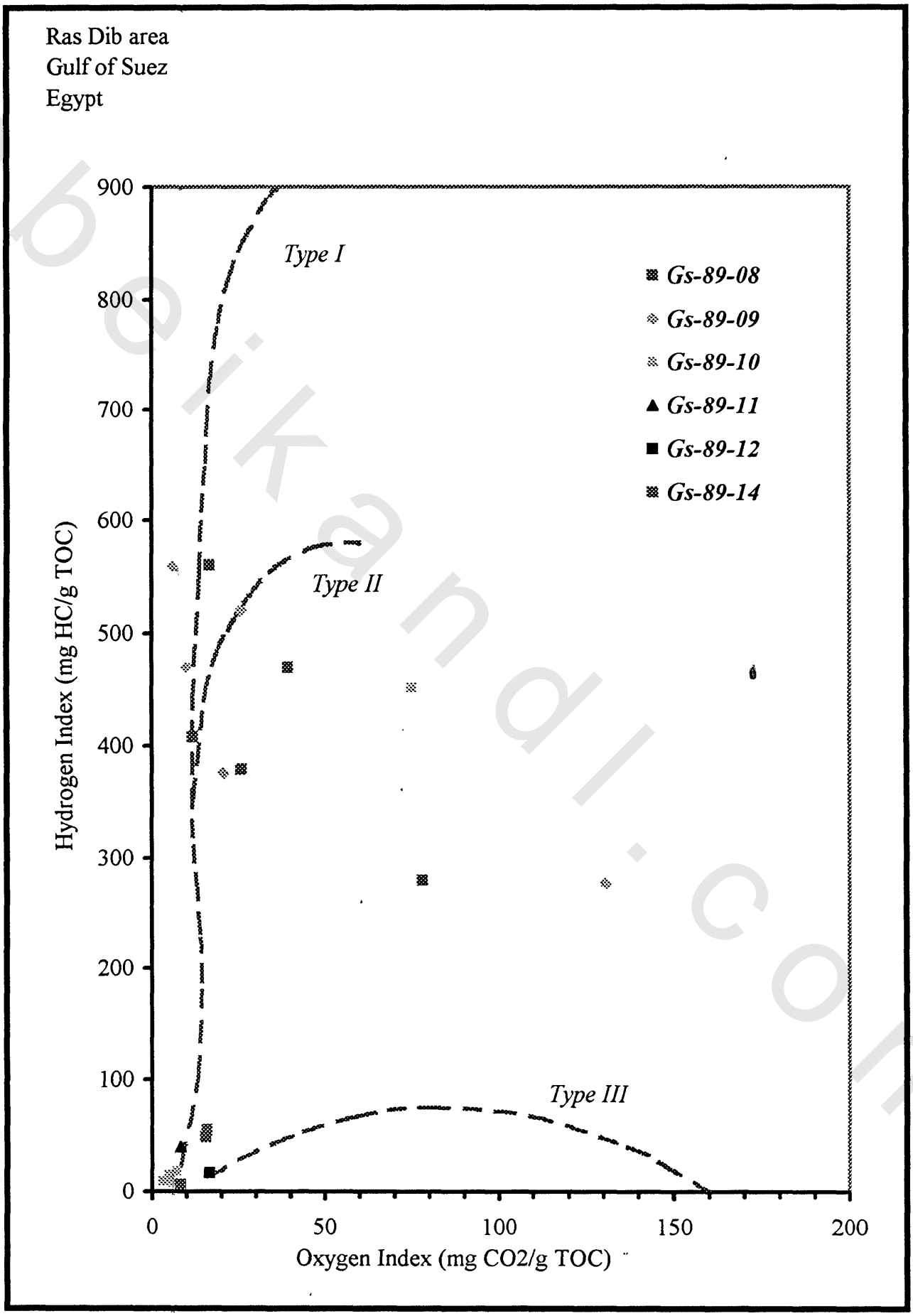

Figure -57: GC diagram of bitumen extracts of subsurface evaporite core samples from Ras Dib area

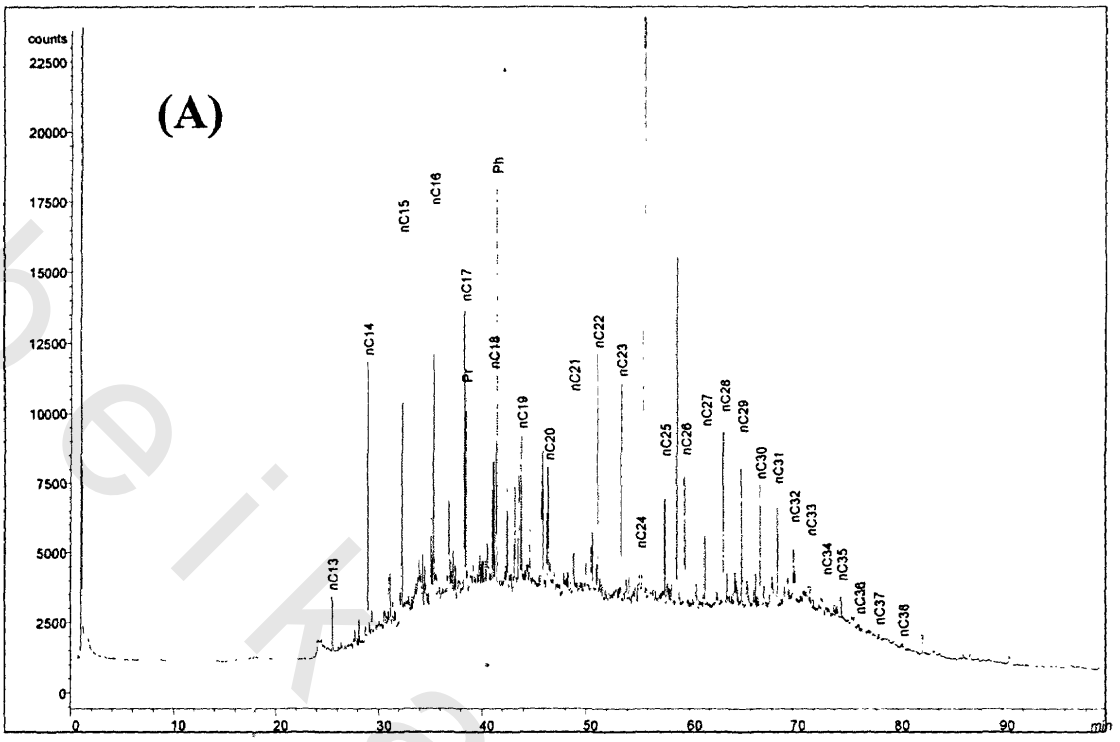

A: Unimodal distribution pattern n-alkane with predominance of phytane which indicates marine (algal and planktonic with bacterial) source of organic matter

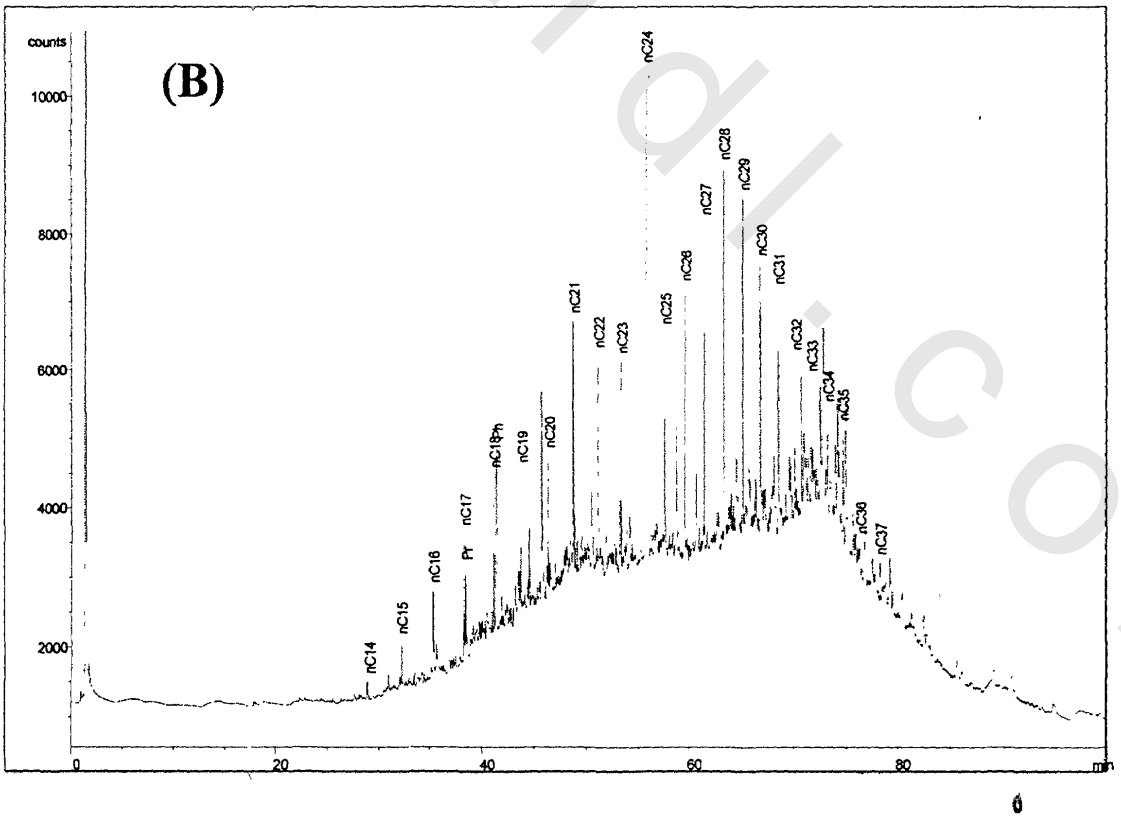

B: The naphthane bluge betwwen C22-C32 indicates the low degree of thermal maturity

Figure -58: GC diagram of bitumen extracts of subsurface evaporite core samples from Ras Dib area

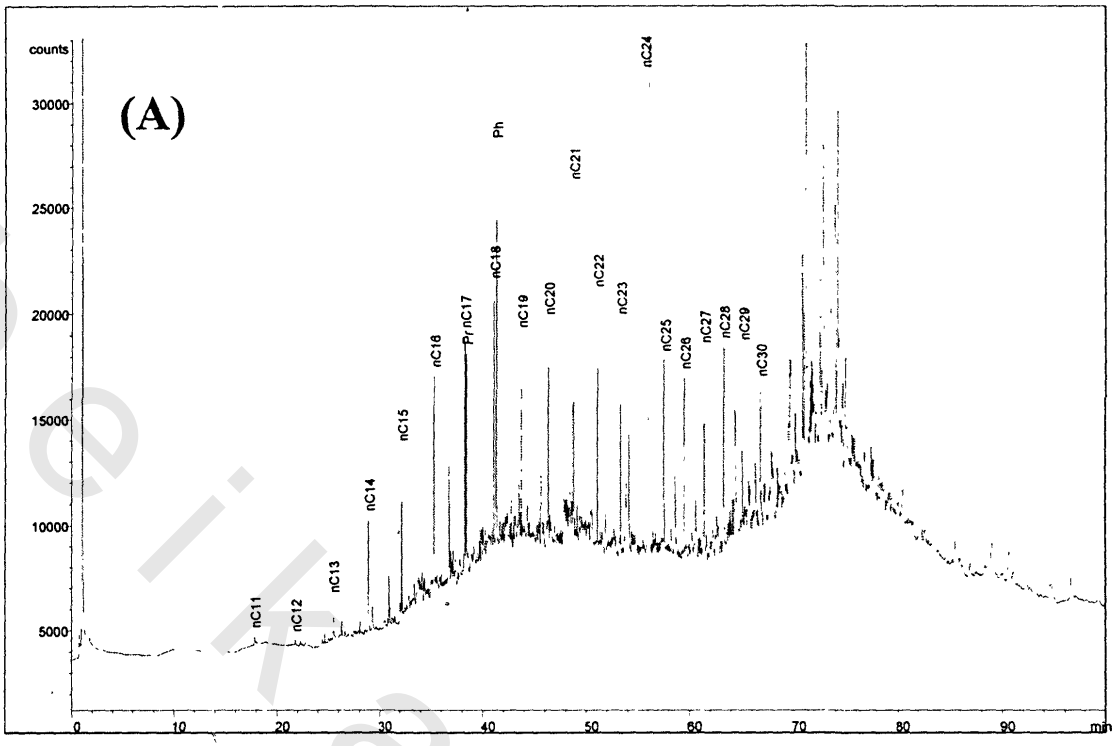

(A) : Bimodal of n-alkane distribution pattern indicates significate contribution of land plants to the source of organic matter

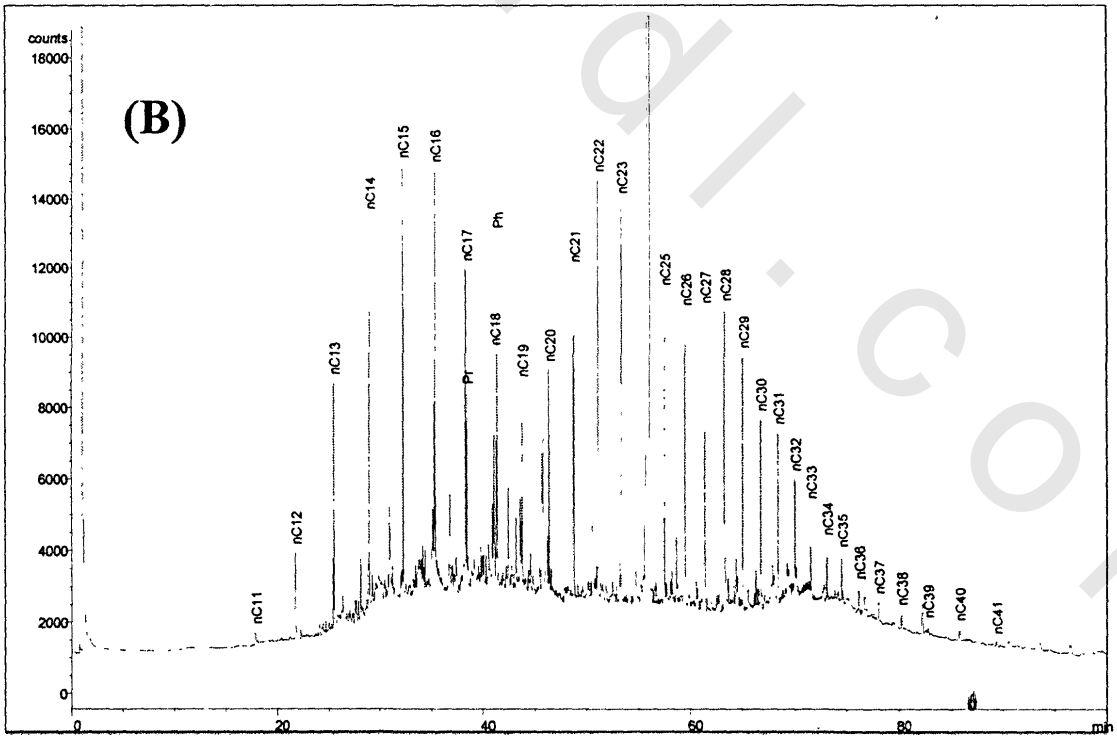

(B):Unimodal distribution pattern with high concenteration of acyclic isopernoids indicates marine source of organic matter

Figure-59

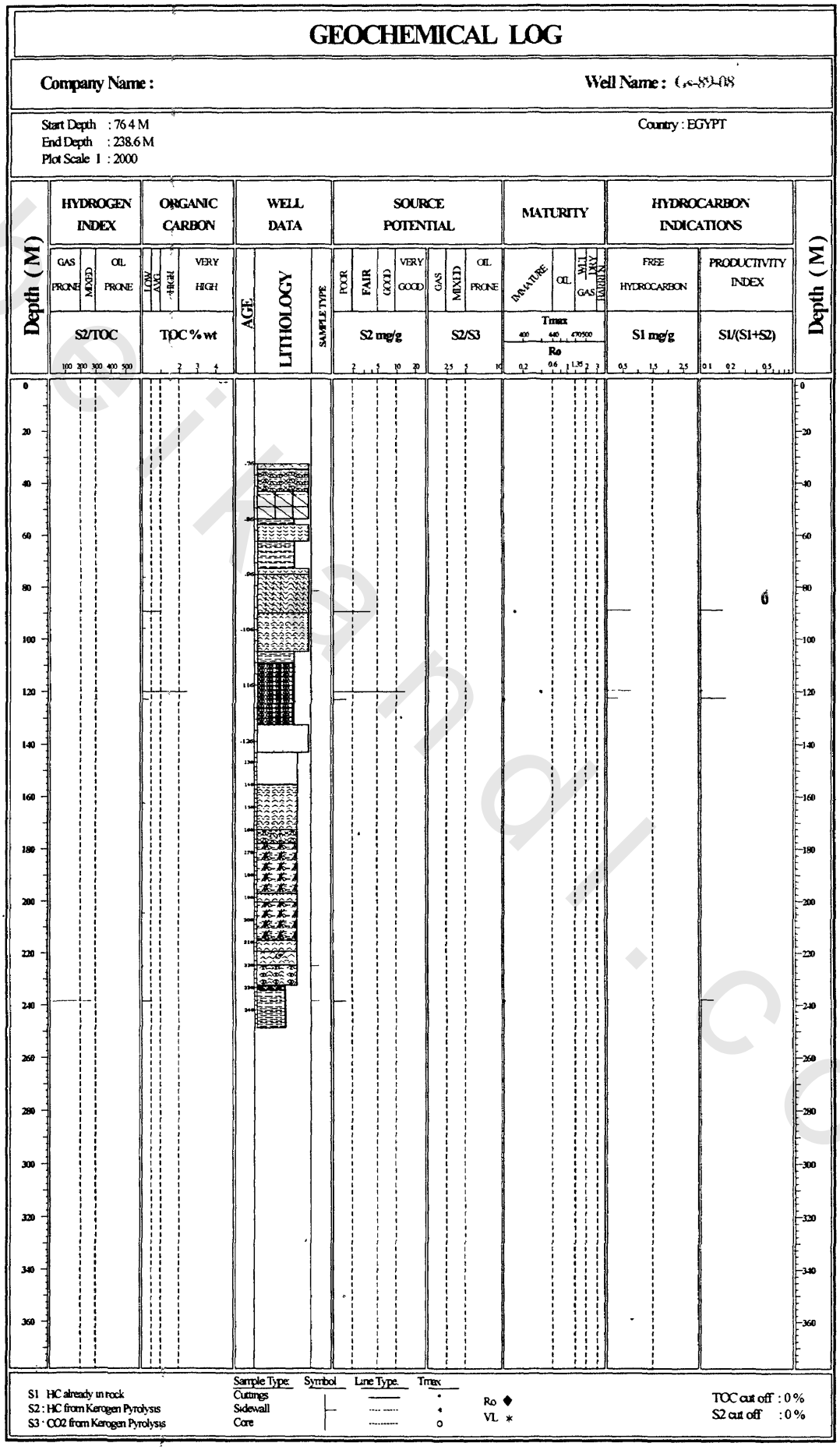
GEOCHEMICAL LOG
Company Name :
Well Name :
Start Depth : 76.4 M
End Depth : 238.6 M
Plot Scale 1 : 2000
Country : EGYPT
Depth (M)
HYDROGEN INDEX
GAS PRONE
MIXED
OIL PRONE
S2/TOC
100 200 300 400 500
ORGANIC CARBON
LOW
AVG.
HIGH
VERY HIGH
TOC % wt
1 2 3 4
WELL DATA
AGE
LITHOLOGY
SAMPLE TYPE
SOURCE POTENTIAL
POOR
FAIR
GOOD
VERY GOOD
S2 mg/g
2 5 10 20
GAS
MIXED
OIL PRONE
S2/S3
2.5 5 10
MATURITY
IMMATURE
OIL
WET GAS
VERY HARMFUL
Tmax
400 440 470 500
Ro
0.2 0.6 1 1.35 2 3
HYDROCARBON INDICATIONS
FREE HYDROCARBON
S1 mg/g
0.5 1.5 2.5
PRODUCTIVITY INDEX
S1/(S1+S2)
0.1 0.2 0.5
Depth (M)
0 20 40 60 80 100 120 140 160 180 200 220 240 260 280 300 320 340 360
S1 HC already in rock
S2 : HC from Kerogen Pyrolysis
S3 : CO2 from Kerogen Pyrolysis
Sample Type
Cuttings
Sidewall
Core
Symbol
Line Type
Tmax
Ro
VL
TOC cut off : 0 %
S2 cut off : 0 %

Figure 60

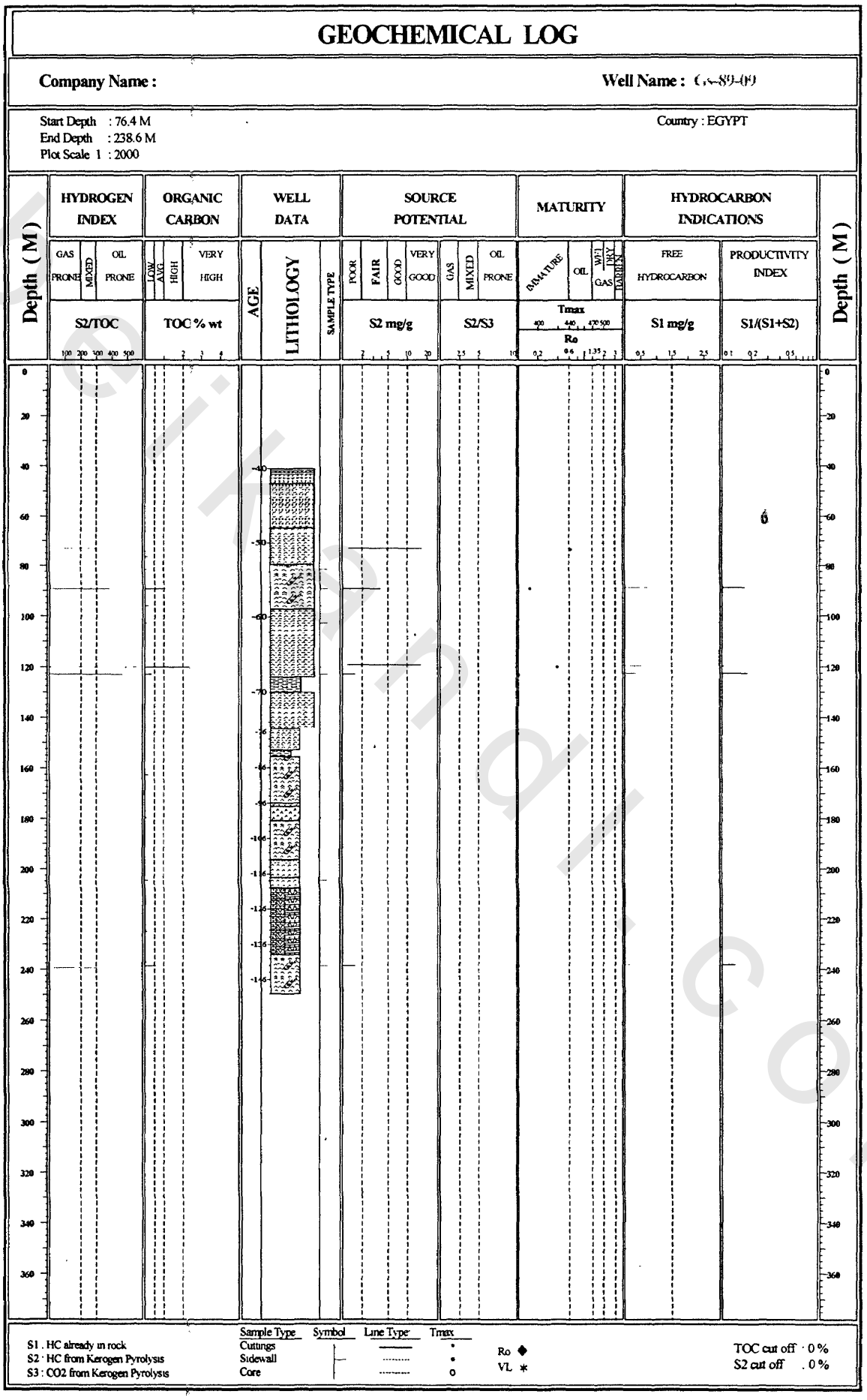
GEOCHEMICAL LOG
Company Name :
Well Name : G-89-09
Start Depth : 76.4 M
End Depth : 238.6 M
Plot Scale 1 : 2000
Country : EGYPT
Depth (M)
HYDROGEN INDEX
GAS PRONE
MIXED
OIL PRONE
S2/TOC
ORGANIC CARBON
LOW
AVG.
HIGH
VERY HIGH
TOC % wt
WELL DATA
AGE
LITHOLOGY
SAMPLE TYPE
SOURCE POTENTIAL
POOR
FAIR
GOOD
VERY GOOD
S2 mg/g
GAS
MIXED
OIL PRONE
S2/S3
MATURITY
IMMATURE
OIL
WET GAS
DRY GAS
Tmax
Ro
HYDROCARBON INDICATIONS
FREE HYDROCARBON
S1 mg/g
PRODUCTIVITY INDEX
S1/(S1+S2)
Depth (M)
S1 . HC already in rock
S2 : HC from Kerogen Pyrolysis
S3 : CO2 from Kerogen Pyrolysis
Sample Type
Cuttings
Sidewall
Core
Symbol
Line Type
Tmax
Ro
VL
TOC cut off : 0 %
S2 cut off : 0 %

Figure -61: Modified Van Krevelen diagram for analyzed samples from Shagar area, Gulf of Suez

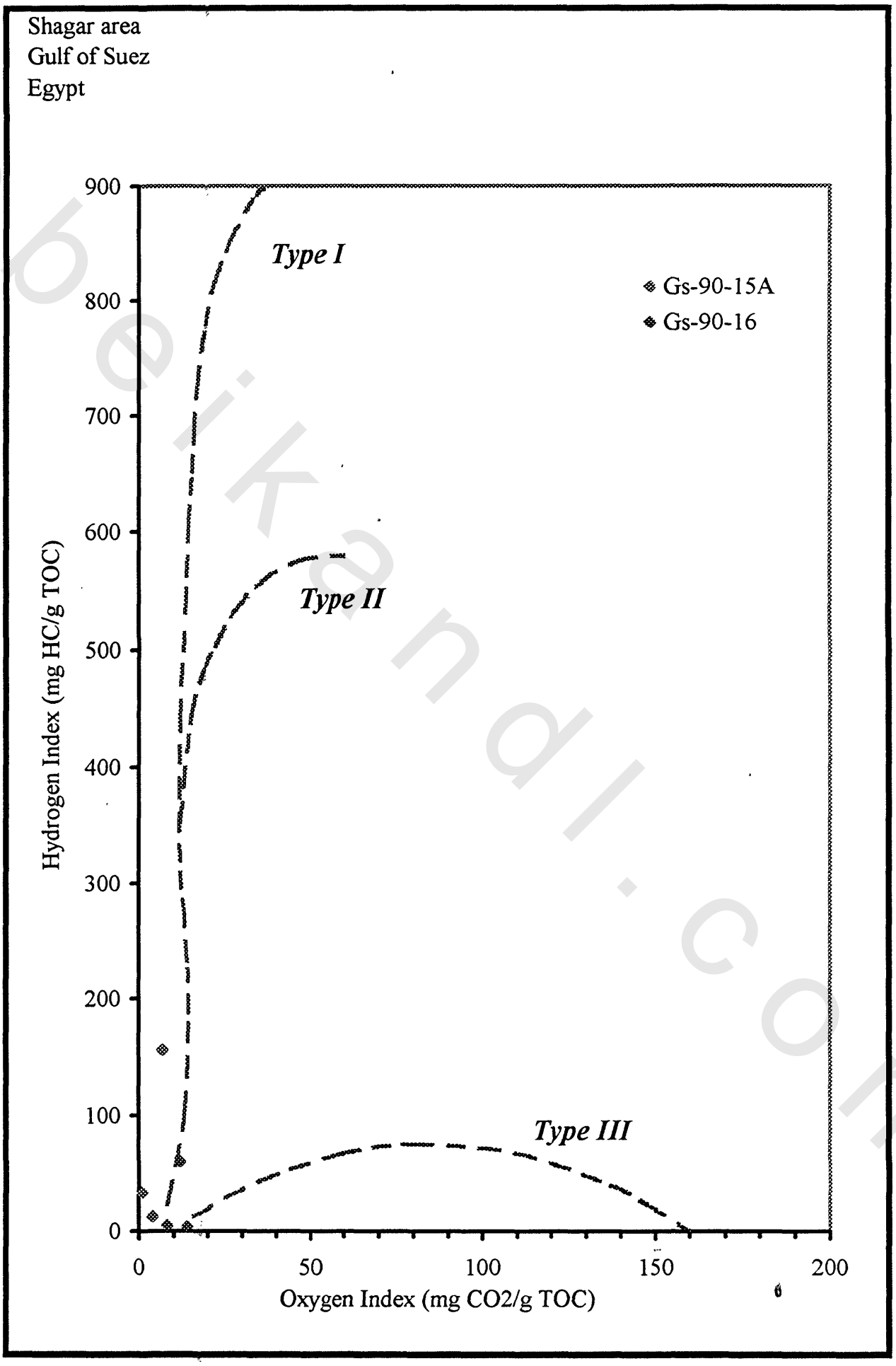

Figure-62: Infrared modified diagram for the investigated samples from Shagar, Gubal Island and Esh-Malaha areas

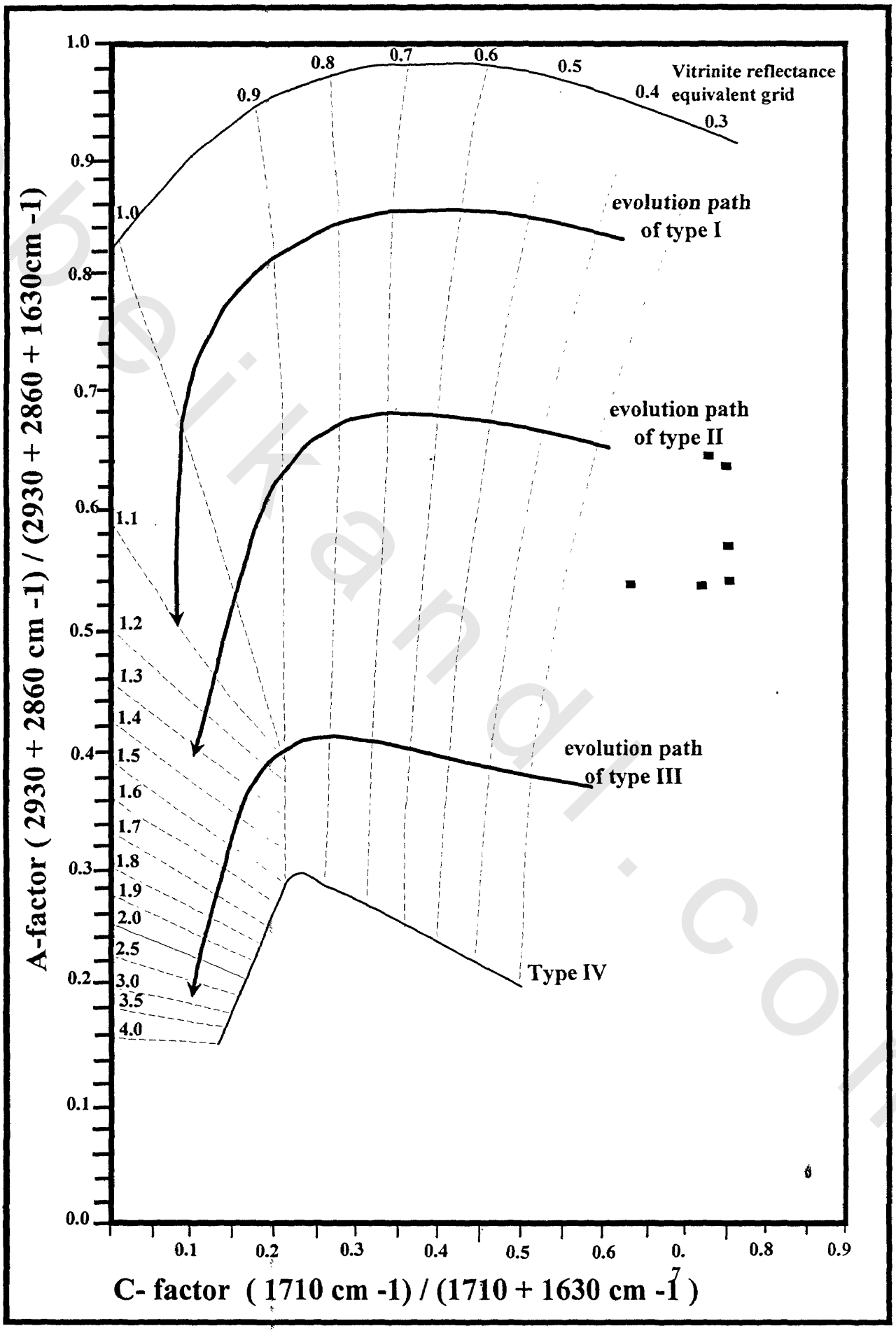

Figure -63: GC diagram of extracts for investigated subsubsurface evaporite core samples from Shagar area

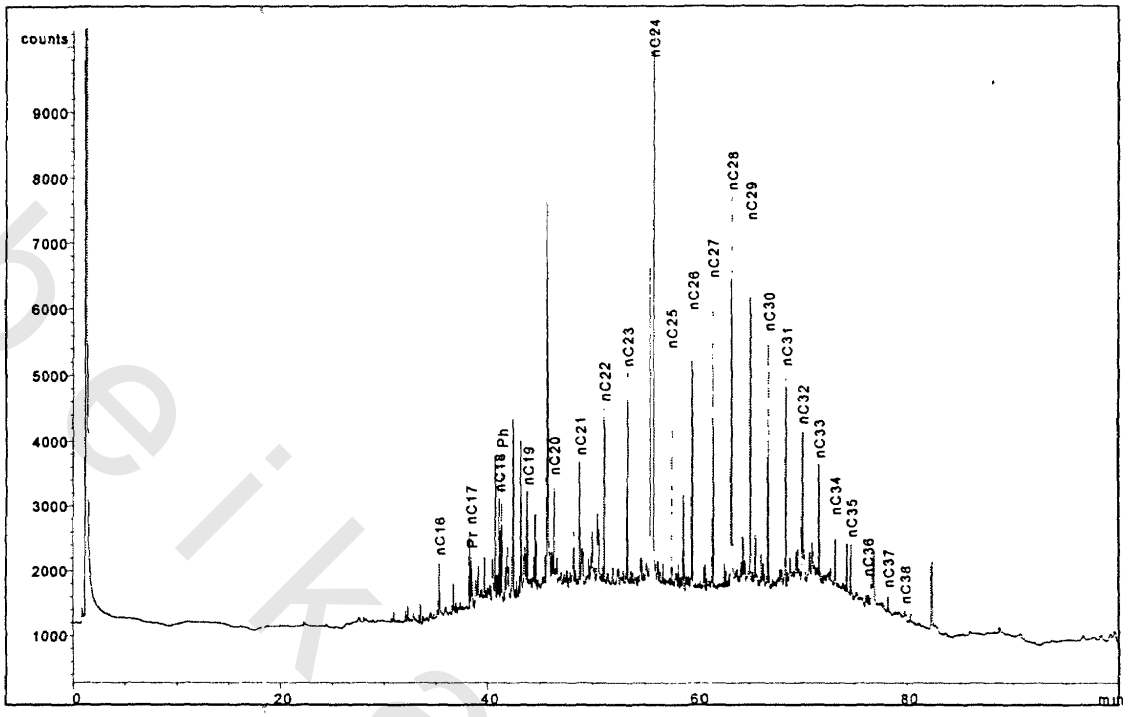

Figure-64: GC diagram of extracts for investigated subsubsurface evaporite core samples from Esh El-Malaha area

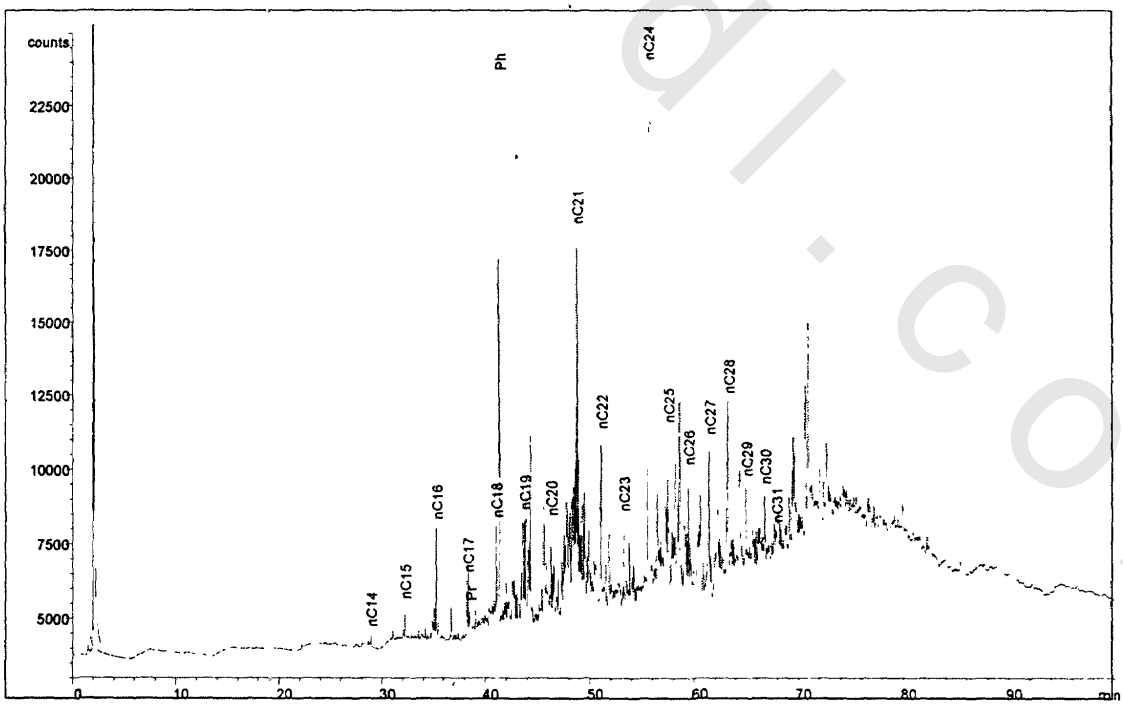

The diagram show : Bimodal distribution
High phytane content
high pristane over n-C17

Figure-65

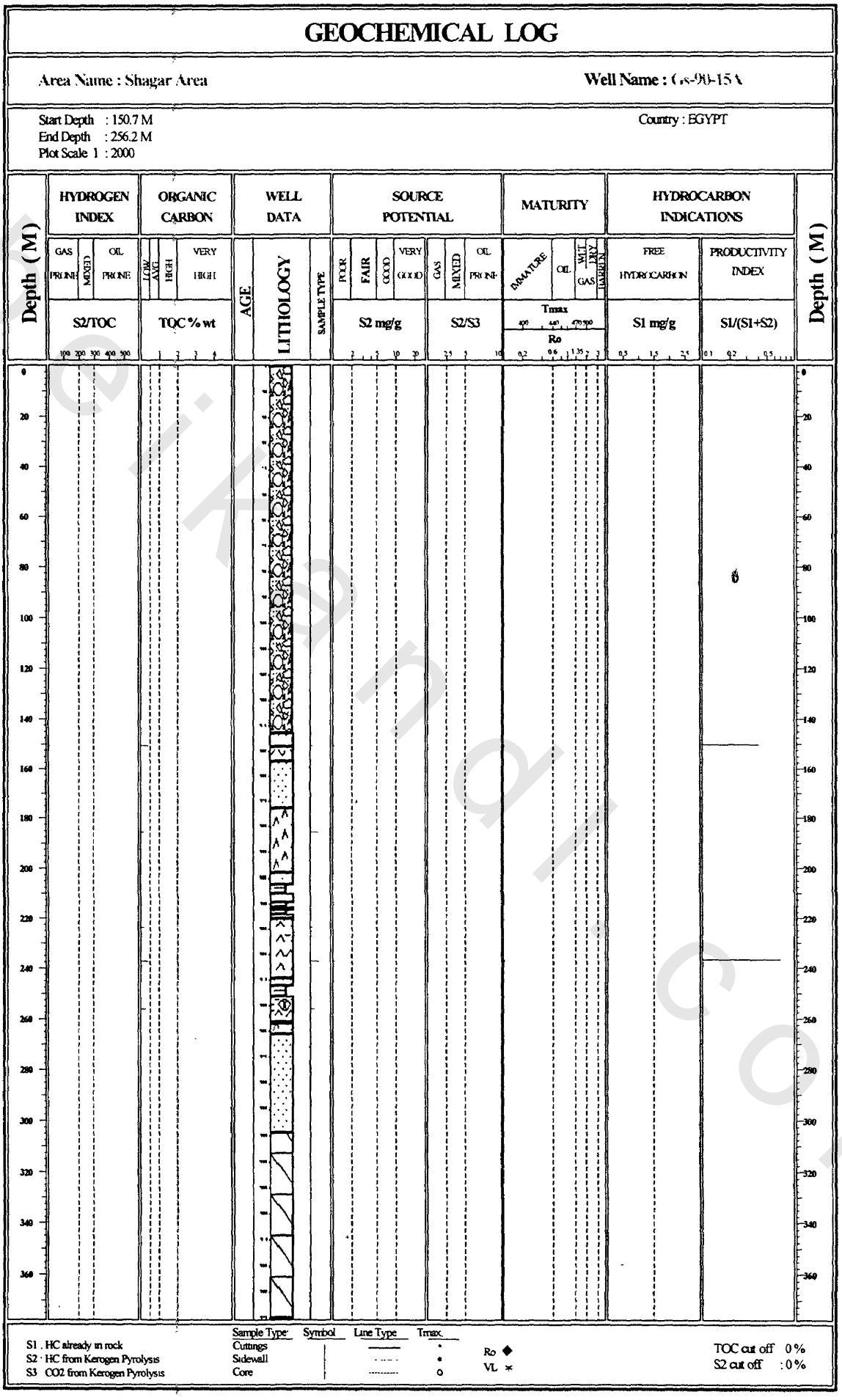
GEOCHEMICAL LOG
Area Name : Shagar Area
Well Name : Gs-98-15A
Start Depth : 150.7 M
End Depth : 256.2 M
Plot Scale 1 : 2000
Country : EGYPT
Depth (M)
HYDROGEN INDEX
GAS PRONE
MIXED
OIL PRONE
S2/TOC
100 200 300 400 500
ORGANIC CARBON
LOW
AVG.
HIGH
VERY HIGH
TOC % wt
1 2 3 4
WELL DATA
AGE
LITHOLOGY
SAMPLE TYPE
SOURCE POTENTIAL
POOR
FAIR
GOOD
VERY GOOD
S2 mg/g
2 5 10 20
GAS
MIXED
OIL PRONE
S2/S3
2.5 5 10
MATURITY
IMMATURE
OIL
WET GAS
DRY GAS
Tmax
400 440 470 500
Ro
0.2 0.6 1.35 2 3
HYDROCARBON INDICATIONS
FREE HYDROCARBON
S1 mg/g
0.5 1.5 2.5
PRODUCTIVITY INDEX
S1/(S1+S2)
0.1 0.2 0.5 1
Depth (M)
0 20 40 60 80 100 120 140 160 180 200 220 240 260 280 300 320 340 360
S1 . HC already in rock
S2 . HC from Kerogen Pyrolysis
S3 CO2 from Kerogen Pyrolysis
Sample Type
Cuttings
Sidewall
Core
Symbol
Line Type
Tmax
Ro
VL
TOC cut off 0 %
S2 cut off : 0 %

Figure-66

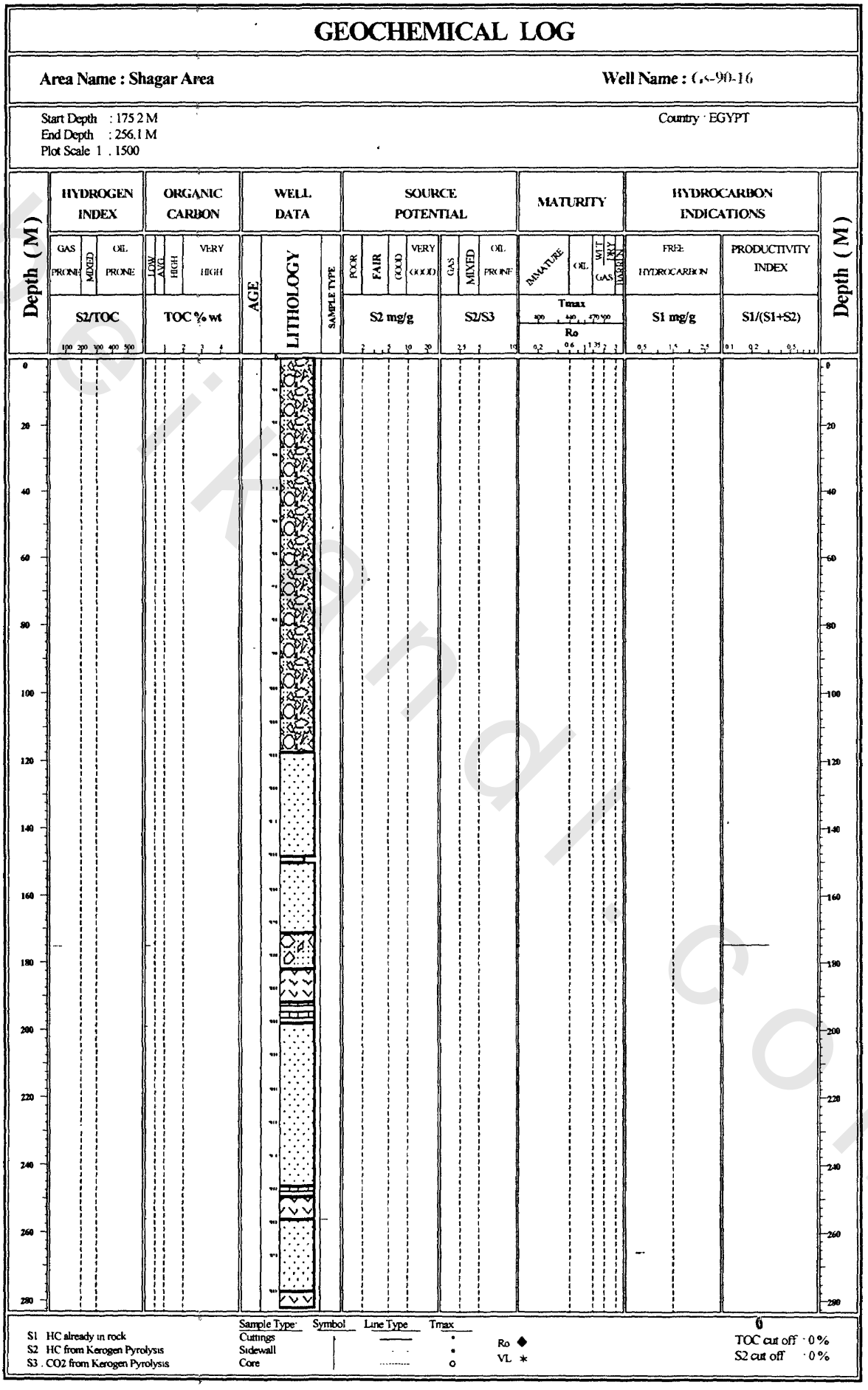
GEOCHEMICAL LOG
Area Name : Shagar Area
Well Name : G-90-16
Start Depth : 175.2 M
End Depth : 256.1 M
Plot Scale 1 : 1500
Country : EGYPT
Depth (M)
HYDROGEN INDEX
GAS PRONE
MIXED
OIL PRONE
S2/TOC
100 200 300 400 500
ORGANIC CARBON
LOW
AVG
HIGH
VERY HIGH
TOC % wt
1 2 3 4
WELL DATA
AGE
LITHOLOGY
SAMPLE TYPE
SOURCE POTENTIAL
POOR
FAIR
GOOD
VERY GOOD
S2 mg/g
2 5 10 20
GAS
MIXED
OIL PRONE
S2/S3
2.5 5 10
MATURITY
IMMATURE
OIL
WET GAS
DRY GAS
Tmax
400 440 470 500
Ro
0.2 0.6 1.35 2 3
HYDROCARBON INDICATIONS
FREE HYDROCARBON
S1 mg/g
0.5 1.5 2.5
PRODUCTIVITY INDEX
S1/(S1+S2)
0.1 0.2 0.5
Depth (M)
0 20 40 60 80 100 120 140 160 180 200 220 240 260 280
S1 HC already in rock
S2 HC from Kerogen Pyrolysis
S3 . CO2 from Kerogen Pyrolysis
Sample Type
Cuttings
Sidewall
Core
Symbol
Line Type
Tmax
Ro
VL
TOC cut off 0 %
S2 cut off 0 %

Figure-67: Modified Van Krevelen diagram for analyzed samples from Gubal Island

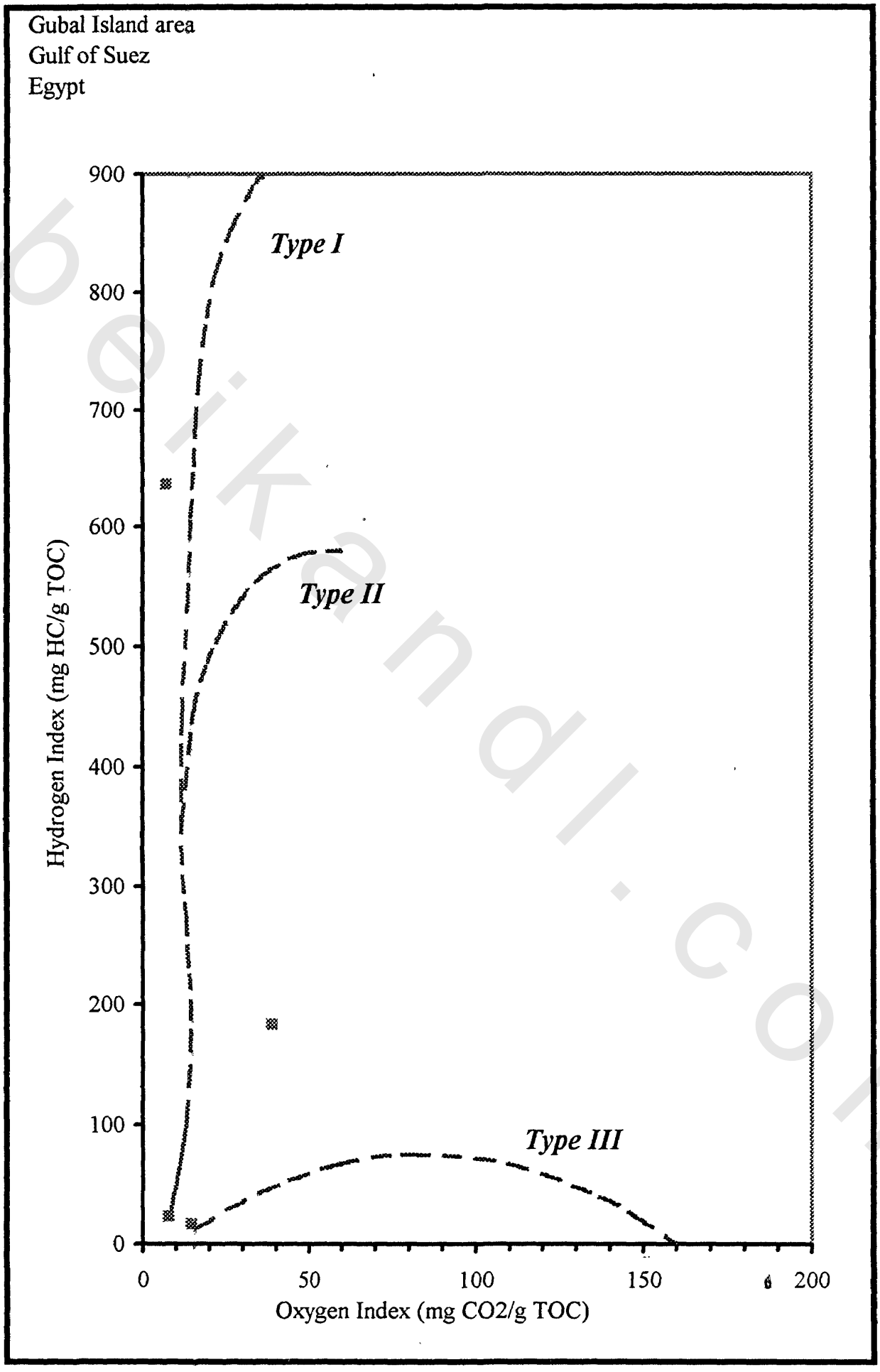

Figure-68: GC diagram of extracts for investigated subsubsurface evaporite core samples from Gubal Island

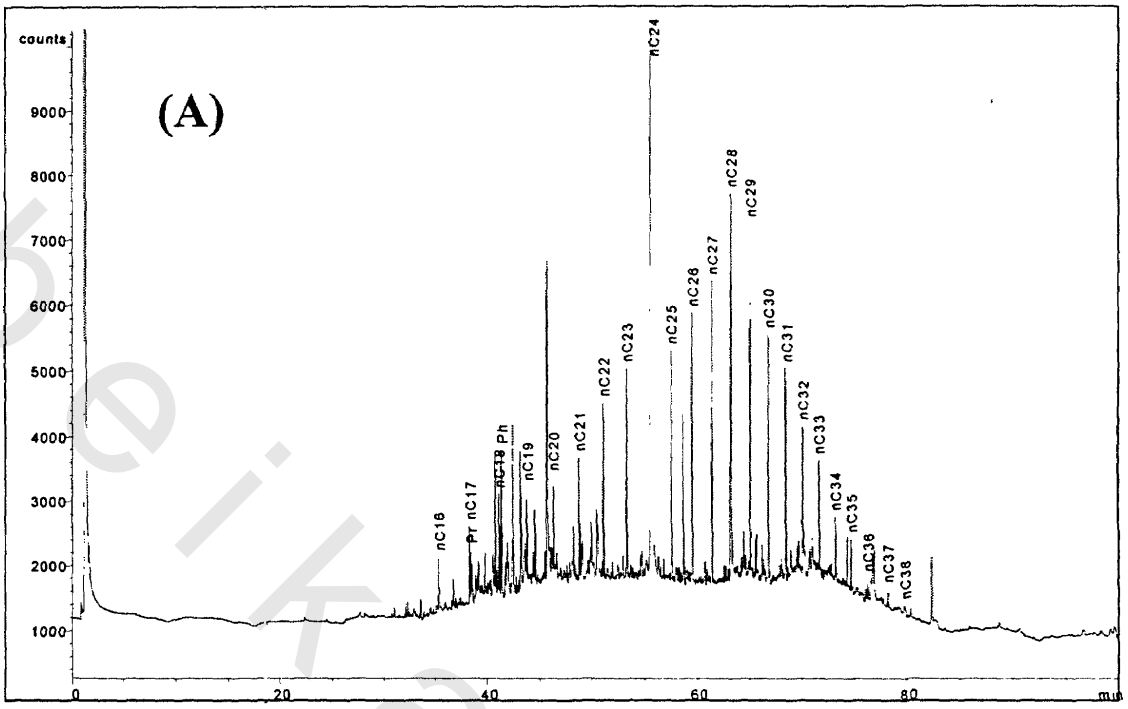

(A) : Unimodal distribution pattern and predominance of phytane over the n-C18

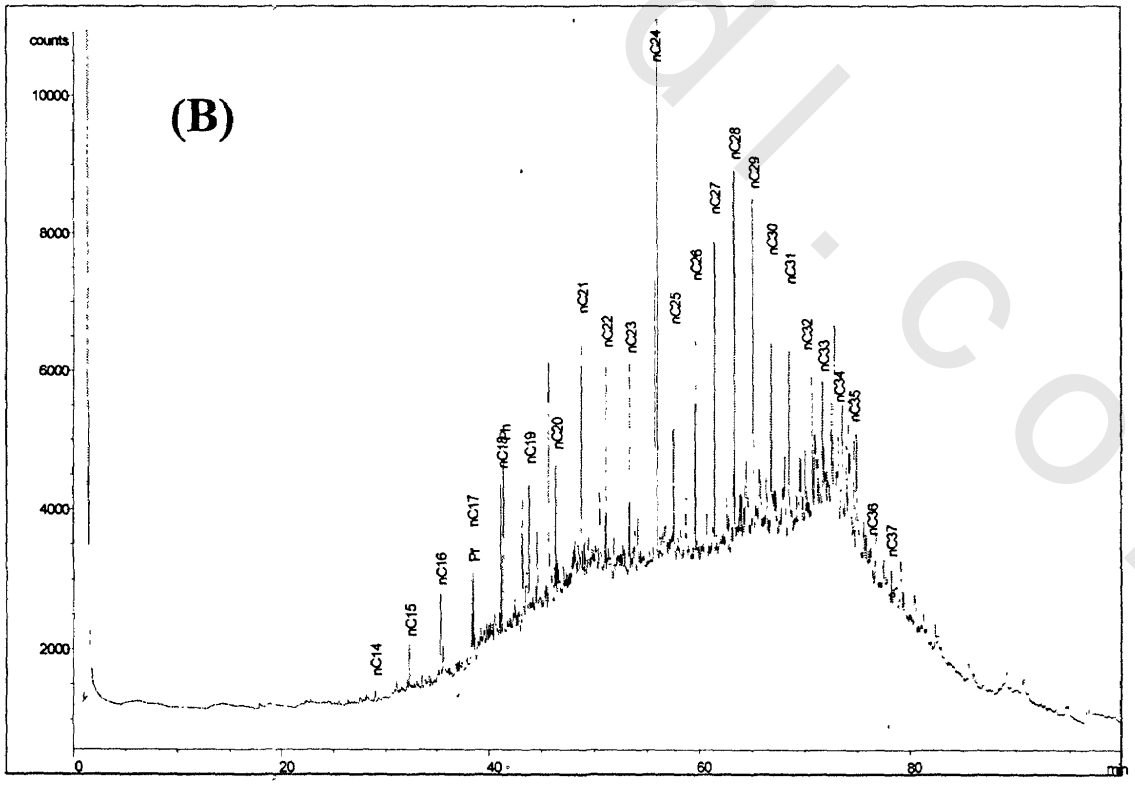

(B) : naphthane bluge between C25 to C31

Figure -69

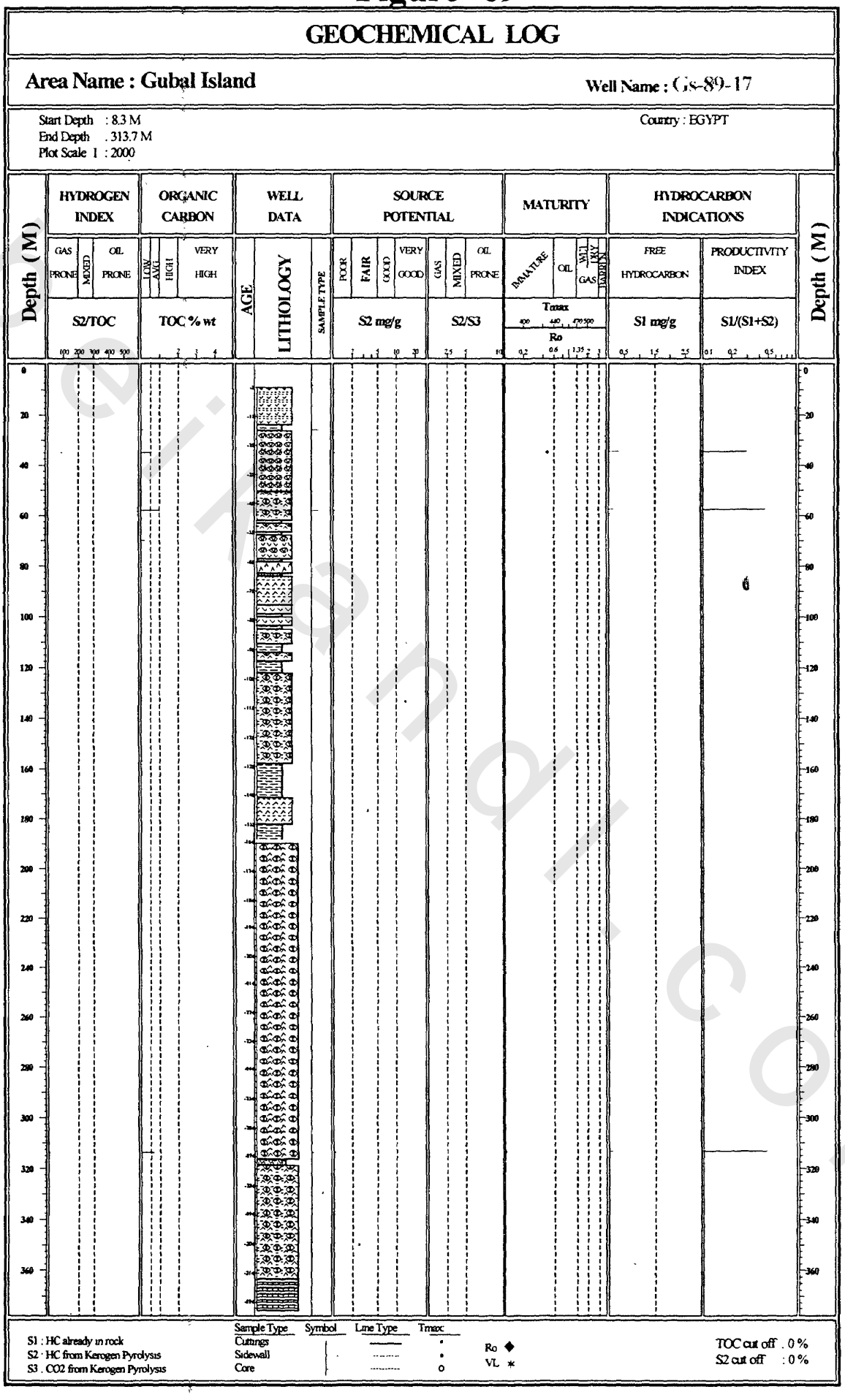
GEOCHEMICAL LOG
Area Name : Gubal Island
Well Name : Gs-89-17
Start Depth : 8.3 M
End Depth . 313.7 M
Plot Scale 1 : 2000
Country : EGYPT
Depth (M)
HYDROGEN INDEX
GAS PRONE
MIXED
OIL PRONE
S2/TOC
100 200 300 400 500
ORGANIC CARBON
LOW
AVG
HIGH
VERY HIGH
TOC % wt
2 3 4
WELL DATA
AGE
LITHOLOGY
SAMPLE TYPE
SOURCE POTENTIAL
POOR
FAIR
GOOD
VERY GOOD
S2 mg/g
2 5 10 20
GAS
MIXED
OIL PRONE
S2/S3
2.5 5 10
MATURITY
IMMATURE
OIL
WET GAS
DRY GAS
Tmax
400 440 470 500
Ro
0.2 0.6 1.35 2 3
HYDROCARBON INDICATIONS
FREE HYDROCARBON
S1 mg/g
0.5 1.5 2.5
PRODUCTIVITY INDEX
S1/(S1+S2)
0.1 0.2 0.5
Depth (M)
0 20 40 60 80 100 120 140 160 180 200 220 240 260 280 300 320 340 360
S1 : HC already in rock
S2 : HC from Kerogen Pyrolysis
S3 . CO2 from Kerogen Pyrolysis
Sample Type
Cuttings
Sidewall
Core
Symbol
Line Type
Tmax
Ro
VL
TOC cut off . 0 %
S2 cut off : 0 %

Figure-70

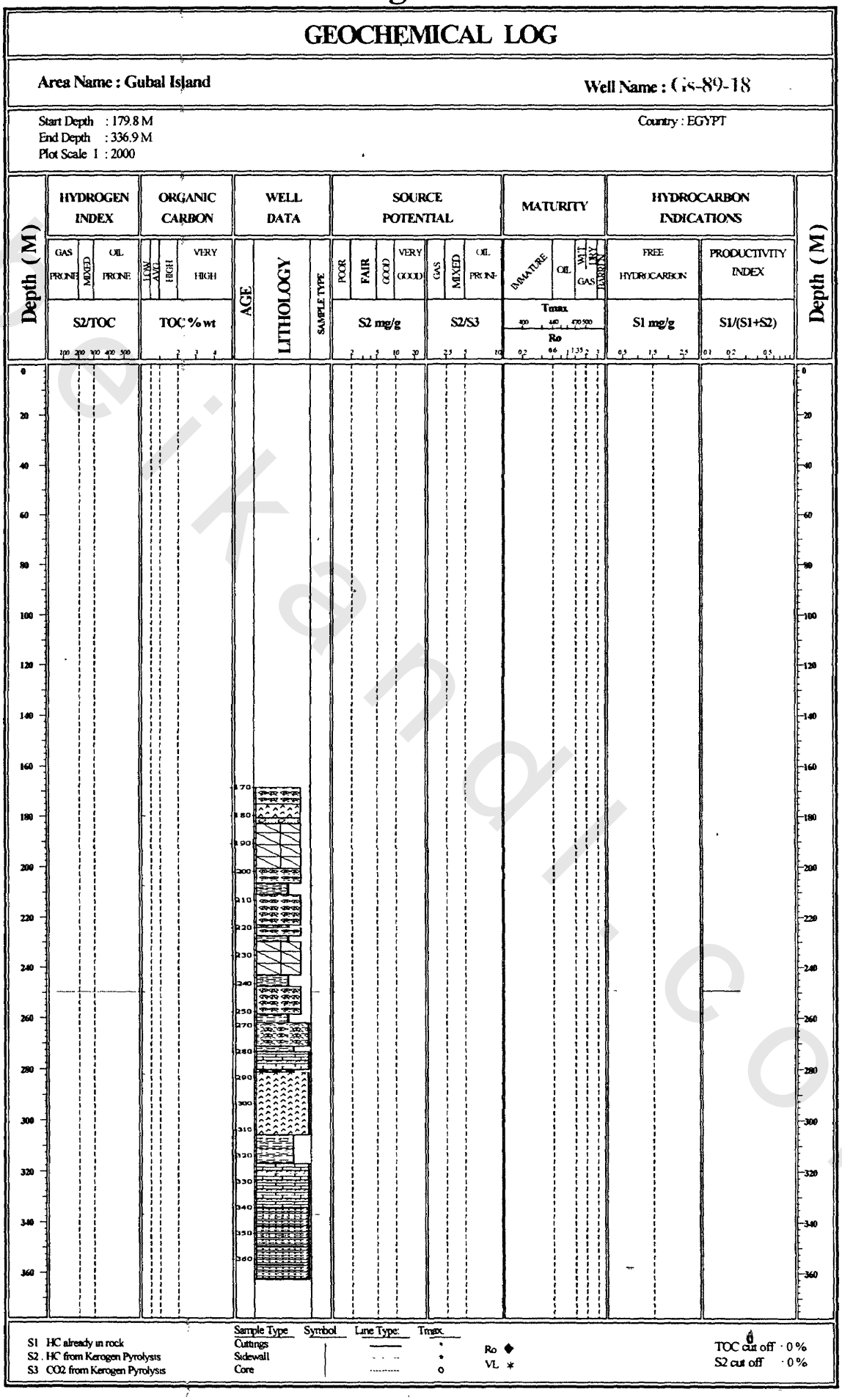
GEOCHEMICAL LOG
Area Name : Gubal Island
Well Name : Gs-89-18
Start Depth : 179.8 M
End Depth : 336.9 M
Plot Scale 1 : 2000
Country : EGYPT
Depth (M)
HYDROGEN INDEX
GAS PRONE
MIXED
OIL PRONE
S2/TOC
100 200 300 400 500
ORGANIC CARBON
LOW
AVG.
HIGH
VERY HIGH
TOC % wt
2 3 4
WELL DATA
AGE
LITHOLOGY
SAMPLE TYPE
SOURCE POTENTIAL
POOR
FAIR
GOOD
VERY GOOD
S2 mg/g
2 5 10 20
GAS
MIXED
OIL PRONE
S2/S3
2.5 5 10
MATURITY
IMMATURE
OIL
WET GAS
DRY GAS
Tmax
400 440 470 500
Ro
0.2 0.6 1.35 2 3
HYDROCARBON INDICATIONS
FREE HYDROCARBON
S1 mg/g
0.5 1.5 2.5
PRODUCTIVITY INDEX
S1/(S1+S2)
0.1 0.2 0.5
0 20 40 60 80 100 120 140 160 180 200 210 220 230 240 250 260 270 280 290 300 310 320 330 340 350 360
S1 HC already in rock
S2 . HC from Kerogen Pyrolysis
S3 CO2 from Kerogen Pyrolysis
Sample Type
Cuttings
Sidewall
Core
Symbol
Line Type:
Tmax
Ro
VL
TOC cut off 0 %
S2 cut off 0 %

Figure-71: Modified Van Krevelen diagram For analyzed samples from Esh El-Malaha Area

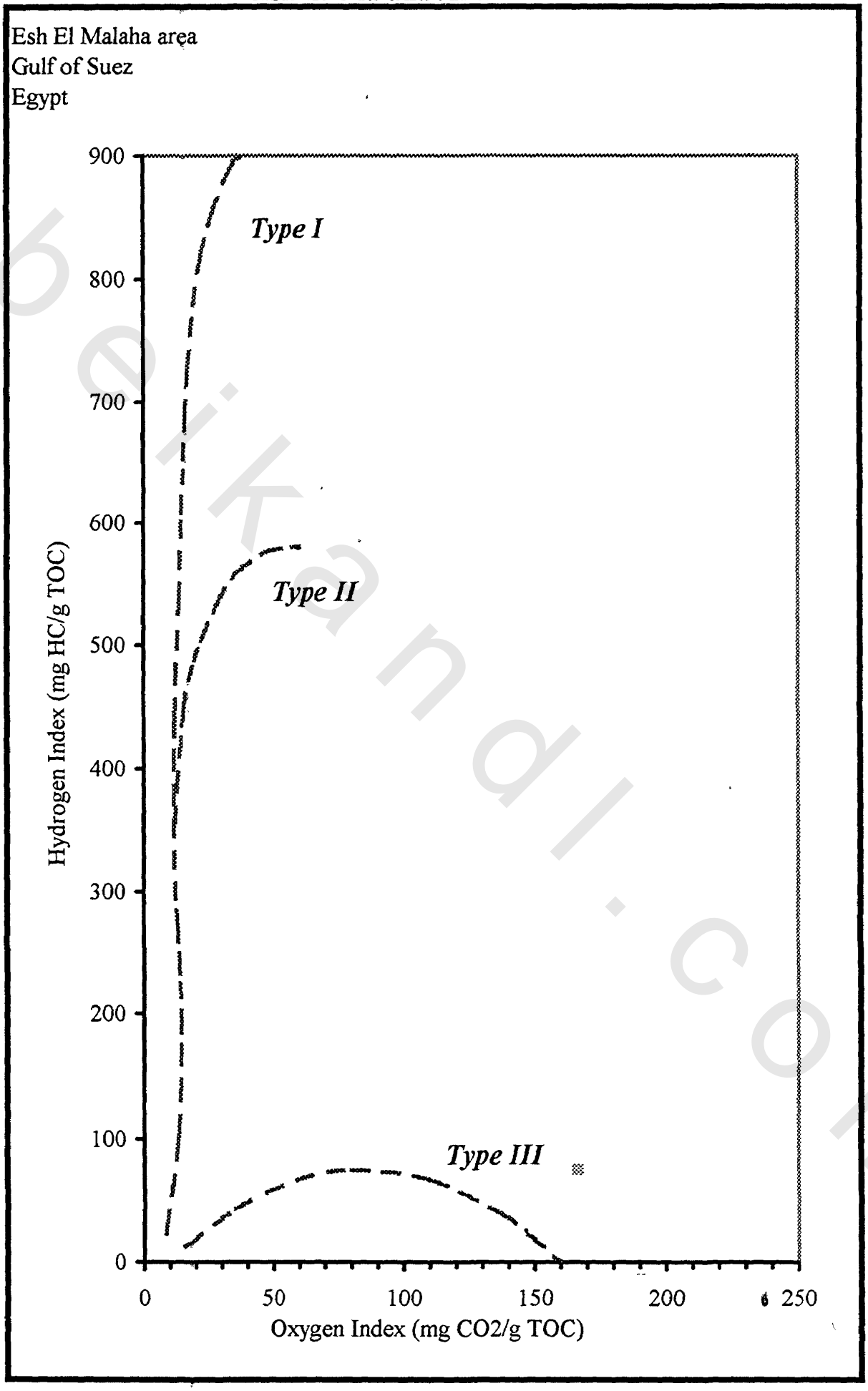

Figure-72: Modified Van Krevelen diagram for analyzed samples from North Sinai.